Distribution Agreement

In presenting this thesis or dissertation as a partial fulfillment of the requirements for an advanced degree from Emory University, I hereby grant to Emory University and its agents the non-exclusive license to archive, make accessible, and display my thesis or dissertation in whole or in part in all forms of media, now or hereafter known, including display on the world wide web. I understand that I may select some access restrictions as part of the online submission of this thesis or dissertation. I retain all ownership rights to the copyright of the thesis or dissertation. I also retain the right to use in future works (such as articles or books) all or part of this thesis or dissertation.

Signature:

_____ _____

Rebecca Faith Rosen Date

Characterization of naturally occurring, pathogenic and benign Aβ multimers
Why don't monkeys get Alzheimer's disease?

By

Rebecca Faith Rosen
Doctor of Philosophy

Graduate Division of Biological and Biomedical Science
Neuroscience

Lary C. Walker, Ph.D.
Advisor

Richard A. Kahn, Ph.D.
Committee Member

James. J. Lah, M.D./Ph.D.
Committee Member

Harry LeVine, III, Ph.D.
Committee Member

Todd M. Preuss, Ph.D.
Committee Member

Accepted:

Lisa A. Tedesco, Ph.D.
Dean of the Graduate School

Date

Characterization of naturally occurring, pathogenic and benign Aβ multimers
Why don't monkeys get Alzheimer's disease?

By

Rebecca Faith Rosen
B.Sc., Yale University, 1999

Advisor: Lary C. Walker, Ph.D.

An abstract of
A dissertation submitted to the Faculty of the Graduate School of Emory University
in partial fulfillment of the requirements for the degree of Doctor of Philosophy
in Graduate Division of Biological and Biomedical Science
Neuroscience
2009

Abstract

Characterization of naturally occurring, pathogenic and benign Aβ multimers
Why don't monkeys get Alzheimer's disease?
By Rebecca Faith Rosen

According to the amyloid cascade hypothesis of Alzheimer's disease (AD) pathogenesis, the aberrant multimerization of the β-amyloid peptide (Aβ) is a crucial early event in AD neurodegeneration and dementia. Aβ is a self-aggregating peptide that accumulates with age in the brains of humans, apes, and monkeys. However, the full spectrum of AD pathology and dementia has never been reported in a nonhuman primate. As our closest living relatives, nonhuman primates are thus unique models of nonpathologic Aβ accumulation. I hypothesized that toxic Aβ aggregates in AD brain are structurally distinct from Aβ multimers formed in nonhuman primate brains. To this end, I extensively characterized Aβ populations in postmortem cortical samples from AD patients, aged great apes (chimpanzees), Old World monkeys (rhesus macaques), and New World monkeys (squirrel monkeys). Using immunohistochemistry, ELISA, immunoprecipitation/MALDI-TOF MS, Western Blot and *in vivo* Aβ-seeding assays, I found that cortical Aβ populations are quantitatively and qualitatively *similar* in AD and aged nonhuman primates. The major cerebral Aβ isoforms (Aβ40 and Aβ42) accumulate at comparable levels and in similar ratios in AD and all nonhuman primate groups examined. Furthermore, post-translationally modified Aβ isoforms and low molecular weight Aβ multimers are strikingly similar in AD and aged nonhuman primate cortical homogenates. I then analyzed higher-order structural features of AD and nonhuman primate Aβ aggregates using Pittsburgh Compound B (PIB), a radioligand designed for *in vivo* PET imaging of β-amyloid. I confirmed that ^{3}H-PIB binding correlates positively with levels of insoluble Aβ40 and Aβ42 in AD cortical homogenates. However, ^{3}H-PIB binds with very low stoichiometry to Aβ in nonhuman primate cortical homogenates, even in cases with levels of Aβ equal to those in AD. These data suggest that, despite a common amino acid sequence, cerebral Aβ multimers are structurally distinct in AD and aged nonhuman primates, and that high-affinity PIB binding may be selective for a pathogenic molecular conformation of Aβ in AD brain. The identification of structural differences between naturally occurring, pathogenic and benign Aβ multimers could yield important clues to the uniquely human susceptibility to AD, and thereby reveal new molecular targets for AD therapeutics.

Characterization of naturally occurring, pathogenic and benign Aβ multimers

Why don't monkeys get Alzheimer's disease?

By

Rebecca Faith Rosen
B.Sc. Yale University, 1999

Advisor: Lary C. Walker, Ph.D.

A dissertation submitted to the Faculty of the Graduate School of Emory University
in partial fulfillment of the requirements for the degree of
Doctor of Philosophy
in Graduate Division of Biological and Biomedical Science
Neuroscience
2009

Contents

List of Figures

List of Tables

Acknowledgements

This dissertation is the product of a worldwide collaborative effort, which I cultivated under the mentorship of Dr. Lary Walker, a modern-day renaissance man. Behind each chapter is a story of learning and discovery, catalyzed by the involvement of numerous knowledgeable and generous scientific colleagues. In my Discussion, I document the story from the beginning, when I entered the graduate program in Neuroscience at Emory. My first acknowledgement goes out to the all-female Neuroscience class of 2003: Zoe, Lizabeth, Andrea, Elyse, Li-Ting, Kelly, Kim, and Liz. I believe we symbolize the new era of women in science, and I continue to be inspired by the passion, intelligence, and success of these eight ladies. I also partially attribute our success as graduate students to the top-notch learning environment fostered by Emory Neuroscience, a program characterized by its unique integration of academic, social, and pedagogical strengths.

Dr. Todd Preuss and Dr. Marie Csete each mentored me through laboratory rotation projects, teaching me the latest cutting-edge techniques while giving me freedom to pursue my own hypotheses. Dr. Preuss remained an integral member of my scientific circle at Emory, and we continue to process the many chimpanzee temporal lobes that we carefully dissected, sectioned, and photographed for our massive stereological undertaking. In Dr. Preuss's lab, I found the expertise and friendship of Carolyn Suwyn. Carolyn's histopathology skills are unmatched and I am lucky to have had the opportunity to learn from the best of the best laboratory technicians: Marcelia Maddox has also been a huge asset. Also at Yerkes, I will always appreciate the help of the

pathology department (Dr. Dan Anderson, Evan Dessasau and Eileen Breding) and Jim Herndon and his lab, who were integral members of our Yerkes aging journal clubs. Thank you to Dr. Yoland Smith's lab for expert assistance with electron microscopy, particularly Dr. Jeff Pare and Susan Maxson, and to the entire Center for Behavioral Neuroscience for sharing just about everything on the fifth floor of the Neuroscience building, no questions asked. And of course thank you to Jeromy Dooyema, our lab manager for the last three years, and my partner in immunohistochemistry, as well as good music. Also in our lab, Aaron Farberg was an undergraduate student who I mentored for two years, after which he came on board as an invaluable research technician for one year before heading off to medical school. I can truly say that I may have learned more from him than he learned from me. He taught me a new understanding of patience and perseverance, as well as faith in my laboratory skills, and I look forward to watching him climb the ladder to unparalleled success in the medical and research fields.

Dr. Lary Walker truly sets the gold standard for a graduate school advisor. I can barely express in words my appreciation for his patience, guidance, and support, both at a personal and an academic level. Within only a year of working in his lab, Lary had already sent me on a visit to Dr. Harry LeVine's laboratory at the University of Kentucky, when I drove up to Lexington with a box of monkey brains on dry ice, and came home with an exciting set of quantitative Aβ ELISA data that jumpstarted my dissertation project. Harry's neighbor, Dr. Paul Murphy, welcomed me into his lab as well, and thus began a fruitful and long-lasting collaboration between all our labs, which I am sure will continue throughout all of our careers. I am thoroughly indebted to Harry for the exciting

twists and turns I experienced while characterizing Aβ peptides in ape and monkey tissue. An expert "amyloidologist", Harry shared his knowledge with me, challenging me to see my experiments from different scientific angles and to truly understand the implications of my data. Most importantly, Harry introduced me to the PIB radioligand, a versatile experimental tool which transformed my dissertation project. Lary also sent me to work in Dr. Jorge Ghiso's laboratory at New York University, where I learned MALDI-TOF mass spectrometry techniques and gained a enthusiastic and friendly collaborator for future publications.

For the "chimpanzee tauopathy" paper, Dr. Bill Hopkins and his lab were eager to share behavioral and MRI data as needed, and have been equally helpful with my chimpanzee temporal lobe project, an endeavor supported strongly by Dr. Chet Sherwood at George Washington University and Dr. Patrick Hof at Mount Sinai School of Medicine. I thank Patrick and his lab for inviting me to New York to meet his colleagues and learn techniques in stereology from the best in the field. Drs. Dan Geschwind and Giovanni Coppola at University of California, Los Angeles sequenced the tau gene locus for this project, but also took the time to attend meetings at Neuroscience conferences, and contribute to the writing of the manuscript.

Here at Emory, the Center for Neurodegenerative Disease has been a laboratory home away from home. Marla Gearing, as the head of the Alzheimer's brain bank, was one of the first scientists I spoke with at the CND, and she has been a reliable source for tissue, pathology advice, and help with our manuscripts. The investigators, technicians, and students in Drs. Jim Lah and Allan Levey's lab welcomed me into their lab, and generously shared with me their lab space, equipment, reagents, and expertise. Dr.

Howard Rees patiently trained me with animal surgeries, confocal microscopy, and immunohistochemistry. Dr. Brian Ciliax was my pharmacology mentor in the CND, and I could never have completed the PIB binding assays and autoradiography without his expert advice and careful explanations. Dr. Rick Kahn, though down the hall in the Biochemistry department, became a valuable member of my thesis committee, and has truly taken the time to involve himself in my project and provide expert advice from a top-notch cell biologist. Thank you also to Mei Hong, Yair Gozal, Dr. Gus Davis, Debbie Cooper, and Dr. Jason Fritz. In the Department of Neurology, Joanne Wuu is a brilliant statistician, who patiently walked me through numerous power analyses and experimental designs. Dr. Thomas Wingo is a newer colleague in Neurology, and I am grateful for his enthusiasm and time commitment on the PIB-refractory AD case project.

Of course there are other collaborators that I must acknowledge, while this list grows ever longer. Dr. Pankaj Mehta and Dr. Peter Davies generously provided our lab with Aβ and tau antibodies. Dr. Mathias Jucker in Tubingen provided overseas consultations for my seeding experiments, taking his valuable time to attend meetings at international Alzheimer's conferences, so we could discuss my progress and design future experiments. I received nonhuman primate tissue from Dr. Mary Lou Voytko at Wake Forest University, Dr. Amy Arnsten at Yale University, Dr. David Lyons at Stanford University, Dr. Elizabeth Head at University of California Irvine, and Dr. Douglas Rosene at Boston University - quite a list!

Finally, I thank my many friends in the Emory Neuroscience program, my parents, my grandparents (in spirit), my sister Jennifer, Michael, and Sara. You have all provided the emotional and intellectual support that carried me through a challenging, yet

exciting six years of graduate school. It is only now that I can look back and acknowledge my immense personal and academic growth throughout the graduate school journey. I can also now look to the future with confidence and anticipation, secure in the knowledge that I will cultivate these friendships and collaborations as part of an exciting career in the fast-paced science of the 21st century.

Funding for my dissertation projects was provided by the University Research Committee of Emory University, RR-00165, PO1AG026423, P50AG025688 and the Woodruff Foundation. Yerkes is approved by AALAC (Association for Assessment and Accreditation of Laboratory Animal Care).

Chapter 1

Introduction and Background

The Evolution of Human Aging and Alzheimer's Disease

One of the most intriguing and complex questions in the biological sciences is "What makes us human?" Human beings live relatively longer than any other extant mammalian species, and their brains are substantially larger than predicted by the allometric relationship of brain and body weight for mammals (Figure 1.1) [126]. Among mammals, humans also an especially broad repertoire of social interactions and understanding, which is driven by their unique ability to communicate through spoken language [228]. The evolutionary forces that selected for brain size and longevity,

however, may also underlie the unique human susceptibility to devastating, age-related neurodegenerative diseases.

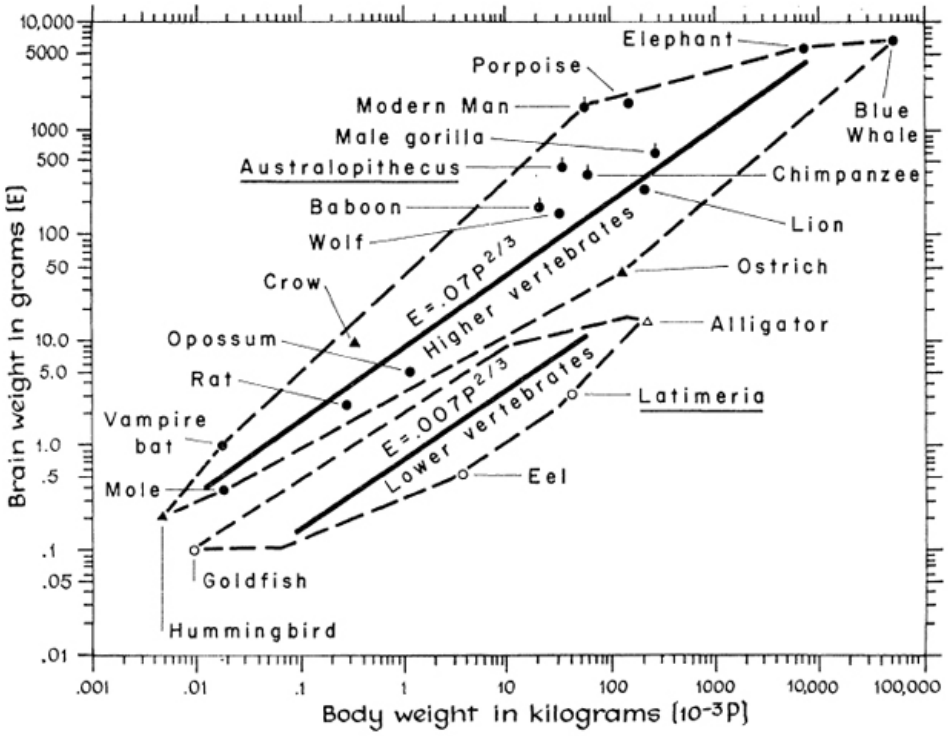

Figure 1.1 "Relation between Brain Weight and Body Weight of Living Vertebrates," reprinted with permission from University of Chicago Press. Original publication: Jerison HJ. (1969) Brain evolution and dinosaur brains. American Naturalist, 103: 575-588. This graph depicts the positive correlation between brain weight and body weight of extant vertebrates. Larger animals have larger brains, and the human brain is larger than predicted by body size than all other vertebrates examined in this study [121].

The human and great ape lineages diverged approximately 6 million years ago (Figure 1.2) [262]. Chimpanzees, our closest living relatives, have a maximum lifespan of 60 years [70, 111], while the maximum human lifespan of 122 years was recorded in 1997, when Jeanne Calment passed away in Arles, France [307]. As exhibited by Mrs. Calment's remarkable lifespan, humans can survive up to 70 years beyond the cessation of reproductive capabilities (reproductive senescence). All other nonhuman primates do not survive long after reproductive senescence, as it is not generally considered to be evolutionarily beneficial [70, 124]. Because of the complex social and physical infrastructure of human society, non-reproducing human grandparents can contribute to the reproductive fitness of their offspring [109]. This "grandmother hypothesis" is one of several viable theories to explain the extended lifespan unique to *Homo sapiens*.

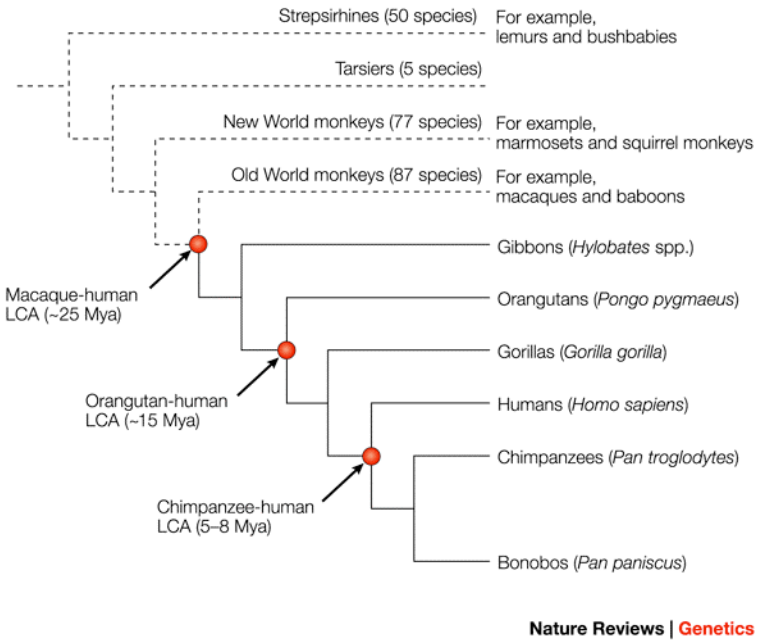

Figure 1.2. Phylogenetic relationships within the primate lineage. Adapted by permission from Macmillan Publishers Ltd: Nature Reviews Genetics, Preuss, T.M. et al, Human brain evolution: insights from microarrays, copyright (2004) [230]. The human and chimpanzee lineage diverged from a common ancestor between 5 and 8 million years ago.

Studies of extant mammalian species reveal a positive correlation between brain size and body mass, i.e. larger mammals have bigger brains. Mammalian brain size also correlates positively with lifespan, and a mammal's lifespan can be predicted by its brain and body weight [7, 12]. Relative to other mammals and, specifically, primates, humans have the largest brains (Figure 1.1; the human data point is the farthest from the estimated regression line in a log-log plot of living vertebrate brain weight versus body weight) [111, 261]. Humans also exhibit the greatest positive deviation from expected lifespan among primates, although one other primate species, the capuchin monkey, also lives substantially longer than the lifespan predicted by its brain and body weight [38].

Along with extended longevity and very large brain size, humans are susceptible to unique age-related diseases of the central nervous system, in what may considered a molecular trade-off of sorts. Several evolutionary theories of aging posit why these detrimental diseases continue to be selected for in human evolution. Peter Medawar's mutation accumulation theory states that the forces of natural selection are weakest on traits expressed during reproductive senescence and old age. These mutations accumulate, leading to higher mortality rates later in life, even though the "late-acting" genes have no benefit on individual reproduction [177]. Alternatively, the antagonistic pleiotropy theory of aging, first described by George Williams, asserts that longevity-associated genes that have been selected during the evolution of the extended human lifespan may have secondary, deleterious effects that are expressed during old age [303]. Such pleiotropic "late-acting" genes would evade selection because their effects are only exerted after the human being's reproductive period has ended. This theory could also be applied to selection for encephalization genes in the human lineage. If the antagonistic

pleiotropy theory holds true, the identification of human-unique genes contributing to longevity and/or encephalization could also lead to a better understanding of the molecular mechanisms underlying human disease of old age.

In 1961, Leonard Hayflick showed that cultured human cells are only capable of a finite number of divisions, providing one of the first indications that the aging phenotype of an organism can also be seen at a cellular level [110]. Later studies with fibroblasts derived from various other mammals demonstrated that cells from longer-lived animals undergo a greater number of cellular divisions *in vitro* than cells derived from animals with a shorter lifespan [240]. With the advent of high-throughput gene microarray technology, we can now undertake high-throughput comparative analyses of gene expression between such cells, to identify genetic mechanisms that underlie species-unique cellular (and potentially organismal) lifespans. Several labs have compared neuronal RNA expression levels in the brains of humans and their nonhuman primate relatives, in order to identify human-specific changes in gene expression that might underlie primate differences in brain size and/or lifespan [37, 64, 131, 183, 278]. These studies revealed several candidate genes of interest, but have yet to identify any single gene with clear phenotypic effects on human lifespan or brain size [230]. Understandably, the complex gene-environment interactions that occur in primate brain aging, as well as the contribution of epigenetic forces, make it unlikely that expression changes in one or two genes alone can determine an entire aging phenotype. In order to determine groups of genes, proteins, or even cells that contribute to the uniqueness of the human brain, a top-down, phenotype-driven approach might be a more productive alternative to high-throughput genome analysis. The initial identification of one human-

unique phenotype is an effective starting point in a comparative analysis of brain aging between humans and their closest nonhuman primate relatives. In other words, what about our aging brains makes us human?[1]

One of the most striking phenotypes of the aged human brain is its unique susceptibility to diseases of protein aggregation, or cerebral proteopathies. Cerebral protein homeostasis is carefully maintained by intracellular signaling pathways that ensure the proper folding of protein transcripts and the disposal of potentially toxic, improperly folded proteins [16, 186]. As the mammalian brain ages, these proteostatic mechanisms lose their efficiency, leading to an increase in the intracellular concentration of misfolded proteins [99]. In both human and nonhuman primate brain, there is a tendency for misfolded proteins to accumulate and deposit with age in the central nervous system and in some peripheral organs [193, 231, 255]. However, only aged humans suffer from the neurodegenerative proteopathies, the most common of which is Alzheimer's disease. Despite the age-related accumulation of cerebral protein aggregates, apes and monkeys seem to be resistant to the neurodegeneration and dementia that afflict humans with Alzheimer's disease [241]. The differential susceptibility to Alzheimer's neurodegeneration is an exciting paradigm with which to study the molecular mechanisms of human longevity.

Scientists have recognized the phenomenon of human longevity and its associated biological decline for thousands of years. As far back as 700 B.C., Pythagoras described five stages of the human life cycle, with the final "senium" stage beginning at 81 years. During this final stage of life, he explained "The system returns to the imbecility of the

[1] It is worth noting that there are also numerous shared biological aspects of aging between humans and nonhuman primates. In that regard, nonhuman primates are valuable experimental models to study the steady decline of physiological systems common to all aging primates.

first epoch of infancy." The perception of old age as a pathology unto itself persisted throughout the Greco-Roman period [20]. The term "senility" was synonymous with "dementia" or "imbecility", despite its origin from the word "senile," or "aged" in Latin. The concept of successful, healthy aging was nonexistent in the scientific literature – in Galen's medical encyclopedia of 180 A.D., old age itself was considered "an inevitable infection of the body [20]." We know now that, while the aged human body no doubt falls victim to long-term wear and tear, there are numerous examples of healthy human aging and that diseases of aging are not inevitable [245, 276, 307]. Throughout the last 200 years, the scientific community has meticulously characterized and categorized the pathological processes of diseases of aging [173]. By expanding our knowledge of the pathogenic mechanisms of these age-related diseases, we may help to extend the human lifespan even beyond 122 years. More importantly, however, biomedical advances in the aging field will serve to enhance the quality of our elderly years.

Alzheimer's disease: History

In the years immediately before and after 1900, European histopathology experienced a series of landmark discoveries, which paved the way for important advances in the identification and characterization of age-related disease pathologies. In the late 1800s, Camillo Golgi revolutionized the field of neuroscience with the discovery of a silver impregnation technique for labeling neurons in cortical tissue sections. In 1894, Franz Nissl developed a staining technique for general labeling of all cortical cells, utilizing a histological stain for ribonucleic acid [20]. The Bielschowsky modification of

the Golgi silver stain was developed in 1902 and used soon after to identify, for the very first time, the hallmark pathological lesions of AD brain [22]. In 1906, the German physician Alois Alzheimer (a colleague of Dr. Nissl) delivered a talk entitled, “An unusual disease of the cerebral cortex” in which he described a female patient at the municipal mental asylum in Frankfurt am Main. Auguste Deter was admitted at the age of 51 years, with a five-year history of short-term memory loss and disorientation, symptoms that rapidly progressed until her death at 55 years. Upon post-mortem examination of her brain, Dr. Alzheimer described cortical thinning, neuron loss and the intracellular accumulations we now call neurofibrillary tangles (Figure 1.3b) [8]. He observed that, within these intracellular bundles, a chemical reaction of the fibrils had taken place. Several months later, in Prague, Dr. Oskar Fischer published a histopathological analysis of the brains from 12 cases of a similar “unusual disease”. In addition to confirming Alzheimer’s description of fibrillar intraneuronal inclusions, he described “miliary sclerosis” (senile plaques) and astutely noted the differences in plaque morphology and progression, as well as the abnormal changes in nerve fibers passing through and around these cortical plaques (Figure 1.3a). Importantly, Dr. Fischer’s study included a large number of non-demented “control” brains, in which he did not find either of the two lesions [71]. This disease of dementia, characterized by senile plaques and neurofibrillary tangles, soon became associated with only one of these two doctor’s names, after it was listed in Dr. Emil Kraepelin’s 1910 edition of his “Textbook of Psychiatry,” as “Alzheimer’s Disease” [20].

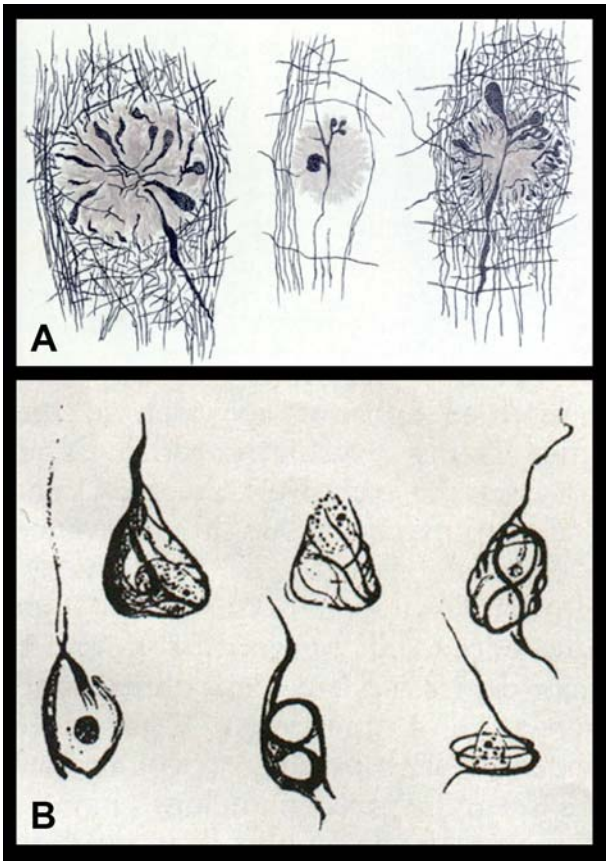

Figure 1.3. Original drawings of amyloid plaques and neurofibrillary tangles in AD brain. (A) In a 1907 paper, Oskar Fischer sketched representations of 3 stages of "miliary plaques", complete with dystrophic neurites and the disruption of passing neuronal fibers. Dr. Fischer also described neurofibrillary tangles, which were first drawn by Dr. Alois Alzheimer in his 1906 publication (B), where he surmised that a chemical modification had taken place within the affected neurons. Figures reproduced from Goedert, Brain 2009, under the terms of a Creative Commons license [88].

Alzheimer's disease (AD) is a progressive neurodegenerative disease characterized by massive neuronal loss, severe dementia and the accumulation of extracellular Aβ plaques and intracellular neurofibrillary tangles throughout the brain. There is currently no disease-modifying treatment available for AD neurodegeneration. The predominant risk factor for AD is simply old age – by the age of 85, there may be as high as a 50% chance of suffering from the disease [254]. The most prevalent genetic risk factor for the sporadic form of the disease is a genetic polymorphism in the ApoE gene, which codes for a lipoprotein of undetermined function in AD pathology. AD afflicts over 5 million people in the US alone and it is projected that nearly 8 million Americans will suffer from the disease by the year 2030. The disease costs the US federal government 149 billion dollars each year, a number that will increase substantially as the baby boomers enter their elderly years [2]. Less than 1% of AD cases can be attributed to known genetic mutations; the remaining 99% cases of AD are "iodiopathic," meaning they are of unknown cause. Alzheimer patients exhibit striking short-term memory loss, delusions, and a progressive inability to communicate. The disease always ends in mortality, although the primary cause of death in AD patients is typically a secondary infection [132].

Alzheimer's disease: Diagnosis

The clinical diagnosis of AD is reliant on physical exams, medical and family histories, and a cognitive neuropsychological exam, usually the Mini-Mental State Examination or a clock-drawing task called the "Mini-Cog". One test commonly used by

health professionals to diagnose probable AD rating scale was established in 1986 by the Consortium to Establish a Registry for Alzheimer's Disease (CERAD) [69]. Another commonly used clinical rating scale was established by the National Institute of Neurological and Communicative Disorders and Stroke and the Alzheimer's Disease and Related Disorders Association (NINCDS-ADRDA) and categorizes the patient as Possible, Probable or Definite AD [59]. The diagnosis of "Definite AD" for both rating scales relies upon a post-mortem cortico-pathologic analysis in which a pathologist scores the region-specific cortical deposition of extracellular senile plaques, made up of aggregated beta-amyloid (Aβ) peptides, and intracellular neurofibrillary tangles, composed of abnormally hyperphosphorylated, aggregated tau protein (Figure 1.4). For Braak staging of AD pathology, cases are scored on a scale of 1 to 6, based on detailed pathological studies of the temporal and regional progression of tau and neuritic amyloid pathology in a large sample of brains from all along the disease continuum [30]. In Braak stages I and II, early AD pathology begins in the transenthorhinal region of the temporal cortex. Pathology in the hippocampus denotes Braak stages III and IV. Finally, in later stages of the disease, plaques and tangles are seen throughout the neocortex, spreading into occipital regions in end-stage AD (Stages V and VI) [30, 270, 271]. For AD diagnosis using the consortium (CERAD), the MMSE score is combined with the Braak stage to calculate a final patient rating. However, Braak staging alone is considered sufficient to establish a final disease diagnosis.

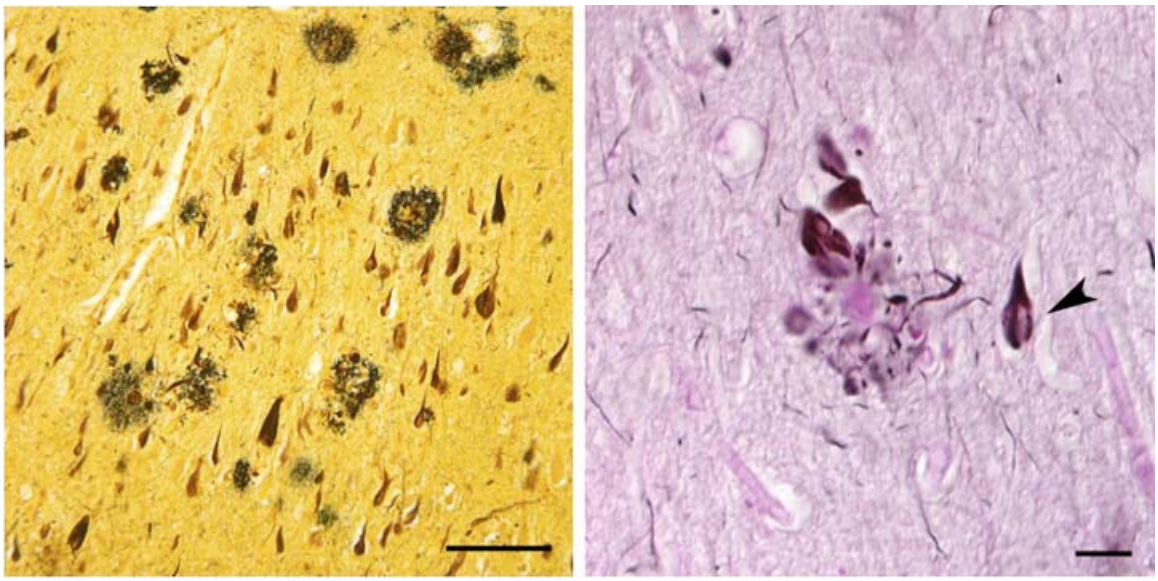

Figure 1.4. Aβ and tau deposition in AD brain. Left panel: Low magnification image of an AD cortical section processed by Bielschowsky silver staining to reveal copious amounts of extracellular plaques and intracellular neurofibrillary tangles. Right panel: Higher magnification image from another silver-stained AD cortical section, showing detailed morphology of a cored senile plaque and NFTs (black arrowhead). Bars = 100μm and 20μm.

There is currently no universally accepted technology to definitively diagnose AD in living persons. Since the advent of molecular imaging techniques, however, several promising new technologies have been developed to image the progression of AD pathology and cortical degeneration *in vivo*. Magnetic resonance neuroanatomical imaging combined with volumetric analysis of cortical regions reveals a significant reduction in cortical volume in regions affected by AD pathology as compared to nondemented control patients [59, 299]. Longitudinal studies of AD-vulnerable brain regions may thus be useful for the early detection of AD-like cortical shrinkage. Positron emission tomography (PET) scanning with ^{18}F-fluoro-2-deoxy-D-glucose (FDG) allows for the *in vivo* measurement of glucose metabolism, a direct measurement of localized brain activity. One longitudinal FDG-PET study revealed progressive hypometabolism in AD-relevant limbic and cortical structures, as nondemented patients progress to a clinical diagnosis of AD dementia. AD pathology and neuronal loss in the hypometabolic regions was confirmed by post-mortem analysis [188]. The use of PET scanning to identify region-specific cerebral hypometabolism is a promising diagnostic tool for AD as well as for numerous age-related dementias that are characterized by neuronal loss in specific cortical and subcortical areas. However, regional brain volume and metabolic activity are indirect measurements of the underlying pathology in neurodegenerative diseases such as AD. In order to image the primary pathological insult in these diseases, we need technologies with higher resolution and lesion specificity.

Recently developed PET radioligands that quickly cross the blood-brain barrier and bind directly to cerebral amyloid may provide the necessary specificity and resolution for *in vivo* diagnosis of AD pathology. These ligands allow for the real-time

visualization of amyloid deposition in the living human brain. One such ligand, Pittsburgh Compound B (PIB), is a benzothiazole derivative of Thioflavin T, the fluorescent histological agent that exhibits a characteristic shift in its emitted fluorescence spectrum upon binding to amyloid structures [142, 295]. In PET studies, ^{11}C-PIB shows significantly increased retention in the brains of clinically diagnosed AD patients when compared to ligand uptake in cognitively normal control subjects as well as subjects with mild cognitive impairment, who exhibit greater PIB retention than the nondemented control subjects (Figure 1.5) [244]. Importantly, the specificity of ^{11}C-PIB for Aβ has been confirmed by postmortem autoradiographic analysis; at specific activity levels achieved in PET scans, the ligand does not bind detectably to neurofibrillary tangles or any other non-Aβ containing lesions [13, 118]. Other radiolabeled amyloid-binding ligands such as ^{18}F-FDDNP and ^{125}I-IMPY have shown moderate success in clinical studies [206, 256]. Not surprisingly, there is a high-paced race among AD and radiology laboratories worldwide to develop even more sensitive ligands with better blood brain barrier penetration. In an ever-growing number of clinical studies, the confirmation of the clinical value of these PET probes suggests that amyloid binding radioligands and PET technology will make the early diagnosis of AD pathology a reality in the near future. The ability to diagnose AD before it manifests clinically, in addition to the possibility of monitoring the progression (or inhibition) of disease pathology, will revolutionize the field of Alzheimer's research and drug development.

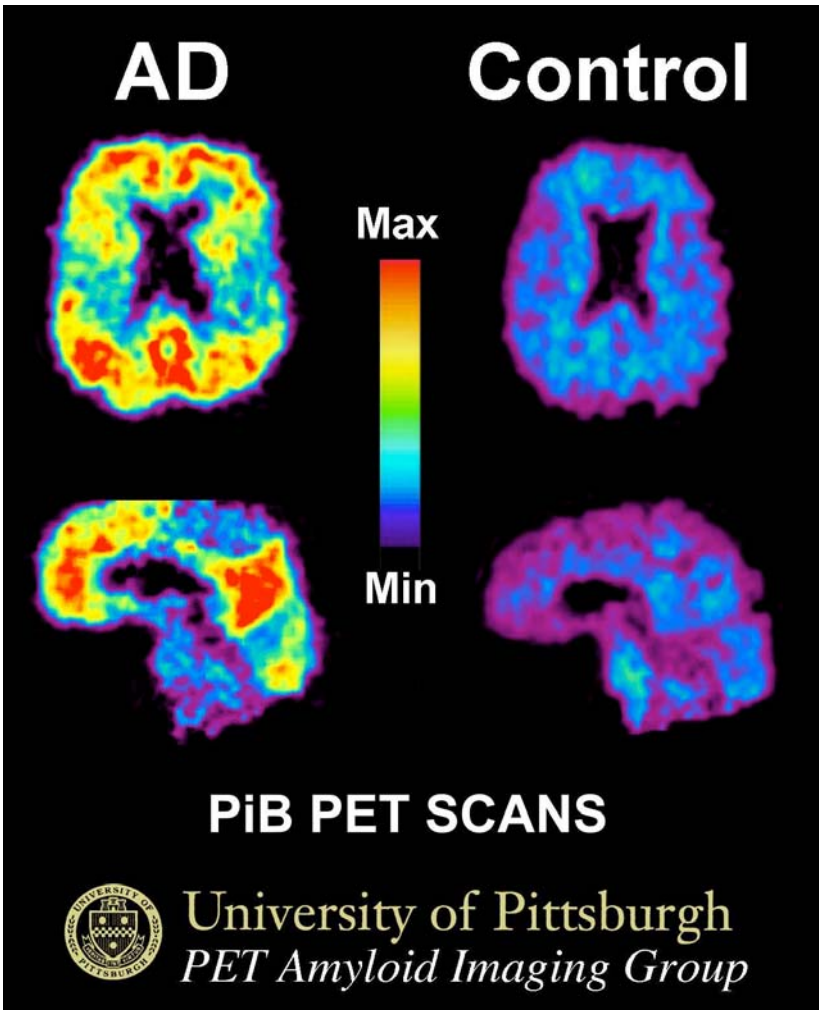

Figure 1.5. Pittsburgh Compound B exhibits increased uptake in AD brain. In this figure originally published by William Klunk with the University of Pittsburgh Amyloid Imaging Group, ^{11}C-PIB uptake is strongly enhanced in the AD case (left) as compared to an elderly subject with normal memory (right). Red and yellow areas indicate high concentrations of PIB in the brain. Image is reproduced under the terms of a Creative Commons license. (http://commons.wikimedia.org/wiki/File:PiB_PET_Images_AD.jpg)

The Aβ Amyloid Cascade Hypothesis of Alzheimer's Pathogenesis

The Aβ peptides that accumulate into senile plaques in AD brain are cleavage products of the amyloid precursor protein (APP). APP is a single-pass trans-membrane protein that has been implicated in normal neuronal development and growth, likely as a component in intracellular trafficking. While the precise cellular function of APP is unknown, the enzymatic cleavage of the ~100 kDa protein and its cleavage products have been extensively characterized [14, 253, 272]. APP is usually cleaved at the plasma membrane or in an endosomal compartment within the secretory pathway. The two major APP cleavage pathways have been termed the "nonamyloidogenic" and, accordingly, the "amyloidogenic" pathways [104]. The nonamyloidogenic cleavage of APP predominates in healthy neurons and is initiated by an α-secretase protease, which cleaves the protein in its transmembrane region to release a soluble ectodomain (sAPPα) into the extracellular space or the cytosol, depending on the cellular location of protein cleavage. The remainder of the protein is then cleaved by the γ-secretase complex, again within the transmembrane region, releasing a small, nontoxic 23 or 25 amino acid "P3" peptide extracellularly [60], and an intracellular 99 amino acid peptide, which binds within a transcriptionally active complex and may regulate gene expression [190]. During amyloidogenic cleavage of APP, the protein is first cleaved within the extracellular domain by β-secretase proteolysis, releasing a soluble sAPPβ protein. The second cleavage event is the same as in the nonamyloidogenic pathway, but a 40-42 amino acid β-amyloid (Aβ) peptide is released instead of the P3 peptide (Figure 1.6). The 17 additional N-terminal amino acids on the Aβ peptide are thought to be essential to the

peptide's strong predilection for self-aggregation and its neurotoxic effects as it accumulates in AD brain [24, 25]. Another important determinant of the peptide's propensity to aggregate is the cellular environment in which APP is cleaved. Protein folding is exquisitely sensitive to small changes in pH and the presence or absence of metal ions and molecular chaperones [10, 36].

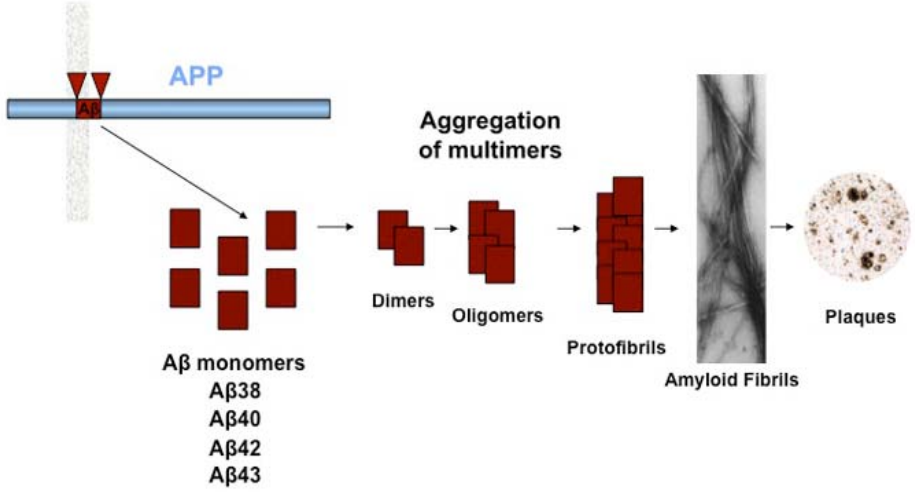

Figure 1.6. Production and aggregation of the Aβ peptide. The APP single-pass transmembrane protein is sequentially cleaved by β-secretase and γ-secretase enzyme complexes to produce Aβ peptides from 38 to 42 amino acids in length. Aβ self-aggregates in a nucleation-dependent manner, forming dimers and trimers and low molecular weight oligomers. Aβ eventually aggregates into β-sheet rich protofibrils and amyloid fibrils that make up senile plaques in AD and aged nonhuman primate brain.

The Aβ amyloid cascade hypothesis holds that it is the abnormal overproduction and/or accumulation of the Aβ peptide that initiates the AD neurodegenerative cascade [104]. Neurofibrillary tangles (NFTs), which are intracellular, fibrillar aggregates of abnormally hyperphosphorylated tau, are the concomitant pathogenic hallmark found in AD brain, and the quantity and regional accumulation of NFTs correlate more strongly with the clinical diagnosis of AD dementia than does senile plaque deposition in AD brain [9, 53]. However, mounting evidence supports the idea that a small, oligomeric form of the Aβ peptide exerts the primary neurotoxic insult in AD brain [40, 157]. We do not yet have an assay with sufficient sensitivity to measure these soluble Aβ oligomers *in vivo*, so it is unclear if the oligomers would better correlate with cognitive decline than amyloid plaques. Experiments with transgenic mouse models of AD pathology suggest this may be the case [157, 191].

Genetic evidence provides the strongest empirical support for a direct link between Aβ accumulation and AD neurodegeneration. Mutations in the tau protein do translate into progressive neurodegenerative disease pathology, as seen with the frontotemporal dementias, but there is no known tau mutation that precipitates AD pathogenesis, i.e. plaques and tangles [89, 153]. All of the 175+ known mutations that cause early-onset familial AD are in the APP protein (either flanking the Aβ cleavage sites or within the Aβ sequence), presenilin 1, or presenilin 2, both of which are protein components of the γ-secretase complex [21]. Every one of these familial AD mutations enhances the total amount of Aβ produced in the brain, leads to a propensity for Aβ42 production, which aggregates more readily than Aβ40, or results in the production of a

mutant Aβ peptide that is more likely to aggregate and/or more toxic than wild-type Aβ40 or Aβ42 [102].

Down's syndrome is a developmental disorder that results in severe mental retardation and a phenotype of early physiological aging. The disease is caused by a third copy of at least part of chromosome 21, which contains the gene for the APP protein. Down's patients produce 50% more cerebral APP than normal cohorts, and they progressively accumulate cerebral Aβ deposits along with neurofibrillary tangles at an earlier age than the general population, with over half of Down's patients presenting full AD neuropathology by their 6^{th} decade [156, 172]. While it can be difficult to diagnose co-morbid Alzheimer's dementia in these patients, it is estimated that approximately 15% of Down's patients suffer from early-onset AD dementia [202], further supporting a causative role for Aβ toxicity in AD.

Transgenic models of AD pathology lend additional support for the amyloid cascade hypothesis, by helping to elucidate the temporal relationship between the aggregation of Aβ and tau *in vivo* [26, 161, 187]. Transgenic mice that overproduce the human Aβ peptide or mutant human tau protein develop senile plaque or neurofibrillary tangle-like pathologies, respectively [58]. When mutant APP and mutant tau transgenes are co-expressed in the same animal, the accumulation of oligomeric Aβ precedes the deposition of intracellular tau aggregates [209]. Additionally, when mutant APP transgenic mice are crossed with human tau transgenic mice, the accumulation of tau pathology is seen at a much earlier time point in the double transgenic animals, yet the temporal course of Aβ deposition is unchanged [27, 95]. Finally, in transgenic mice overexpressing human tau protein, intracerebral injections of aggregated Aβ peptide or

Aβ-rich cortical extract induce the early formation of intracellular tau pathology. A similar effect of aggregated tau on Aβ deposition has not been seen [27, 96]. These *in vivo* data suggest that anomalous Aβ aggregation precedes the abnormal accumulation of intracellular tau protein.

Transgenic mice overexpressing normal human APP do not accumulate Aβ deposits but do exhibit age-related cognitive decline, which has been attributed to potential physiological effects of oligomeric Aβ that is then cleared from the brain before it can aggregate [189]. Intriguingly, when these mice are crossed with tau knockout mice, the cognitive deficits are entirely eliminated, suggesting that tau protein is necessary for detrimental cellular effects of Aβ oligomers [236]. These experiments both provide additional support for the amyloid hypothesis and present a more unified theory of Aβ-induced neurodegeneration that integrates the contribution of the tau protein.

Alzheimer's disease: Therapeutics[2]

There are currently no disease-modifying pharmaceutical treatments available for Alzheimer's dementia. In the 1970's and early 1980's, biochemical and neuropathological evidence emerged implicating the degeneration of basal forebrain cholinergic neurons in Alzheimer's disease (AD) [18]. The *cholinergic hypothesis* of AD held that cholinergic dysfunction causes cognitive decline, and that dementia therefore might be mitigated by augmentation of acetylcholine activity in brain. The logical therapeutic objective was to boost the levels of the transmitter by inhibiting its catabolic

[2] Edited from L.C. Walker and R.F. Rosen (2006). "Alzheimer's therapeutics – what after the cholinesterase inhibitors?" Age Ageing, 35:332-5.

enzyme, acetylcholinesterase. Today, several cholinesterase inhibitors are marketed for the treatment of mild-to-moderate dementia. They have been demonstrated to improve, relative to placebo, various cognitive and functional capacities [250] and there is evidence that they can slow the pathogenesis of AD [108]. Additionally, an inhibitor of ionotropic glutamatergic neurotransmitter receptors (memantine) was approved for use in moderate to severe dementia [144]. However, because multiple neuronal systems are severely damaged in AD, the benefits of agents that selectively target transmitter function are limited, a concern highlighted by the 2005 proposal (and its repercussions) of the British National Institute of Clinical Excellence (NICE) not to recommend donepezil, rivastigmine, galantamine or memantine for the treatment of dementia. While these drugs offer hope, and probably some benefit, to many patients, the improvements are modest and mainly symptomatic, and the drugs cannot halt the progression of dementia.

At present, the most promising approach to treating or preventing AD is based on the hypothesis that the buildup and cytotoxicity of Aβ are central to the disease process. At some point, the cascade includes other pathological processes that characterize AD: tauopathy, inflammation, and neurodegeneration. These later stages of the disease are reasonable targets, but disease prevention, or intervention at a very early stage, is the ideal goal of therapeutics. To halt the Aβ cascade, several strategies suggest themselves: 1) Block the cellular production of Aβ; 2) prevent the self-assembly of Aβ; 3) promote the catabolism of Aβ; 4) stimulate the removal of Aβ; and 5) counteract the cytotoxicity of multimeric Aβ.

R-flurbiprofen (Flurizan^{TM}), the R-enantiomer of the anti-inflammatory agent flurbiprofen, selectively lowers Aβ42 production via allosteric modulation of γ-secretase

activity, preserving the activity of γ-secretase on Notch and other substrates. The agent is well tolerated, and limited efficacy recently was reported in mild AD subjects[300], but the drug failed to improve cognition or daily living in a recent phase III clinical study [212]. Tramiprosate (Alzhemed^{TM}), a sulfated glycosaminoglycan mimetic developed to block the interactions of proteoglycans with amyloid fibrils and thereby impede amyloid aggregation, has been reported to reduce senile plaque load in a mouse model of β-amyloidosis [5]. Yet in phase III clinical trials, the drug failed to demonstrate any long-term effects on cognitive improvement [5, 249]. While theoretically attractive, impeding protein-protein interactions can be difficult pharmacologically [289]. Additionally, it may be necessary to interrupt the Aβ self-assembly process *prior to the formation of small oligomers*, as inhibiting fibril formation conceivably could cause the accumulation of prefibrillar oligomers, and thereby exacerbate cytotoxicity.

Aβ can be broken down by several endopeptidases, notably neprilysin and insulin-degrading enzyme (IDE) [195]. Experimentally increasing the activity of these enzymes in βAPP-transgenic mice reduces brain Aβ levels and senile plaque load [155]. Thus, pharmacological augmentation of Aβ-degrading enzyme activity in the brain is conceivably a promising technique with which to slow the course of AD. In the absence of proven methodologies for safely and selectively achieving this objective (both enzymes are involved in neuropeptide and peptide hormone metabolism) blocking the enzymatic liberation of Aβ (above) is a more attractive approach [195].

An auspicious strategy for halting the AD pathogenic cascade is to promote the elimination of Aβ, either immunologically or by enhancing the transcellular efflux of the peptide from the brain. Active or passive anti-Aβ immunization reduces Aβ load and

improves behavioral performance in βAPP-transgenic mice [92], and active immunization has even shown hints of disease-modifying efficacy in early AD [34]. Unforeseen adverse events, particularly aseptic meningoencephalitis, have hindered the clinical application of Aβ-immunotherapy in AD [211], but the effectiveness of immunization in preclinical models validates the current intensity of research in this arena. Basic and clinical research on Aβ-immunization therapy is proceeding apace, with numerous clinical trials currently underway [205]. However, the increasingly compelling data implicating aberrant Aβ multimerization in the genesis of AD argues for a sustained and diversified effort to abrogate the proteopathic cascade.

Toxic Aβ multimers in AD brain

Aβ is a 38 to 43 amino acid amphiphilic peptide that rapidly self-aggregates into low and high molecular weight oligomers, protofibrils, and the β-sheet rich amyloid fibrils found in senile plaques (Figure 1.7) [158]. In 1984, Aβ was first identified as a major component of senile plaques [86, 174]. Mounting evidence now suggests that the fibrillar form of the peptide is not necessarily highly toxic, and rather represents a mechanism by which cells sequester toxic oligomers into a relatively inert, extracellular mass [40, 43, 151, 297]. This would explain the lack of a strong correlation between senile plaque load and dementia in AD subjects. Aβ aggregation is a nucleation-dependent event, occurring once a critical protein concentration has been reached [105]. The aggregation pathways and their intermediate structures have not been fully elucidated, in part due to the rapid and intractable nature of the aggregation [25]. Further,

it is not clear if all Aβ oligomers are intermediates of the amyloid aggregation pathway, or endpoints of a distinct Aβ aggregation pathway [24, 196]. However, detergent-soluble, low molecular weight Aβ oligomers have been identified in human AD and Aβ-producing transgenic mouse brain, as well as in cell cultures that overexpress the APP protein [40, 43, 148, 157]. In transgenic mouse brain, a 56 kDa species of Aβ oligomers correlates with cognitive decline detected in aged animals [157]. Various species of multimeric Aβ40 and Aβ42 have been synthesized *in vitro* and characterized both in cell culture and in animal models of AD pathology [294]. In William Klein's laboratory at Northwestern, Aβ-derived diffusible ligands (ADDLs) were first isolated from AD (and not normal) human brain, and have since been identified as multimeric Aβ structures containing anywhere from 3 to 48 individual Aβ peptides [259]. Both synthetic and brain-derived ADDLs are toxic to cultured neurons, and cause a decrease in LTP and hippocampal-dependent tasks when administered to rodent subjects [40]. Importantly, these effects are reversed by the infusion of Aβ-specific antibodies [259]. Other labs have confirmed that naturally-occurring oligomeric Aβ is neurotoxic both *in vitro* and *in vivo* and adversely affects rodent performance on memory tasks, confirming the relevance of the experimental effects to the progression of AD dementia [100, 258].

Despite a lack of concordance on the precise structural nature of Aβ oligomers, it is widely accepted that oligomeric Aβ species are detrimental to living cells [23, 100]. Both synthetic and naturally-occurring Aβ oligomers bind to the plasma membrane and neuronal synapses in cell culture, where they are positioned to interfere with intracellular signaling pathways. The full complement of cellular machinery required to produce the Aβ peptide is found in lipid raft fractions of plasma membranes, suggesting that the

peptide can aggregate and then disrupt normal cell function, all proximate to the plasma membrane where it is originally secreted [265, 294]. However, β- and γ-secretase both have acidic pH optima, suggesting that the Aβ peptide is actually produced within the endocytic pathway, rather than at the plasma membrane [282]. One intriguing explanation for Aβ oligomer-induced toxicity is via the formation of amyloid pores. Pre-fibrillar Aβ multimers have increasing amounts of β-sheet structure and naturally form annular β-sheet rich structures that can insert into the plasma membrane and conduct ions between the cytosol and extracellular space. β-amyloid "channels" can form during the treatment with synthetic oligomers but it is not clear if these structures generally occur in AD brain [152, 163, 233]. Alterations in ion homeostasis induced by such anomalous ion channels would have devastating effects on neuronal viability.

There is convincing genetic, biochemical, and pathologic evidence in support of the amyloid cascade hypothesis of AD. However, the neurotoxic effects of Aβ aggregation have thus far only been seen in human brain, despite heavy Aβ amyloid deposition in aged nonhuman primate [287], canine [51], and APP transgenic mouse brain. These naturally occurring (primate and canine) and transgenic (mouse) models of amyloid deposition indicate that the overproduction and accumulation of cerebral Aβ is not always neurotoxic. Rather, the AD brain is unique in its susceptibility to multimeric Aβ-induced neurotoxicity.

Animal Models of Cerebral Aβ Accumulation

In 1996, Karen Hsiao and colleagues published one of the first reports of a transgenic mouse that exhibited copious amounts of age-related plaques containing the human-sequence Aβ peptide [79, 116]. The mouse was genetically engineered to produce the full-length sequence of human APP containing a mutation that was first identified in a Swedish family with early-onset familial AD. The double mutation is located in the extracellular region flanking the Aβ peptide sequence and it enhances the β-secretase cleavage of APP, resulting in an increased production of Aβ40 and Aβ42. By 9 months of age, APPSwe transgenic mice begin to accumulate amyloid plaques in the cortex, hippocampus, and other limbic regions, and plaque deposition increases rapidly with age. Also at 9 months, the mice begin to exhibit deficits in attention and memory-related behavioral tasks. However, no significant neuronal loss has been detected in these mice at any age, despite progressive and substantial age-related Aβ deposition [119].

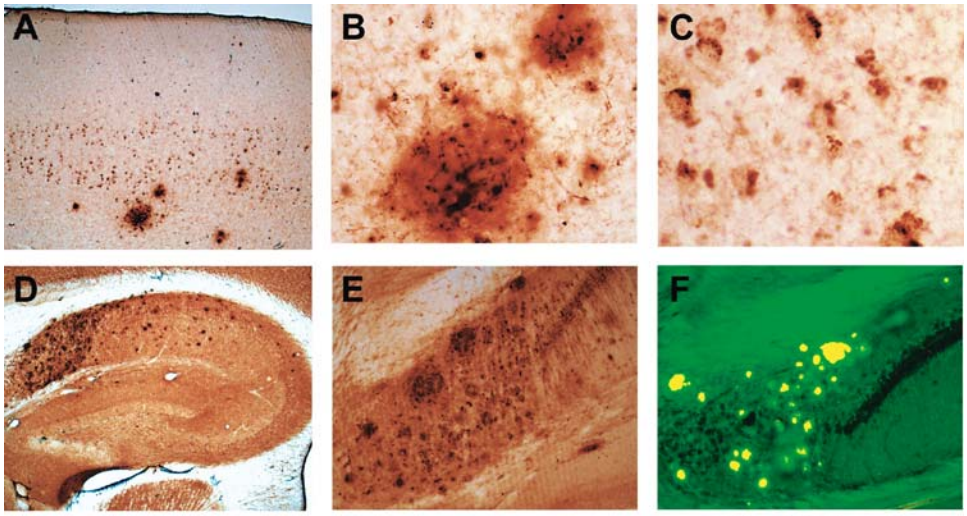

Figure 1.7. Aβ deposition in an 18-month-old triple transgenic mouse expressing human APPSwe, tau P301L, and PSl M146V proteins. Panels A-C: Early Aβ42 depostition in the neocortex, at increasing magnifications. Panels D and E: low and high magnification of Aβ42-immunoreactive deposits in the hippocampus and F: an adjacent section stained with ThioflavinS. Not shown: Aβ and tau immunoreactivity are detected within the same pyramidal neurons. Reprinted from Neurobiology of Aging, 24:8, Oddo S, et al, Amyloid deposition precedes tangle formation in a triple transgenic model of Alzheimer's disease, Copyright (2003), with permission from Elsevier [208].

In the last 13 years, over 70 varieties of Aβ-depositing transgenic mice have been produced and made available to the research community. These animals express either a single transgene for mutant APP, APP in combination with mutant presenilin or mutant tau, or even all 3 transgenes together (Figure 1.7). Each mouse exhibits a unique phenotype of parenchymal and/or vascular amyloid deposition, due in part to the transgene promotor and the nature of the transgene, but also influenced by the background mouse strain. Rodent models of Aβ pathology are valuable research models for the study of *in vivo* protein aggregation and its effects at the cellular, network, and behavioral levels. Many of these animals do exhibit some sort of age-related cognitive deficits [95, 187] as well as regional neuronal loss [39]. Recently developed rat models of cerebral Aβ amyloidosis promise exciting advancements in AD research, as these animals exhibit a broader behavioral repertoire with which to study the cognitive and physical effects of Aβ overproduction and deposition in the CNS [3, 54, 73, 164]. Thus far, however, no single rodent model of cerebral Aβ accumulation or tau pathology convincingly recapitulates the full spectrum of Alzheimer's pathology and dementia.

Nearly all of the transgenic rodent models of AD pathology overexpress disease-relevant, mutant forms of human APP or tau. Yet less than 1% of human AD cases actually involve APP mutations and no tau mutation is known to induce AD. Additionally, the Aβ plaques in AD mouse models often contain rodent Aβ co-aggregated with human Aβ [120, 280]. Rodent Aβ differs from human-sequence Aβ by 3 N-terminal amino acids, and, upon *in vitro* co-incubation, changes the aggregation properties of human-sequence Aβ [305]. The effect of rodent Aβ on the toxicity of

human Aβ multimers has not been characterized, but rodent Aβ alone is not toxic, and does not readily self-aggregate [120].

The Aβ plaques in transgenic mice may develop over a period of one or two years and can even form in under 24 hours [182], while human AD plaques may develop and mature over long periods of time, often several decades. During this plaque maturation period, Aβ accumulates various post-translational modifications (including crosslinking) that affect its solubility and quaternary structure [248]. As such, transgenic mouse plaques are much more readily solubilized than human AD plaques and do not contain the same non-Aβ components found in AD plaques [150]. For these reasons, we need long-lived animal models of naturally-occurring Aβ amyloidosis in order to study the long-term effects of the aggregation and maturation of multimeric Aβ on cortical infrastructure and function.

Cerebral Aβ Deposition in Nonhuman Primates

Nonhuman primates are a biologically relevant, long-lived model of age-related cerebral Aβ amylodiosis. The Aβ sequence is 100% conserved in extant primates, and both amyloidogenic and nonamyloidogenic pathyways of APP processing occur in nonhuman primate cortex [221]. New World Monkeys, Old World Monkeys and apes, our closest living relatives, all accumulate significant levels of cerebral Aβ deposits with age [287]. As in humans, apes, monkeys, and transgenic mice first show signs of Aβ deposition approximately midway through their maximum lifespan [70]. Parenchymal Aβ plaques can be highly similar to those seen in AD brain, including cloudy, diffuse

deposits and compact, senile plaques surrounded by tau- and APP-immunoreactive neurites. Some monkeys also exhibit a unique type of compact, spherical plaque without any neuritic halo [241, 243, 287]. All nonhuman primate parenchymal plaques contain Aβ40 and Aβ42 as well as other post-translationally modified Aβ isoforms that likely accumulate over years of plaque maturation, as seen in human brain [242]. The quantity and morphology of parenchymal Aβ deposits vary widely, both within and between nonhuman primate species. Much more consistent is the deposition of Aβ amyloid in the cerebral vasculature of aged nonhuman primate brain. Aβ40 and Aβ42-immunoreactive material is found in small capillaries as well as large vessels in nearly all aged nonhuman primates (Figure 1.8) [80-82, 130, 137, 222, 241]. Because most studies of cerebral amyloidosis in nonhuman primates are limited to immunohistochemical analyses of Aβ40 and Aβ42 deposits in formalin-fixed cortical tissue, we know little about the biochemical activity or higher-order structure of Aβ multimers in nonhuman primate brain.

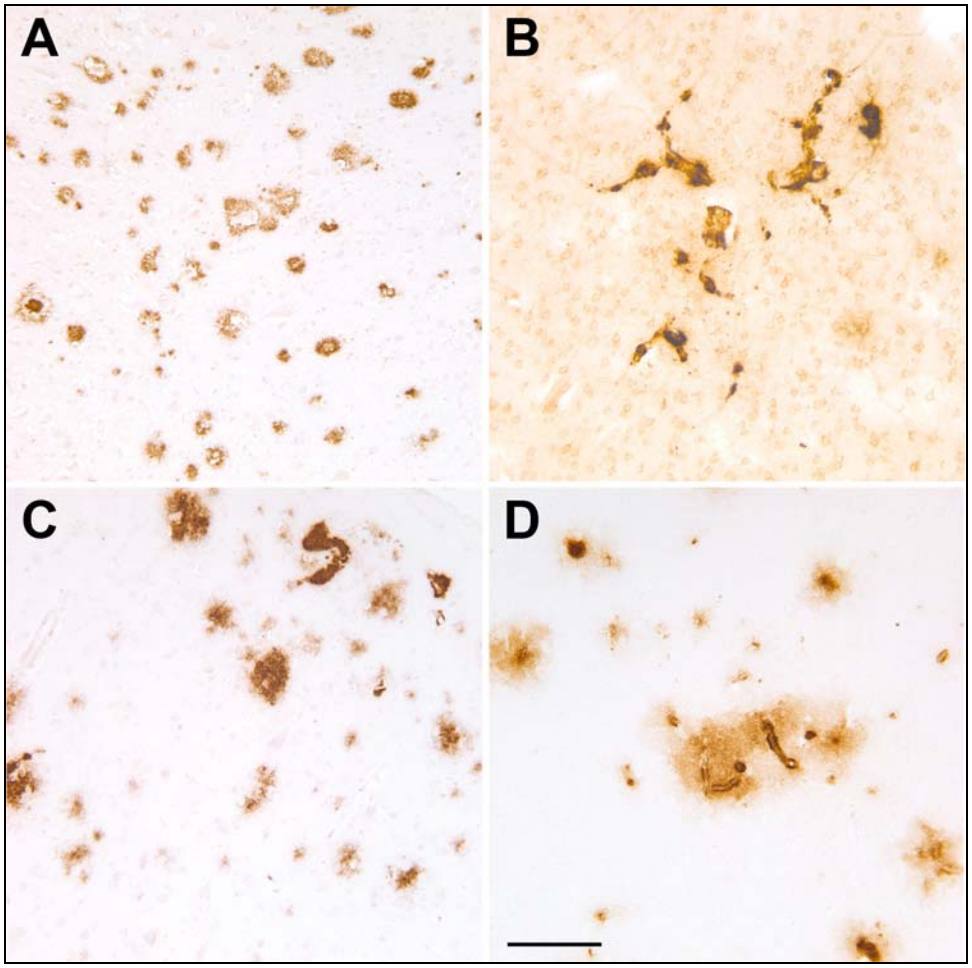

Figure 1.8. Aβ deposition in AD and aged nonhuman primate temporal cortex. Immunohistochemistry with an antibody to Aβ1-x (6E10) reveals heavy amyloid deposition in the cerebral parenchyma and vasculature of AD and aged nonhuman primate subjects. (A) In AD brain, diffuse and cored Aβ plaques are spread throughout the cortex, while cerebral amyloid angiopathy is less common. In chimpanzee (B), rhesus macaque (C), and squirrel monkey (D) temporal cortex, Aβ has a predilection to accumulate in large vessels and capillaries. Diffuse and compact Aβ plaques are also commonly detected in rhesus macaque and squirrel monkey cortex but the plaques tend

to be focal and less widely distributed, except in brains of the oldest animals, which may exhibit AD-like quantities of parenchymal senile plaques. Bar = 100μm.

The tau protein is 100% identical between humans and chimpanzees, and both Old World and New World monkeys express all 6 tau isoforms found in human brain [201, 241]. In AD, the tau protein in neurofibrillary tangles is hyperphosphorylated and forms fibrillar inclusions that impede normal neuronal function and are believed to precede cell death [17, 171]. The tau protein can also be abnormally hyperphosphorylated in aged nonhuman primates, and even aggregates into intracellular inclusions [137, 251], yet nonhumans do not develop AD-like tau pathology and very rarely develop filamentous intraneuronal tau aggregates [241]. Nonhuman primates also do not exhibit the massive neuronal loss or dementia seen in any human neurodegenerative disease. Nonhuman primate brains do contain the molecular mechanisms for AD pathogenesis, and can accumulate insoluble Aβ deposits at comparable levels to that seen in human AD. As such, the comparative study of cerebral Aβ in humans, apes and monkeys is an invaluable paradigm with which to explore how a single protein can be both toxic and benign, depending on the cellular and cortical environment where it is produced and aggregates.

The Evolution of ApoE and Alzheimer's Disease

The strongest genetic risk factor for Alzheimer's disease is the allelic polymorphism in the ApoE gene on chromosome 19 [223]. ApoE, or Apolipoprotein E, is a lipoprotein that can bind to the Aβ peptide and co-aggregates with the peptide in AD senile plaques. The protein is necessary for triglyceride catabolism and may be involved in Aβ proteolysis or clearance, but its precise role in AD pathology has not yet been

determined [168]. The human population contains 3 ApoE alleles: ε2, ε3, and ε4, each of which code for distinct protein isoforms with different lipoprotein binding characteristics. ApoEε3 is the predominant human isoform, while the ApoEε4 allele, present in less than 15% of the population, can increase the risk of developing AD by up to 20 times in homozygotes. In all other primates, there is only one ApoE allele and it is considered homologous to ApoEε4, based on an amino acid transition at codon 112. However, the lipoprotein binding behavior of primate ApoEε4, which would be considered the ancestral form of the protein, is actually more similar to human ApoEε3 – it binds preferentially to high-density lipoproteins [169]. In a recent comparative genomic study of disease-related genes in a broad group of mammalian species used in biomedical research, the ApoE gene was identified as a positively selected gene uniquely in the hominid lineage [279]. The significance of the evolutionary selection for variant ApoE isoforms and its relationship to AD pathogenesis are not yet clear. Some groups hypothesize that the ApoE-Aβ interaction is involved in Aβ clearance, and that differences in ApoE isoforms result in differential abilities of cells to dispose of aggregated Aβ [247]. If this is the case, then the ancestral form of ApoE found in all nonhuman primates might allow for the enhanced clearance of Aβ into the extracellular space, where it can accumulate into relatively benign fibrillar plaques. It is also possible that the ApoE-Aβ interaction affects the folding and aggregation of Aβ multimers, as the structure of aggregated Aβ is a significant determinant of its biochemical activity.

Toxic and Benign Aβ "Strains"

The accumulation of cerebral Aβ deposits is not always associated with frank dementia or neurodegeneration, as seen in nonhuman primate cerebral amyloidosis as well as in the many transgenic rodent models of AD pathology. Aβ can also accumulate in the brains of cognitively normal, aged humans. The existence of structurally and functionally polymorphic Aβ "strains", akin to that seen in the prion diseases, reconciles the amyloid cascade hypothesis of AD with these manifestations of seemingly nonpathogenic Aβ deposition.

The term "strain" was initially used in the microbiology field, and refers to structural and/or functional varieties of a given species. Different bacterial strains retain the essential features of that species, while concomitantly exhibiting strain-specific properties, such as pathogenicity or resistance to antibiotics. A defining characteristic of a strain is its ability to faithfully propagate, both at a structural and a functional level [273]. In prion diseases such as Creutzfield-Jakob and Bovine Spongiform Encephalopathy ("Mad Cow disease"), an abnormally misfolded protein is the sole infectious agent [232]. Investigations into the nature of the infectious protein revealed structural variants of prion proteins that are identical at an amino acid level, but can be characterized by differential susceptibility to experimental conditions such as proteolytic digestion as well as distinct incubation times and pathogenicity [4, 42, 77]. The distinct secondary and quaternary structures of prion "strains" underlie their benign or toxic nature [268]. Upon introduction to the central nervous system, either by ingestion or through a stochastic folding event, the β-sheet-rich, corrupted prion protein recruits and

templates the misfolding of naïve, endogenously produced prion proteins, which then self-aggregate into toxic oligomers (Figure 1.9) [4, 285]. Importantly, sequential passaging of prion-infected cortical tissue between animals confirms that, like bacterial strains, these prion strains retain their structural and functional properties between generations [78, 266, 267].

Aggregated Aβ peptides can also form fibrils that are structurally polymorphic, and molecular polymorphisms (i.e. fibril periodicity and thickness) in both naturally-occurring and synthetic Aβ fibrils have been revealed using both electron microscopy and nuclear magnetic resonance spectroscopy [214, 217]. These polymorphic Aβ fibrils can be propagated with high fidelity using *in vitro* seeding experiments. Soluble Aβ monomers that are added to a solution of fibrillar Aβ will fibrillize, and the molecular structure of the induced, or seeded, fibrils will retain the same structural features as the parent fibrils [215, 216, 277]. Further, structurally polymorphic Aβ fibrils can exhibit differential toxicity in neuronal cell cultures [57, 216]. β-sheet-rich Aβ aggregates can also template the folding and aggregation of monomeric, naïve Aβ *in vivo*, although the nature of the seeded amyloid has not yet been fully characterized [129, 181, 215, 216].

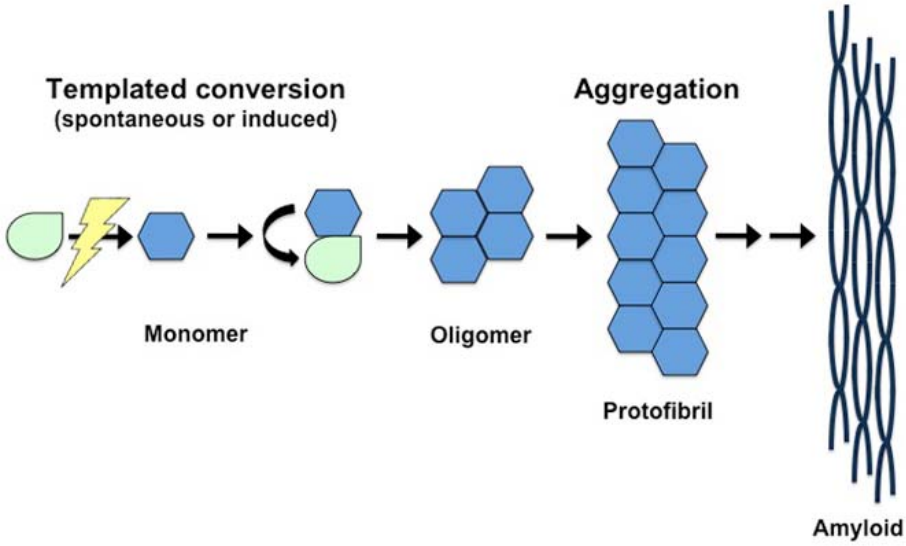

Figure 1.9. Mechanism of aberrant protein misfolding and templating in the cerebral proteopathies. When an anomalously folded peptide is exogenously introduced into the CNS, or is produced by a stochastic cellular event, the peptide subsequently induces the like misfolding of protein monomers by a process of templated conversion. Misfolded proteins have a predilection to self-aggregate into toxic oligomers and larger protofibrils, finally forming β-sheet rich amyloid fibrils. Figure adapted from Trends in Neurosciences, 29 (8), Walker et al, Inducible proteopathies, Copyright (2006), with permission from Elsevier [290].

AD and prion diseases belong to the family of neurodegenerative cerebral proteopathies, or diseases of protein misfolding. The phenomenon of self-propagating protein strains is highly relevant to all cerebral proteopathies, which include Parkinson's disease, frontotemporal dementia, and Huntington's disease [290]. These diseases are characterized by the abnormal cerebral accumulation of α-synuclein, tau, and polyglutamine-rich huntingtin protein, respectively [100]. There is evidence for a common structural motif between prefibrillar aggregates of such disease-causing amyloidogenic proteins, which may underlie a common mechanism of cytotoxicity [133]. Further, *in vitro* experiments with α-synuclein and tau have shown that structural and functional polymorphisms in protein fibrils can be mechanically or chemically induced and that these polymorphisms can be templated, or "seeded", onto unfolded protein monomers [55, 76]. Each of the cerebral proteopathies is initiated by the aggregation of a unique protein within the nucleus, cytoplasm, or extracellular space. The diseases can be further distinguished by region-specific susceptibility to lesion deposition and neurodegeneration. The broad spectrum of lesion phenotypes suggests that there is an important effect of intracellular and extracellular environments on protein folding, misfolding, and clearance.

Conclusions and Hypotheses

In order to reconcile the neurotoxicity of Aβ accumulation in humans but not in nonhuman primates, I hypothesize that cerebral Aβ aggregates are structurally polymorphic between humans and nonhuman primates. I further hypothesize that

aggregated Aβ from AD brain is toxic, while nonhuman primate Aβ multimers are relatively benign. It is important to note that Aβ can also aggregate without initiating a neurotoxic cascade in the brains of cognitively normal humans. However, it is nearly impossible to determine if such cases are truly nondemented "control" humans or simply cases of incipient AD that had not yet reached criteria for clinical diagnosis. The nonhuman primate is therefore an ideal model of normal human brain aging that can be used for the comparative study of healthy and pathologic aging. If aggregated Aβ is uniquely toxic in AD brain, the comparative study of aggregated Aβ from AD and nonhuman brain could reveal species-specific differences in the folding and/or binding partners of the peptide that underlie its cellular effects. Using a top-down approach to the comparative neurobiology of aging in primates, I have identified characteristics of multimeric Aβ that are unique to AD brain and may underlie its toxicity. In an aging cortical environment where neurons have a decreased ability to maintain protein homeostasis, a shift in the secondary folding structure of a peptide can rapidly proliferate and wreak havoc in the brain. The characterization of this toxic structural motif and its permissive environment will provide enticing therapeutic targets for prevention or intervention in Alzheimer's disease and possibly the other cerebral proteopathies.

Chapter 2

Is Alzheimer's a human-specific disease?[3]

Introduction

Chimpanzees and humans diverged from a common ancestor approximately 6 million years ago and the two extant species of chimpanzees (*Pan troglodytes and Pan paniscus*) are our closest living relatives (see Figure 1.2) [260]. In 2005, two years after the human genome was successfully sequenced, the chimpanzee genome was sequenced from a middle-aged male at the Yerkes National Primate Research Center. An early

[3] Article previously published as Rosen, R.F., et al, "Tauopathy with paired helical filaments in an aged chimpanzee." (2008) J Comp Neur, 509:259-270. Substantial revisions have been made to the Introduction.

comparison of the two genomes indicated that the species share over 98% gene-sequence homology [1, 281]. The media response to the "98.5%" touted the striking similarities between the two genomes, with headlines such as Time Magazine's "How We Became Human: Chimps and humans share almost 99% of their DNA. New discoveries reveal how we can be so alike – and yet so different" (October 9, 2006). Given the biological similarities between the two species, scientists can utilize data acquired from great ape research to extrapolate a better understanding of human physiology and nervous system function. However, we now know that the genetic variation is closer to 4% and that, in combination with epigenetic differences, there are quite distinct human and chimpanzee "phenomes", or phenotypic expression of the genome [56, 278, 281]. The study of such trait differences between humans and chimpanzees may eventually lead to the identification of human-specific genes that play important roles in shaping the human phenotype.

One way to determine if a particular phenotype is specific to the hominin lineage (genus *Homo*) is to conduct a comparative trait analysis between humans and chimpanzees, using a more distantly related primate (i.e. Old World or New World monkey) as an "out-group". If the phenotype is unique to human subjects in such a study, the trait likely evolved after the chimpanzee-human divergence [131, 278].

There has not been any report in the scientific literature of age-related neurodegenerative disease or dementia in a chimpanzee or other nonhuman primate animal. A comparative analysis of neurodegenerative disease phenotypes in very old primates would support the idea that humans are unique in their susceptibility to age-

related diseases that are caused by the aggregation and accumulation of aberrantly folded proteins [85].

The tauopathies are a class of human neurodegenerative disorders characterized by the intracellular aggregation of abnormally phosphorylated tau protein and selective neuronal loss [153]. Tau dysfunction likely plays a primary role in disease pathogenesis, as mutations in the MAPT locus are associated with several of these tauopathies [89]. In the mammalian nervous system, tau normally interacts with tubulin to stabilize microtubules and promote their assembly [171]. In the neurodegenerative tauopathies, tau is hyperphosphorylated by intracellular kinases, which impedes the normal binding of the protein to cytoskeletal elements and thereby augments its tendency to polymerize into higher molecular weight assemblies such as neurofibrillary tangles [17, 171]. More than 20 human tauopathies are known, each with a disease-specific clinical presentation and pattern of atypical tau aggregation in neurons and/or glial cells [87, 153, 302].

The most frequently occurring tauopathy is Alzheimer's disease (AD), a dementing disorder in which specific regions of the brain are beset by neurofibrillary tangles as well as deposits of the Aβ peptide in senile plaques in the walls of cerebral blood vessels [61, 102]. The neurofibrillary tangles in AD consist mostly of *paired helical filaments*, twisting ribbons of tau that have a helical half-periodicity of ~80nm and an apparent diameter that alternates between ~8 and 20nm [52]. Although genetic and biochemical evidence indicates that the pathogenic cascade of AD is initiated by aberrant Aβ, particularly the 42-amino acid form (Aβ42) [104], the degree of tau pathology correlates strongly with cognitive decline [9, 53, 84, 301].

Humans are particularly, and perhaps uniquely, susceptible to Alzheimer's disease and other tauopathies [201, 284]. However, amino acid sequence similarities in extant species indicate that both the Aβ-precursor protein (APP) and tau protein are highly conserved evolutionarily. The amino acid sequence of APP695 is >99% identical in humans and chimpanzees [41] and the tau sequence is 100% identical in the two species [115]. Additionally, all six tau isoforms that are found in the human brain also have been identified in nonhuman primates [115, 201].

In the normal course of senescence, many mammalian species exhibit cerebral Aβ-amyloidosis [48, 63, 65, 81-83, 106, 137, 178, 192, 194, 222, 237, 284, 291], and Aβ accumulation in the brains of aged nonhuman primates can sometimes reach levels comparable to those in AD [63](R.F. Rosen, unpublished data). Aggregated tau has been histologically identified in glia and neurons of a number of aged mammals [31, 48, 106, 134, 198-200, 237, 252], but no documented case of nonhuman tau pathology fully recapitulates the degree and localization of intraneuronal tau accumulation seen in the human tauopathies. Furthermore, neuronal tau pathology with AD-like paired helical filaments has never been identified in a nonhuman primate [65, 284].

Here we present the first evidence of tauopathy with human-like paired helical filaments in an aged chimpanzee. We further present genetic, biochemical, and pathologic analyses of cerebral tau and Aβ in the animal, in order to determine whether or not this represents the first case of Alzheimer's disease pathology in a nonhuman animal.

Materials and Methods

Subjects

A 41-year old, socially housed female chimpanzee (*Pan troglodytes*)(CO494) at the Yerkes National Primate Research Center spontaneously developed acute lethargy and rapidly progressive motor dysfunction suggestive of stroke. A T2-weighted magnetic resonance (MR) scan revealed a massive, left-hemispheric lesion involving mainly the temporal, parietal and occipital lobes (Fig. 2.1E-H). At necropsy, gross examination of the brain confirmed a substantial region of ischemic (non-hemorrhagic) necrosis in the left hemisphere. The right hemisphere was grossly normal. The total brain weight was 287.5 grams, less than the average weight of an adult chimpanzee brain (348.8 grams) [111], possibly due to necrosis in the left hemisphere. The previous medical history was unremarkable except for a chronic systolic heart murmur first diagnosed at 15 years of age, moderate obesity (weight at death 61.5 kg) and high serum cholesterol (total cholesterol levels in 1995, 2000 and 2005 were 262, 244 and 359mg/dl, respectively). A T1-weighted MR scan performed in 1995 showed no obvious abnormalities of the brain (Fig. 1A).

For comparison, age-related Aβ and tau lesions were examined in available archival neocortical and/or hippocampal tissue samples from eight additional chimpanzees aged 30 to 59 years (Table 2.1). Furthermore, as a reference group for the MAPT genotyping, frozen cerebella from 7 chimpanzees were selected from the Yerkes archives for tau gene sequence analysis. All studies were conducted in accordance with federal and local guidelines for the humane care and use of animals.

Collection and Preparation of Cerebral Tissue Samples

Fresh, unfixed tissue blocks (~500 mg) were excised from the right (non-infarcted) superior temporal cortex for analysis by enzyme-linked immunosorbance assay (ELISA). Unfixed tissue samples for ELISA also were taken from the superior temporal cortex of 5 end-stage AD cases for comparison (Table 2.2). The brain then was coronally slabbed at ~2cm thickness and immersion-fixed in 10% neutral-buffered formalin for at least 7 days. A set of bilateral, matched tissue blocks from the prefrontal, temporal, and occipital cortices (avoiding the infarct core), as well as samples from the diencephalon, globus pallidus, putamen, lower brainstem and cerebellum, were sectioned at 50μm thickness on a vibratome and stored at 4°C in phosphate-buffered saline (PBS) prior to immunostaining. Additional fixed brain samples from the right temporal lobe were cryoprotected in 30% sucrose, frozen, and cut at 50μm thickness on a freezing-sliding microtome. Frozen sections from the eight reference chimpanzees were sectioned and stored similarly, and all frozen sections were maintained in an antifreeze solution (30% sucrose/30% ethylene glycol in PBS) at -20°C until immunostaining. Separate, bilateral tissue blocks from the prefrontal, temporal and occipital lobes of chimpanzee CO494 were paraffin-embedded, sectioned at 8μm thickness, and mounted onto silanized slides (Newcomer Supply, Middleton, WI) for silver- and immuno-staining, as well as for additional histopathological stains (below).

Antibodies and Reagents

The following antibodies were used for immunohistochemistry: **AT8** (1:5000) mouse IgG1 monoclonal antibody from Pierce Biotechnology (Rockford, IL), Cat#MN1020, in PBS, raised against partially purified human PHF-tau, has an epitope in the region around phosphoserine 202/phosphothreonine 205 and does not cross-react with normal tau [90]; **CP13** (1:10,000) mouse IgG1 monoclonal antibody, a generous gift from Dr. Peter Davies (Albert Einstein College of Medicine, Bronx, NY), was produced from mice immunized with PHF-tau purified from Alzheimer brain tissue by the method described in detail in Jicha et al. (1999). The antibody was selected for reactivity with the phosphopeptide GYSSPG(phosphoS**)**PGTPGSRS, where the phosphoS is phosphoserine 202 of tau. No reactivity with any other phosphoserine of tau was detected (Jicha et al., 1999); **PHF1** (1:10,000) mouse IgG1 monoclonal antibody, also from Dr. Davies, was raised against detergent-extracted PHF preparations, and has been epitope-mapped to the region around phosphoserine 396/404 [97, 213]. Specificity was confirmed with Western blots of transfected cell lysates (Otvos et al., 1994); **MC1** (1:10,000) mouse IgG1 monoclonal, also from Dr. Davies, was raised against Alz50-immunopurified PHFs and then epitope-mapped to similar conformation-specific regions as Alz50, but not FAC1 [122] (in the same study, western blot and dot blot showed specificity of MC1 to PHFs of tau protein); **6E10** (1:5000) mouse IgG1 monoclonal antibody from Covance (Princeton, NJ), Cat# SIG-39320, Protein G-purified, in PBS, was raised against residues 1-16 of Aβ peptide, with an epitope at residues 3-8 [136]; **4G8** (1:5000) mouse IgG2b monoclonal antibody from Covance, Cat# SIG-39220, Protein G-purified, in PBS, was raised against residues 17-24 of Aβ peptide, with an epitope at residues 18-22 [136]. The specificity of

both 6E10 and 4G8 antibodies was characterized in the source reference. Rabbit polyclonal antibodies **R361** and **R398** (both at 1:15,000), a generous gift from Dr. Pankaj Mehta (Institute for Basic Research on Developmental Disabilities, Staten Island, NY), were raised against synthetic Aβ32-40 and Aβ33-42 (AnaSpec, San Jose, CA), respectively, conjugated to keyhole limpet hemocyanin in PBS. Specificity of these antibodies was examined by sandwich ELISA and Western blot analysis [227]. All antibodies to phosphorylated tau and Aβ were tested immunohistochemically with human AD tissue sections and specifically stained only abnormal tau accumulations and parenchymal and vascular amyloid deposits, respectively. **Anti-ubiquitin** (1:10000) rabbit polyclonal antibody from Dako (Carpinteria, CA), Cat#Z-0458, was raised against ubiquitin isolated from cow erythrocytes and conjugated to chicken gamma globulins with glutaraldehyde, purified by solid-phase absorption with human plasma proteins (in western blotting, the antibody labels bands corresponding to free ubiquitin and ubiquitin conjugates); **anti-GFAP** (1:5000) purified immunoglobulin fraction of rabbit antiserum from Dako (Carpinteria, CA), Cat# Z0334, was raised against glial fibrillary acidic protein isolated from cow spinal cord, purified by solid-phase absorption with human and cow serum proteins (it shows no cross reactivity with human plasma or cow serum by crossed immunoelectrophoresis and indirect ELISA). Immunohistochemistry with the antibody revealed the expected pattern of astrocytic staining in human AD and chimpanzee tissue sections. **Anti-Iba1** (1:10000) rabbit polyclonal antibody from Wako (Osaka, Japan), Cat# 019-19741, in TBS, purified by affinity antigen chromatography from rabbit antisera, was raised against a synthetic peptide (PTGPPAKKAISELP) corresponding to the C-terminus of Iba1, a 17-kDa EF hand protein that is specifically

expressed in macrophages/ microglia and is upregulated during the activation of these cells. Specificity was confirmed by Western Blot (Imai et al, 1996) and immunohistochemistry with the antibody revealed the expected pattern of microglial staining in human AD and chimpanzee tissue sections**. Anti-α-synuclein** (1:300) rabbit polyclonal antibody, a gift of Dr. Bernardino Ghetti (Indiana University, Indianapolis, Indiana), was raised against a peptide containing residues 119-137 (DPDNEAYEMPSEEGYODYE) of the C-terminus of α-synuclein (Piccardo et al, 1998). Specificity was confirmed by specific immunolabeling of Lewy bodies in Parkinson's disease. Vectastain Elite kits (Vector Laboratories, Burlingame, CA) were used for ABC-based immunodetection of antigen-antibody complexes.

Histochemistry

Endogenous peroxidase in tissue sections was inactivated with 3% H_2O_2 in methanol, and nonspecific reagent binding was blocked with 2% normal serum in 0.2% Tween, each for one hour at room temperature. For Aβ-immunodetection, sections were pretreated for 10 minutes in 90% formic acid to expose antigenic sites. Sections were incubated in primary antibody (diluted in buffer with blocking serum) overnight at 4°C. After rinsing, sections were incubated for one hour at room temperature in biotinylated secondary antibody, rinsed, immersed for 30 minutes in avidin-biotin complex, and then developed with diaminobenzidine (DAB) or DAB complexed to nickel (Vector Laboratories). Tissue from human AD cases was used as positive control material, and non-immune mouse IgG or rabbit sera were used in place of the primary antibodies as

negative controls. In some instances, a light hematoxylin counterstain was applied after immunostaining.

Double immunostaining was employed to localize multiple antigens in tissue sections. For fluorescence immunostaining, sections were blocked in 2% normal goat serum / 0.1% Triton X-100 in PBS for one hour at room temperature, incubated in a mouse monoclonal antibody (diluted in 2% normal goat serum) overnight at 4°C, rinsed well, and then incubated for 90 minutes in Cy2-conjugated anti-mouse secondary antibody (1:200; Jackson Labs, West Grove, PA). Sections were again rinsed thoroughly, incubated overnight in diluted rabbit polyclonal antibody at 4°C, rinsed, and placed for 90 minutes in Rhodamine-Red-X goat anti-rabbit secondary antibody (1:200; Jackson). To block endogenous autofluorescence, double-stained sections were mounted on gel-coated slides, rinsed for 5 minutes in 70% ethanol and immersed in 1% Sudan black (in 70% ethanol, filtered before each use) for 30 minutes at room temperature. Excess Sudan black was removed via 3 rinses in ethanol, and sections were coverslipped from PBS with Faramount aqueous mounting medium (Dako) for fluorescence microscopy. To visualize multiple antigens in the same sections by standard transillumination light microscopy, antibodies were applied as described above for single antigen/DAB immunohistochemistry, except that the first antibody-antigen complex was marked with DAB+nickel (black), and the subsequent antibody was marked with DAB only (brown).

Finally, we stained selected sections with the Congo Red, Bielschowsky and Campbell-Gallyas stains for AD-type lesions, with the Prussian Blue (Perls) stain for iron, with hematoxylin and eosin, and with a Gram stain (there was no evidence of bacterial infection in any brain region). Light-microscopic photomicrographs were taken

with a Leica DMLB microscope (Wetzlar, Germany) and SPOT XPlorer and FLEX digital cameras (Diagnostic Instruments, Sterling Heights, MI). Confocal images were captured with a Zeiss LSM 510 laser scanning confocal microscope. All images were edited in Photoshop (Adobe) without any further manipulations.

Quantitative Mapping of Tau and Aβ Lesions

Tau lesions (intrasomatic neurofibrillary tangles and plaque-like clusters of immunoreactive neurites) and Aβ lesions (cerebral Aβ-amyloid angiopathy [CAA] and parenchymal [senile] Aβ plaques) were mapped and quantitated bilaterally in matched CP13-, R361- and R398-immunostained sections from the prefrontal, temporal, and occipital cortices using the Neurolucida image analysis system (MBF Biosciences, Williston, VT). The prefrontal cortical sections were taken at the level of the rostral end of the middle frontal gyrus (Bailey & Bonin FE/FD; Brodmann area 10/9/46) [15, 33]; temporal cortical sections taken at the level anterior to the primary auditory cortex (A1) (TA/TE, Brodmann area 20/21/22); and the occipital cortical sections were from a level between the lunate sulcus and the occipital pole, containing both area V1 and extrastriate cortex (OB/OC; Brodmann area 18/17).

A single researcher used the Neurolucida system to count every tau or Aβ lesion found in each section. Every discrete cell soma or cluster of tau-immunoreactive elements was counted as a single lesion. Two morphologically distinct types of tau plaques were identified and counted: neuritic and punctate. Similarly, each distinct Aβ-plaque or Aβ-reactive vascular profile was indicated on the tissue map. R361- and R398-positive vessels that were spatially continuous within the section were counted as a single

lesion; otherwise, discrete vascular profiles were counted separately. The numeric densities of immunoreactive lesions were calculated from the total planar area of each section [63]. Lesion densities in the two hemispheres were compared statistically using paired *t*-tests, with a set limit of $p < 0.05$ for significance. Neuropil threads (tau-positive processes that were not organized into plaques) were profuse and widely distributed in brain (see Fig. 2.2) and were not quantitated histologically.

Electron Microscopy

For ultrastructural analysis, tissue samples from the left prefrontal cortex were postfixed in 4% paraformaldehyde and 0.5% glutaraldehyde, washed in phosphate buffer (0.1M, pH 7.4) and immersed in osmium tetroxide (1% in phosphate buffer) for 20 minutes. They were then rinsed in phosphate buffer and dehydrated in a graded series of ethanol and propylene oxide. Uranyl acetate (1%) was added to the 70% ethanol (35 minute immersion) to improve contrast in the electron microscope. The sections were then embedded in epoxy resin (Durcupan ACM; Fluka, Ft. Washington, PA) on microscope slides and heated for 48 hours at 60°C. Areas of interest were selected, excised from the slide and glued onto resin blocks. Ultrathin sections were cut with a Leica Ultracut T2 (Nussloch, Germany), collected onto single-slot copper grids, and stained with lead citrate.

For immunogold EM, non-postfixed sections were preincubated in PBS containing 5% nonfat dry milk and then washed in Tris-buffered saline (TBS)-gelatin buffer (0.02 M Tris, 0.15 M NaCl, 1 µl/ml fish gelatin, pH 7.6) to block nonspecific sites. Sections were then incubated for 48 hours at 4°C in CP13 antibody (1:10,000)

diluted in PBS-BSA, rinsed in TBS-gelatin, and incubated for 2 hours at room temperature in gold-conjugated goat anti-mouse Fab' fragments (dilution 1:100; Nanogold [Nanoprobes Inc., Yaphank, NY]). Gold particles (1.4 nm) were silver-enhanced with the HQ Silver kit (Nanoprobes). As a control for the specificity of immunolabeling, omission of the primary antibody from incubation solutions completely abolished immunostaining for the corresponding antigens. The tissue was then embedded and cut as described above.

All thin sections were examined with a Zeiss EM10-C electron microscope (Oberkochen, Germany) and digital images were captured using the Dual View camera (Gatan Inc., Pleasanton, CA).

Aβ ELISA

Unfixed, right temporal cortical tissue was Dounce-homogenized in 5 volumes of homogenization buffer (50mM Tris-HCl, 150mM NaCl, and protease inhibitor tablets [Santa Cruz Biochemicals, Santa Cruz, CA]) and then centrifuged at 100,000g for 60 minutes at 4°C to generate the "soluble" supernatant. The pellet was probe-sonicated in 70% formic acid and centrifuged at 14,000rpm for 60 minutes at 4°C to generate the "insoluble" supernatant. Aβ40 and Aβ42 were measured in each extract by ELISA (The Genetics Company, Schlieren, Switzerland) according to the manufacturer's instructions. Soluble extracts were diluted in sample buffer at a 1:50 dilution, and insoluble extracts were neutralized in 1.0M Tris base, pH 11 (1:20 dilution) and diluted in sample buffer to a 1:1000 total dilution. All samples were run in duplicate. Plates were read at 450 nm

and the average optical density values for each extract were interpolated on a 4-parameter standard curve to determine Aβ concentrations.

DNA Extraction and MAPT Genotyping

Genomic DNA from unfixed liver of the 41-year old subject (and, as a reference group, from unfixed cerebellar tissue from 7 additional chimpanzees) was purified using large-scale, automated template purification systems employing solid-phase reversible immobilization (Agencourt Bioscience Corporation, Beverly, MA). The purified DNA samples were then sequenced using ABI dye-terminator chemistry. All subsequent steps were based on sequencing by automated DNA sequencing methods. The ABI dye terminator sequence reads were run on ABI 3700/3730 (Applied Biosystems) machines and the data were transferred to Linux machines. Base calls and quality scores were determined using the program PHRED [66, 67].

Tables

Table 2.1. Supplemental chimpanzees examined for Aβ and tau pathology (archival material).

Subject	Sex	Age (years)
N00-39Pt	f	30
N00-40Pt	m	34
N00-34Pt	m	37
N01-20Pt	f	41
Y06-147Pt	m	43
Y07-25Pt	f	44
Y06-108Pt	f	47
C-612	f	56

Table 2.2. AD cases examined by Aβ ELISA.

Subject	Sex	Age (years)	PMI (hours)
OS02-159	m	61	5.5
OS03-300	f	75	12
OS02-106	f	81	2
E04-172	f	87	6
OS01-128	f	91	2.5

PMI: postmortem interval

Table 2.3. Quantitative mapping data of intrasomatic neurofibrillary tangles and tau plaque-like clusters of immunoreactive neurites in location-matched tissue blocks from the bilateral prefrontal, temporal, and occipital cortices of chimpanzee CO494. Lesion densities are expressed as number of lesions per unit area of tissue analyzed. Antibody CP13.

Region	# N-Plaque	# P-Plaque	# Cell Bodies	N-Plaque density (#/mm²)	# P-Plaque density (#/mm²)	Cell Body Density (#/mm²)
LFC	158	79	349	0.6132	0.3066	1.3546
LOC	5	8	22	0.0182	0.0291	0.0802
LTC	22	43	138	0.0672	0.1314	0.4215
RFC	39	46	81	0.1246	0.1469	0.2587
ROC	0	0	0	0.0000	0.0000	0.0000
RTC	1	20	25	0.0072	0.1436	0.1795

L: left; R: right; FC: prefrontal cortex; OC: occipital cortex; TC: temporal cortex; N-plaque: tau neuritic plaque; P-Plaque: tau punctate plaque

Table 2.4. Quantitative mapping data of Aβ parenchymal plaques and CAA in location-matched tissue blocks from the bilateral prefrontal, temporal, and occipital cortices of chimpanzee CO494. Lesion densities are expressed as number of lesions per unit area of tissue analyzed Antibodies R361 and R398 to Aβ40 and Aβ42, respectively.

Region	Total Aβ40-CAA	Total Aβ42-CAA	Total Aβ40-Plaques	Total Aβ42-Plaques	Aβ40-CAA density (#/mm²)	Aβ42-CAA density (#/mm²)	Aβ40-Plaque density (#/mm²)	Aβ42-Plaque density (#/mm²)
LFC	162	298	2	0	0.5512	1.0147	0.0068	0.0000
LOC	45	78	0	0	0.1723	0.2957	0.0000	0.0000
LTC	67	112	12	10	0.2505	0.3329	0.0449	0.0297
RFC	358	666	57	26	1.2227	2.1810	0.1947	0.0851
ROC	289	966	3	0	0.9947	3.1774	0.0103	0.0000
RTC	118	284	43	50	0.8592	2.0315	0.3131	0.3577

L: left: R: right; FC: prefrontal cortex; OC: occipital cortex; TC: temporal cortex

Figures

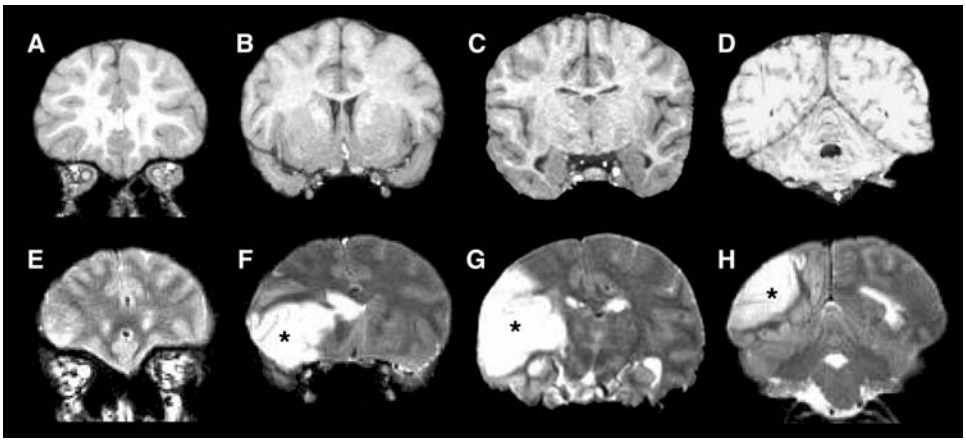

Figure 2.1. MR images of the chimpanzee brain before and during the stroke. **A-D** An Anterior-posterior series of coronal, T1-weighted MR images made 10 years prior to death. **E-H:** T2-weighted MR images captured after the symptoms had emerged, with the location of affected tissue in the left hemisphere indicated by asterisks. (A T2-weighted scan was not run prior to the stroke.)

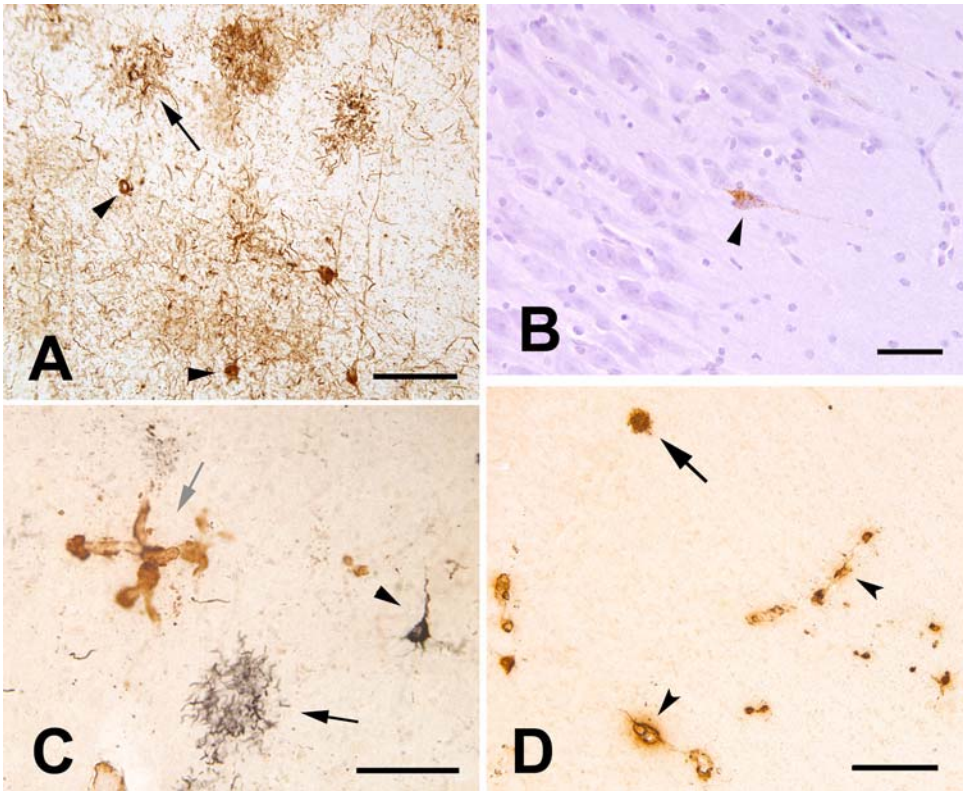

Figure 2.2. Tau- and Aβ-pathology in the aged chimpanzee. A: Tau-immunoreactive somata (2 indicated by arrowheads) and neuritic tau plaques (1 indicated by arrow) in the left prefrontal cortex. Numerous tau-immunoreactive processes (threads) occupy the intervening neuropil. Antibody AT8. B: Tau-immunoreactive neuron (arrowhead) in area CA1 of the right hippocampus; note the integrity of the nearby pyramidal cells. Antibody AT8, Hematoxylin counterstain. C: Double-immunostained section showing tau- (CP13/Nickel-DAB, black, developed first) and Aβ- (R398/DAB, brown) immunoreactivity in the left prefrontal cortex. A tau plaque (black arrow) and a tau-positive pyramidal neuron (arrowhead) are present. A focus of Aβ-immunoreactive CAA is indicated by the grey arrow. Note the absence of an Aβ-core in the tau plaques, which was typical of focal accumulations of tau neurites in this animal. D: Cerebral amyloid angiopathy (arrowheads denote two blood vessels) and a senile

plaque (arrow) in the right temporal neocortex. Antibody 6E10. Bars = 100 μm (A, C), 50 μm (B), 200 μm (D).

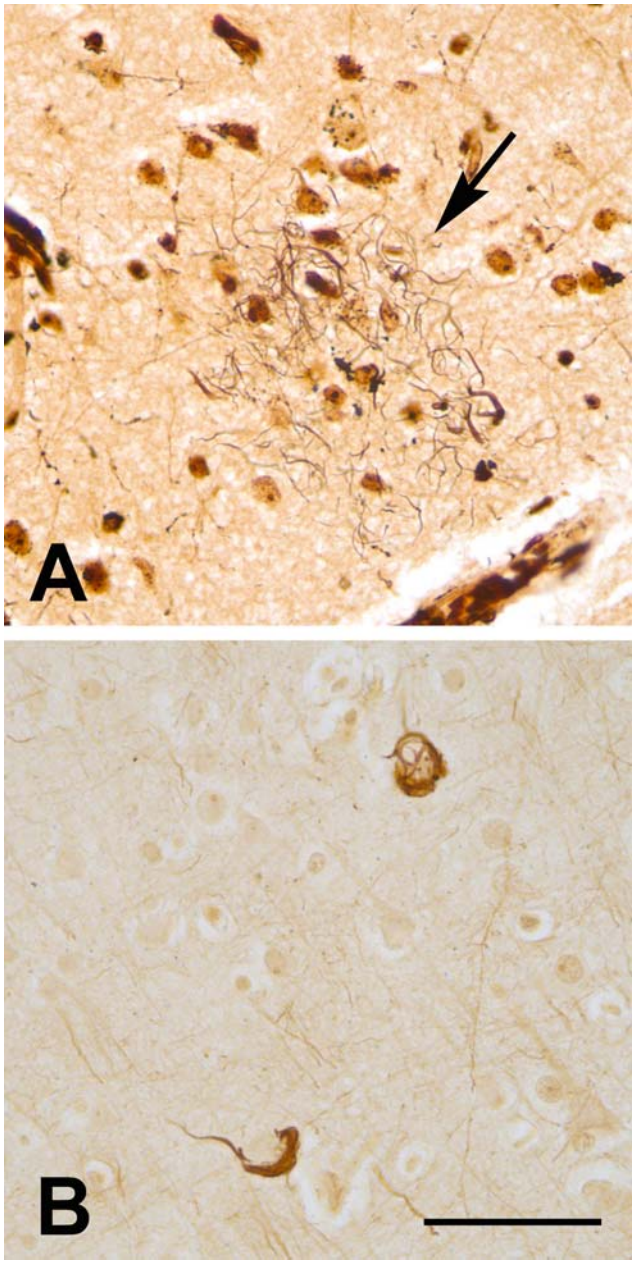

Figure 2.3. Silver-stained lesions in the left prefrontal neocortex of the aged chimpanzee. A: Campbell-Gallyas-stained neuritic plaque (tortuous black neurites, arrow). This plaque was positive with the anti-tau antibody CP-13 in an adjacent section (not shown). B: Two cortical cells stained with the Bielschowsky silver method. Bar = 50 μm for both A and B.

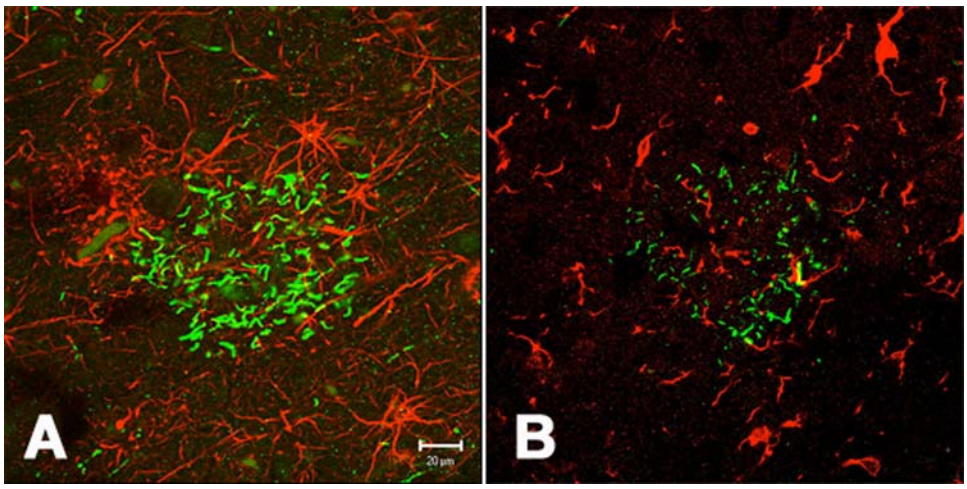

Figure 2.4. Double-fluorescence immunostaining of tau-neurites and reactive glia in the left prefrontal cortex of the aged chimpanzee. By confocal microscopy, CP13-positive neurites (green) in tau plaques do not colocalize with GFAP-stained astrocytes (magenta) (A), nor do they colocalize with Iba1-immunoreactive microglia (magenta) (B). Neuropil threads also are negative for these glial markers. Bar = 20 μm for A and B.

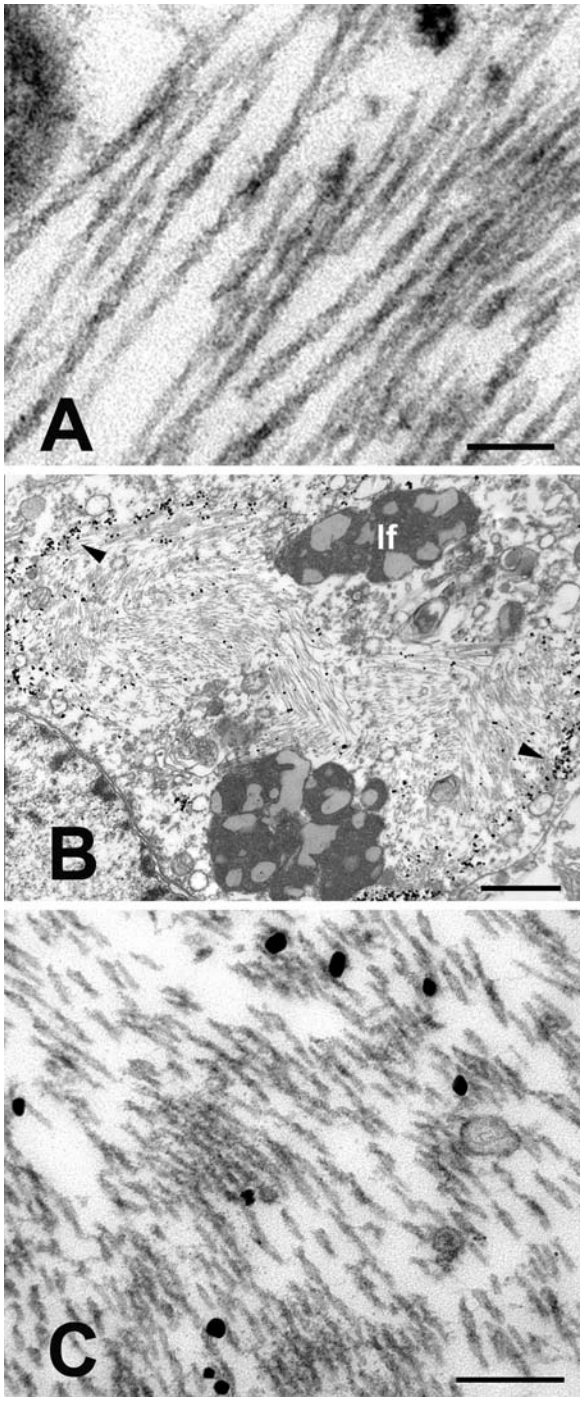

Figure 2.5. Ultrastructure of paired helical filaments in neurons from the left prefrontal cortex of the aged chimpanzee. A: High magnification view of intraneuronal paired helical filaments. The twisting, filamentous ribbons have a mean half-periodicity of ~79nm, a maximum width of ~20nm and a minimum width of ~10nm. B-C:

CP13/immunogold-labeled, intraneuronal paired helical filaments. B is a low magnification view of a CP13-immunoreactive neuron; the nucleus is to the lower left. Because the thick section was immunostained prior to sectioning, the immunogold preferentially decorates the periphery of the mass of PHFs (arrowheads). Note the heavy bundles of paired helical filaments in the cytoplasm. C shows a higher magnification view of CP13/immunogold-labeled PHFs from the cell in B. lf: lipofuscin. Bars = 100nm (A), 1μm (B) and 200nm (C).

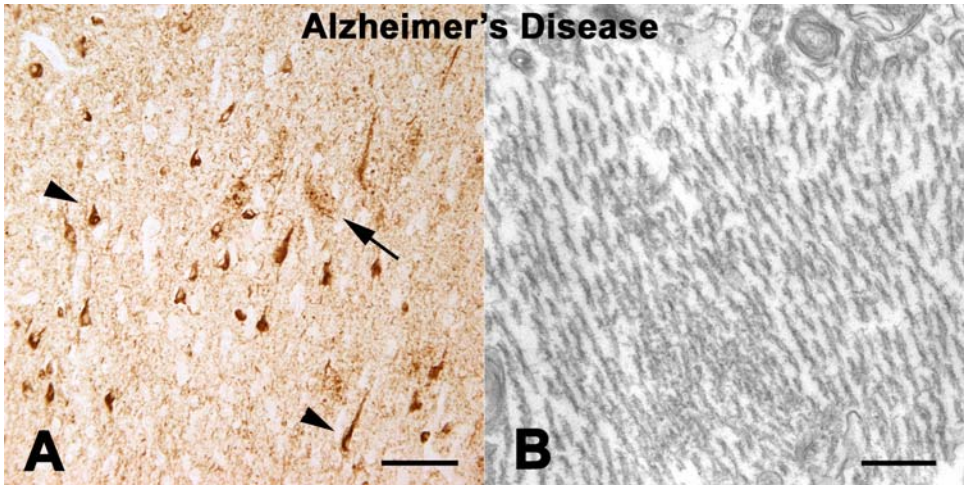

Figure 2.6. Tauopathy in a human with Alzheimer's disease. **A**: Light micrograph showing tau-immunoreactive neurons (two indicated by arrowheads) and clusters of neurites (one indicated by arrow) in Alzheimer's disease; antibody AT8. **B**: Electron micrograph of intraneuronal paired helical filaments in Alzheimer's disease. The size and helical periodicity of the filaments are highly similar to those in chimpanzee CO494 (Figure 2.5). Bars = 100um (A) and 200nm (B).

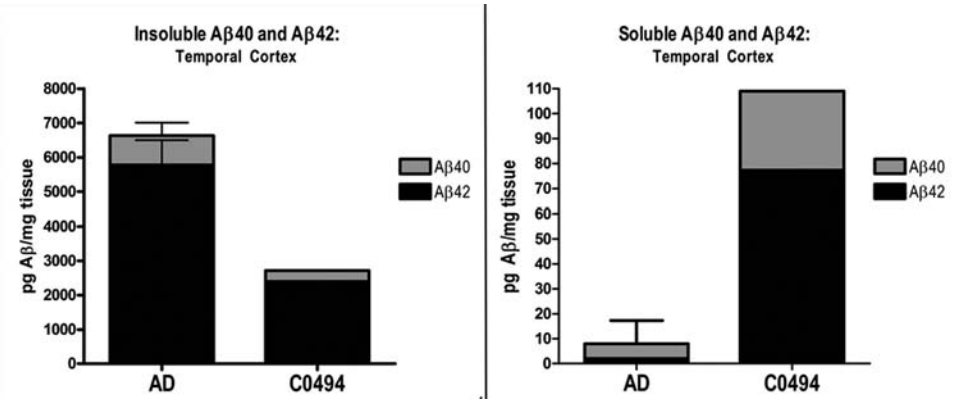

Figure 2.7. Aβ levels in the right temporal neocortex of the chimpanzee (CO494), relative to the levels in a comparison group of 5 confirmed AD patients, measured by ELISA. **A**: Insoluble Aβ40 (gray, top) and Aβ42 (black, bottom) levels. **B**: Soluble Aβ40 and Aβ42 levels. Note the different scales on the y axes for insoluble and soluble Aβ. Bars = standard deviations for the AD group.

Results

Tau Histopathology

Postmortem immunohistochemical analysis using antibodies to pathologic forms of tau revealed abnormal intracellular tau immunoreactivity in multiple cortical regions of both hemispheres and, to a lesser extent, in subcortical structures. Throughout the neocortex (the most severely affected brain structure), the lesions included tau-laden neurons, neuropil threads, and diverse, plaque-like clusters of neurites ('tau plaques') (Fig. 2.2A-C). The regional density of tau lesions varied among and within cortical areas, and there were foci of particularly intense pathology (Fig. 2.2A). The lesions were most abundant in the prefrontal cortical samples, followed by the temporal cortex and the occipital cortex, which had the least tauopathy of the neocortical regions examined (Table 2.3). In the hippocampus, occasional tau-positive neurons (Fig. 2.2B), neuropil threads and tau plaques were present, but these were much less numerous than in most regions of neocortex. The tau plaques generally were not associated with a core of aggregated Aβ (Fig 2.2C). Subcortically, tau immunoreactivity, mostly in thread-like processes, was present to varying degrees in the globus pallidus, neostriatum and diencephalon, and occasionally in white matter pathways. Scattered immunoreactive profiles also were present in the lower brainstem and, very infrequently, in the cerebellum. Overall, subcortical tauopathy was sparse relative to that in neocortex.

In nearby frontal, temporal, and occipital cortical sections, antibodies AT8 and CP13 consistently detected the most tau lesions. Antibody PHF1 detected somewhat fewer lesions, and antibody MC1, which recognizes AD-type conformational epitopes on

tau, detected the fewest tangles, tau plaques, and neuropil threads of the four anti-tau antibodies. A subset of neurons, plaque neurites and neuropil threads were immunoreactive for ubiquitin (not shown). Neuritic plaques and neurofibrillary tangles also were evident by Campbell-Gallyas and Bielschowsky silver stains (Fig. 2.3). Granulovacuolar degeneration was not seen. The presence of tau-only plaques in this animal prompted us to determine whether the tau-neurites might originate from astrocytes, as in the case of 'astrocytic plaques' in corticobasal degeneration (CBD) [145]. Double-immunostaining for GFAP and CP13 in left and right frontal cortex showed that the neurites are not astrocytic processes (Fig. 2.4A). The neurites also were negative for the microglial marker Iba-1 (Fig. 2.4B) and α-synuclein (not shown).

Ultrastructurally, the neurofibrillary tangles consisted of dense, intraneuronal bundles of paired helical filaments that were identical in size and helical periodicity to those in humans with Alzheimer's disease [52, 179] (Fig. 2.5, Fig. 2.6B). Immunogold labeling with antibody CP13 confirmed the presence of phospho-tau epitopes on the paired helical filaments (Fig. 2.5B,C).

Aβ Histopathology

Immunohistochemistry with antibodies to Aβ disclosed a moderate degree of CAA (Figs. 2.2C, D) in all of the neocortical regions examined, as well as mild, focal Aβ-plaque pathology (Fig. 2.2D) (Table 2.4). As in humans, Aβ deposits were sparse in the hippocampus compared to temporal neocortex, and were essentially absent in the basal ganglia, diencephalon, and lower brainstem. The cerebellum manifested very mild CAA. In affected regions, most Aβ-immunopositive senile plaques were diffuse in

nature, as confirmed by a paucity of Congo Red staining/birefringence in parenchymal deposits. The number of Aβ42-positive plaques did not differ significantly from the number of Aβ40-positive plaques, but CAA was marginally more likely to be immunoreactive for Aβ42 than for Aβ40 (t=2.560; p= .0506). Surprisingly, the degree of total CAA was significantly greater in the right, non-stroke hemisphere than in the left hemisphere (t=4.668; p=.043) (Table 2.4).

Aβ ELISA

Insoluble Aβ40 and Aβ42 levels in a sample of temporal neocortex from the non-infarcted hemisphere were lower than in the 5 reference AD brains when assessed by ELISA. Soluble Aβ levels, however, were higher in the chimpanzee than in the AD cases (Fig. 2.7).

MAPT Genotyping

Sequence analysis of genomic DNA revealed no mutations of functional significance at the tau locus (including saitohin, a polymorphic gene nested within the MAPT locus). Two synonymous base pair changes in exons 7 and 9 were identified, while all other polymorphisms were located in noncoding regions at distances from the nearest splicing sites ranging from 40 to 145 base pairs. One unusual, 4-base pair deletion was identified in intron 3 only in this chimpanzee, but this deletion was deemed unlikely to be of pathogenic significance because it lies 67 base pairs from the nearest predicted splicing site.

Discussion

This is the first report of cerebral tauopathy with paired helical filaments in an aged chimpanzee. The tau lesions included neurofibrillary tangles, neuropil threads, and neuritic tau plaques. The neurofibrillary tangles consisted of paired helical filaments that were indistinguishable from those occurring in humans with Alzheimer's disease (Fig. 2.2, Fig. 2.5, Fig. 2.6) [52, 179]. This aged chimpanzee also exhibited a species-typical profile of cerebral β-amyloid angiopathy and infrequent Aβ-immunoreactive senile plaques [80, 81].

The impetus for human-like tau pathology in this chimpanzee is uncertain. Any influence on the expression or splicing of tau, whether environmental or genetic, could alter the probability of developing tauopathy [103]. Several mutations in the tau gene are associated with human primary tauopathies [89, 153]. However, sequencing of the exons and associated introns in the genomic *MAPT* locus of this subject disclosed no known tauopathy-associated mutations, nor any other genetic changes of obvious functional significance. The two extended MAPT haplotypes that occur in human populations (H1 and H2) are thought to differentially influence the probability of developing neurofibrillary tangles [103]. The tau haplotype in chimpanzees, however, is a mixture of the human H1 and H2 haplotypes [46, 115, 220], and at present it is unclear whether this gene structure affects the likelihood that chimpanzees will manifest tau lesions. While genetic or epigenetic changes might yet be discovered that regulate the pathogenicity of tau, our analysis shows that this animal did not harbor a sequence modification in the tau gene that would be expected to precipitate a human-like tauopathy.

Old age is the most important risk factor for AD and other neurodegenerative diseases in humans [132], and age probably contributed to the emergence of tau pathology in this chimpanzee. The documented maximum lifespan of *Pan troglodytes* is 59 years [111]. Chimpanzees in their 40's and 50's have been shown previously to exhibit cerebral Aβ-amyloidosis, primarily in the form of CAA [49, 50, 65, 80, 81, 284], but significant intraneuronal tau pathology has not been documented previously in chimpanzees [49, 80, 81, 284]. Although it is not unusual to encounter occasional tau-immunoreactive neurons and processes in older animals, immunohistochemical examination of archival, postmortem tissue samples from eight additional chimpanzees ranging from 30 to 59 years of age revealed little abnormal tau immunoreactivity (R.F. Rosen, unpublished). Thus, while age probably played a role in the ontogeny of tauopathy in this 41-year old animal, the paucity of tau lesions in other chimpanzees of similar or greater age suggests that additional factors are involved.

Tau pathology also could be related to conditions that engendered the ischemic stroke, which appears to be a rare occurrence in nonhuman primates [29, 72]. The chimpanzee in this study had high levels of cholesterol throughout her adult life, and hypercholesterolemia has been implicated as a risk factor both for stroke and tauopathy [210]. Furthermore, the ischemic lesion itself may have directly initiated AD-like tau pathology in this chimpanzee. In humans, epidemiological evidence suggests a relationship between cerebral ischemia and dementia, and nearly one-third of AD patients exhibit postmortem evidence of cerebral infarct [127]. Experimental evidence for a relationship between ischemia and tau pathology is ambiguous, however. Total tau has been found to increase in CSF after stroke in humans, although phospho-tau in brain

appears not to be elevated [112]. In rats, tau is rapidly hyperphosphorylated, via a cdk5-associated mechanism, in neurons at the site of experimental ischemia [298]. However, the hyperphosphorylation occurs only in neurons in the infarcted region, and paired helical filaments and neuritic tau-plaques were not observed. Tauopathy in the chimpanzee in this investigation was advanced and widespread in both hemispheres, and was not increased in the infarcted region proper, or in the adjacent neocortex, suggesting that the lesions probably were present prior to the acute ischemic incident. Although the Perls iron stain did not reveal evidence of prior microinfarcts in the tissue sections that we sampled, the possibility that clinically silent microinfarcts may have precipitated tau pathology in the years before the chimpanzee's death cannot be eliminated.

The amyloid cascade hypothesis implicates the multimerization of Aβ as the critical upstream effector in the pathogenic process that ultimately results in the generation of neurofibrillary tangles in AD [104]. *In vivo* and *in vitro* evidence indicates that aberrantly folded Aβ can induce tau hyperphosphorylation and polymerization in neurons [26, 94]. The Aβ42:Aβ40 ratio, in particular, has been hypothesized to govern the risk of developing AD [135, 176], and soluble Aβ oligomers are increasingly thought to play a crucial role [40, 294]. ELISA of (non-stroke) temporal neocortex from this chimpanzee revealed a relatively high ratio of Aβ42:Aβ40, similar to that in humans with AD. Furthermore, levels of buffer-soluble Aβ (low molecular weight monomers and oligomers) in the temporal cortex were well above the mean levels of soluble Aβ in AD (Fig. 2.7). This Aβ profile, co-present with neurofibrillary tangles, therefore suggests the possibility that excess soluble cerebral Aβ42 may have contributed to the emergence of tauopathy. The soluble Aβ quantities in this animal should be interpreted with caution,

however, as the Aβ-precursor protein can be upregulated by the conditions associated with brain injury [234], including stroke [224].

In summary, we report an unprecedented case of tauopathy with intraneuronal paired helical filaments, neuropil threads and neuritic tau plaques in an aged chimpanzee. The subject also exhibited a moderate degree of cerebral Aβ deposition, mainly in the brain vasculature. Despite tantalizing similarities, there are also important pathologic differences between this chimpanzee and humans with AD, notably in the rarity of neurofibrillary tangles in the hippocampus, the presence of unusual, tau-only neuritic plaques lacking β-amyloid cores, and the paucity of parenchymal Aβ- (senile) plaques. However, the occurrence of both tau- and Aβ-pathology indicates that the cellular and molecular machinery for generating two key hallmarks of AD – neurofibrillary tangles and Aβ-amyloidosis – is fully present in aged chimpanzees. In addition to providing evidence for biological similarities between humans and chimpanzees even late in the lifespan, these findings compel us to reconsider the assumption that humans are the only primates to manifest Alzheimer-like tauopathy with age.

Supplementary Figures

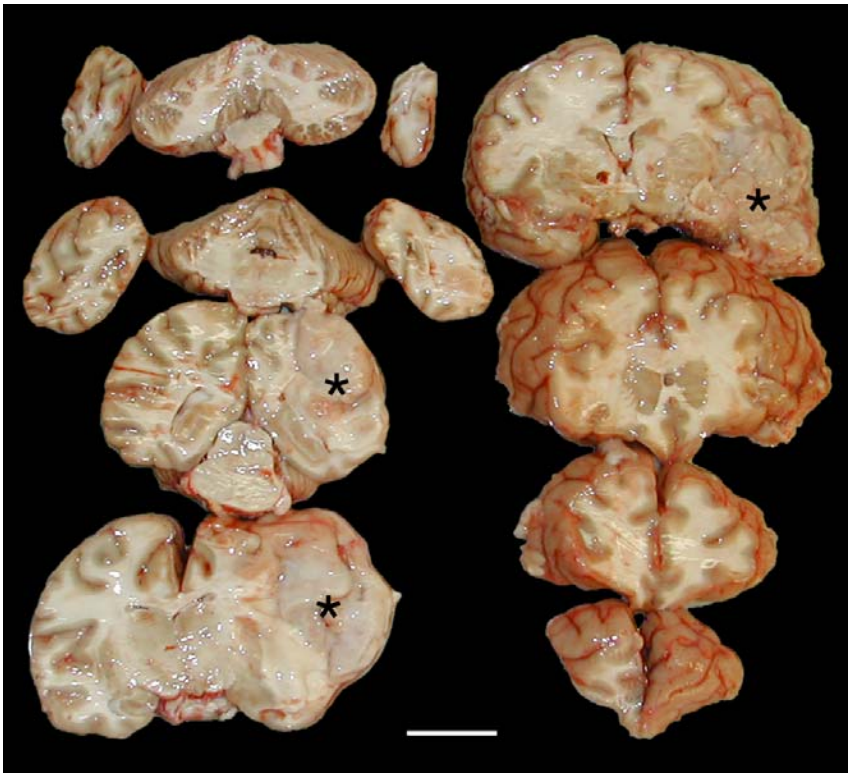

Figure S2.1. Gross photos of brain slabs from chimpanzee CO494 at necropsy. The brain was blocked into ~2cm coronal slabs and photographed with the anterior face up; the left hemisphere is to the right. Regions of ischemic necrosis are indicated with asterisks (compare to Figure 2.1, which is reversed relative to these blocks). Bar = 2.54 cm.

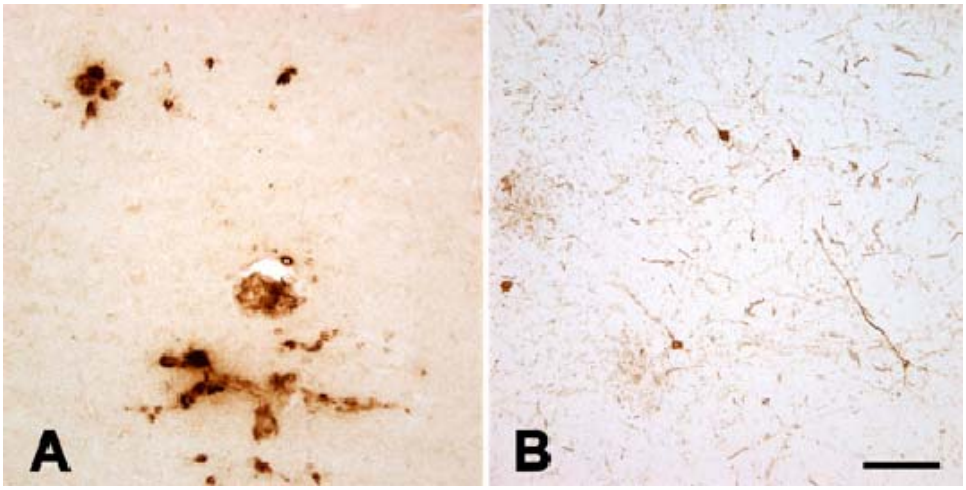

Figure S2.2. Supplementary images of Aβ- and tau-pathology in chimpanzee CO494. **A**: Cerebral β-amyloid angiopathy in the left temporal neocortex; Antibody, 6E10. **B**: Tau-immunoreactive somata and a neuritic tau plaques in the right prefrontal cortex. Note also the profusion of neuropil threads; Antibody AT8. Bars = 100μm for A and B.

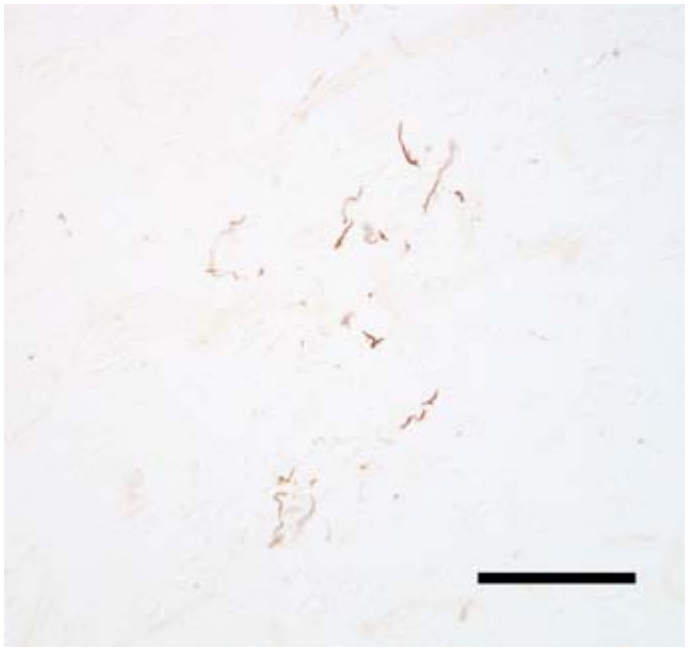

Figure S2.3. Phospho-tau-immunoreactive processes in the temporal neocortex of another 41 year old female chimpanzee (NO1-20Pt). Occasional tau-immunoreactive processes and/or cells sometimes can be found in older chimpanzees and other primates, particularly using antibodies to phosphotau 202/205, but in the chimpanzee samples that we examined, such lesions were generally infrequent and focal compared to CO494. Antibody AT8. Bar = 100μm.

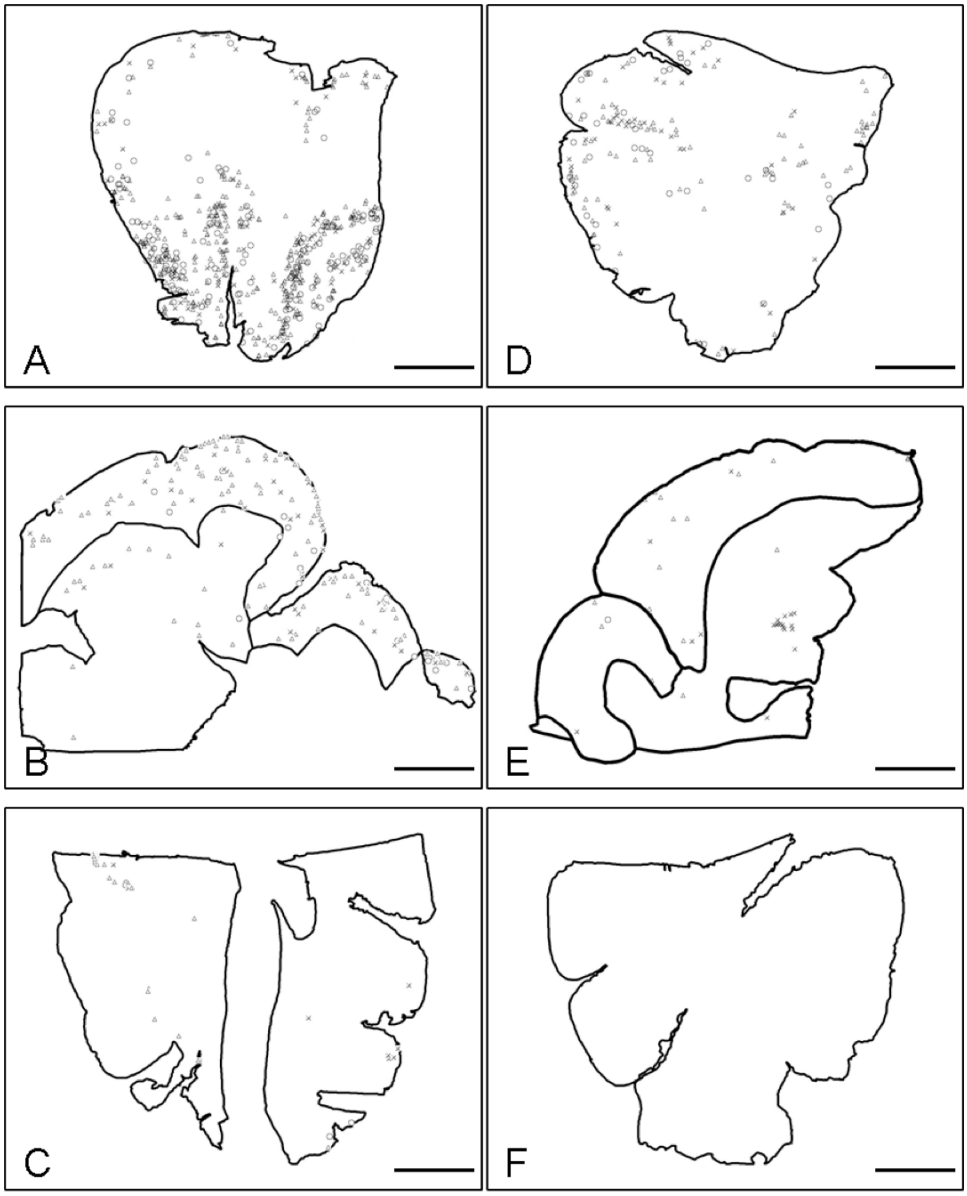

Figure S2.4. Point counting maps of tau-immunoreactive lesions in three brain areas of chimpanzee CO494. Low magnification, computer-assisted diagrams of tau-immunoreactive lesions point-counted throughout entire tissue sections (created with Neurolucida image analysis software, MBF Biosciences). Sections taken from left prefrontal (A), temporal (B), and occipital (C) and right prefrontal (D), temporal (E), and occipital cortices (F); Legend: ○ - neuritic tau plaque; x – punctate tau plaque; Δ – immunoreactive cell body; SFG – superior frontal gyrus; MFG – medial frontal gyrus;

ITG – inferior temporal gyrus; PH – parahippocampal cortex; M – medial; L – lateral; D – dorsal. Antibody CP13. Although there was a trend toward more lesions in the left hemisphere, the overall number of tau lesions did not differ significantly between hemispheres.

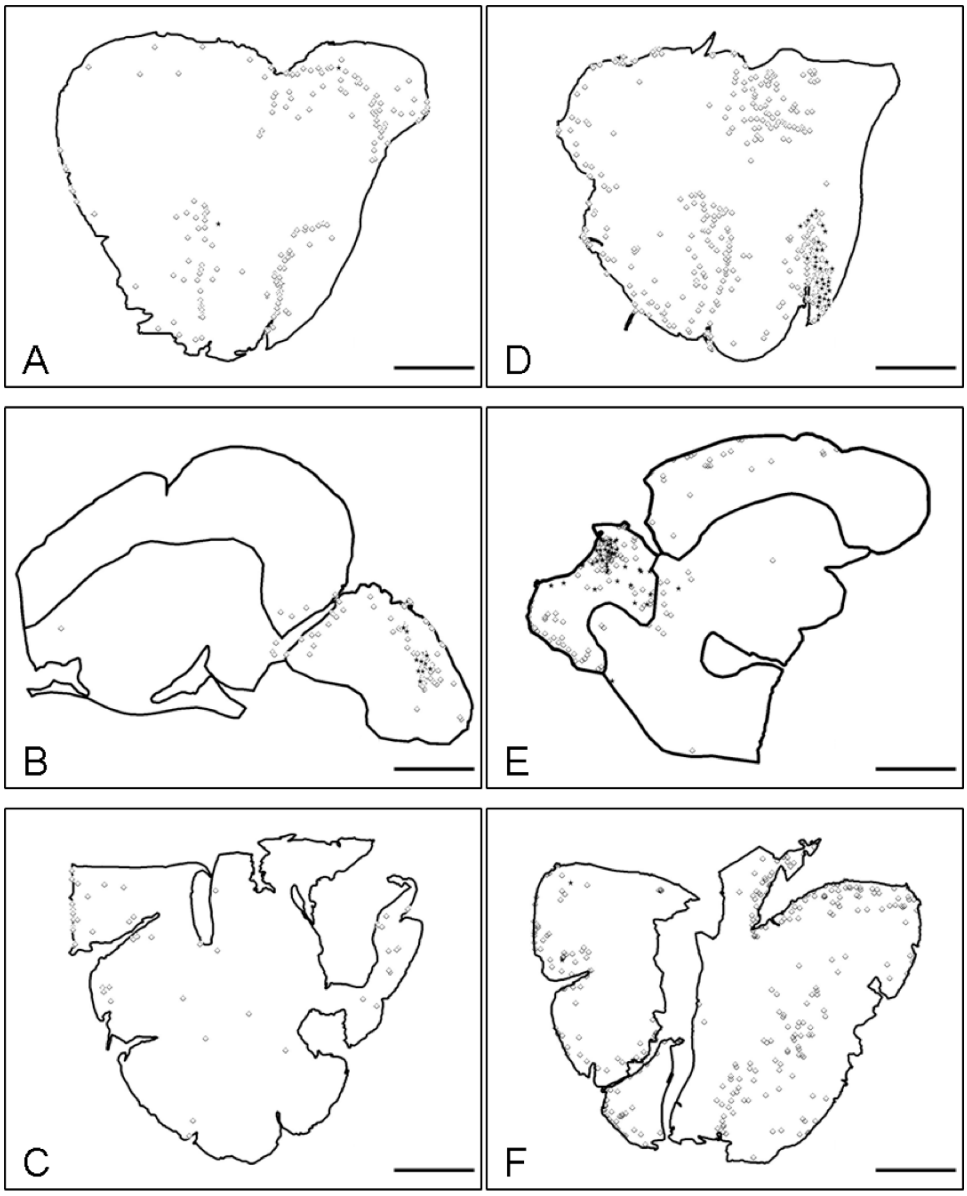

Figure S2.5. Point counting maps of Aβ40-immunoreactive lesions in three brain areas of chimpanzee CO494. Low magnification, computer-assisted diagrams of Aβ40-immunoreactive lesions point-counted throughout entire tissue sections (created with Neurolucida image analysis software, MBF Biosciences). Sections taken from left prefrontal (A), temporal (B), and occipital (C) and right prefrontal (D), temporal (E), and occipital cortices (F); Legend: ◊ - cerebral amyloid angiopathy; * - parenchymal plaque; SFG – superior frontal gyrus; MFG – medial frontal gyrus; ITG – inferior temporal

gyrus; PH – parahippocampal cortex; M – medial; L – lateral; D – dorsal. Antibody R361. There were significantly more CAA profiles in the right hemisphere than in the left ($t=11.052$, $p=0.008$).

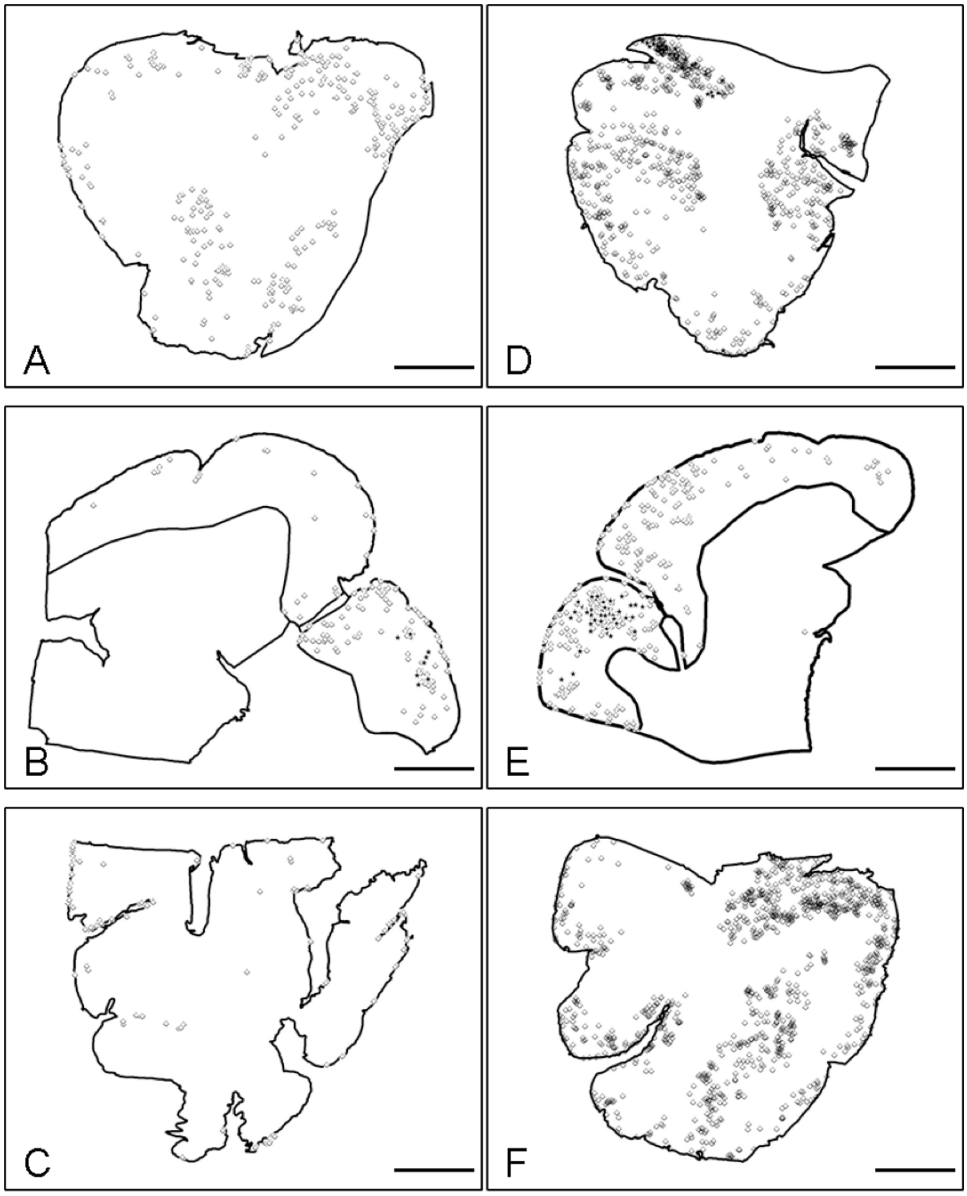

Figure S2.6. Point counting maps of Aβ42-immunoreactive lesions in three brain areas of chimpanzee CO494. Low magnification, computer-assisted diagrams of Aβ42-immunoreactive lesions point-counted throughout entire tissue sections (created with Neurolucida image analysis software, MBF Biosciences). Sections from left prefrontal (A), temporal (B), and occipital (C) and right prefrontal (D), temporal (E), and occipital cortices (F); Legend: ◊ - cerebral amyloid angiopathy; * - parenchymal plaque, SFG – superior frontal gyrus; MFG – medial frontal gyrus; ITG – inferior temporal gyrus; PH –

parahippocampal cortex; M – medial; L – lateral; D – dorsal. Antibody R398. There were marginally more CAA profiles in the right hemisphere than in the left (t=3.779, p=0.063).

Chapter 3

Characterization of Aβ peptide populations in aged human and nonhuman primate brain

Introduction

The Alzheimer's disease (AD) brain is characterized by copious deposition of intracellular neurofibrillary tangles and extracellular senile plaques [253]. Neurofibrillary tangles, which are composed of abnormally hyperphosphorylated and aggregated tau protein, interfere with normal cytoskeletal function, presumably leading to neuronal death [91]. Senile plaques in the AD brain are β-sheet rich amyloid deposits

composed of aggregated β-amyloid (Aβ) peptides. The temporal and regional patterns of neurofibrillary tangle deposition are highly stereotyped in AD brain, and correlate with the progressive development of cognitive decline [32]. However, genetic, pathologic, and biochemical evidence strongly supports the amyloid cascade hypothesis of AD, which implicates the overproduction and aggregation of the Aβ peptide as the primary, upstream events in the AD neurodegenerative cascade [104]. All known genetic mutations that underlie early-onset, familial AD result in an increased production of cerebral Aβ or an enhanced ability of the peptide to aggregate in the brain [21]. Aβ is an amphiphilic peptide that rapidly self-aggregates, and mounting evidence indicates that soluble oligomeric forms of the Aβ peptide, rather than senile plaques, are the likely culprits in AD synaptotoxicity and neurotoxicity [23, 40].

Aβ is an extracellular cleavage product of the sequential proteolytic processing of the APP transmembrane protein by β-secretase and then the γ-secretase enzyme complex [272]. The predominant cerebral Aβ isoforms are 40 and 42 amino acids in length, but β- and γ-secretases are not sequence-specific proteases; additional Aβ isoforms of various lengths are produced, and the ratio of these Aβ isoforms may play a crucial role in the peptide's toxicity. β-secretase cleavage also occurs in front of glutamate amino acid residues 3 and 11 (where 1 and 42 are the first and last amino acid residues in full-length Aβ42), after which the free N-terminal glutamate can cyclize chemically or can be cyclized by glutaminyl cyclase, forming a pyroglutamate residue. N-truncated, cyclized Aβ 3pyrE-x and 11pyrE-x isoforms have a higher tendency to aggregate than Aβ1-40 and Aβ1-42, are more resistant to proteolysis, and are less soluble as a result of enhanced hydrophobicity. Aβ can also be altered at its C-terminus, with the most common

isoforms ending at the 38th and 43rd amino acids [149, 185, 239]. The C-terminal residues contribute to the physical oligomerization properties of the peptide, and may therefore underlie the peptide's toxicity [24]. Both full-length Aβ and truncated Aβ are also subject to post-translational modifications, including N-terminal truncation by endopeptidases, isomerization and racemization of aspartate residues (1 and 7), and methionine oxidation (35), all of which enhance the peptide's resistance to proteolytic degradation. As plaques mature over periods of years (and sometimes decades) in the AD brain, Aβ peptides within the plaques undergo enzyme-induced post-translational modifications [149, 248]. However, modified Aβ peptides have been identified in both soluble cortical extracts *and* within amyloid deposits, suggesting that Aβ polymerization is a dynamic process, and that dissociating senile plaques in AD may be a source of soluble, oligomeric Aβ peptides [150, 248, 269].

Aβ plaque morphology is strikingly heterogeneous in the AD brain, ranging from amorphous, diffuse deposits to highly structured, cored senile plaques. While Aβ isoform composition does not entirely determine plaque morphology, Aβ42 predominates in diffuse-type Aβ lesions and cored senile plaques are composed of varying combinations of full-length and modified Aβ peptides [270]. The broad morphological spectrum of plaque morphology may be attributable to the existence of "strains" of folded peptides, akin to those seen with the prion protein. In the prion diseases, a single prion protein folds into structurally and functionally diverse strains. Molecular polymorphisms dictate the prion strain's toxicity, and these structural and bioactive characteristics can then be transmitted to unfolded proteins via a templated protein folding mechanism [4].

Like the prionoses, Alzheimer's disease belongs to the cerebral proteopathy family of diseases, which are characterized by aberrant protein aggregation and, frequently, cerebral amyloid deposition [288]. As in AD, soluble protein oligomers are implicated in the pathogenesis, region-specific neurodegeneration, and dementia of other cerebral proteopathies, which include Parkinson's disease and Huntington's disease [100]. In each of the cerebral proteopathies, the disease-relevant aggregates are composed of entirely different proteins. However, conformation-specific antibodies to protein oligomers exhibit striking pan-immunoreactivity to oligomeric proteins from several different diseases, suggesting a common structural motif among disease-causing protein aggregates. This common structure suggests a shared mechanism of protein toxicity [85]. Aβ oligomers, which have been studied most extensively, bind specifically to the plasma membrane at neuronal synapses, and also have been shown to form annular structures that can insert into the membrane, forming anomalous ion channels [57, 152].

We use animal models of cerebral Aβ amyloidosis in order to study the *in vivo* formation of Aβ aggregates and the mechanisms of Aβ-induced synaptotoxicity and neurotoxicity. Aβ-producing transgenic mouse models of AD overexpress mutant APP protein and accumulate cortical, hippocampal, and vascular Aβ amyloid deposits in an age-related fashion. However, no mouse model fully recapitulates the pathological and behavioral spectrum of AD [187]. In contrast to the extensive plaque maturation period in the human brain, Aβ plaques in the transgenic mouse brain are relatively dynamic and have a paucity of post-translationally modified Aβ isoforms [128, 148, 150]. Human-sequence Aβ plaques can form (and disappear) in a matter of 24 hours in the mouse brain [182]. Additionally, rodent Aβ, which differs from human Aβ by 3 amino acids, is

produced in nearly all APP transgenic mouse models and is found to co-aggregate within a subset of plaque deposits in these mice [280]. Rodent Aβ alone is benign and does not tend to self-aggregate, but it alters the folding dynamics and biological activity of human-sequence Aβ when the two synthetic peptides are co-incubated [305]. For these reasons, we need a longer-lived, more biologically relevant animal model of cerebral Aβ amyloidosis with which to study Aβ aggregation dynamics and potential long-term toxic effects of cerebral Aβ deposition.

The Aβ peptide sequence has been 100% conserved throughout primate evolution, and nonhuman primates, our closest living relatives, accumulate significant cerebral Aβ deposition with age [221]. Aβ deposition in aged nonhuman primates closely recapitulates the temporal and regional accumulation of diffuse and compact parenchymal plaques and congophilic vascular amyloid in the human AD brain. Additionally, cerebral Aβ lesions in aged nonhuman primates mature over many years, and are subject to similar post-translational modifications as the Aβ in AD. Both Aβ40 and Aβ42 are detected in plaques and vessels in aged ape and monkey brains, although Aβ40 is reported to be the predominant deposited isoform in immunohistochemical studies (epitope availability and antibody penetration are variable in such studies, and may result in the underestimation of the contribution of certain peptide isoforms to brain lesions) [63, 81, 192, 231]. The nonhuman primate brain exhibits additional AD-relevant cortical changes with age, such as the overexpression of tau protein, tau protein kinases, and Apolipoprotein E at nerve endings [137]. However, nonhuman primates do not develop the full pathological spectrum of AD lesions, nor do they suffer from AD-like dementia [241]. Rather, nonhuman primates are a unique model of age-related cerebral

Aβ amyloidosis in the absence of neurodegeneration or dementia. Our closest living primate relatives can be utilized for the comparative study of healthy and pathological brain aging, in order to clarify the nature of toxic protein aggregation unique to the human brain.

Aβ peptides also accumulate with age in the brains of cognitively normal humans, without apparent neurodegeneration or dementia [6]. In nondemented aged humans, Aβ aggregates into soluble oligomeric species, but the peptide isoform composition of these oligomers may be different from soluble Aβ oligomers in the AD brain [148]. In one study, the predominant peptides identified in soluble extracts from nondemented and AD human brains were Aβ42, Aβpyr3-42, and Aβpyr11-42, but the two groups differed in the relative contribution of Aβpyr3-42 to total soluble Aβ populations, with the AD brain containing over 50% Aβpyr3-42. Synthetic Aβ42/Aβpyr3-42/Aβpyr11-42 peptide preparations with AD-like ratios of the three peptides exhibited enhanced toxicity relative to nondemented human-like peptide preparations, indicating that the component *ratio* of full-length and modified Aβ peptides may underlie the peptide's toxicity unique to AD brain [218]. These data help to reconcile the Aβ amyloid hypothesis with pathological findings of benign cerebral Aβ deposition in nondemented humans and nonhuman primates. However, the use of a nondemented human control group introduces an important confound: it is nearly impossible to determine if the amyloid-laden brain from a nondemented human subject is truly "normal" and not actually a case of preclinical AD. The nonhuman primate model of benign cerebral amyloidosis circumvents this issue.

We hypothesize that there is an AD-specific population of full-length and modified Aβ isoforms that underlies the peptide's unique toxicity in the AD brain, and

that these peptides can be experimentally distinguished from the benign Aβ that deposits in the brains of nondemented aged nonhuman primates. There has not yet been a comprehensive biochemical analysis of the contribution of truncated and post-translationally modified Aβ to cerebral amyloidosis in the brains of both apes and monkeys. In this study, we used immunohistochemistry, ELISA, MALDI-TOF mass spectrometry, and immunoblotting to characterize total Aβ peptide populations in human and nonhuman primate subjects. Fixed and unfixed temporal and occipital cortical tissue was collected from the brains of a large cohort of aged chimpanzees (apes), rhesus macaques (Old World monkeys), and squirrel monkeys (New World monkeys), in addition to end-stage AD and "nondemented human" cases. While we were unable to identify an AD-unique population of Aβ peptides, our immunoblotting data suggest that Aβ oligomers in AD and aged nonhuman primate brain may be structurally distinct, akin to the protein strains seen in prion diseases. Further structural analysis of Aβ aggregates in AD and nonhuman primate brain might help to clarify a structural motif that underlies the unique toxicity of Aβ in the AD brain.

Methods

Subjects

We analyzed postmortem brain tissue from 9 rhesus monkeys (*Macaca mulatta*) (3 females, 6 males), 6 squirrel monkeys (*Saimiri sciureus*) (1 female, 5 males), 3 female chimpanzees (*Pan troglodytes*), 9 humans with end-stage AD (6 females, 3 males), and 3

nondemented elderly humans (2 females, 1 male) (Table 3.1). Human tissues were obtained from the Emory University Alzheimer's Disease Research Center Brain Bank in accordance with federal and institutional guidelines, and were coded to ensure the anonymity of subjects. Animal tissues were collected in accordance with federal and institutional guidelines for the humane care and use of experimental animals. The Yerkes Center is fully accredited by AAALAC International.

Tissue Collection and Preparation

For quantitative and qualitative biochemical analyses, unfixed, fresh-frozen temporal and occipital cortical tissue blocks were weighed and Dounce-homogenized in 5 volumes of homogenization buffer (50mM Tris-HCl and 150mM NaCl, pH 7.5, containing complete protease inhibitor tablets [Santa Cruz Biochemicals, Santa Cruz, CA, USA]). Cortical homogenates were centrifuged at 100,000g for 60 minutes at 4°C in a TLA 100.4 rotor (Beckman Coulter, Fullerton, CA, USA) and the supernatant ("soluble extract") aliquoted and stored at -80°C until use. The resulting buffer-insoluble pellet was probe-sonicated in 70% formic acid, centrifuged at 16,110g for 60 minutes at 4°C, and the clear supernatant ("insoluble extract") aliquoted and stored at -80°C until use.

For SDS-PAGE analysis, unfixed, fresh-frozen temporal and occipital cortical tissue blocks were weighed and Dounce-homogenized in 4 volumes of sterile, ice-cold 0.01M phosphate buffered-saline, 137mmol NaCl, 2.7 mmol KCl (1x PBS), pH 7.4. 20% weight/volume homogenates were sonicated 3 x 5 seconds, vortexed, centrifuged for 5 minutes at 3,000g, and the supernatants stored at -80°C until use.

For immunohistochemistry, brains were fixed for at least 7 days in 0.1M PBS-buffered 4% paraformaldehyde at 4°C. Temporal and occipital blocks were coronally bisected so that both frozen and paraffin sections could be made from the same general region. For the frozen sections, tissue blocks were cryoprotected in a graded series of 10%-30% sucrose, embedded in frozen Tissue-Tek OCT mounting medium (Sakura, Torrance CA) and sectioned at 50μm thickness on a cryostat at -20°C. Sections were stored in antifreeze (30% ethylene glycol in 30% sucrose/PBS) at -20°C until use. The remaining blocks were paraffin-embedded, sectioned at 8μm thickness and mounted onto silanized slides.

Antibodies

The following antibodies were used for immunohistochemistry, immunoprecipitation, and/or immunoblotting: Monoclonal antibodies 6E10 and 4G8 to residues 3-8 and 17-24 of the Aβ peptide, respectively (both at 1:5000; Covance Research Products, Denver, PA, USA); rabbit polyclonal antibodies R361 and R398 to C-terminal residues 32-40 and 33-42 of Aβ40 and Aβ42, respectively (both at 1:15,000; provided by Dr. Pankaj Mehta, Institute for Basic Research on Developmental Disabilities, Staten Island, NY, USA); monoclonal antibody 8E1 to Aβpyr3-x (0.75μg/ml, IBL, Gunma, Japan); monoclonal antibodies CP13 to phospho-tau 202 (1:10,000), PHF1 to phospho-tau 396/404 (1:10,000), and MC1 to aggregated tau (1:10,000) (all provided by Dr. Peter Davies, Albert Einstein College of Medicine, Bronx, NY, USA); and monoclonal antibody AT8 to phospho-tau 202/205 (1:5000; Covance) [241].

Immunohistochemistry

To prepare slide-mounted paraffin sections for immunohistochemistry, sections were de-paraffinized by heating in an oven for 30 minutes at 60°C followed by 1 minute incubations in xylene, 100% ethanol, 95% ethanol, 70% ethanol, and ddH2O. Paraffin and frozen (floating) sections were washed in 0.1M PBS, pH 7.4, and then endogenous peroxidases were inactivated with 3% H_2O_2 in methanol. To block nonspecific reagent binding, sections were incubated in 2% normal serum (horse serum for monoclonals and goat serum for polyclonals) and 0.2% Tween-20 (Sigma-Aldrich, St. Louis, MO) in PBS (blocking solution) for one hour at room temperature. As an antigen-retrieval technique for Aβ-immunodetection, sections were pretreated for 10 minutes with 100% formic and then incubated in primary antibody (diluted in blocking solution) for one hour at room temperature and then overnight at 4°C. On the second day, Vectastain Elite kits (Vector Laboratories, Burlingame, CA, USA) were used for avidin-biotin complex (ABC)-based horseradish peroxidase immunodetection of antigen-antibody complexes. After rinsing, sections were placed for one hour at room temperature in biotinylated secondary antibody (1:200 in blocking solution), rinsed, immersed for 30 minutes in avidin-biotin complex, and then developed with 3,3'-diaminobenzidine (DAB) (Vector Laboratories). Tissue from pathologically verified human AD cases was used as positive control material, and non-immune mouse IgG or rabbit serum was used in place of the primary antibodies as negative controls.

Aβ load was assessed histopathologically in 6E10-immunostained paraffin sections of temporal and occipital cortices. For each section, two researchers rated the

levels of diffuse plaques, compact plaques, and CAA in capillaries and large vessels (+++ frequent, ++ moderate, + rare, - absent) [165].

Quantitative Aβ ELISA

To quantify total Aβx-40 and Aβx-42 levels in soluble and insoluble cortical extracts, formic acid extracts were first neutralized with 1.0M Tris base, pH 11 (1:20 dilution), and then extracts were diluted in sample buffer as necessary (between 1:2 and 1:10,000). Diluted samples were added to 96-well microplates coated with a C-terminal-specific capture antibody, and an N-terminal-specific detection antibody then was added according to the manufacturer's instructions (The Genetics Company, Schlieren, Switzerland). Aβ content is expressed relative to the wet weight of tissue. All samples were assayed in duplicate. After stopping the tetramethylbenzidine-peroxidase reaction with sulfuric acid, plates were read at 450 nm on a Biotek Synergy HT Multidetection plate reader (Biotek, Winooski, VT, USA).

Aβ Immunoprecipitation/MALDI-TOF Mass spectrometry

To immunoprecipitate total Aβ from the cortical extracts, paramagnetic beads were coated with antibodies 4G8 and 6E10, and the precipitates run on Tricine SDS-PAGE gels or by matrix assisted laser desorption/ionization-time of flight mass spectrometry (MALDI-TOF MS), as previously described [274]. Briefly, 50µl Dynal M-280 Dynabeads (Invitrogen, Carlsbad, CA) coated with sheep anti-mouse antibodies were washed 3 times with 50µl 0.1M PBS, and incubated, rotating end-over-end for 24 hours at 4°C, with monoclonal 4G8 and 6E10 antibodies at a concentration of 120µg/ml (3µg of

each antibody/50µl beads). Antibody-coated beads were then blocked with 50µl 0.1% bovine serum albumin (Sigma-Aldrich, St. Louis, MO). To control for nonspecific binding, 25µl of blocked uncoated beads were added to 1.0ml soluble cortical extract or a solution of 100µl formic acid extract, neutralized with 1.0M Tris to pH 7.4 and then diluted up to 10ml with deionized water, and incubated, rotating end-over-end, for one hour at room temperature. For each immunoprecipitation (IP) reaction, 50µl of Aβ antibody-coated beads were added to the "cleared" extracts and incubated, rotating, for 3 hours at room temperature then 12 hours at 4°C. As a negative control, blocked beads with no antibodies were incubated with cortical extracts from each group. Synthetic Aβ40 incubated with antibody-coated beads was used as a positive control.

For analysis of immunoprecipitated Aβ by Western blotting, dried beads were resuspended in 20µl total volume of 2x SDS-PAGE buffer and 10x reducing agent (Invitrogen, Carlsbad, CA), boiled for 5 minutes, quickly vortexed and loaded onto 10-20% Tris-Tricine gels (see below for continuation of the immunoblotting protocol). For analysis of immunoprecipitated Aβ by MALDI-TOF MS, beads were washed 3 times with ice-cold 0.1M PBS, 1 time with 50 mM ammonium bicarbonate pH 7.3, completely dried in a SpeedVac, and then eluted with 20µl 0.5% formic acid. Samples were dried under a cold stream of nitrogen gas and then resuspended in 4µl 0.1% formic acid/20% acetonitrile in deionized water. At the New York University protein facility, 1µl of IP eluate was mixed with 500µl ethanol and 500µl ACN in 0.1%TFA and then analyzed in a Micromass TofSpec-2E MALDI-TOF instrument. Major peaks within all spectra were identified with ExPASy's FindPept software (http://us.expasy.org/tools/findpept.html).

Peaks that were detected in the negative control (mock immunoprecipitation with no antibodies) were not included in the final analysis.

Western blot

To determine total protein concentrations in clarified 20% cortical homogenates, samples were diluted 1:10 in 0.1M PBS in a 96 well microplate, and incubated with 200μl of a solution of buffered bicinchoninic acid and 4% cupric sulfate, for 30 minutes at 37°C, according to the manufacturer's instructions (Thermo Scientific, Rockford, IL). Plates were immediately read at 562 nm on a Biotek Synergy HT Multidetection plate reader, and total protein concentration was determined by interpolation on a 4-parameter standard curve. For each sample, 60μg of total protein was incubated with 2x Tricine loading buffer, 10x reducing agent, and deionized water, boiled at 100°C for 5 minutes, quickly vortexed, and loaded onto a 10-20% Tris-Tricine gel (Invitrogen). SeeBlue 2 molecular marker (Invitrogen) and 20ng synthetic, aggregated Aβ42 (rPeptide, Athens, GA) were run on each gel as a molecular weight marker and positive control, respectively. Protein was transferred to nitrocellulose membranes that were then boiled for 15 minutes in 0.1M PBS.

For immunoblotting, membranes were blocked for 30 minutes at room temperature in 2.5% milk in Tris-buffered saline with 0.05% Tween-20 (TBS-T). After a 30 minute rinse in TBS-T, membranes were incubated in primary antibodies, diluted in 2.5% milk/TBS-T (6E10, 1:1000, 4G8, 1:2500, R361, 1:1000, R398, 1:1000, CP13, 1:1000, 8E1, 2.5μg/ml) for one hour at room temperature and then 12 hours at 4°C. On day 2, the membranes were rinsed for 30 minutes in TBS-T, incubated for 90 minutes in

α-mouse IgG or α-rabbit IgG electrochemiluminescence secondary antibody (diluted in 2.5% milk/TBS-T at 1:10,000 Amersham Biosciences, UK), then rinsed for 30 minutes in TBS-T, all shaking at room temperature. To visualize the ECL-conjugated secondary antibodies, the membranes were incubated in Pierce ECL Western Blotting Substrate (Thermo Scientific, Waltham, MA) for 10 minutes, exposed to Kodak BioMax MS film (Kodak, Rochester, NY) for 30 seconds to 5 minutes, then developed in a Kodak processor. Films were scanned with a Canon flatbed scanner and images were edited in Photoshop, using only the cropping tool.

Statistical analyses

We used the Kruskal-Wallis nonparametric one-way analysis of variance (ANOVA) to detect group differences in Aβ levels in the soluble and insoluble extracts of both brain regions examined. Dunn's post-hoc t-tests were then employed to detect differences in Aβ40, Aβ42, or total Aβ levels between individual groups for soluble and insoluble cortical extracts from both regions.

Tables

Table 3.1. Case list

Group	Case	[Δ]Age(y)	Sex	[§]PMI(h)	Braak Stage	*ApoE
ND Human	E04-46	40	m	31	Braak 0	3/4
	E04-34	57	f	17	Braak 0	3/3
	OS02-35	75	f	6	Braak 0	3/3
Human AD	E04-33	57	f	20	Braak V/VI	3/4
	E04-172	87	f	6	Braak V/VI	3/4
	OS03-300	75	f	12	Braak V/VI	4/4
	OS02-159	61	m	5.5	Braak V/VI	3/4
	OS01-128	91	f	2.5	Braak V/VI	3/4
	OS02-106	81	f	2	Braak >IV	3/3
	E05-87	61	m	4	Braak V/VI	3/4
	E08-41	84	m	4.5	Braak VI	3/4
	E05-04	64	f	4.5	Braak VI	3/4
Chimpanzee	YN06-108Pt	44	f	3		
	YN07-25Pt	47	f	1		
	YN05-400Pt	41	f	1		
Rhesus	06-1Mm	35	f	<3		
macaque	AM109	26.6	m	1		
	AM120	26.5	f	1		
	554	38	m	<3		
	1201	35	m	<3		
	1203	33	f	<3		
	1210	30	m	<3		
	1211	25	f	<3		
	1313	>20	m	<3		
Squirrel	84L	21	m	1		
monkey	83GO	20	m	1		
	86J	17	m	1		
	06-5Ss	23	f	<3		
	90T	17	m	1		
	92AH	15	m	1		

[Δ]Age (y): Age (years)
[§]PMI (h): Postmortem interval (hours)
*ApoE: Apolipoprotein E genotype

Table 3.2. Soluble Aβ levels (pmol Aβ/100μg wet weight tissue)

		Temporal Cortex			Occipital Cortex		
Group	**Case**	**Aβ40**	**Aβ42**	**Total Aβ**	**Aβ40**	**Aβ42**	**Total Aβ**
ND Human	E04-46	0	293	293	133	123.1	136.4
	E04-34	0	22	22	0	0	0
	OS02-35	0	99	99	0	29	29
Human AD	E04-33	0	167	167	233	833	106.6
	E04-172	53	315	368	2801.4	513.6	331.5
	OS03-300	81.4	37.7	119.2	18.3	50.3	78.6
	OS02-159	502.2	48.5	550.7	204.9	77.8	282.7
	OS01-128	77.2	71.4	148.7	1341.6	163.4	1505
	OS02-106	1.1	28.3	29.4	0	47.2	47.2
	E05-87	1594	86.2	1680.3	n/a	n/a	n/a
	E08-41	21.4	39.2	60.5	n/a	n/a	n/a
	E05-04	73.7	116.5	190.1	n/a	n/a	n/a
Chimpanzee	YN06-108Pt	221.2	799.2	1020.4	1689.6	532.7	2222.3
	YN07-25Pt	6.2	27.3	33.5	23.4	777.6	801.1
	YN05-400Pt	714.8	1669.1	2383.9	n/a	n/a	n/a
Rhesus	06-1Mm	183.2	194.3	377.5	260.1	3328.8	3588.8
macaque	AM109	n/a	n/a	n/a	5.5	16.1	21.6
	AM120	n/a	n/a	n/a	12.8	224	236.8
	554	n/a	n/a	n/a	9.5	20.7	30.2
	1201	n/a	n/a	n/a	31002.3	5442.7	36445.1
	1203	n/a	n/a	n/a	399.8	2323.7	2723.8
	1210	n/a	n/a	n/a	10.9	560.6	571.6
	1211	n/a	n/a	n/a	12.1	53.2	65.3
	1313	n/a	n/a	n/a	11.7	618.6	630.2
Squirrel	84L	8117.4	2072.9	10190.3	6570.3	2501.3	9071.5
monkey	83GO	7110.6	1408.6	8519.2	11566.1	2508.6	14074.7
	86J	309.5	321.1	630.6	174.8	95.6	270.4
	06-5Ss	18.0	68.7	86.8	299.5	216.2	515.8
	90T	29.4	104.9	134.3	104.8	403.5	508.3
	92AH	7.6	22.3	29.8	7.0	10.5	17.5

n/a: Not available

Table 3.3. Insoluble Aβ levels (fmol Aβ/100μg wet weight tissue)

		Temporal Cortex			Occipital Cortex		
Group	**Case**	**Aβ40**	**Aβ42**	**Total Aβ**	**Aβ40**	**Aβ42**	**Total Aβ**
ND Human	E04-46	0	1	1	0	1	1
	E04-34	0	0	0	0	0	0
	OS02-35	0	0	0	0	1	1
Human AD	E04-33	3	83	86	2	211	213
	E04-172	8	217	225	11	176	187
	OS03-300	62	98	160	5	187	192
	OS02-159	40	175	215	15	298	313
	OS01-128	18	196	214	10	191	202
	OS02-106	1	146	146	0	59	60
	E05-87	275	353	628	n/a	n/a	n/a
	E08-41	4	156	160	n/a	n/a	n/a
	E05-04	4	445	449	n/a	n/a	n/a
Chimpanzee	YN06-108Pt	15	93	109	249	179	428
	YN07-25Pt	0	24	24	1	62	63
	YN05-400Pt	10	69	79	n/a	n/a	n/a
Rhesus	06-1Mm	100	250	350	15	190	205
macaque	AM109	n/a	n/a	n/a	0	29	29
	AM120	n/a	n/a	n/a	0	18	19
	554	n/a	n/a	n/a	7	24	31
	1201	n/a	n/a	n/a	843	487	1330
	1203	n/a	n/a	n/a	10	228	238
	1210	n/a	n/a	n/a	0	104	105
	1211	n/a	n/a	n/a	2	90	93
	1313	n/a	n/a	n/a	0	67	67
Squirrel	84L	367	230	597	396	618	1014
monkey	83GO	497	252	750	1121	508	1629
	86J	8	91	99	1	174	176
	06-5Ss	19	318	337	26	370	396
	90T	3	357	360	43	178	221
	92AH	0	51	52	0	2	2

n/a: Not available

Figures

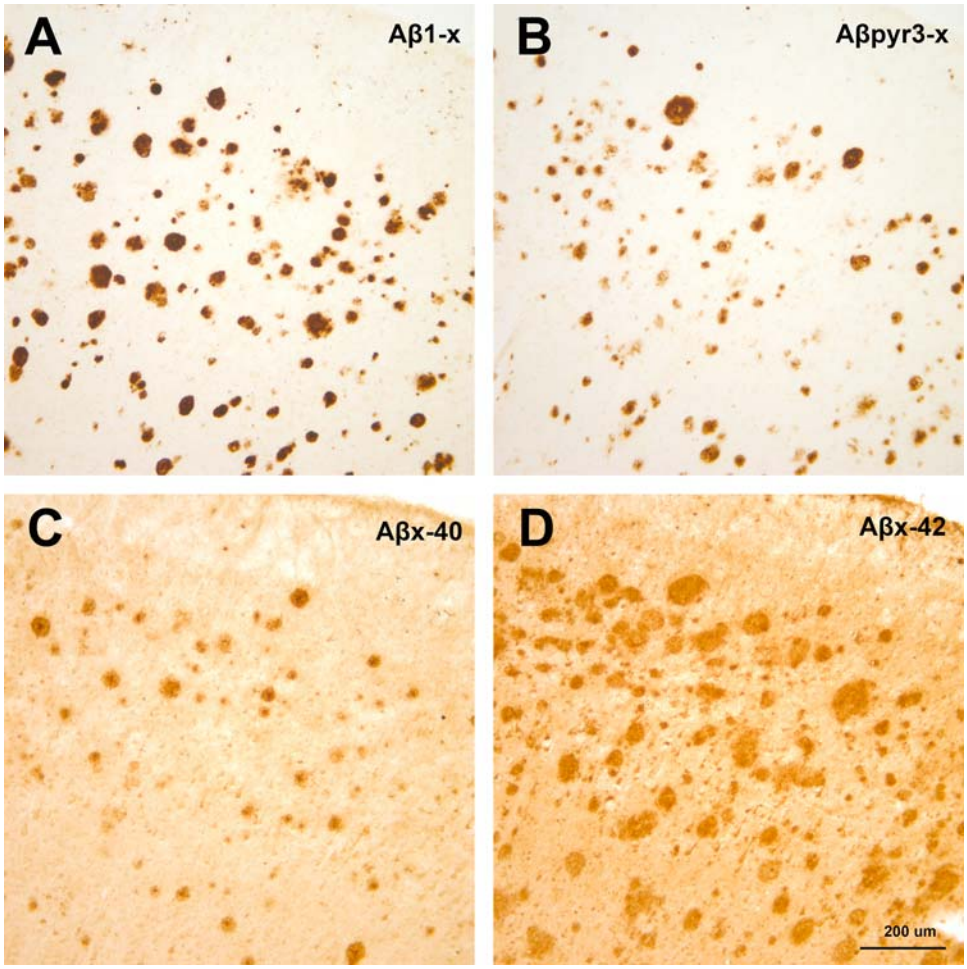

Figure 3.1. Aβ deposition in Alzheimer's temporal cortex.

Immunohistochemistry with antibodies to various epitopes within the Aβ peptide revealed extensive plaque deposition throughout cortical layers 2 to 6 of the superior temporal gyrus in a typical AD brain, while only rare deposits of vascular amyloid were seen. In several other AD subjects, heavy plaque deposition was also detected along the superficial pial layer of the cortex. (A) The majority of compact and diffuse plaques contain Aβ peptides beginning at amino acid residue 1, as detected with antibody 6E10. In panel (B), the 8E1 antibody to the pyroglutamized residue of N-terminally cleaved

Aβ3-x reacts with a large subset of 6E10-immunoreactive cored and diffuse plaques as well as occasional CAA. In panels (C) and (D), immunostaining with C-terminal Aβ antibodies (R361 in [C] and R398 in [D]) show that Aβx-40 peptides are less common in diffuse plaques, and are found in the central core of compact plaques. Aβx-42 is found in many more compact and diffuse plaques, and is localized both at the center and around the perimeter of senile plaques. Diffuse Aβ-immunoreactive deposits were also detected within the white matter of most AD subjects in this study (data not shown). Bar = 200μm.

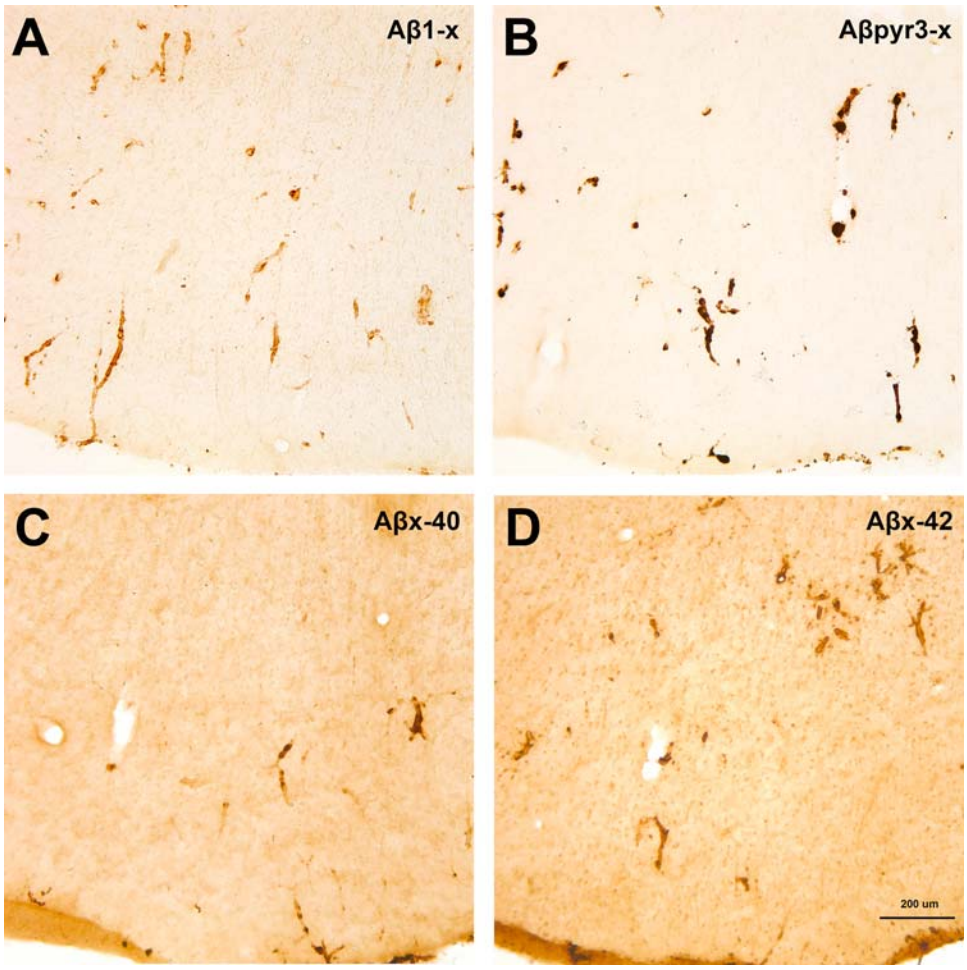

Figure 3.2. Aβ deposition in aged chimpanzee temporal cortex. In the superior temporal gyrus of this 41-year old female chimpanzee, immunohistochemistry with four Aβ-specific antibodies revealed species-typical accumulation of large-vessel cerebral amyloid angiopathy. Also detected were small Aβ-immunoreactive plaques associated with large cortical vessels. Antibodies to Aβ1-x (A) and $Aβ_{pyroglutamate}$3-x (B) both revealed dense vascular amyloid deposits throughout the cortical layers and along the pial surface (antibodies 6E10 in [A] and 8E1 in [B]). Vascular amyloid along the pial layer was also immunoreactive for antibodies R361 (C) and R398 (D), which are specific for C-terminal Aβ ending at residues 40 and 42, respectively. Both Aβx-40 and Aβx-42 are deposited in chimpanzee CAA, however Aβx-42 was the predominant isoform

detected in this animal. Note several large vessels that were not at all affected by CAA. Bar = 200μm.

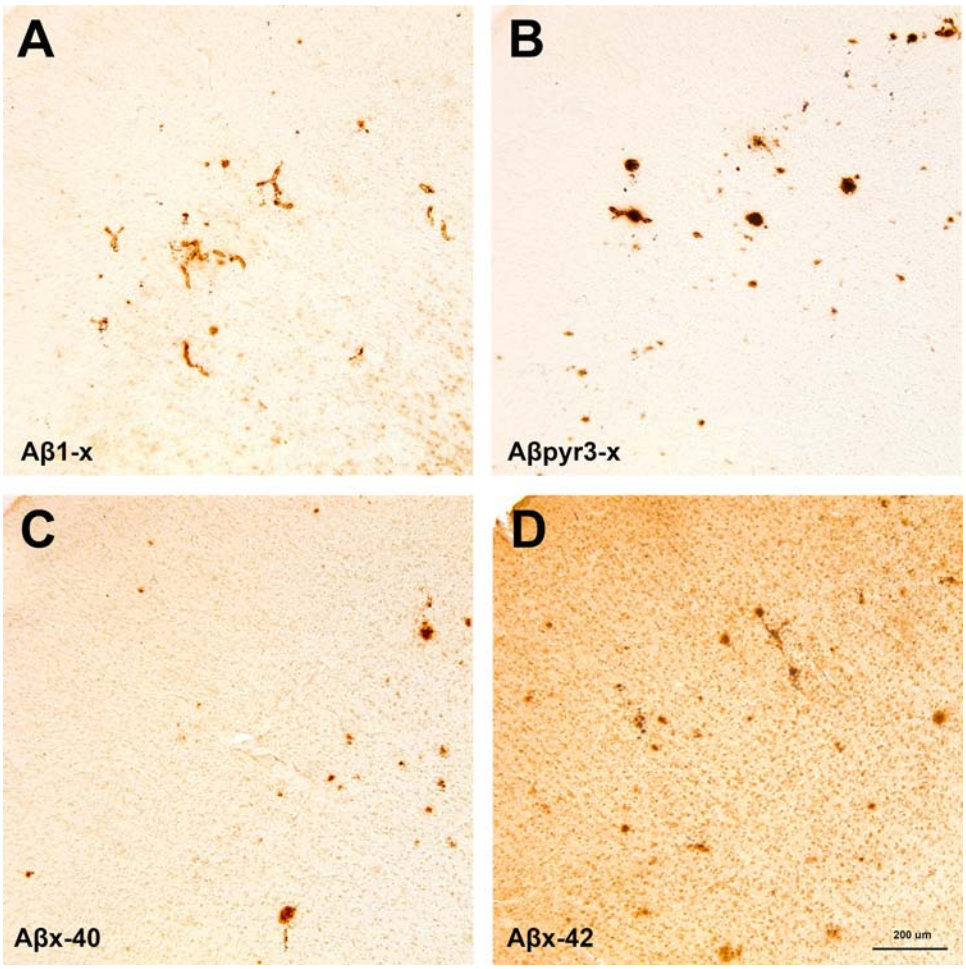

Figure 3.3. Aβ deposition in the superior temporal gyrus of an aged rhesus macaque. Immunohistochemistry with antibodies to 4 distinct Aβ epitopes revealed species-typical accumulation of cerebral amyloid angiopathy and, occasionally, small compact and diffuse plaques in rhesus monkeys. The lesions were spread throughout cortical layers 2 to 6 in this case, although, as in all simians and humans, their morphology and distribution can vary among cortical regions. (A) Antibody 6E10, specific for the N-terminal region of Aβ, labeled large vessel and capillary CAA and, less frequently, compact and diffuse parenchymal plaques. (B) Antibody 8E1, which binds to N-terminally truncated and modified $A\beta_{pyroglutamate}3$-x peptides, showed occasional immunoreactivity in large vessel CAA but more often in small diffuse and compact

plaques. (C) Polyclonal antibody R361 revealed Aβx-40 accumulation in various morphologies of compact plaques. (D) Aβx-42, as revealed with antibody R398, was found in all types of vascular and parenchymal Aβ lesions in this subject. Overall, Aβ deposits contained slightly more Aβx-42 than Aβx-40 in this animal. Rhesus monkeys exhibit significant within-species variability, and some of the oldest rhesus macaques accumulate heavier amounts of parenchymal plaque deposition in the more superficial cortical layers. Bar = 200μm.

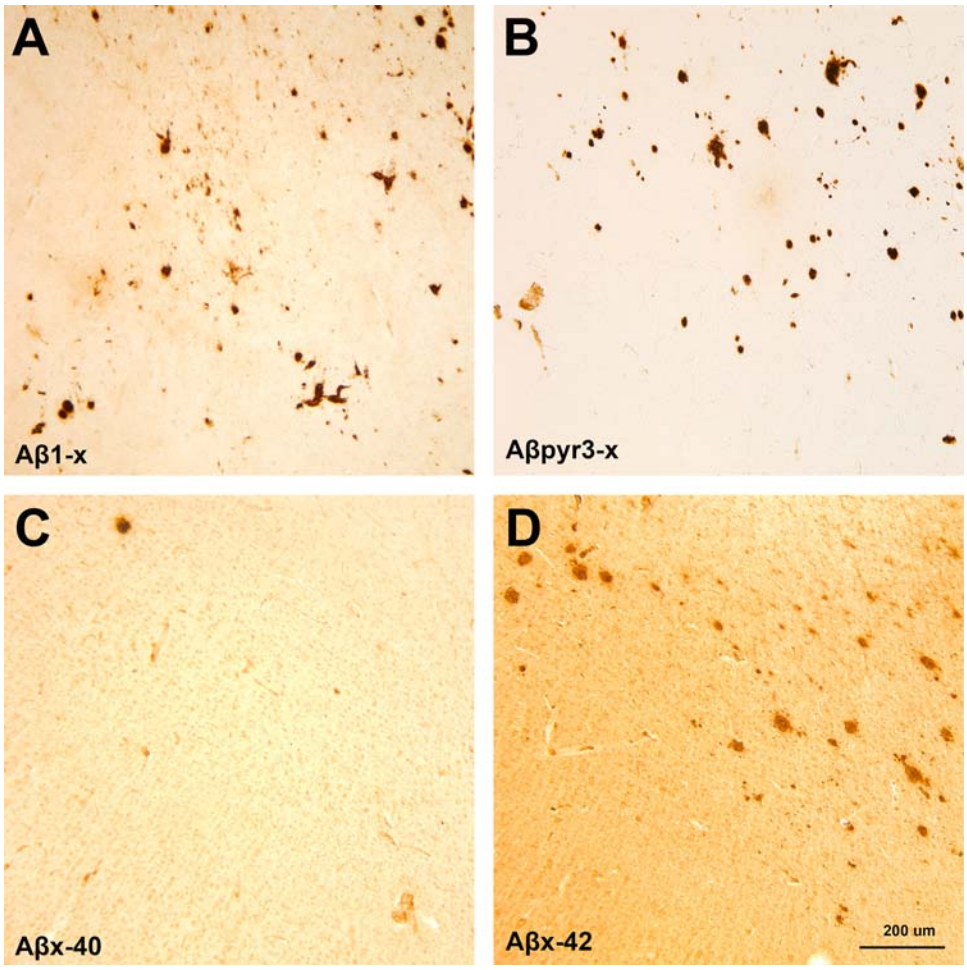

Figure 3.4. Aβ deposition in aged squirrel monkey temporal cortex. Aged squirrel monkeys manifest significant vascular and parenchymal Aβ deposition that is generally found in the deeper cortical layers and spreads to layer 2 in older animals. (A) In this 18-year-old subject, immunostaining with antibody 6E10 revealed Aβ1-x peptides in large vessel and capillary CAA, as well as diffuse and small, compact senile plaques. (B) $A\beta_{pyroglutamate}3$-x peptides were detected in a subset of 6E10-immunoreactive lesions, and the modified peptide tended to be located in the core of compact plaques (antibody 8E1). (C) In this animal, Aβx-40-positive lesions were rarely detected, while Aβx-42 (D) accumulated in plaques and vessels throughout the cortex, particularly in deep-layer diffuse deposits, which are probably composed of full-length Aβ42, based on comparison

with the adjacent 6E10-immunostained section (antibody R361 in [A] and antibody R398 in [B]). Bar = 200μm.

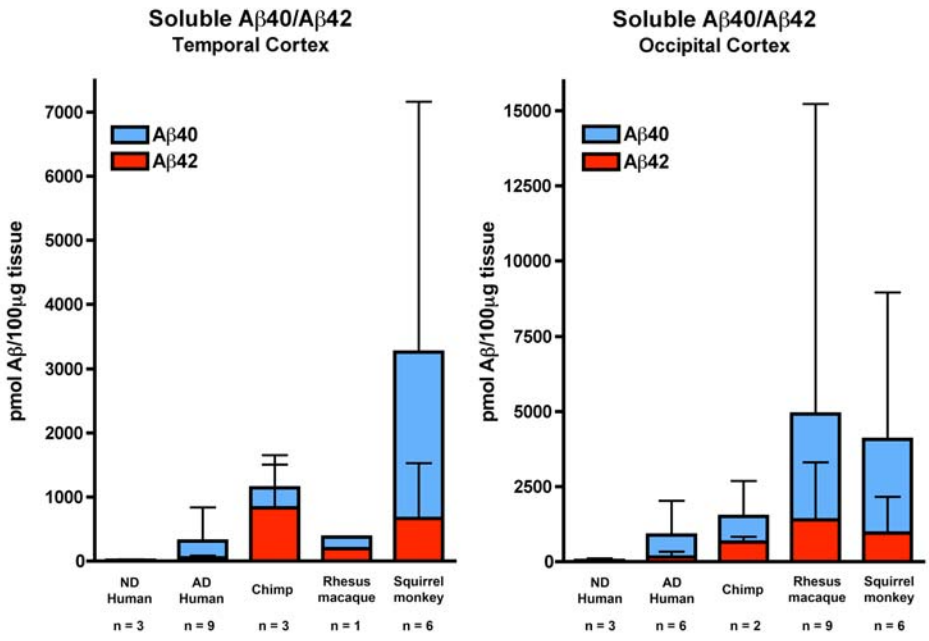

Figure 3.5. ELISA quantification of soluble Aβ40 and Aβ42 in human and aged nonhuman primate brain. Using capture antibodies specific to the C-termini of Aβx-40 and Aβx-42 and an N-terminal-specific detection antibody, we quantified the total amount of full length Aβ40 and Aβ42 in buffer-soluble temporal and occipital cortical extracts from 3 nondemented humans, 9 end-stage AD cases, 3 chimpanzees, 9 rhesus macaques, and 6 squirrel monkeys. (A) In the temporal cortex, no soluble Aβ40 and very low levels of Aβ42 were detected in the nondemented human cases (n=3, means = 0 pmol Aβ40/100μg [S.D.=0] and 13.82 pmol Aβ42/100μg [S.D.=13.97]). Mean soluble Aβ40 and Aβ42 levels were higher in all 3 nonhuman primate groups compared to AD subjects, except for Aβ40 in the one rhesus macaque. In both cortical regions, the mean Aβ40:Aβ42 ratio was greater than one for AD and all nonhuman primate groups, with the exception of the temporal cortex in the chimpanzees. Note the different scales on the y-axes of the two graphs, as peptide levels were substantially higher in the occipital cortex. By nonparametric ANOVA, total soluble Aβ levels were significantly

different between nondemented human and squirrel monkey groups ($p<0.05$) but no other significant differences were detected between any of the groups in either cortical region, probably because of the variability of values within groups. ND = nondemented human, AD = Alzheimer's disease human. Bars = standard deviations.

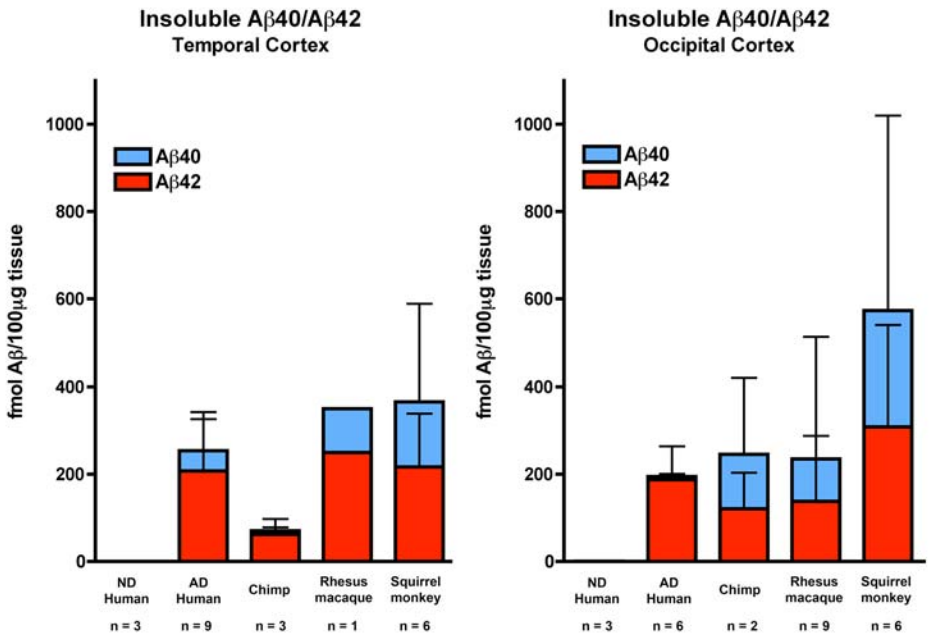

Figure 3.6. Insoluble Aβ accumulates at comparable levels in AD and aged nonhuman primate brain. By ELISA, full-length Aβ40 and Aβ42 peptides were quantified in formic-acid solubilized protein extracts from temporal and occipital cortical samples from 3 nondemented humans, 9 end-stage AD cases, 3 chimpanzees, 9 rhesus macaques, and 6 squirrel monkeys. (A) Insoluble temporal cortical extracts from the nondemented human cases contained significantly lower levels of Aβ42 and total Aβ than were detected in both AD and squirrel monkey temporal cortex ($p<0.05$). (B) Insoluble extracts from the occipital cortex of nondemented humans also contained negligible detectable Aβ40 or Aβ42, as compared to Aβ load in AD cases, but these differences were not significant by nonparametric ANOVA. In both cortical regions examined, Aβ42 and total Aβ levels were only significantly different between squirrel monkey and nondemented human subjects. No significant differences were detected between temporal or occipital cortical Aβ levels in AD and any nonhuman primate group. In both cortical regions of all groups, the insoluble Aβ40:Aβ42 ratio was less than one.

However, there was a trend towards relatively more Aβ40 in the aged nonhuman primate brains. ND = nondemented human, AD = Alzheimer's disease human. Bars = standard deviations.

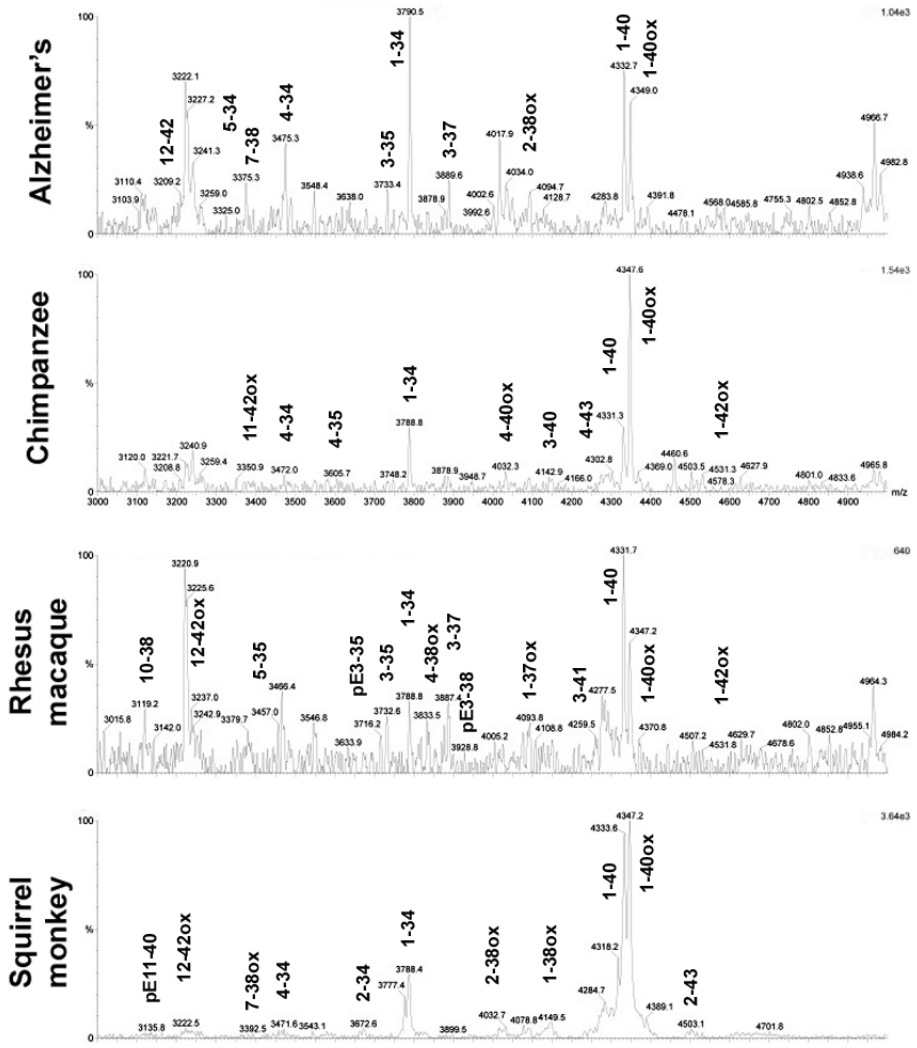

Figure 3.7. MALDI-TOF mass spectrometric analysis of soluble Aβ peptides in AD and aged nonhuman primate temporal cortex. Total Aβ peptide populations were immunoprecipitated from soluble cortical extracts and analyzed by MALDI-TOF MS, using antibodies 6E10 and 4G8, to the N-terminus and central hydrophobic region of the Aβ peptide, respectively. Each spectral peak represents one peptide, each of which has a unique mass-to-charge value (m/z). Shown are representative spectra of temporal cortical extracts from each group (AD Human: OS0-159, Chimp: Y05-400Pt, Rhesus

macaque: 06-1Mm, Squirrel monkey: 83GO), with labeled peaks that correspond to full-length, truncated, or modified Aβ peptides. Soluble Aβ40 and Aβ40ox (oxidized at Met35 residue) were detected in all cases but soluble Aβ42 was only detected in its oxidized form. The Aβ1-34 peptide was consistently detected in soluble extracts from most AD and nonhuman primate cases, but not in any of the nondemented human cases. Furthermore, no full-length Aβ40 and Aβ42 was detected in any soluble extracts from the nondemented human group. Similar results were obtained with soluble extracts from the occipital cortex (data not shown). For a complete list of soluble Aβ peptides detected in both temporal and occipital cortical extracts from all subjects, see Figure 3.9.

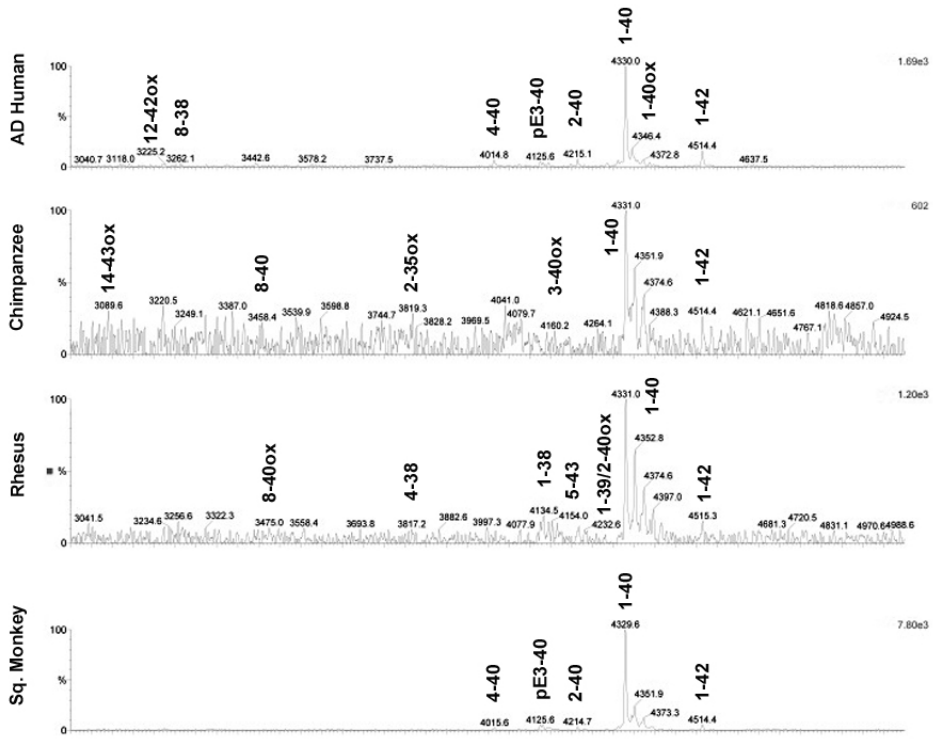

Figure 3.8. MALDI-TOF mass spectrometric analysis of insoluble Aβ peptides in AD and aged nonhuman primate temporal cortex. Aβ peptides were immunoprecipitated from formic acid-solubilized cortical extracts that had been neutralized with 1.0M Tris buffer and diluted with deionized water. In order to isolate full-length, fragmented, and modified Aβ peptides, paramagnetic beads were coated with antibodies 6E10 and 4G8, which bind to the N-terminus and central hydrophobic region of the Aβ peptide, respectively. Concentrated immunoprecipitate was analyzed by MALDI-TOF MS to identify individual peptides by their unique mass-to-charge value. Representative spectra of insoluble Aβ populations are shown for each group (AD Human: OS0-159, Chimp: Y05-400Pt, Rhesus macaque: 06-1Mm, Squirrel monkey: 83GO). Nondemented human cortical extracts had few detectable formic acid-soluble Aβ peptides, and no full-length Aβ40 or Aβ42 (data not shown). In addition to full length

Aβ40, Aβ42, and the oxidized isoforms of the peptides, other common fragments detected in all four groups include, but are not limited to, Aβ2-40, AβpE3-40, and Aβ4-40. There was no group of Aβ peptides, nor an individual Aβ peptide, that was exclusively detected in AD or nonhuman primate brain. Figure 3.9 contains a meta-analysis of fragments detected in both cortical regions examined, including Aβ peptides detected in occipital cortical samples (data not shown).

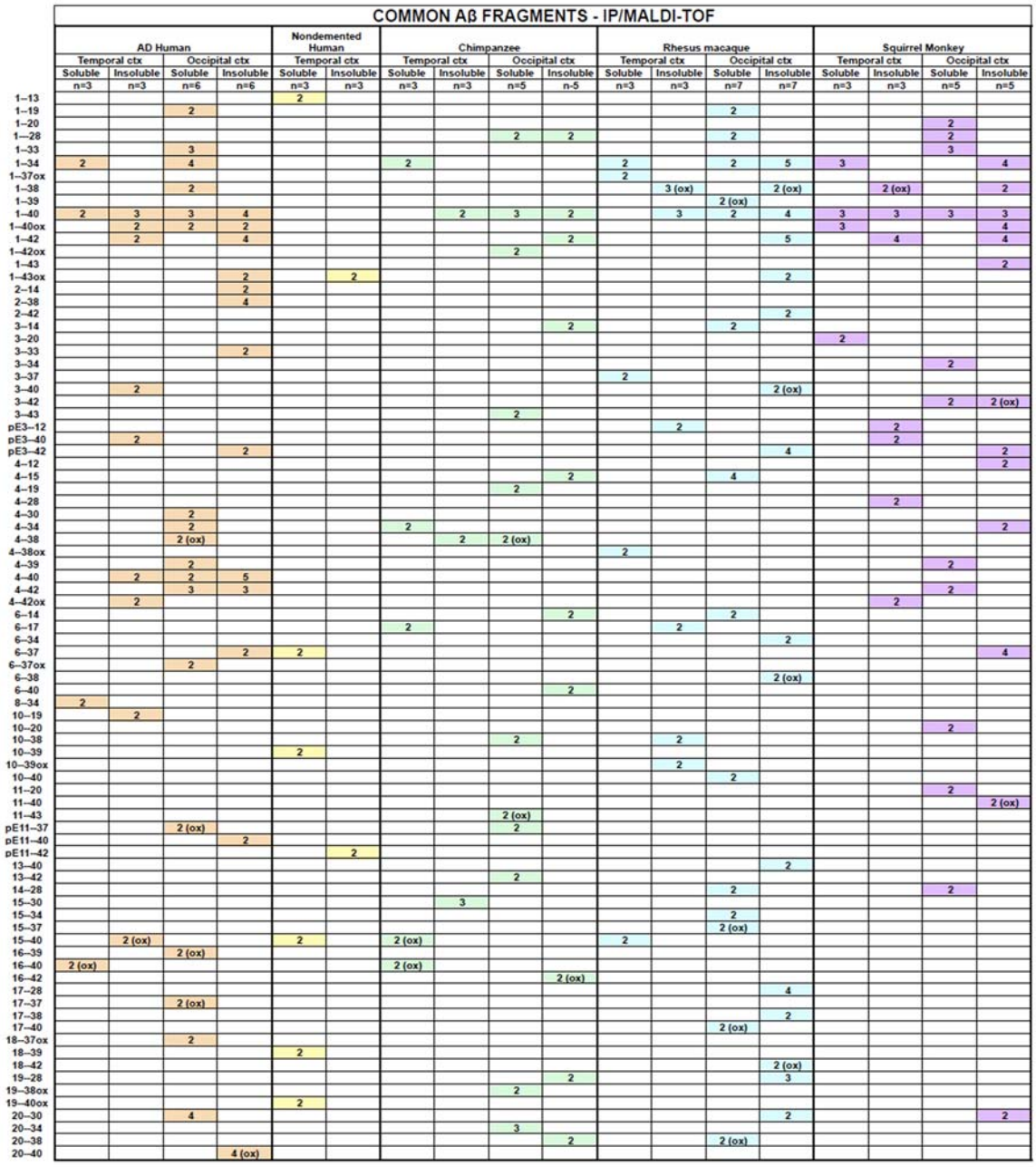

Figure 3.9. Analysis of common Aβ fragments detected by MALDI-TOF in buffer-soluble and insoluble temporal and occipital cortical extracts from human and nonhuman primate subjects. Major peaks that were detected in linear mode MALDI-TOF MS were entered into ExPASy's FindPept software (http://us.expasy.org/tools/findpept.html) in order to match m/z values with potential Aβ

peptides. Peaks that were also detected in negative control samples (sham immunoprecipitations with no primary antibodies) were eliminated from the analysis. Based on antibody specificity, all feasible Aβ fragments are listed in column 1. Shaded boxes indicate that the Aβ peptide in that row was detected in at least 2 cases from that column's group. Numbers in the shaded boxes indicate the number of cases in which the Aβ peptide was detected and "(ox)" indicates that at least one of the detected peptides was in its oxidized form. AD: temporal cortex, n=3, occipital cortex, n=6; ND: temporal cortex, n=3; Chimpanzee: temporal cortex, n=3, occipital cortex, n=5; Rhesus macaque: temporal cortex, n=3, occipital cortex, n=7; Squirrel monkey: temporal cortex, n=3, occipital cortex, n=5.

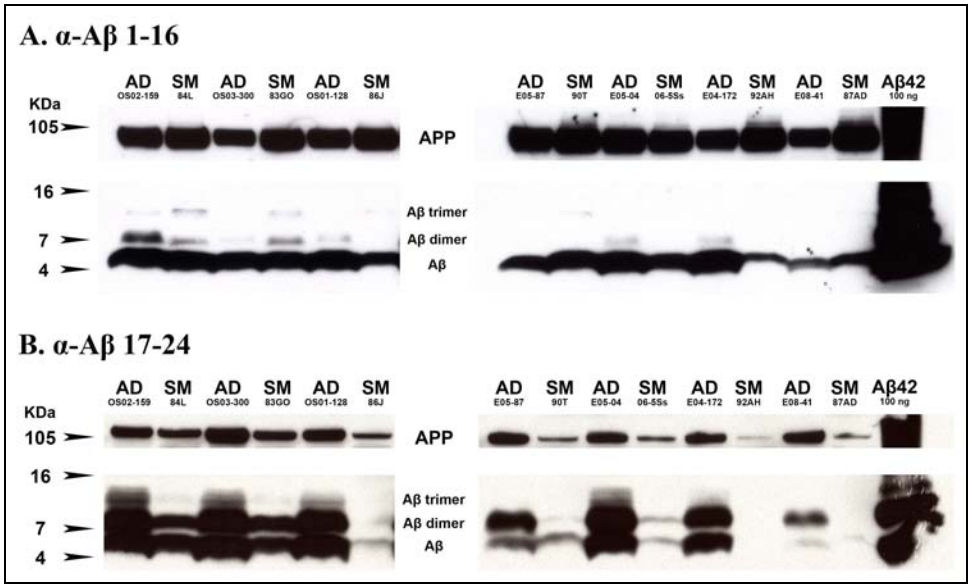

Figure 3.10. Western blot analysis of multimeric Aβ distribution in AD and aged squirrel monkey temporal cortex. Clarified temporal cortical homogenates from 7 end-stage AD cases and 7 aged squirrel monkeys, normalized for total protein, were electrophoretically separated by molecular weight on a Tris-Tricine 10-20% gel and immunoblotted with anti-Aβ antibodies 6E10 and 4G8. (A) Immunoblotting with antibody 6E10 revealed strong bands running at approximately 4 KDa in all homogenates, which correspond to monomeric Aβ40 and Aβ42. Dimeric and trimeric Aβ species were also detected in some AD and squirrel monkey samples, particularly in the cases shown to have higher levels of insoluble Aβ by ELISA (Figure 3.6). (B) The 4G8 antibody also detected strong bands of Aβ monomers in nearly all AD and squirrel monkey homogenates. 4G8-immunoreactive bands corresponding to Aβ dimers and trimers were substantially stronger in most AD samples than in squirrel monkeys with comparable levels of total Aβ. Both antibodies bound to a band migrating around 100KDa, or full-length APP, in all samples. SDS-PAGE/Immunoblotting did not reveal

any apparent differences in the distribution of aggregated Aβ between the AD and squirrel monkey samples. In the last lane, 100ng of fibrillar synthetic Aβ42 was run as a positive control. AD: Alzheimer's disease, SM: Squirrel monkey.

Results

Aβ Immunohistochemistry

In fixed temporal and occipital cortical tissue, Aβ-immunoreactive amyloid deposits were detected in all AD and aged nonhuman primate cases. Aβ plaque deposition was dense and widespread throughout cortical layers 2 to 6 in all AD cases examined (Figure 3.1). Diffuse and compact plaques were seen along layer 1 in some cases, and diffuse Aβ-immunoreactive plaques in the white matter were detected in most cases. In the nonhuman primate cases, plaque deposition was more focal in nature. Parenchymal plaques were composed predominantly of Aβ42 in both AD and nonhuman primate brain, with a smaller subset of plaques containing Aβ40 peptides. Aβ amyloid was detected in the vasculature of all nonhuman primate cases, while cerebral amyloid angiopathy (CAA) was relatively rare in the 9 AD cases examined. The contribution of Aβ40 and Aβ42 to vascular lesions varied substantially within and between nonhuman primate groups (Figures 3.2-3.4).

Aβ immunohistochemistry revealed species-typical patterns of Aβ deposition, which may be due to species variations in APP processing and/or Aβ clearance. In the aged chimpanzee brain, parenchymal plaques were rare and focal in occurrence, while the majority of Aβ-immunoreactive amyloid was located in large vessels (Figure 3.2). Rhesus macaques accumulated diffuse and compact parenchymal plaques along with vascular Aβ deposits, and, like chimpanzees, the Aβ tended to deposit heavily only in the final third of the animal's lifespan (Figure 3.3). In aged squirrel monkey brains, however, heavy Aβ deposition was often detected by 15-17 years old, halfway through

the animal's maximum lifespan. Aβ had a predilection to accumulate as CAA in the squirrel monkey brain, although some squirrel monkeys in this study exhibited extracellular Aβ deposits throughout the cortex, both compact and diffuse in nature (Figure 3.4). In the squirrel monkey brain, Aβ plaques tended to accumulate first in the deep cortical layers throughout the cortex, and then spread to more superficial layers in the oldest animals, which presumably represents a more advanced stage of Aβ proteopathy. Previous studies have reported a rostro-caudal gradient of Aβ deposition in aged monkeys, with higher levels of Aβ lesions in frontal cortex compared to more caudal regions, with the lowest number of lesions in the occipital cortex. Our immunohistochemical data in temporal and occipital cortex generally confirmed this finding, although, with quantitative ELISAs we detected more insoluble Aβ in nonhuman primate occipital cortex than temporal cortex.

Quantification of Aβ40 and Aβ42

In this study, we quantified Aβ40 and Aβ42 isoforms in buffer-soluble and insoluble, temporal and occipital cortical extracts from a substantial cohort of aged chimpanzees, rhesus macaques, and squirrel monkeys, alongside samples from humans with AD and nondemented human control cases. As expected, we detected only negligible levels of both soluble Aβ isoforms in nondemented aged human cases. Compared to the 3 nonhuman primate groups in this study (with the exception of rhesus macaque temporal cortex), we found lower levels of soluble Aβ40 and Aβ42 in both the temporal and occipital cortex of AD cases (Figure 3.5).

We also found that both Aβ40 and Aβ42 formed insoluble deposits in the aged nonhuman primate brain at similar or higher levels than in the end-stage AD brain, while the nondemented human cases contained substantially less insoluble peptide than either the simians or AD cases (Figure 3.6). By ELISA of temporal cortical samples, insoluble Aβ40 and Aβ42 levels were not significantly different between AD and any aged nonhuman primate group, although Aβ levels were substantially lower in the chimpanzee cohort. In this regard, it is worth noting that the chimpanzees in this group were younger (relative to their maximum known lifespan of 60 years) than were the other nonhuman primates. In the occipital cortex, there were also no significant differences between Aβ40, Aβ42 or total Aβ levels between AD cases and any nonhuman primate group.

Because a predominance of the Aβ42 isoform has been implicated in the toxicity and aggregability of the peptide in AD brain [107, 176], we calculated the Aβ40:Aβ42 ratios for each case and cortical region. Soluble Aβ40:Aβ42 ratios were highly variable for all groups except for the rhesus macaque occipital cortex, in which 8 of the 9 cases had more Aβ42 than Aβ40. However, *insoluble* Aβ42 was more abundant than was Aβ40 in both cortical regions of the humans and nonhuman primates, although the relative levels of Aβ40 in the occipital cortex were somewhat higher in the nonhuman primates (Figure 3.6). The Aβ40:Aβ42 ratio was less than 1.0 in every AD case examined, and exceeded 1.0 in at least one cortical region of only four nonhuman primates (YN06-108Pt, 1201, 84L and 83G0; see Table 3).

Because this is a comparative study of the primary Aβ structure in AD and aged nonhuman primate brain, we have taken into consideration that Aβ from human subjects may be subject to relatively higher levels of *ex vivo* proteolysis during the longer

postmortem intervals. However, in both human and nonhuman primate subjects, we did not detect significant differences in Aβ40 or Aβ42 levels by ELISA in frontal cortical tissue that was either snap-frozen at necropsy or stored at 4°C for 18 hours prior to freezing (data not shown).

MALDI-TOF MS

In order to identify species-unique populations of full-length and modified Aβ, total Aβ peptide populations were immunoprecipitated and ionized in a MALDI-TOF mass spectrometer to measure the mass and charge for each protein in the immunoprecipitate. Full length Aβ was not detected in temporal cortical samples from nondemented human cases (n=3). Peptides that were detected in at least 2 cases per group were designated as common isoforms for that group. Fragments that were seen in both oxidized and unmodified states are designated by "(ox)". In soluble extracts from temporal cortex (n=3 for all 5 groups), Aβ34 was the most commonly detected isoform, and was seen in at least 2 cases from each group (AD, chimpanzee, rhesus macaque and squirrel monkey) (Figure 3.7). Other common fragments in temporal cortex soluble extracts were Aβ8-34 and Aβ16-40(ox) in AD subjects, Aβ1-13, Aβ6-37, Aβ10-39, Aβ15-40, Aβ18-39ox and Aβ19-40ox in nondemented human, Aβ4-34, Aβ15-40(ox) and Aβ16-40(ox) in chimpanzee, Aβ1-37ox, Aβ3-38, Aβ4-38ox, and Aβ15-40 in rhesus macaques, and Aβ3-20 in squirrel monkeys. No soluble Aβ42 was detected, possibly due to decreased ionization efficiency of the longer Aβ isoform. In soluble extracts from occipital cortical samples, Aβ1-40, both oxidized and not, was seen in all 4 groups examined (AD, chimpanzee, rhesus macaque, and squirrel monkey), and Aβ1-34 also

was a common fragment, but only in AD and rhesus macaque samples. Overall, there were many more Aβ peptides in occipital cortical samples than in temporal cortex. Common soluble fragments in occipital cortex were Aβ1-19, Aβ1-33, Aβ1-38, Aβ4-30, Aβ4-34, Aβ4-38(ox), Aβ4-39ox, Aβ4-40, Aβ4-42, Aβ6-37ox, AβpE11-37(ox), Aβ16-39(ox), Aβ17-37(ox) and Aβ18-37ox in AD subjects (n=6), Aβ1-28, Aβ1-42ox, Aβ3-43, Aβ4-19, Aβ4-38(ox), Aβ10-38, Aβ11-43(ox), AβpE11-37, Aβ13-42, Aβ19-38ox, Aβ20-34 in chimpanzee subjects (n=5), Aβ1-19, Aβ1-28, Aβ1-39(ox), Aβ3-14, Aβ4-15, Aβ6-14, Aβ10-40, Aβ14-28, Aβ15-34, Aβ15-37(ox), Aβ17-40(ox), Aβ20-38(ox) in rhesus macaque subjects (n=7), and Aβ1-20, Aβ1-28, Aβ1-33, Aβ3-34, A3-42, Aβ4-39ox, Aβ4-42, Aβ10-20, Aβ11-20, and Aβ14-28 in squirrel monkey subjects (n=5).

Insoluble Aβ40 (oxidized and not) was detected in insoluble extracts of temporal cortex from AD and all nonhuman primate groups, while insoluble Aβ42 was seen in at least 2 cases in only the AD and squirrel monkey groups (n=3 for all groups) (Figure 3.8). Additional insoluble Aβ peptides in the temporal cortex were Aβ3-40, AβpE3-20, Aβ4-40, Aβ4-42ox, Aβ10-19, Aβ15-40(ox) in AD subjects, Aβ1-43ox and AβpE11-42 in nondemented humans, Aβ4-38 and Aβ15-30 in chimpanzees, Aβ1-39, AβpE3-12, Aβ6-17, Aβ10-38 and Aβ10-39ox in rhesus macaques, and Aβ1-39, AβpE3-12, Aβ3-40, Aβ4-28, and Aβ4-42ox in squirrel monkeys. In insoluble extracts from occipital cortical samples, peaks corresponding to Aβ40, Aβ40ox, Aβ42 and Aβ42ox were identified in AD and all 3 nonhuman primate groups and there were more Aβ fragments detected overall, as compared to insoluble temporal cortex extracts. Other common insoluble Aβ fragments detected in occipital cortex were Aβ1-43ox, Aβ2-14, Aβ2-38, Aβ3-33, AβpE3-42, Aβ 4-40, Aβ4-42, Aβ6-38, AβpE11-40, and Aβ2-40(ox) in AD cases (n=6),

Aβ1-28, Aβ3-14, Aβ4-15, Aβ6-14, Aβ6-40, Aβ16-42(ox), Aβ19-28, and Aβ20-38 in chimpanzees (n=5), Aβ1-34, Aβ1-38(ox) Aβ2-42, Aβ3-40(ox), AβpE3-42, Aβ6-34, Aβ6-38(ox), Aβ13-40, Aβ17-28, Aβ17-38ox, Aβ18-42(ox), Aβ19-28, and Aβ20-30 in rhesus macaques (n=7), and Aβ1-34, Aβ1-38, Aβ1-43, Aβ3-43(ox), AβpE3-42, Aβ4-12, Aβ4-34, Aβ6-37, Aβ11-40(ox), and Aβ2-30 in squirrel monkeys (n=5). Common fragments and the number of cases within each group in which the fragments were detected are listed in Figure 3.9.

Aβ Immunoblot

To characterize the distribution of monomeric and multimeric Aβ peptide populations in AD and aged nonhuman primate brain, temporal cortical homogenates from 7 AD and 7 squirrel monkey cases were separated by molecular weight with SDS-PAGE and immunoblotted with antibodies 6E10 and 4G8 to the N-terminus and central region of the Aβ peptide, respectively (Figure 3.10). Both antibodies detected strong monomeric Aβ bands at 4kDa in every case examined. In the 6E10 immunoblot, Aβ dimers (~8 kDa) were detected in 5 of the 7 AD cases, and 3 of the 7 squirrel monkeys, while trimeric Aβ (~12KDa) bands were seen in only 1 AD case and 4 squirrel monkey samples. Duplicate membranes were probed with the 4G8 antibody, revealing strong bands of monomeric Aβ in all but one squirrel monkey (92AH). Dimeric Aβ bands were 4G8-immunoreactive in all AD samples and 5 of 7 squirrel monkeys, similar to that seen with 6E10. However, 4G8 detected 12 kDa Aβ multimers (trimers) in 4 AD cases and 2 squirrel monkeys, a staining pattern markedly distinct from 6E10. Both antibodies labeled bands around 100KDa, corresponding to the APP protein. The 4G8 antibody had

a substantially higher predilection for putative Aβ dimers and trimers, while 6E10-labeled monomer bands were stronger than 4G8-labeled monomer bands in duplicate samples. In several cases, Aβ dimers were detected with 4G8 and not at all with 6E10 immunoblotting.

Discussion

Because it is nearly impossible to distinguish nondemented humans with senile plaque accumulation from humans with preclinical, incipient AD, the aged nonhuman primate is a biologically relevant model of benign cerebral Aβ-amyloidosis with which we have conducted a comparative phenotypic analysis of the long-term accumulation of toxic and benign cerebral Aβ. In this study, we characterized cerebral Aβ peptide populations in aged nonhuman primates and AD subjects, in order to identify an AD-unique set of Aβ peptides that might underlie its human-specific toxicity and serve as a potential therapeutic target for AD. We found that cerebral Aβ peptides from humans and nonhuman primates are practically indistinguishable at a primary structural level, but that the folded structures of multimeric Aβ may be distinct in AD and nonhuman primates. Mounting evidence points to these low molecular weight Aβ oligomers as the neurotoxic and synaptotoxic culprits in AD pathology and dementia [93, 148, 246, 258, 297] and also suggests that structural polymorphisms may dictate the relative toxicity of protein oligomers [216, 266, 268].

Aβ Immunohistochemistry

We used immunohistochemistry with Aβ-specific antibodies to the N-terminal, C-terminal and central regions of the peptide to characterize age-related cerebral Aβ accumulation in a broad evolutionary spectrum of nonhuman primates. We confirmed previous reports that Aβ tends to aggregate into CAA in aged nonhuman primates [63, 81]. However, we saw extensive variability in cortical Aβ lesion morphology between species and within species, and the Aβ isoform content of amyloid deposits also was highly variable. In chimpanzees, vascular amyloid containing both Aβ40 and Aβ42 was predominantly located in large vessels (Figure 3.2). The squirrel monkey cortex was beset by amyloidotic capillaries (Figure 3.4), a pattern we reported previously in a comprehensive histological study of the morphology and regional distribution of Aβ deposition in aged squirrel monkeys [63]. While parenchymal plaques were infrequent in the chimpanzee brain, plaques were detected throughout the cortex of several rhesus macaques and squirrel monkeys in this study. Aβ plaques in the rhesus cortex tended to be more diffuse in nature, whereas squirrel monkeys accumulated a unique type of small, spherical plaque that is not generally seen in the AD or rhesus brain (Figures 3.3, 3.4). N-terminally truncated, pyroglutamized Aβpyr3-x was detected within Aβ deposits in all nonhuman primate cases (Figures 3.2-3.4), indicating that, in both nonhuman primate and AD brain, Aβ is subject to variable β-secretase cleavage events as well as to post-translational modifications that are not seen in shorter-lived, transgenic mouse models of cerebral amyloidosis.

Despite extensive morphological variability in nonhuman primate Aβ deposition, all lesion types identified in the AD brain except for cored, halo senile plaques were seen

in at least one case from each nonhuman primate group in this study, and AD-relevant Aβ isoforms were identified in each of these lesions (Figures 3.1-3.4). Additionally, while the predilection for CAA in the nonhuman primate brain presents a striking phenotypic difference from AD, the accumulation of vascular Aβ by no means represents a benign peptide aggregation pathway. Rather, CAA is a histopathological hallmark of a family of sporadic and familial human vascular disorders characterized by lobar hemorrhage [146].

Quantification of Aβ Isoforms

A mounting body of evidence implicates buffer-soluble Aβ oligomers in the AD neurodegenerative cascade [100, 258, 294, 297]. Aβ40 and Aβ42 levels have been quantified by ELISA in the cortex, white matter and CSF in numerous studies of nondemented, mild cognitively impaired, and demented humans, revealing an increase in insoluble Aβ42 and a decrease in soluble Aβ42 in the brain as patients progress towards end-stage AD [68, 148, 191, 225, 297]. In the AD and nonhuman primate brain cohorts in this study, we used ELISA to quantify Aβx-40 and Aβx-42 peptides in buffer-soluble cortical extracts (which contains predominantly Aβ monomers and low molecular weight oligomers) and formic acid-soluble extracts made up mostly of solubilized peptides from higher molecular weight Aβ oligomers and Aβ-containing amyloid fibrils. Surprisingly, we found no significant differences in cortical levels of soluble or insoluble, Aβ40 *or* Aβ42 between humans with AD and any of the nonhuman primate groups examined. In fact, with the exception of insoluble Aβ in the chimpanzee temporal cortex, mean soluble and insoluble Aβ levels were higher in all three nonhuman primate groups than in AD cases (Figures 3.5, 3.6). This finding was unexpected in light of our

immunohistochemical data, which indicate that temporal cortical Aβ amyloid accumulation is comparable among AD and nonhuman primate groups, and that there is substantially more total Aβ deposition in the occipital cortex of AD patients than in aged nonhuman primates. These differences may be attributable to variations in tissue preparation, antibody penetration and/or epitope availability between the experimental techniques.

The ratio of Aβ40 and Aβ42 isoforms influences the toxicity of the peptide, and Aβ40, when >1 may actually be protective against Aβ-induced neurotoxicity [135, 176]. Surprisingly, Aβ40:Aβ42 ratios were similar between AD and all nonhuman primate cortical extracts, with the exception of the insoluble fraction of chimpanzee temporal cortex. Aβ40 predominated in soluble fractions, whereas Aβ42 was the predominant insoluble Aβ isoform in all groups. We can conclude from these results that neither the overall quantity of Aβ peptide, nor the ratio of Aβ40:Aβ42, is sufficient to initiate and/or sustain the neurodegenerative cascade seen in AD brain.

Mass Spectrometric Detection of Modified Aβ Isoforms

Full-length Aβ is predominantly 40 and 42 amino acids in length, but the peptide can be truncated at both its N- and C-termini and is also subject to post-translational modifications, including pyroglutamization at a truncated N-terminus and oxidation of the methionine residue [238, 248]. Aβ truncation and post-translational modifications can affect the peptide's disease-relevant properties: toxicity, tendency to aggregate, and solubility [218]. Using highly sensitive MALDI-TOF MS analysis of cerebrospinal fluid from AD and nondemented human patients, Portelius and colleagues identified an AD-

specific “signature” combination of peptides: Aβ1-16, Aβ1-33, Aβ1-39, and Aβ1-42. This fragment signature could be used to distinguish sporadic AD from nondemented patients with a high level of accuracy [225]. Piccini and colleagues used Western blotting to identify and quantify an AD-specific population of soluble Aβ1-42, AβpE3-42, and AβpE11-42 peptides in frontal cortical extracts, and showed that synthetic “AD-like” solutions of these 3 Aβ isoforms had enhanced cytotoxicity when compared to synthetic Aβ peptides prepared in ratios detected in nondemented humans [218].

Using nonhuman primates as a pure model of nontoxic cerebral Aβ accumulation, we employed MALDI-TOF MS to identify Aβ isoforms that may be found uniquely in the AD brain (where they are toxic), or in the nonhuman primate brain (where they are relatively benign, and possibly even protective). We were unable to identify any single Aβ peptide or group of Aβ isoforms that occurred in the majority of AD subjects, but was not found in any nonhuman primate brain. In fact, MALDI spectra from AD and squirrel monkey insoluble extracts were strikingly similar (Figures 3.7, 3.8). The accumulation of numerous cleaved Aβ fragments in the nonhuman primate brain suggests that similar endopeptidases are proteolyzing Aβ aggregates in both AD and nonhuman primates, and that the presence or absence of any of these Aβ fragments may not confer enhanced toxicity to multimeric Aβ *in vivo.*

Multimeric Aβ in AD and Nonhuman Primate Brain

Species-typical phenotypes of cerebral Aβ amyloidosis revealed in our immunohistochemical analyses may be a result of distinct Aβ aggregation pathways in the brains of different primates. It has been shown previously that Aβ dimers and trimers

isolated from the AD brain reduce LTP both *in vitro* and *in vivo*, presumably through the disruption of synaptic transmission [258]. We used Western blotting to identify, in whole cortical homogenates, populations of SDS-insoluble, low molecular weight Aβ oligomers in AD and monkey brain. We identified 8 and 12 kDa SDS-insoluble Aβ multimers in the AD brain, as expected, but we also detected these multimers in several older squirrel monkey subjects (Figure 3.10). However, 12 kDa multimers from squirrel monkey brain exhibited enhanced immunoreactivity to an N-terminal Aβ antibody, as compared to AD brain-derived trimers. Conversely, the 4G8 antibody to Aβ17-24 showed enhanced binding to 12 kDa multimers from the AD brain compared to the squirrel monkey brain. Our immunoblotting data suggest that multimeric Aβ species in humans and aged nonhuman primates have distinct epitope availabilities, possibly due to differences in tertiary folded structure. However, because Aβ aggregates are highly sensitive to experimental manipulation, these experiments should be confirmed with nondenaturing gels in combination with alternative blotting membrane materials.

In additional to the histological and biophysical techniques used in this study, conformational differences in Aβ amyloid can be detected with luminescent conjugated polyelectrolyte probes, which are flexible amyloid-binding ligands that experience a change in emitted fluorescence spectra upon binding to polymorphic amyloid structures [293]. These ligands reveal structural polymorphisms in multimeric Aβ species. Our data suggest that the distinct bioactive properties of Aβ aggregates formed in AD and nonhuman primate brain may be attributable to differences in tertiary structure of peptide multimers. Further *in vitro* and *in vivo* characterization with luminescent conjugated

probes may reveal species differences in the higher-order structure and/or neurotoxicity of naturally-occurring Aβ oligomers.

The toxicity of soluble protein oligomers in Alzheimer's disease may be a common disease mechanism shared by misfolded proteins that underlie several other neurodegenerative diseases, such as Parkinson's disease, Huntington's disease and the prion diseases. The higher-order folded structure of the prion protein confers its toxic properties, and diverse "strains" of folded proteins have distinct toxicities and aggregation dynamics. The nonhuman primate model of cerebral Aβ-amyloidosis may represent naturally occurring strains of aggregated Aβ that form amyloid-related lesions without the toxic intermediates that are seen in AD. The comparative study of these naturally occurring, benign Aβ multimers and the toxic Aβ multimers from the AD brain may help to clarify the nature of the toxic structural motif that is unique to Aβ in humans with AD. Furthermore, as nonhuman primates are relatively resistant to the neurodegenerative proteopathies that affect so many elderly humans, further comparative studies of the aging brain in humans and nonhuman primates may help us understand why the aging human brain is a particularly conducive environment for the formation and propagation of toxic protein oligomers.

Chapter 4

PIB Binding in Aged Primate Brain: Enrichment of High-Affinity Sites in Humans with Alzheimer's Disease[4]

Introduction

The Aβ-cascade hypothesis of Alzheimer's disease (AD) holds that the intracerebral accumulation of multimeric Aβ is a key early event in the pathogenesis of

[4] Reproduced with minor edits from original publication: Rosen, R.F. et al (2009). PIB binding in aged primate brain: Enrichment of high-affinity sites in humans Alzheimer's disease. Neurobiol Aging.

the disease [104]. However, the deposition of Aβ in the human brain is not invariably associated with frank dementia, inasmuch as abundant Aβ lesions sometimes occur in aged humans in the absence of overt cognitive impairment [19, 53]. Nonhuman primates and other mammals produce Aβ that is identical in amino acid sequence to human Aβ, and many species naturally accumulate senile plaques and cerebral β-amyloid angiopathy (CAA) with age [159, 287]. However, no nonhuman species has been shown to exhibit the full behavioral or pathological characteristics of AD [241]. In light of the substantial evidence for a key role of Aβ in the etiology of AD, these findings, along with *in vitro* and *in vivo* studies [180, 216], can be reconciled by the possibility that aggregated Aβ takes the form of polymorphic molecular strains, some of which are more pathogenic than others [160]. The possible existence of functionally heterogeneous protein polymorphs has important implications for understanding the pathogenesis of neurodegenerative disorders such as AD, and for developing specific diagnostic and therapeutic agents. The identification of molecular probes for pathogenic features of Aβ and related molecules will help to address this issue [160].

Pittsburgh compound B (PIB), a synthetic, radiolabeled benzothiazole ligand based on the chemical structure of the amyloid dye Thioflavin-T, has been developed for imaging Aβ deposits *in vivo* by positron-emission tomography (PET) [140, 207]. Radiolabeled PIB binds with high-affinity and high specificity, at concentrations typically achieved in imaging (~1 nM), to Aβ plaques and CAA [13, 123, 139, 154], but only weakly to neurofibrillary tangles and Lewy Bodies [74, 118, 139, 306]. *In vitro* studies have identified high- and low-affinity binding sites on Aβ assemblies [141, 304]. The stoichiometry of high-affinity PIB binding in AD brain homogenates indicates that

PIB binds directly to Aβ amyloid, with more than 500 binding sites per 1000 molecules of Aβ. However, PIB binds at high-affinity with significantly lower stoichiometry (fewer than one binding site per 1000 Aβ molecules) in synthetic Aβ fibril preparations, as well as in deposit-rich, β-amyloid precursor protein (APP)-transgenic mouse brain [141, 167, 257, 275]. With a Kd of 1-2 nM, only the high-affinity PIB binding sites in cerebral Aβ deposits are significantly occupied at the ligand concentrations achieved in PET scans [175].

Several groups have demonstrated only negligible ^{11}C-PIB or ^{18}F-PIB uptake in microPET experiments with APP-transgenic mouse models [141, 257, 275]. Because APP-transgenic mice lack the profound neurodegeneration and cognitive dysfunction seen in AD patients [58, 159], these findings suggest that PIB has the potential to differentiate between pathogenic (AD-related) and relatively benign forms of multimeric Aβ, and possibly to reveal structural characteristics that render Aβ especially toxic in the AD brain. Most current transgenic mouse models express artificially high levels of mutant APP, often coexpressed with mutant presenilin [58]. The majority of these models produce human-type Aβ in the context of endogenous murine Aβ, which is relatively refractory to aggregation and, when co-aggregated with synthetic human-sequence Aβ, reduces *in vitro* PIB binding [125, 305]. Furthermore, in APP-transgenic mouse models, the Aβ deposits lack many of the post-translational modifications that contribute to the insolubility of the lesions in humans [147]. For these reasons, it is important to evaluate PIB binding in longer-lived animal models that naturally form deposits of human-sequence Aβ, such as aged nonhuman primates. We hypothesized that the differential pathogenicity of multimeric Aβ in humans and nonhuman primates is

related to structural variations in the molecule that can be distinguished by the high-affinity binding of PIB. Here we present a quantitative analysis of ^{3}H-PIB binding in postmortem cortical homogenates from AD patients, nondemented elderly humans, aged chimpanzees, rhesus macaques, and squirrel monkeys. Despite levels of Aβ that sometimes exceeded those in AD, high-affinity ^{3}H-PIB binding in nonhuman primates was strikingly less than that in humans with AD, suggesting that PIB might serve as a selective probe for human-specific molecular markers of AD.

Methods

Subjects

We analyzed postmortem brain tissue from 9 rhesus monkeys (*Macaca mulatta*) (3 females, 6 males), 6 squirrel monkeys (*Saimiri sciureus*) (1 female, 5 males), 3 female chimpanzees (*Pan troglodytes*), 9 humans with end-stage AD (6 females, 3 males), and 3 nondemented elderly humans (2 females, 1 male) (Table 4.1). Human tissues were obtained from the Emory University Alzheimer's Disease Research Center Brain Bank in accordance with federal and institutional guidelines, and were coded to ensure the anonymity of subjects. Animal tissues were collected in accordance with federal and institutional guidelines for the humane care and use of experimental animals. The Yerkes Center is fully accredited by AAALAC International.

Preparation of tissue samples

For quantitative biochemical analyses, unfixed, fresh-frozen temporal and occipital cortical tissue blocks were weighed, Dounce-homogenized in 5 volumes of homogenization buffer (50mM Tris-HCl and 150mM NaCl, pH 7.5, containing complete protease inhibitor tablets [Santa Cruz Biochemicals, Santa Cruz, CA, USA]), and stored at -80°C until use. For immunohistochemistry, brains were fixed for at least 7 days in 4%, 0.1M Phosphate-buffered saline (PBS)-buffered paraformaldehyde at 4°C. Temporal and occipital cortical blocks from the contralateral hemisphere were paraffin-embedded, sectioned at 8μm thickness and mounted onto silanized slides. For autoradiography and immunohistochemistry, cryosections from unfixed temporal cortical blocks were cut at 10μm, mounted onto silanized slides, and stored in air-tight containers at -80°C until use.

ELISA quantification of cortical Aβ40 and Aβ42

Cortical homogenates were centrifuged at 100,000g for 60 minutes at 4°C in a TLA 100.4 rotor (Beckman Coulter, Fullerton, CA, USA). The resulting buffer-insoluble pellet was probe-sonicated in 70% formic acid and centrifuged at 16,110g for 60 minutes at 4°C, and the supernatant containing formic acid-solubilized, buffer-insoluble Aβ was retained. Formic acid extracts were neutralized with 1.0M Tris base, pH 11 (1:20 dilution) and diluted in sample buffer. Aβ ending at amino acids 40 or 42 (Aβx-40 and Aβx-42) was measured in each extract by ELISA, using C-terminal specific capture antibodies and an N-terminal specific detection antibody according to the manufacturer's instructions (The Genetics Company, Schlieren, Switzerland). Aβ content is expressed

relative to wet weight of tissue. All samples were assayed in duplicate. After stopping the tetramethylbenzidine-peroxidase reaction with sulfuric acid, plates were read at 450 nm on a Biotek Synergy HT Multidetection plate reader (Biotek, Winooski, VT, USA).

^{3}H-PIB binding assay

PIB binding assays were conducted on the same tissue samples as were the Aβ ELISAs. Cortical homogenates were prepared as described above, at an original concentration of 167 mg wet tissue weight /ml. Homogenates were further diluted 1:33.3 in 0.1M PBS (pH 7.4) to a final concentration of 5mg wet weight/ml. In a 96 well polypropylene plate, 20µl of diluted homogenate (100µg wet tissue weight) were added to each of duplicate wells. 200µl of 1 nM ^{3}H-PIB (SA=82 Ci/mmol, custom synthesis, GE Healthcare, UK) were quickly added to each well. Samples were incubated at ambient temperature for 2.5 hours, without shaking, transferred to a 96 well Multiscreen HTS Hi Flow FB filter plate, and filtered with a vacuum manifold (Millipore Corporation, Bedford, MA, USA). Nonspecific binding was defined as the counts retained in the presence of 1 µM unlabeled PIB. Kd and Bmax values were determined for all groups using a competition binding assay with a constant concentration of 1.2nM ^{3H}-PIB and concentrations of unlabeled PIB between 0.1 nM and 1.0 µM. Filters were rapidly washed with 4 X 200µl of PBS at room temperature and dried on the manifold, after which 50µl of MicroScint 20 scintillation fluid (PerkinElmer, Waltham, MA, USA) was added to each well. After 24 hours incubation on an orbital shaker, ^{3}H-PIB binding was quantified in a TopCount scintillation counter (PerkinElmer) and specific binding was calculated by subtracting nonspecific counts per minute (CPM). Using 1 nM ^{3}H-

PIB, ligand binding was linear between 25 and 150μg wet weight AD tissue per well. CPMs were converted to femtomoles using an experimentally-determined 15% counting efficiency in the scintillation counter. Similar results were obtained when the filters were placed in vials and counted with scintillation fluid. Finally, to determine whether species-specific molecules might enhance or inhibit ^{3}H-PIB binding, we performed this *in vitro* binding assay using 1:1 mixtures of AD and nonhuman primate cortical homogenates.

Immunohistochemistry

The following antibodies were used for immunohistochemistry: Monoclonal antibodies 6E10 and 4G8 to residues 3-8 and 17-24 of the Aβ peptide, respectively (both at 1:5000; Covance Research Products, Denver, PA, USA); rabbit polyclonal antibodies R361 and R398 to C-terminal residues 32-40 and 33-42 of Aβ40 and Aβ42, respectively (both at 1:15,000; provided by Dr. Pankaj Mehta, Institute for Basic Research on Developmental Disabilities, Staten Island, NY, USA); monoclonal antibodies CP13 to phospho-tau 202 (1:10,000), PHF1 to phospho-tau 396/404 (1:10,000), and MC1 to aggregated tau (1:10,000) (all provided by Dr. Peter Davies, Albert Einstein College of Medicine, Bronx, NY, USA); and monoclonal antibody AT8 to phospho-tau 202/205 (1:5000; Covance) [241]. Vectastain Elite kits (Vector Laboratories, Burlingame, CA, USA) were used for avidin-biotin complex (ABC)-based horseradish peroxidase immunodetection of antigen-antibody complexes.

Endogenous peroxidase was inactivated with 3% H_2O_2 in methanol, and nonspecific reagent binding was blocked with 2% normal horse serum (for monoclonals)

or normal goat serum (for polyclonals) in 0.2% Tween 20 in PBS (blocking solution) for one hour at room temperature. For Aβ-immunodetection, sections were pretreated for 10 minutes with 100% formic acid to expose antigenic sites and then incubated in primary antibody (diluted in blocking solution) overnight at 4°C. After rinsing, sections were placed for one hour at room temperature in biotinylated secondary antibody (1:200 in blocking solution), rinsed, immersed for 30 minutes in avidin-biotin complex, and then developed with 3,3'-diaminobenzidine (DAB) (Vector Laboratories). Tissue from pathologically verified human AD cases was used as positive control material, and non-immune mouse IgG or rabbit serum was used in place of the primary antibodies as negative controls. In some instances, a hematoxylin counterstain was applied after immunostaining.

Aβ load was assessed histopathologically in 6E10-immunostained sections of temporal and occipital cortices. For each section, two researchers rated the levels of diffuse plaques, compact plaques, and CAA in capillaries and large vessels (+++ frequent, ++ moderate, + rare, - absent) [165].

^{3}H-PIB autoradiography

Cryosections were thawed for 10 minutes, immersed in 10% ethanol for 20 minutes, and incubated for 1 hour in 1.0nM ^{3}H-PIB in 5% ethanol/PBS, at room temperature. Nonspecific binding was determined in the presence of 1.0μM unlabeled PIB. Sections were then quickly rinsed twice with 10% ethanol and twice with deionized water, both at 4°C. After drying under a cold air stream, sections were directly apposed to Hyperfilm ^{3}H (GE Amersham, UK). After a 2-week exposure, film was developed

with D19 developer solution (Kodak, New Haven, CT) and images were captured with a QICAM digital camera (QImaging, BC, Canada). Except for size cropping, images were not digitally manipulated prior to publication.

For confirmation of Aβ deposition in the regions analyzed by autoradiography, adjacent cryosections were fixed for 30 minutes in 70% ethanol at room temperature and immunohistochemistry with antibody 6E10 was performed as described above, except that the sections were incubated in 100% formic acid for 2 minutes.

Statistical analysis

Analysis of variance (ANOVA) was used to determine group differences in insoluble Aβ levels between AD and the three nonhuman primate groups. ANOVA also was used to assess potential group differences in PIB binding among the nonhuman primates. Because PIB binding did not differ significantly among the three nonhuman primate species in either the temporal or occipital cortical samples (see also Figure 4.2), and because of the small number of samples in some groups, we combined the nonhuman primate cases for subsequent analyses, in which we conducted nonparametric Mann-Whitney U tests (two-tailed, CI=95%) to compare PIB binding between humans with AD and nonhuman primates. We also employed nonparametric Mann-Whitney U tests to compare PIB binding between AD and nondemented human cases and between nondemented human cases and nonhuman primates. For the determination of PIB binding site characteristics in cortical homogenates, we conducted a curve-fit analysis of the displacement binding data using a nonlinear homologous competition equation. To assess the relationship between PIB binding and insoluble Aβ in the temporal and

occipital cortices of AD cases, we applied the two-tailed Pearson product-moment correlation coefficient (Pearson's *r*, CI=95%). For the homogenate “mixing experiments” (Figure 3.4), we used ANOVA followed by post-hoc t-tests to detect possible synergistic effects of mixing cortical homogenates on PIB binding levels.

Tables

Table 4.1. Case List

Group	Case	[Δ]Age(y)	Sex	[§]PMI(h)	Braak Stage	*ApoE
ND Human	E04-46	40	m	31	Braak 0	3/4
	E04-34	57	f	17	Braak 0	3/3
	OS02-35	75	f	6	Braak 0	3/3
Human AD	E04-33	57	f	20	Braak V/VI	3/4
	E04-172	87	f	6	Braak V/VI	3/4
	OS03-300	75	f	12	Braak V/VI	4/4
	OS02-159	61	m	5.5	Braak V/VI	3/4
	OS01-128	91	f	2.5	Braak V/VI	3/4
	OS02-106	81	f	2	Braak >IV	3/3
	E05-87	61	m	4	Braak V/VI	3/4
	E08-41	84	m	4.5	Braak VI	3/4
	E05-04	64	f	4.5	Braak VI	3/4
Chimpanzee	YN06-108Pt	44	f	3		
	YN07-25Pt	47	f	1		
	YN05-400Pt	41	f	1		
Rhesus macaque	06-1Mm	35	f	<3		
	AM109	26.6	m	1		
	AM120	26.5	f	1		
	554	38	m	<3		
	1201	35	m	<3		
	1203	33	f	<3		
	1210	30	m	<3		
	1211	25	f	<3		
	1313	>20	m	<3		
Squirrel monkey	84L	21	m	1		
	83GO	20	m	1		
	86J	17	m	1		
	06-5Ss	23	f	<3		
	90T	17	m	1		
	92AH	15	m	1		

[Δ]Age (y): Age (years)

[§]PMI (h): Postmortem interval (hours)

*ApoE: Apolipoprotein E genotype

Table 4.2. Histopathological assessment of Aβ-plaques and cerebral amyloid angiopathy

		Temporal Cortex				Occipital Cortex			
Group	**Case**	**DP**	**CP**	**CaAA**	**LVAA**	**DP**	**CP**	**CaAA**	**LVAA**
ND Human	E04-46	-	-	-	-	-	-	-	+
	E04-34	-	-	-	-	-	-	-	-
	OS02-35	-	-	-	-	-	-	-	-
Human AD	E04-33	++	+++	++	+	++	+++	+	+
	E04-172	+++	+++	++	++	++	+++	+	+
	OS03-300	+++	+++	+	++	+++	+++	++	++
	OS02-159	+++	+++	++	++	+++	+++	++	++
	OS01-128	+++	+	+	-	+++	+++	++	++
	OS02-106	++	++	+	+	++	++	++	++
	E05-87	+++	+++	+	++	n/a	n/a	n/a	n/a
	E08-41	+++	+++	+	+	n/a	n/a	n/a	n/a
	E05-04	++	+++	-	+	n/a	n/a	n/a	n/a
Chimpanzee	YN06-108Pt	-	-	+	++	-	-	++	++
	YN07-25Pt	-	+	+	+	n/a	n/a	n/a	n/a
	YN05-400Pt	-	+	++	+	n/a	n/a	n/a	n/a
Rhesus macaque	06-1Mm	++	+	+	+	+++	++	+++	++
	AM109	n/a	n/a	n/a	n/a	n/a	n/a	n/a	n/a
	AM120	n/a	n/a	n/a	n/a	n/a	n/a	n/a	n/a
	554	n/a	n/a	n/a	n/a	++	-	+	-
	1201	n/a	n/a	n/a	n/a	+++	++	++	++
	1203	n/a	n/a	n/a	n/a	++	+	++	++
	1210	n/a	n/a	n/a	n/a	+	-	-	+
	1211	n/a	n/a	n/a	n/a	n/a	n/a	n/a	n/a
	1313	n/a	n/a	n/a	n/a	+	-	++	-
Squirrel monkey	84L	++	++	+++	+	-	-	+	++
	83GO	-	++	++	++	++	+	++	+++
	86J	+++	++	++	+	n/a	n/a	n/a	n/a
	06-5Ss	+++	++	++	+	-	-	++	+
	90T	++	+++	++	++	++	-	+	++
	92AH	++	+	++	+	-	-	-	+

DP: Diffuse plaques

CP: Compact plaques

CaAA: Capillary amyloid angiopathy

LVAA: Large vessel amyloid angiopathy

n/a: Not available

Table 4.3. Insoluble Aβ levels and PIB binding (fmol /100µg wet weight tissue)

		Temporal Cortex				Occipital Cortex			
Group	**Case**	**Aβ40**	**Aβ42**	**Total Aβ**	**PIB binding**	**Aβ40**	**Aβ42**	**Total Aβ**	**PIB binding**
ND Human	E04-46	0	1	1	0	0	1	1	0
	E04-34	0	0	0	1	0	0	0	1
	OS02-35	0	0	0	0	0	1	1	0
Human AD	E04-33	3	83	86	17	2	211	213	31
	E04-172	8	217	225	17	11	176	187	18
	OS03-300	62	98	160	26	5	187	192	34
	OS02-159	40	175	215	23	15	298	313	43
	OS01-128	18	196	214	35	10	191	202	24
	OS02-106	1	146	146	10	0	59	60	24
	E05-87	275	353	628	26	n/a	n/a	n/a	n/a
	E08-41	4	156	160	25	n/a	n/a	n/a	n/a
	E05-04	4	445	449	22	n/a	n/a	n/a	n/a
Chimpanzee	YN06-108Pt	15	93	109	3	249	179	428	0
	YN07-25Pt	0	24	24	1	1	62	63	0
	YN05-400Pt	10	69	79	0	n/a	n/a	n/a	n/a
Rhesus macaque	06-1Mm 100	250	350	2		15	190	205	2
	AM109	n/a	n/a	n/a	n/a	0	29	29	2
	AM120	n/a	n/a	n/a	n/a	0	18	19	2
	554	n/a	n/a	n/a	n/a	7	24	31	0
	1201	n/a	n/a	n/a	n/a	843	487	1330	0
	1203	n/a	n/a	n/a	n/a	10	228	238	2
	1210	n/a	n/a	n/a	n/a	0	104	105	2
	1211	n/a	n/a	n/a	n/a	2	90	93	0
	1313	n/a	n/a	n/a	n/a	0	67	67	0
Squirrel monkey	84L	367	230	597	1	396	618	1014	3
	83GO	497	252	750	0	1121	508	1629	3
	86J	8	91	99	3	1	174	176	3
	06-5Ss	19	318	337	1	26	370	396	1
	90T	3	357	360	1	43	178	221	0
	92AH	0	51	52	1	0	2	2	3

n/a: Not available

Figures

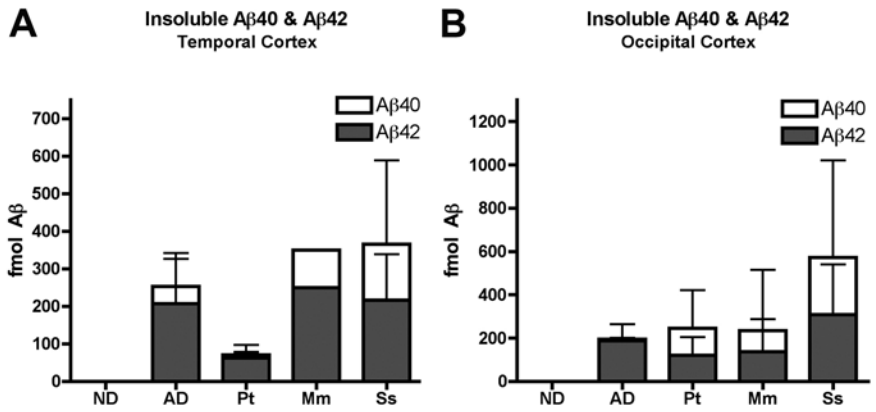

Figure 4.1. ELISA quantitation of insoluble Aβx-40 and Aβx-42 in temporal (A) and occipital (B) cortical homogenates from aged humans and nonhuman primates.

A: Insoluble Aβ in temporal cortex (ND, n=3; AD, n=9; Chimpanzee, n=3; Rhesus macaque, n=1; Squirrel monkey, n=6). Mean Aβ42 levels were higher than Aβ40 levels in the temporal cortex of all 4 groups. **B**: Insoluble Aβ in occipital cortex (ND, n=3; AD, n=6; Chimpanzee, n=2; Rhesus macaque, n=9; Squirrel monkey, n=6). In nonhuman primates, the occipital cortical Aβ40:Aβ42 ratio was somewhat higher than in AD. However, no statistically significant differences in Aβ levels were detected between AD and nonhuman primate groups in either cortical region. ND: Nondemented human; AD: Alzheimer's disease; Pt: *Pan troglodytes* (Chimpanzee); Mm: *Macaca mulatta* (Rhesus macaque); Ss: *Saimiri sciureus* (Squirrel monkey). Bars = standard deviations.

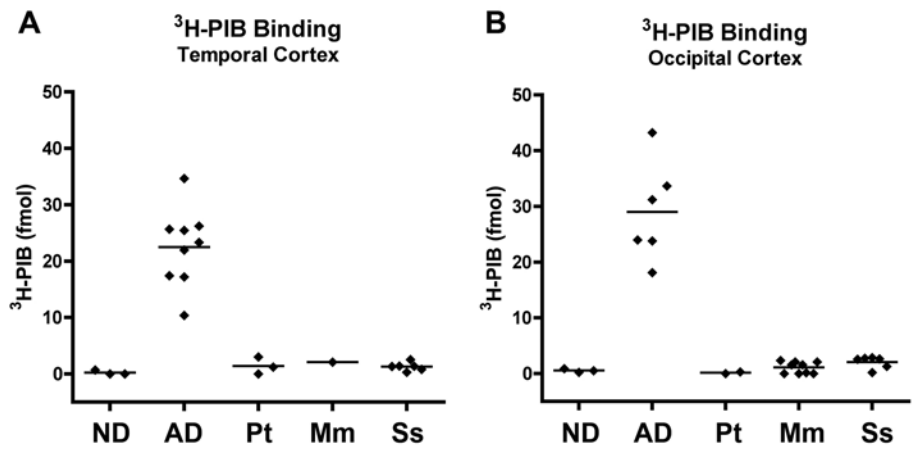

Figure 4.2. **Postmortem quantification of ^{3}H-PIB binding in cortical homogenates from aged humans and nonhuman primates.** Despite comparable mean levels of insoluble Aβ, ^{3}H-PIB (1 nM) binding is low to undetectable in aged nonhuman primate temporal (**A**) and occipital (**B**) cortices compared to the same regions from humans with Alzheimer's disease. (AD vs. nonhuman primates, temporal cortex [Mann-Whitney]: $p<0.0001$, occipital cortex: $p=0.0004$). Note also the low binding of PIB in nondemented control humans (ND vs. AD, temporal cortex: $p=0.0091$, occipital cortex: $p=0.0238$). No significant difference in PIB binding was detected between nondemented humans and nonhuman primates. [Temporal cortex: ND, n= 3; AD, n=9; Chimpanzee, n=3; Rhesus macaque, n=1; Squirrel monkey, n=6. Occipital cortex: ND, n=3 ; AD, n=6; Chimpanzee, n=2; Rhesus macaque, n=9; Squirrel monkey, n=6]. ND: Nondemented human; AD: Alzheimer's disease; Pt: *Pan troglodytes* (Chimpanzee); Mm: *Macaca mulatta* (Rhesus macaque); Ss: *Saimiri sciureus* (Squirrel monkey). Bars = means.

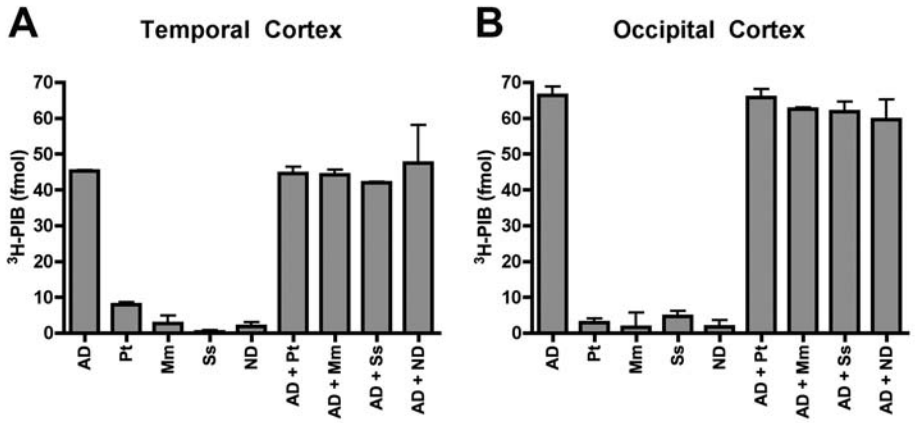

Figure 4.3. Cortical homogenate mixing experiments do not indicate a species-specific factor that modulates ^{3}H-PIB binding in aged humans or nonhuman primates. Homogenates from AD temporal (A) and occipital (B) cortices (100μg tissue) were incubated with temporal and occipital cortical homogenates (100μg tissue) from nondemented humans, chimpanzees, rhesus macaques, and squirrel monkeys in an *in vitro* ^{3}H-PIB binding assay. The amount of ligand binding to homogenate mixtures approximately equaled the sum of ^{3}H-PIB binding to each mixture component, indicating an absence of species-specific, auxiliary factors that enhance or suppress PIB binding. ND: Nondemented human; AD: Alzheimer's disease; Pt: *Pan troglodytes* (Chimpanzee); Mm: *Macaca mulatta* (Rhesus macaque); Ss: *Saimiri sciureus* (Squirrel monkey). Bars = Standard deviations.

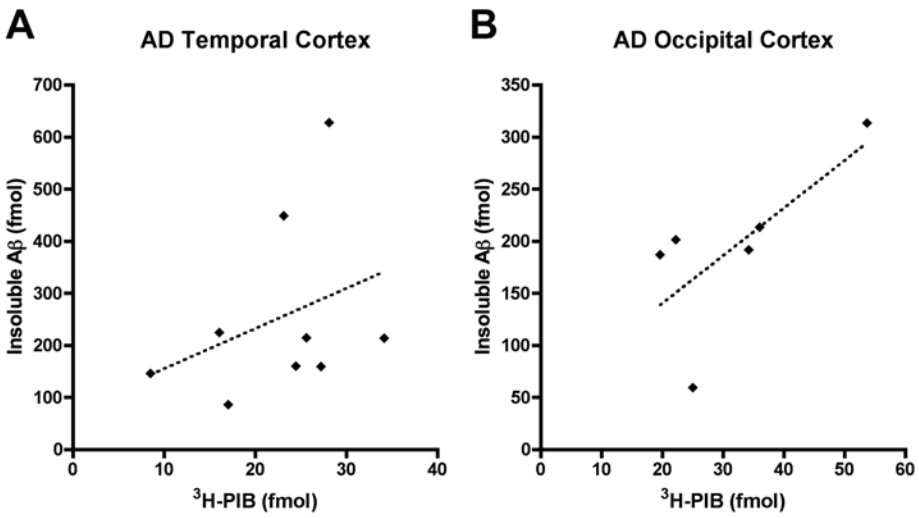

Figure 4.4. Relationship between insoluble Aβ levels and ^{3}H-PIB binding in AD cortical homogenates. Total levels of insoluble Aβ (Aβ40 and Aβ42) correlate positively with ^{3}H-PIB binding to AD temporal and occipital cortical homogenates. The correlation was not statistically significant in either cortical region, however (temporal cortex, r=0.3417, p=0.3682; occipital cortex, r=0.7088, p=0.1149).

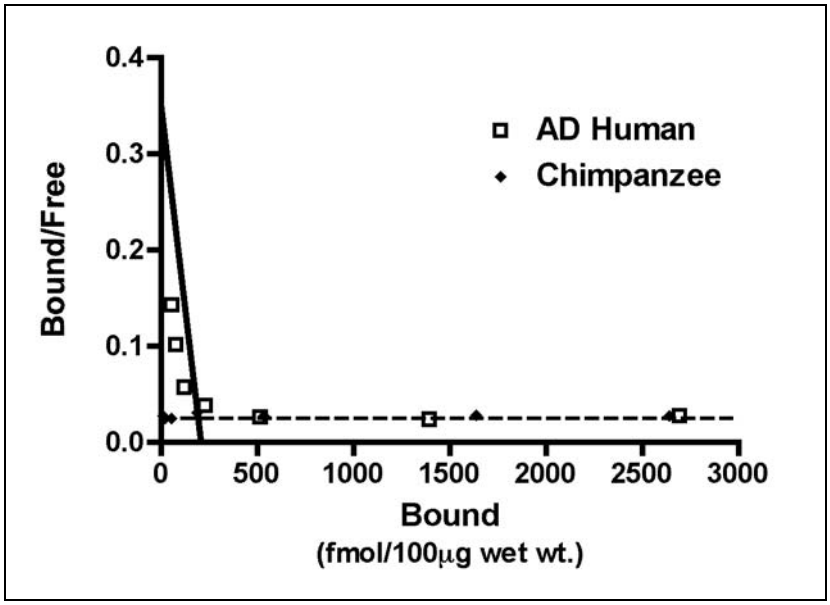

Figure 4.5. Analysis of high-affinity ^{3}H-PIB binding in AD and chimpanzee cortical homogenate. A homologous competition binding analysis with 1.2nM ^{3}H-PIB and unlabeled PIB between 1.0 nM and 1.0μM reveals a high-affinity PIB binding component in AD temporal cortical homogenate (Kd = 3.0nM, Bmax = 209.28 fmol/100μg wet tissue) but no detectable high-affinity PIB binding components in chimpanzee temporal cortical homogenate (AD human: open squares, Chimpanzee: filled diamonds). Similar results were seen with rhesus macaque and squirrel monkey cortical homogenates (data not shown).

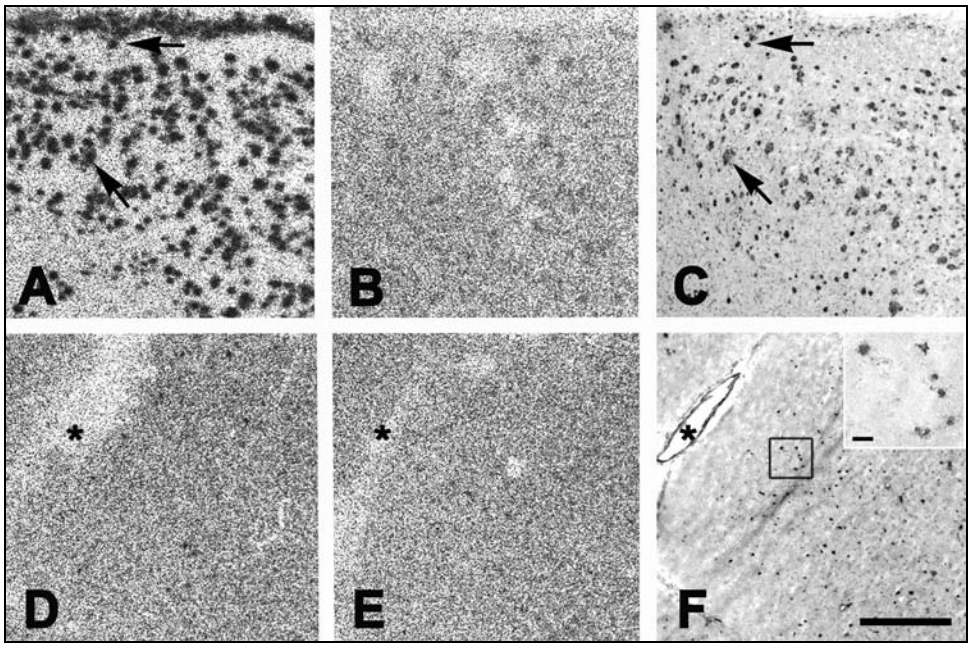

Figure 4.6. ^{3}H-PIB Autoradiography in AD and aged squirrel monkey cortical tissue sections. 1.0nM ^{3}H-PIB binds to Aβ lesions throughout the cortex and, to a lesser extent, in the white matter of AD temporal cortical cryosections (**A**). This binding is mostly, but not entirely, blocked by 1μM unlabeled PIB (**B**), and corresponds to 6E10-immunoreactive Aβ lesions in adjacent cryosections (arrows in **A** and **C**). In cryosections from squirrel monkey temporal cortex, negligible ^{3}H-PIB binding is detected (**D**), despite the presence of heavy vascular and parenchymal Aβ deposition, as shown with 6E10 immunohistochemistry in adjacent cryosections (**F**) (asterisks denote the same large blood vessel in panels D-F). Note that the Aβ-positive lesions in squirrel monkeys consist largely of microvascular deposits and small parenchymal plaques (**inset** in F), as previously described [63]. When ^{3}H-PIB was incubated in the presence of 1μM unlabeled PIB, binding was mostly blocked (**E**); however, as in the AD cases, ^{3}H-PIB binding was mostly, but not entirely eliminated by unlabeled PIB. Bar in F = 1mm for panels A-F; bar in the inset = 50μm.

Results

Aβ and tau pathology in human and nonhuman primate brain

Immunohistochemistry with antibodies to Aβ revealed species-typical Aβ-immunoreactivity patterns in cortical sections from every AD and aged nonhuman primate subject examined in this study, whereas the nondemented humans were largely devoid of Aβ-lesions (Table 4.2). Humans with AD showed abundant parenchymal Aβ deposits, as well as occasional CAA, whereas the aged nonhuman primates displayed relatively more CAA accompanied by parenchymal Aβ deposits. Immunohistochemistry using antibodies to pathological forms of tau revealed widespread neurofibrillary tangles in all AD cases examined. We detected little or no aberrant tau immunoreactivity in the nondemented humans or in the nonhuman primates, with the exception of one aged chimpanzee (Y05-400Pt) that presented with tauopathy in addition to moderate CAA, as previously described [241].

Quantification of Aβ40 and Aβ42

Because previous studies have shown that PIB binding positively correlates with the levels of buffer-insoluble, but not soluble Aβ [13, 118, 141, 143, 263], our quantitative analysis focused on insoluble Aβ, which constitutes the great majority of the protein in senile plaque cores and CAA. We found that Aβ40 and Aβ42 accumulate in the aged nonhuman primate brain to similar or higher levels than in the end-stage AD brain; by ELISA of temporal cortical samples, aged squirrel monkeys had higher mean levels of total insoluble Aβ than did the AD cases (365.6 fmol/100μg wet tissue [n=6,

SD=272.48 fmol] vs. 253.58 fmol/100μg [n=9, SD=172.91 fmol], respectively). Mean levels of total Aβ in nondemented human (n=3), rhesus macaque (n=1) and chimpanzee (n=3) temporal cortex were 0.41 fmol/100μg wet tissue (SD=0.51 fmol), 349.95 fmol/100μg, and 70.43 fmol/100μg (SD=42.76 fmol), respectively (Figure 4.1). In the occipital cortex, total insoluble Aβ levels in nonhuman primates were consistently higher than in AD (AD mean=194.49 fmol/100μg wet tissue [n=6, SD=81.02 fmol], chimpanzee mean=245.62 fmol/100μg [n=2, SD=257.7 fmol], rhesus macaque mean=235.06 fmol/100μg [n=9, SD=417.68 fmol], squirrel monkey mean=573.01 fmol/100μg [n=6, SD=624.28 fmol]) (Figure 4.1). Statistically, however, Aβ levels did not differ significantly between the AD cases and the nonhuman primates in either cortical region, probably because of the high inter-individual variability in the groups.

Because a predominance of the Aβ42 isoform has been implicated in the toxicity and aggregability of the peptide in AD brain [107, 176], we calculated the Aβ40:Aβ42 ratios for each case and cortical region. Overall, Aβ42 was more abundant than was Aβ40 in both cortical regions of the humans and nonhuman primates, although the relative levels of Aβ40 in the occipital cortex were somewhat higher in the nonhuman primates (Figure 4.1). The Aβ40:Aβ42 ratio was less than 1.0 in every AD case examined, and exceeded 1.0 in at least one cortical region of only four nonhuman primates (YN06-108Pt, 1201, 84L and 83G0; see Table 3).

In vitro ^{3}H-PIB binding

The binding of one nanomolar ^{3}H-PIB was strikingly less in cortical homogenates from all nonhuman primates compared to samples from the AD cases (temporal cortex:

p<0.0001; occipital cortex: p=0.0004). We found high levels of specific PIB binding in the AD cases (temporal cortex: mean = 22.48 fmol/100μg wet tissue [SD=6.91], occipital cortex: mean = 29.01 fmol/100μg wet tissue [SD=8.93]) that correlated positively, but not significantly, with the amount of Aβ measured by ELISA (temporal cortex, r=0.3417, p=0.3682; occipital cortex, r=0.7088, p=0.1149) (Figure 4.4). PIB binding in the AD cases was consistently greater in occipital cortex than in temporal cortex, despite similar or lower levels of Aβ in this region by ELISA (Figures 4.1, 4.2). Nonlinear regression analysis of the homologous competition binding data reveals a Kd of 3.0 nM and Bmax of 209.28 fmol/100ug wet tissue for high-affinity PIB binding sites in AD temporal cortex, and a Kd of 3.0nM and Bmax of 234.48 fmol/100ug wet tissue for the ligand in AD occipital cortex (Figure 4.5). We were unable to detect a high-affinity binding site in cortical homogenates from any of the three nonhuman primate groups.

In the nonhuman primates, only background PIB binding was observed in temporal and occipital cortices of all subjects examined (Table 4.2; temporal cortex: mean = 1.41 fmol/100μg wet tissue [SD=0.93], occipital cortex: mean = 1.33 fmol/100μg [SD=1.15]), even though the levels of total Aβ in most simians were at least as high as those in the AD brain (Figure 4.1). In the cerebellar cortex, which is relatively unaffected by Aβ plaque deposition or neurodegeneration, only background levels of ^{3}H-PIB binding were detected in the AD cases (data not shown).

To address the possibility that species-specific molecules might enhance or inhibit ^{3}H-PIB binding, we performed the same *in vitro* binding assay with 1:1 mixtures of AD and nonhuman primate cortical homogenates. There was only an additive effect of

combining homogenates from AD cases with those from the nonhuman primates (Figure 4.3), indicating an absence of species-specific binding-modulatory factors.

^{3}H-PIB autoradiography

To determine if ^{3}H-PIB binds to a particular subset of amyloid lesions in AD or nonhuman primate brain, we performed ^{3}H-PIB autoradiography on unfixed cryosections from the superior temporal gyrus of nondemented human, AD, and squirrel monkey subjects (n=2 for all groups). At the same ligand concentration used in the cortical homogenate binding assays (1.0 nM), we detected strong, specific binding to a broad morphological range of senile plaques in the grey matter of the AD superior temporal gyrus (Figure 4.6) but not to neurofibrillary tangles (data not shown). PIB also bound to a smaller number of lesions in the subcortical white matter (Figure 4.6). In the two squirrel monkey cases examined, we did not detect specific ^{3}H-PIB binding to any Aβ lesions, despite heavy cortical and vascular amyloid deposition in both cases, as shown by Aβ immunohistochemistry of adjacent cryosections (Figure 4.6). No ^{3}H-PIB binding was detected in cortical sections from nondemented human subjects who lacked Aβ deposition (data not shown).

Discussion

We describe the first evidence that Pittsburgh compound B (PIB), a high-affinity molecular probe for Aβ deposits in the AD brain, binds at substantially diminished stoichiometry to cortical homogenates from aged nonhuman primates, despite total Aβ levels equal to, or greater than, the levels measured in AD brains. The virtual absence of

PIB binding in monkeys and chimpanzees under the conditions that we employed suggests a paucity of high-affinity PIB binding sites on Aβ multimers in nonhuman primates, similar to that reported for APP/presenilin-1-transgenic mice [141]. Klunk, Lockhart, and colleagues have provided evidence for high- and low-affinity PIB binding sites located within the fibrillar Aβ assembly [143, 166]. The AD brain contains approximately 500-fold more high-affinity PIB binding sites per Aβ molecule than does synthetic Aβ or Aβ from transgenic mouse brains [141]. In the present study, PIB binding to nonhuman primate cortical homogenates was negligible at a 1 nM ligand concentration, which is selective for the high-affinity PIB binding sites that are the primary target in PET studies [139]. To the best of our knowledge, this is the first report of deficient PIB binding to cortical tissue containing profuse, naturally occurring Aβ plaques and cerebral β-amyloid angiopathy. Our findings suggest that, unless ultra-high specific-activity PIB is used [167], PIB would not be an effective β-amyloid imaging agent in nonhuman primates [206], even in aged animals with heavy Aβ deposition.

The dearth of high-affinity cortical PIB binding sites in simians may be attributable to structural variants of multimeric Aβ. *In vitro* [216] and *in vivo* [180] evidence increasingly favors the existence of polymorphic Aβ multimers, analogous to structurally and functionally diverse prion strains [42, 45, 170]. Under different *in vitro* conditions, distinct Aβ strains, distinguishable by biophysical and/or imaging techniques, can be generated from the identical starting peptide [216]. *In vivo*, morphologically distinct Aβ-deposits can be seeded in the brains of transgenic mice by Aβ-rich cortical extracts from different types of APP-transgenic mice [180]. Our findings support the

hypothesis that Aβ can form polymorphic molecular assemblies that are distinguishable by their PIB-binding characteristics.

Histological observations using the fluorescent PIB analog, 6-CN-PIB, further indicate that PIB binds selectively to a structural motif within fibrillar Aβ assemblies. Denaturation of proteins in cortical tissue sections from AD cases abolishes the binding of 6-CN-PIB [118], indicating a conformation-sensitive binding substrate for PIB. Diffuse Aβ plaques in the cerebellum (a region of the brain that usually shows little degenerative change in AD) do not bind 6-CN-PIB or unlabeled PIB in AD cases [118, 263], suggesting variations in the molecular structure of these lesions even within the same case. 6-CN-PIB binds to a subset of extracellular neurofibrillary tangles in AD tissue sections [118], but these 'ghost' tangles also can be immunoreactive for Aβ [292], and the 6-CN-PIB concentrations used for histostaining are 100- to 10,000-fold higher than the brain concentrations attained in PET studies. This and other autoradiographic studies show that ^{3}H-PIB does not bind to neurofibrillary tangles at a 1-nanomolar concentration [165]. The high selectivity of PIB for aggregated Aβ, as opposed to tau (neurofibrillary tangles) or α-synuclein (Lewy Bodies) [74, 118, 143], makes it unlikely that the strong PIB signal in human AD brain is due to the presence of such lesions, which are rare or nonexistent in most nonhuman primates. Furthermore, one aged chimpanzee that we examined (YN05-400Pt) had significant tauopathy [241], but the ^{3}H-PIB binding in this case was very low, similar to that in nonhuman primates that were mostly devoid of tauopathy (Table 4.3).

In the present study, PIB binding to AD brain homogenates correlated positively with total insoluble Aβ, as previously reported [118, 141, 263]. The variability in

published reports of PIB binding levels and insoluble Aβ levels in AD cortical homogenates may be attributable to the heterogeneity of Aβ deposition among brain regions and among individuals [283], and/or to minor differences in the assay conditions in different laboratories. In these four studies, quantitative Aβ ELISAs were performed with different capture and detection antibody pairs, on insoluble Aβ samples prepared with distinct buffers and extraction techniques. Further, our ^{3}H-PIB assay employed a scaled-down microplate version of the cell harvester protocols utilized in the other studies. Importantly, the positive correlation between PIB binding and Aβ levels in our study confirms previous findings, and supports the view that PIB is a useful probe for the pathologic accumulation of Aβ in the human brain.

In autoradiographic experiments using the same tracer levels and specific activity employed in our binding assays, ^{3}H-PIB specifically labels a wide morphological variety of Aβ deposits in cortex and subcortical white matter of AD cases, but not of squirrel monkeys. The intensity of binding is not explained by the unique presence of a particular fragment of Aβ, since previous MALDI-TOF mass-spectrometric studies indicate that all Aβ fragments, including pyroglutamate Aβ pE3-40 and pE3-42, are present in the neocortices of humans with AD and aged nonhuman primates [242]. The ratio of Aβ40:Aβ42 could influence PIB binding[141], but our ELISA data indicate that the relative amounts of Aβ peptides ending at amino acids 40 and 42 are largely similar in human and nonhuman primates, especially in the temporal neocortex. Together, these data strengthen the hypothesis that high-affinity PIB binding is dependent upon quaternary structural motifs of assembled fibrillar Aβ, and thus the high-affinity binding element may not be quantifiable with techniques that detect only histologic or primary

structural characteristics of the Aβ peptide. Finally, our homogenate-mixing experiments (as well as those of Klunk et al, 2005) do not support the existence of a species-specific factor that modulates PIB binding.

In summary, we show that high-affinity PIB binding sites are significantly deficient in Aβ-rich cortical extracts from aged nonhuman primates compared to extracts from humans with Alzheimer's disease. Considerable evidence supports a central role for Aβ in AD neurodegeneration [104], yet AD-like dementia has not been reported in any nonhuman primate [287]. PIB thus could be a useful experimental tool for clarifying the molecular underpinnings of the uniquely human predisposition to Alzheimer's disease.

Chapter 5

Deficient High-Affinity Binding of Pittsburgh Compound B in a Case of Alzheimer's Disease[5]

Introduction

Radiolabeled Pittsburgh compound B (PIB; [N-methyl-^{11}C]2-(4'-methylaminophenyl)-6-hydroxybenzothiazole) is a promising *in vivo* imaging agent that can bind with high affinity, specificity and stoichiometry to parenchymal amyloid-β deposits [140, 207, 244] and cerebral β-amyloid angiopathy (CAA) [13, 123] in patients with Alzheimer's disease (AD). Positron-emission tomography (PET) imaging studies

[5] Reproduced with minor edits from original publication: Rosen, R.F. et al (2009). Deficient high-affinity PIB binding in case of Alzheimer's disease. Acta Neuropath, *accepted.*

indicate that ^{11}C-labeled PIB rapidly enters the brain, where it is retained significantly longer in Aβ-rich regions than in brain areas that lack Aβ deposits [140, 207]. Thus, PIB may be a useful tool to aid in the diagnosis of AD plaque pathology in living patients [184, 219].

Evaluation of post-mortem or biopsied brain samples from patients who exhibited cortical PIB retention in PET scans indicates that PIB binding *in vivo* correlates with heavy cerebral Aβ deposition [13, 118, 154]. However, some instances of unexpectedly high uptake in nondemented cases [244], or unexpectedly low retention in clinically diagnosed AD cases [62, 140, 162, 197], have been reported, and some Aβ lesions appear to be refractory to PIB binding [118, 264]. Studies *in vitro* and in animal models furnish additional evidence that, at nanomolar concentrations similar to those achieved in PET imaging, PIB does not bind to all multimeric assemblies of Aβ equally [141, 243, 264]. Specifically, the density of high-affinity PIB binding sites per molecule of Aβ is much lower in β-amyloid precursor protein (APP)-transgenic mice [141] and in normal aged nonhuman primates [243] compared to AD patients, despite profuse cerebral Aβ deposition in the animal models.

These experiments suggest that PIB may recognize a polymorphic molecular site on multimeric Aβ that is enriched in human AD cases but is altered or concealed in nonhuman species [160, 243]. The occasionally weak correlations between PIB binding and Aβ levels [62, 140, 162, 197, 243, 244] and the presence of poorly binding lesions in some brain regions [118, 264] suggest the possible existence of polymorphic Aβ aggregates in humans as well. Here we report a case of clinically and pathologically confirmed AD with heavy Aβ burden yet strikingly reduced high-affinity PIB binding *in*

vitro compared to a series of nine other AD cases. This finding raises the possibility that some cases of clinicopathologically verifiable AD might not show significant retention of radiolabeled PIB in diagnostic PET scans, and further suggests that PIB can discriminate among naturally-occurring, polymorphic forms of multimeric Aβ in humans.

Materials and Methods

Subject

A 72 year-old woman (case AD1) was clinically diagnosed with possible Alzheimer's disease four years prior to death. Her initial symptoms began six years prior to her diagnosis, and included impairments in short-term memory and visuospatial function. Neuropsychological testing corroborated these findings, and she experienced a gradual worsening of cognition in the subsequent years, in addition to worsening gait disturbance and incontinence. Nine years after her initial symptoms, she underwent ventriculoperitoneal shunt placement for possible normal pressure hydrocephalus. Her family reported transient improvement in her gait and incontinence, which then regressed within one month of the shunt placement, possibly due to shunt malfunction. Subsequent shunt revisions did not improve her symptoms, and she died shortly thereafter. Aside from her mother, who had Parkinson's disease but normal cognition, she had no family history of dementia or other neurodegenerative diseases.

At autopsy, the brain weighed 1110 grams and showed no significant atrophy over the convexity. Vessels of the circle of Willis showed mild-to-moderate, patchy

atherosclerosis with 50% occlusion of the right middle cerebral artery. A lesion approximately 1 cm in diameter was noted in the right frontal cortex corresponding to the site of entry of the ventricular shunt, and an old infarct approximately 1.5 cm in diameter was identified in the right medial posterior parieto-occipital cortex. The lateral and third ventricles were markedly dilated, and the hippocampus, amygdala and entorhinal cortex showed moderate atrophy. The caudate nucleus was slightly flattened, but the substantia nigra was normally pigmented. Histopathologically, the case was assigned a Braak AD stage of 6 (Table 5.1); the apolipoprotein E genotype was *ApoE3/4*.

Comparison subjects

Nine additional, clinically and pathologically confirmed AD cases and three age-matched, nondemented subjects were analyzed for comparison with AD1 (Table 1) in the core analysis. These subjects were part of an earlier comparative study of Aβ in humans and nonhuman primates [243]. Tissue samples from three additional clinically and pathologically confirmed AD cases (which were verified to be PIB-sensitive by *in vitro* ^{3}H-PIB binding analysis) and one age-matched control (Table 5.1) were used as comparison subjects only in the MALDI-TOF mass spectrometry analyses (below).

Tissue preparation

Bilateral tissue slabs from the core subjects were dissected from the superior temporal gyrus (AD, n=10; ND, n=3) and the paracalcarine occipital cortex (AD, n=7; ND, n=3). The samples from one hemisphere were quickly frozen and stored at -80°C. Frozen tissue later was weighed and Dounce-homogenized in 5 volumes of Tris-buffered

saline (TBS) homogenization buffer (50mM Tris-HCl and 150mM NaCl containing complete protease inhibitor [Santa Cruz Biochemicals, Santa Cruz, CA, USA]). Aliquots of the homogenates were stored at -80°C until use in the PIB binding analysis, Aβ-ELISAs, immunoblots and mass spectrometry. Additional blocks of frozen tissue were sectioned at 10μm on a cryostat and mounted onto silanized slides (Fisher Scientific, Waltham, MA, USA). Location-matched tissue from the contralateral hemisphere was fixed in phosphate-buffered, 4% paraformaldehyde, embedded in paraffin wax, and processed for histochemical analysis. In two AD cases, fixed, non-embedded samples from the temporal neocortex were used for ultrastructural investigation (below). All tissue samples were obtained from the Emory University Alzheimer's Disease Research Center Brain Bank and the New York University Alzheimer's Disease Center Brain Bank, in accordance with federal and institutional guidelines, and the samples were coded to ensure the anonymity of the subjects.

DNA Sequencing for the β-Amyloid Precursor Protein (APP), Presenilin 1 (PSEN-1), and Presenilin 2 (PSEN-2)

Coding exons 3-18 with the corresponding 50bp of intronic junctions of *APP* and all coding exons from both *PSEN-1* and *PSEN-2*, along with at least 25 base pairs of flanking sequence, were sequenced from genomic DNA extracted from AD1 brain tissue, using primers described in the supplementary material (Tables S5.1, S5.2 and S5.3).

Immunohistochemistry

Tissue sections from all AD cases were processed immunohistochemically using monoclonal anti-Aβ antibodies *6E10* to Aβ1-16 (1:25,000), *4G8* to Aβ17-24 (1:5,000; both from Covance, Princeton, NJ, USA), and *8E1* to the pyroglutamized amino terminus of $A\beta_{pyr\text{-}glu}3\text{-}x$ (1:5,000; Immuno-Biological Laboratories, Gunma, Japan); polyclonal antibodies *R361* to Aβ32-40 and *R398* to Aβ33-42 (both at 1:15,000, courtesy of Pankaj Mehta, Institute for Basic Research on Developmental Disabilities, Staten Island, NY, USA); monoclonal anti-tau antibodies *CP13* to phosphorylated tau serine 202 (1:10,000), *MC1* to a pathologic conformation of tau (1:5,000; both courtesy of Peter Davies, Albert Einstein College of Medicine, Bronx, NY, USA), and *AT8* to phosphorylated tau serine 202/phosphothreonine 205 (1:5,000; Covance). To rule out the presence of synucleinopathy, we employed a polyclonal antibody to α-synuclein (1:300, courtesy of Bernardino Ghetti, Indiana University, Indianapolis, IN, USA) (see Rosen et al., 2008 for antibody details).

Vectastain Elite kits (Vector Laboratories, Burlingame, CA, USA) were used for avidin-biotin complex (ABC)/horseradish peroxidase immunodetection of antigen-antibody complexes, with diaminobenzidine (DAB) or DAB + nickel as chromogens. Appropriate positive control specimens from cases with previously confirmed pathology were included in all immunostaining experiments. In some instances, sections were lightly counterstained with hematoxylin. Non-immune mouse IgG or rabbit serum was used in place of the monoclonal and polyclonal primary antibodies, respectively, as negative controls. Some additional sections were stained with Congo Red, Thioflavin-T, hematoxylin and eosin, or the Campbell-Gallyas AD-silver stain [243].

Electron microscopy

Fixed tissue slabs from the temporal neocortex of two AD cases (the PIB-refractory case [AD1] and a PIB-sensitive case [AD6]) were cut on a vibratome at 70μm thickness, and regions of heavy Aβ load were identified in adjoining sections immunostained with antibody 6E10. Samples from these regions were dissected from the adjacent, non-immunostained section, washed in phosphate buffer (0.1M, pH 7.4) and immersed in osmium tetroxide (1% in phosphate buffer) for 20 minutes. They were then rinsed in phosphate buffer and dehydrated in graded concentrations of ethanol and propylene oxide. Uranyl acetate (1%) was added to the 70% ethanol (35 minute immersion) to improve contrast in the electron microscope. Next, the blocks were embedded in epoxy resin (Durcupan ACM; Fluka, Ft. Washington, PA, USA) and heated for 48 hours at 60°C. Ultrathin sections were cut with a Leica Ultracut T2 (Nussloch, Germany), collected onto single-slot copper grids, and stained with lead citrate. Thin sections were examined with a Zeiss EM10-C electron microscope (Oberkochen, Germany) and digital images were captured with a Dual View camera (Gatan Inc., Pleasanton, CA, USA).

^{3}H-PIB binding assay

To measure high-affinity PIB binding in cortical homogenates, all samples were simultaneously incubated with 1.0nM ^{3}H-PIB (specific activity=82 Ci/mmol, custom synthesis, GE Healthcare, UK) in a microplate radioligand binding assay [243]. At 1.0nM, the concentration of free ^{3}H-PIB used in our *in vitro* experiments is comparable to that achieved with ^{11}C-PIB in PET scans [244], and is selective for the high-affinity

binding sites on Aβ [13, 123, 139, 141]. The same tissue homogenates used in Aβ ELISAs (below) were diluted 1:33.3 in phosphate-buffered saline (PBS) (pH 7.4) to a final concentration of 5mg wet weight tissue/ml. In a 96 well polypropylene plate, 100µg of wet cortical tissue (20µl of diluted homogenate) from each sample were incubated, in duplicate, with 200µl of 1.0 nM ^{3}H-PIB in 5% ethanol/PBS (nonspecific binding was defined as counts detected in the presence of 1.0 µM unlabeled PIB). After a 2.5-hour incubation (at room temperature, without shaking), samples were quickly transferred to a 96 well Multiscreen HTS Hi Flow FB filter plate and filtered with a vacuum manifold (Millipore Corporation, Billerica, MA, USA). Filters were rinsed 4 times with PBS at room temperature. The filters were dried for 30 minutes at 37°C, after which 50µl of MicroScint 20 (PerkinElmer, Waltham, MA, USA) scintillation fluid were added to each well and the plate was incubated at room temperature for 24 hours, shaking at 100 rpm. ^{3}H-PIB binding was quantified in a TopCount scintillation counter (PerkinElmer) and specific binding was calculated by subtracting nonspecific counts per minute (CPM) (+1.0μM unlabeled PIB). Based on a 15% counting efficiency (established empirically), CPM were converted to femtomoles of bound PIB. PIB binding was linear between 25 and 200µg (wet weight) of AD cortical tissue homogenate added per well with 1.0nM ^{3}H-PIB. To characterize the high-affinity binding components in case AD1 and other AD homogenates, samples were incubated in 1.2nM ^{3}H-PIB with concentrations of unlabeled PIB between 0.1 nM and 1.0µM in a competition binding experiment.

^{3}H-PIB Autoradiography

Slide-mounted, unfixed cryosections were brought to room temperature in air-tight containers and then immersion-fixed in 10% ethanol/PBS for 20 minutes. Sections were incubated in 1.0nM ^{3}H-PIB (specific activity=82Ci/mmol) in 5% ethanol/PBS for one hour at room temperature, rinsed twice with 10% ethanol/PBS and 2 times with ddH_2O, both on ice, and then air-dried before exposing directly to a BAS-TR2040 tritium imaging plate (Fujifilm, Stamford, CT, USA). After 2 weeks of exposure, the plate was developed in a BAS-5000 Image Plate Scanner and images were captured with MultiGauge software (Fujifilm). Adjacent cryosections were immunostained with Aβ antibody 6E10, as described above.

ELISA Quantification of Aβ40 and Aβ42

Cortical homogenates were spun at 100,000 x g for one hour at 4°C in a TLA-100.4 ultracentrifuge rotor (Beckman Coulter, Fullerton, CA USA). After collecting buffer-soluble supernatants, the pellet was sonicated in 70% formic acid, spun at 16,100 x g for 60 min at 4°C, and the clear supernatant was collected as the buffer-insoluble extract. For both extracts, total Aβx-40 and Aβx-42 levels were measured by enzyme-linked immunosorbent assays (ELISA) using standardized kits (The Genetics Company, Schlieren, Switzerland) as previously described [241, 243]. Aβ content is expressed relative to the wet weight of the tissue samples (Tables 5.2, 5.3).

Western blot

Unfixed cortical tissue blocks were Dounce-homogenized in 4 volumes of PBS. The 20% homogenate was vortexed, probe-sonicated 3 x 5 seconds (level 4, Model 100 ultrasonic dismembrator, Fisher Scientific), centrifuged at 3,000 x g for 5 minutes at 4°C, and the supernatant stored at -80°C until use. Total protein was quantified in the sample with a microplate bicinchoninic acid (BCA) assay (Pierce Biotechnology, Rockford, IL, USA). 60μg of protein was boiled for 5 minutes in 2x Tricine sample buffer and 10x Reducing Agent (Invitrogen, Carlsbad, CA, USA), run on a 10-20% Tricine gel (Invitrogen) and blotted onto a nitrocellulose membrane. The membrane was boiled for 15 minutes in 1xPBS, then blocked at room temperature in 2.5% nonfat milk/0.05% Tween-20 (blocking buffer) for 60 minutes, incubated in primary antibody to Aβ (6E10, 1:1000 diluted in blocking buffer) for 48 hours at 4°C, followed by 90 minutes in horseradish peroxidase-conjugated anti-mouse IgG antibody (1:10,000 in blocking buffer, GE Healthcare, Piscataway, NJ, USA). Antibody binding was detected with Super Signal West Pico electrochemiluminescence substrate (Fisher Scientific) and exposed to Kodak MR Biomax film (Kodak, New Haven, CT, USA).

Immunoprecipitation/MALDI-TOF MS

For mass spectrometry, cortical homogenates were ultracentrifuged to isolate buffer-soluble Aβ (see above). Pellets were resuspended in 2% SDS, spun at 100,000 x g for 60 minutes at 10°C to extract detergent-soluble Aβ, and the pellet containing buffer-insoluble proteins was sequentially extracted with 70% and 90% formic acid (above). Immunoprecipitation of Aβ was performed using paramagnetic beads coated with a

cocktail of antibodies 4G8 and 6E10, or C-terminal specific antibody 12F4 to Aβx-42, and the precipitates analyzed by matrix-assisted laser desorption/ionization-time-of-flight (MALDI-TOF) mass spectrometry, as previously described [274]. Briefly, Dynal M-280 Dynabeads (Invitrogen) coated with sheep anti-mouse antibodies were then coated with monoclonal antibodies 4G8 and 6E10, each at a concentration of 60 μg/ml, or monoclonal antibody 12F4 (Covance) at 120 μg/ul. 50μl of coated beads were added to 1.0ml soluble cortical extract, 1.0ml detergent-soluble extract (after detergent removal using SDS-OUT, according to manufacturer's instructions, Pierce Biotechnology), or a solution of 100μl formic acid extract, neutralized with 1.0M Tris buffer to pH 7.4 and then diluted up to 10ml volume with deionized water. Following immunoprecipitation and washing, beads were completely dried in a SpeedVac, eluted with 20μl of 0.5% formic acid, dried in a SpeedVac and resuspended in 4μl of 0.1% formic acid. 1μl of IP eluate was mixed with 500μl ethanol and 500μl acetonitrile in 0.1% trifluoroacetic acid and then analyzed in a Micromass TofSpec-2E MALDI-TOF instrument. Major peaks within all spectra were identified with ExPASy's FindPept software (http://us.expasy.org/tools/findpept.html).

Tables

Table 5.1. Case List.

Case	Group	Age	Sex	PMI (hr)	Braak stage	*ApoE* type
AD1	**AD**	**72**	**f**	**3**	**VI**	**3/4**
AD2	AD	61	m	5.5	V/VI	3/4
AD3	AD	75	f	12	V/VI	4/4
AD4	AD	91	f	2.5	V/VI	3/4
AD5	AD	61	m	4	V or VI	3/4
AD6	AD	64	f	4.5	VI	3/4
AD7	AD	87	f	6	V/VI	3/4
AD8	AD	84	m	4.5	VI	3/4
AD9	AD	81	f	2	V/VI	3/3
AD10	AD	57	f	20	V/VI	3/4
AD11*	AD	86	f	2.5	V	3/3
AD12*	AD	74	f	2.8	VI	2/4
AD13*	AD	84	f	3.5	VI	3/4
ND1	Ctrl	40	m	31	0	3/4
ND2	Ctrl	57	f	17	0	3/3
ND3	Ctrl	75	f	6	0	3/3
ND4*	Ctrl	78	m	1.6	0	3/3

* Only included in MALDI-TOF MS analysis
PMI: Postmortem interval (hours)
ApoE type: Apolipoprotein E genotype

Table 5.2. Soluble Aβ40 and Aβ42 levels in temporal and occipital cortices of the core Alzheimer's disease and nondemented control cases, as measured by ELISA. Aβ levels are presented relative to wet tissue weight (fmol Aβ/100μg wet weight tissue).

		Temporal Cortex			**Occipital Cortex**		
Group	**Case**	**Aβ40**	**Aβ42**	**Total Aβ**	**Aβ40**	**Aβ42**	**Total Aβ**
Alzheimer's	AD1	21.63	0.13	21.76	24.56	2.42	26.98
	AD2	0.50	0.05	0.55	0.20	0.08	0.28
	AD3	0.08	0.04	0.12	0.02	0.06	0.08
	AD4	0.08	0.07	0.15	1.34	0.16	1.51
	AD5	1.59	0.09	1.68	n/a	n/a	n/a
	AD6	0.07	0.12	0.19	n/a	n/a	n/a
	AD7	0.01	0.01	0.04	2.80	0.51	3.31
	AD8	0.02	0.04	0.06	n/a	n/a	n/a
	AD9	0	0.03	0.03	0	0.05	0.05
	AD10	0	0.01	0.02	0.02	0.08	0.11
	AD means:	**2.40**	**0.06**	**2.46**	**4.14**	**0.48**	**4.62**
Nondemented	ND1	0	0.03	0.03	0.01	0.12	0.14
	ND2	0	0	0	0	0	0
	ND3	0	0.01	0.01	0	0	0
	ND means:	**0.00**	**0.01**	**0.01**	**0.00**	**0.04**	**0.05**

Table 5.3. Insoluble Aβ40 and Aβ42 levels in temporal and occipital cortices of the core Alzheimer's disease and nondemented control cases, as measured by ELISA. Aβ levels are presented relative to wet tissue weight (fmol Aβ/100μg wet weight tissue).

		Temporal Cortex			**Occipital Cortex**		
Group	**Case**	**Aβ40**	**Aβ42**	**Total Aβ**	**Aβ40**	**Aβ42**	**Total Aβ**
Alzheimer's	AD1	1126.13	790.51	1916.63	2685.25	912.84	3598.09
	AD2	39.84	174.88	214.72	15.49	297.96	313.45
	AD3	62.48	97.56	160.04	5.23	186.51	191.73
	AD4	17.75	196.38	214.13	10.29	191.29	201.58
	AD5	275.37	352.57	627.94	n/a	n/a	n/a
	AD6	3.88	444.72	448.59	n/a	n/a	n/a
	AD7	7.65	217.09	224.74	10.97	176.23	187.21
	AD8	4.07	155.58	159.66	n/a	n/a	n/a
	AD9	0.62	145.53	146.15	0.21	59.36	59.57
	AD10	3.37	82.91	86.28	2.18	211.23	213.41
	AD means:	**154.12**	**265.77**	**419.89**	**389.95**	**290.77**	**680.72**
Nondemented	ND1	0	0	0	0.19	0.22	0.41
	ND2	0	0.98	0.98	0.23	1.27	1.50
	ND3	0.03	0.23	0.26	0	0.62	0.62
	ND means:	**0.01**	**0.40**	**0.41**	**0.14**	**0.70**	**0.84**

Figures

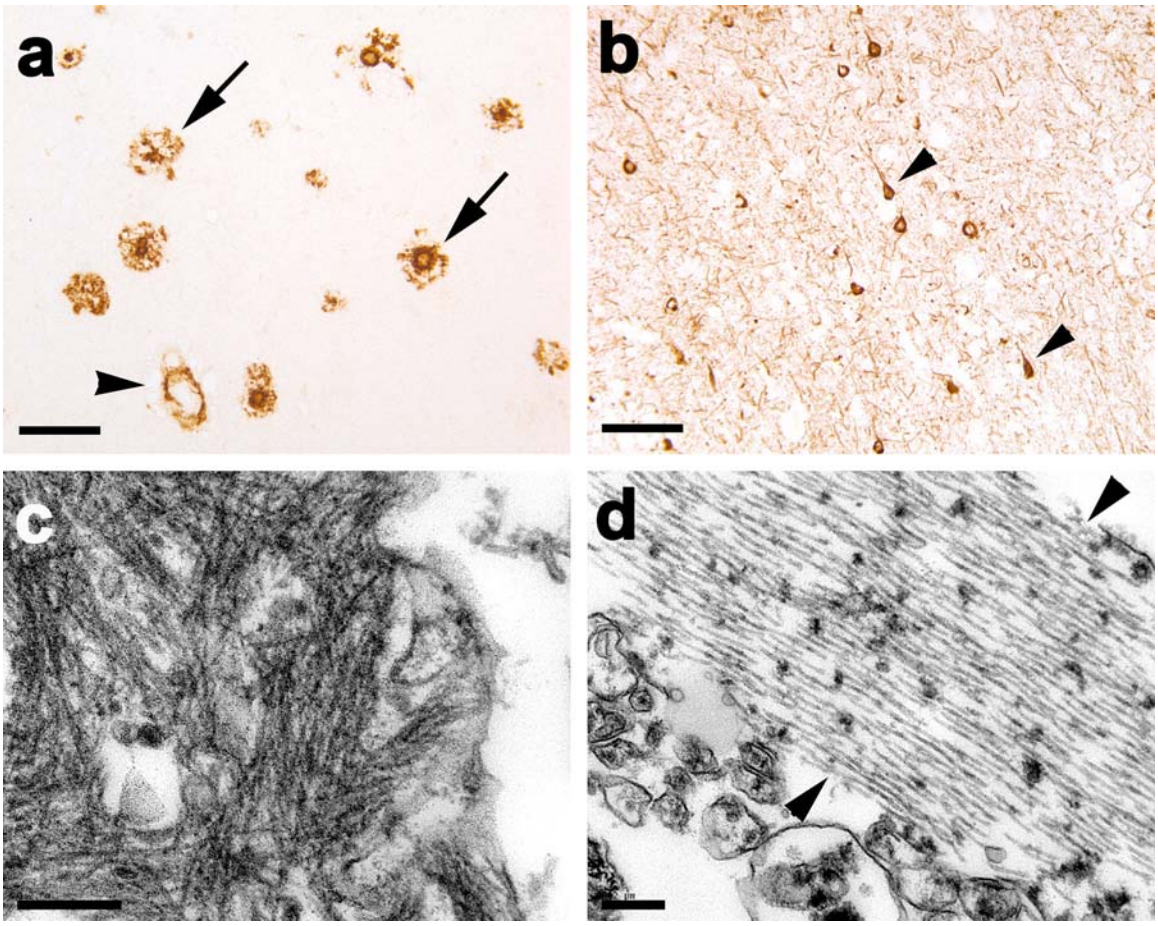

Figure 5.1. Aβ and tau pathology in the superior temporal gyrus of the PIB-refractory Alzheimer's case AD1. (A) Antibody 6E10-immunoreactive senile plaques (two denoted by arrows) and large-vessel CAA (black arrowhead). (B) Antibody CP13-immunoreactive, intra-somatal neurofibrillary tangles (two denoted by arrowheads) and abundant neuropil threads. (C) Ultrastructure of amyloid fibrils in the periphery of a senile plaque. (D) Ultrastructure of a bundle of paired helical filaments (marked by two arrowheads). Case AD1 had significant CAA, and the senile plaques sometimes showed diminished immunostaining in the central region (right-hand arrow in a), but otherwise

the histopathology did not differ remarkably from that of the other AD cases. Bar = 100μm in A and B and 200nm in C and D).

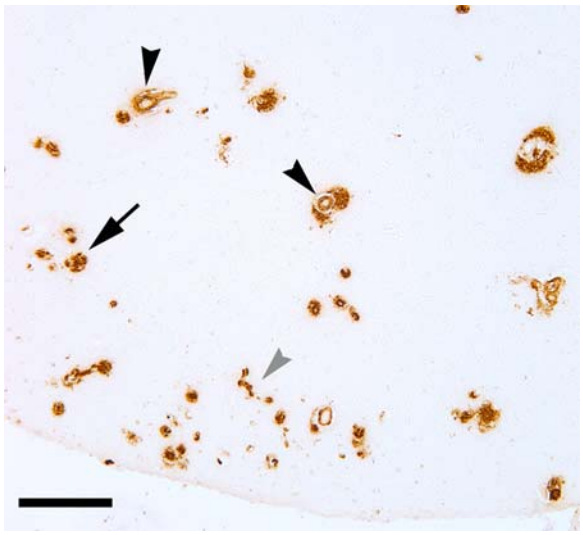

Figure 5.2. Cerebral β-amyloid angiopathy in the occipital cortex of case AD1. Both large vessels (black arrowheads) and capillaries (grey arrowhead) were affected. CAA of both types was more abundant in the occipital cortex than in the temporal cortex. A plaque-like parenchymal deposit of Aβ is denoted by the arrow. Antibody 4G8; Bar = 200μm.

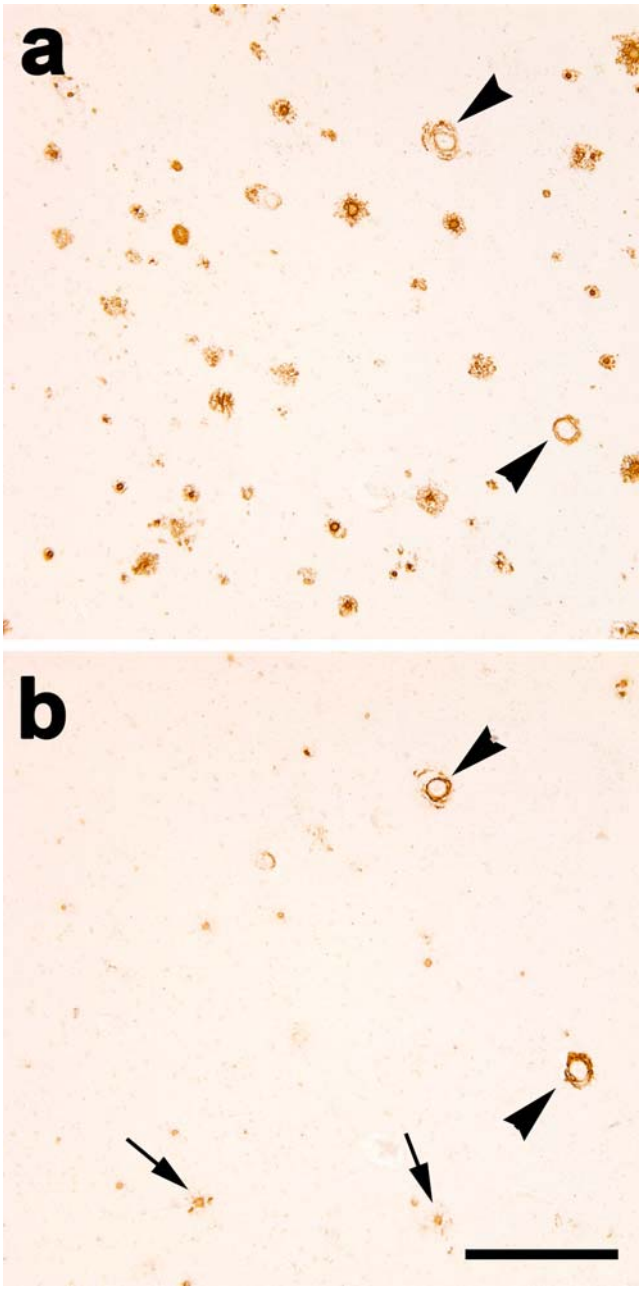

Figure 5.3. Immunostaining for Aβ42 (A) and Aβ40 (B) in nearby temporal cortical sections from case AD1. The antibody to Aβ42 stained a variety of diffuse and dense parenchymal lesions as well as CAA, but the antibody to Aβ40 stained mainly CAA (the same two immunoreactive blood vessels are marked by arrowheads in both panels) and dense plaque cores (two denoted by arrows in b). Bar = 300μm.

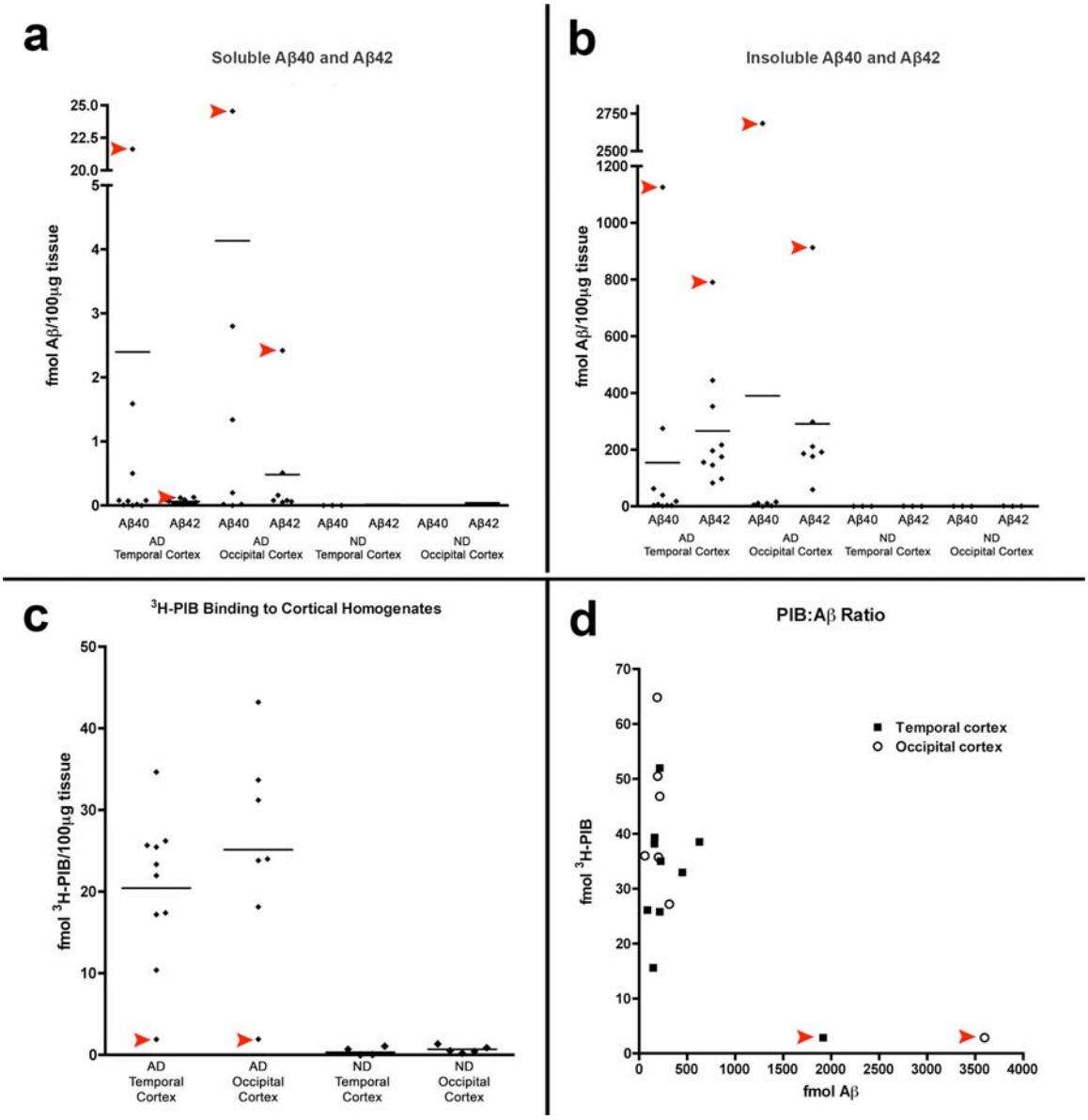

Figure 5.4. Aβ levels and ^{3}H-PIB binding in temporal and occipital cortical homogenates from AD1, nine comparison AD cases and three nondemented control (ND) cases. (A, B). By ELISA of soluble and insoluble extracts, AD1 (red arrowheads) exhibited substantially more soluble and insoluble Aβ40 and Aβ42 than did all other AD cases examined in this study. Negligible Aβ was detected in both regions of the 3 ND cases (group means are indicated by the horizontal lines). Levels of soluble Aβ40 and Aβ42 (A) and levels of insoluble Aβ40 and Aβ42 (B) are expressed in fmol Aβ per 100μg wet

tissue for each subject. (C) Radioligand binding assays with ^{3}H-PIB reveal high levels of PIB binding to temporal and occipital cortical tissue from all AD cases in this study except AD1, which showed only background levels of PIB binding. (D) The ratio of PIB binding to total Aβ in two cortical regions. When AD1 data points were excluded from the analysis, total levels of insoluble Aβ (Aβ40 and Aβ42) correlate positively with ^{3}H-PIB binding to AD temporal (*n*=9) and occipital (*n*=7) cortical homogenates from the comparison AD cases [29].

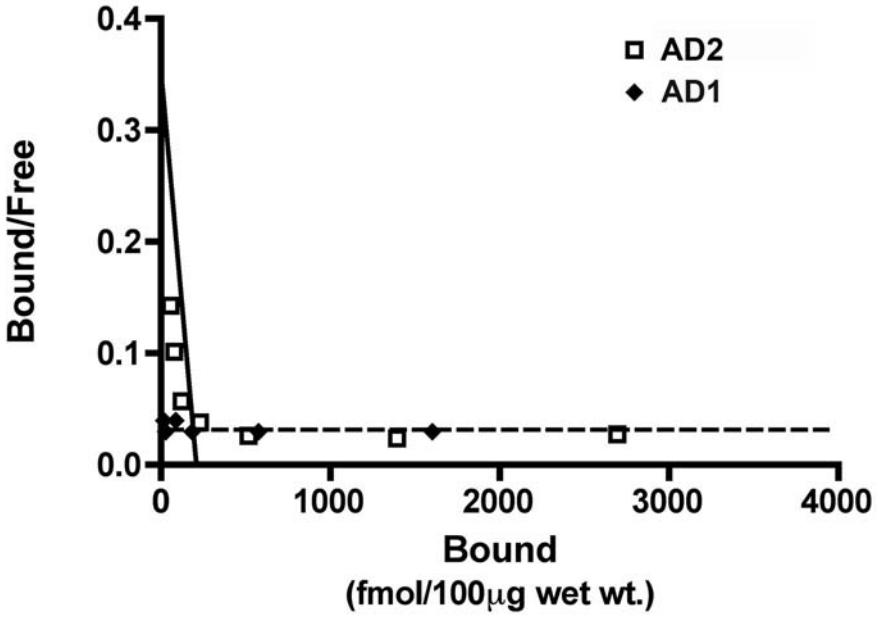

Figure 5.5. Analysis of high-affinity ^{3}H-PIB binding in temporal cortical homogenates from two AD cases. A homologous competition binding analysis of PIB binding levels in temporal cortical homogenates incubated with 1.2nM ^{3}H-PIB alone and with 1.2nM ^{3}H-PIB co-incubated with concentrations of unlabeled PIB between 1.0 nM and 1.0μM did not reveal a measurable high-affinity PIB binding component in case AD1 (dotted line). In case AD2 (continuous line), a high-affinity PIB binding component was detected with a Kd = 3.0nM and Bmax = 209.28 fmol/100μg wet tissue (AD2: open squares, AD1: filled diamonds). Comparable results were obtained with occipital cortical homogenates (data not shown).

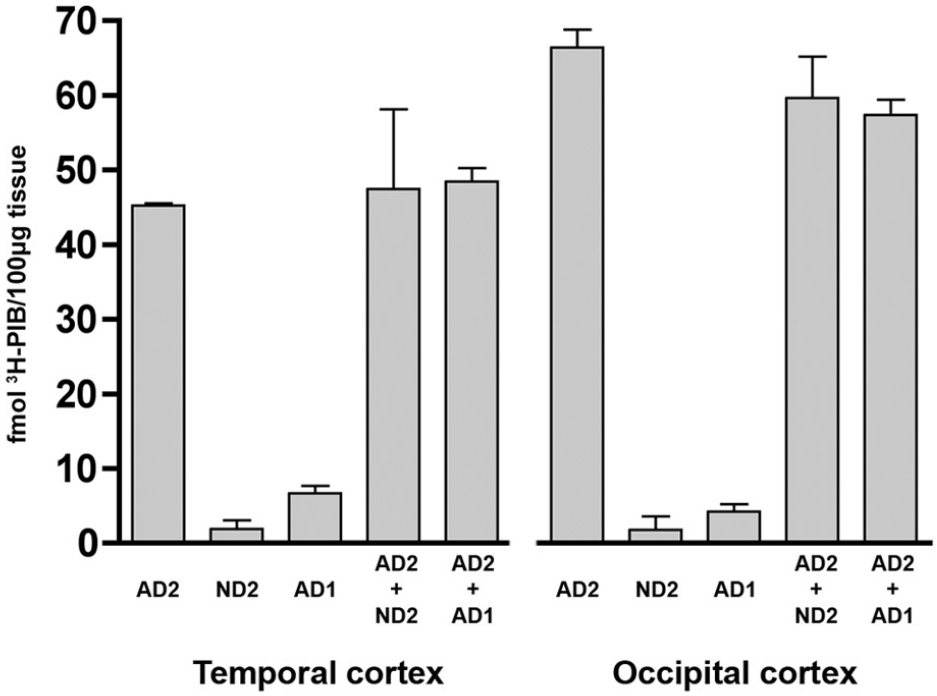

Figure 5.6. ^{3}H-PIB binding experiments with mixtures of AD and ND cortical homogenates. To detect the potential presence of a diffusible element in AD1 cortical tissue that inhibits PIB binding *in vitro*, we incubated 1.0nM ^{3}H-PIB with 1:1 mixtures of cortical homogenates from a typical PIB-sensitive AD case (AD2) and the PIB-refractory case AD1. We did not identify an inhibitory or synergistic effect on PIB binding in either the temporal or occipital cortical homogenates. Rather, the quantity of PIB binding to mixed homogenates was approximately the sum of total PIB binding to each individual homogenate. Similar results were seen when 1.0nM ^{3}H-PIB was incubated with mixtures of temporal and occipital cortical homogenate from AD2 and a nondemented control case (ND2) that alone exhibited negligible high-affinity PIB binding.

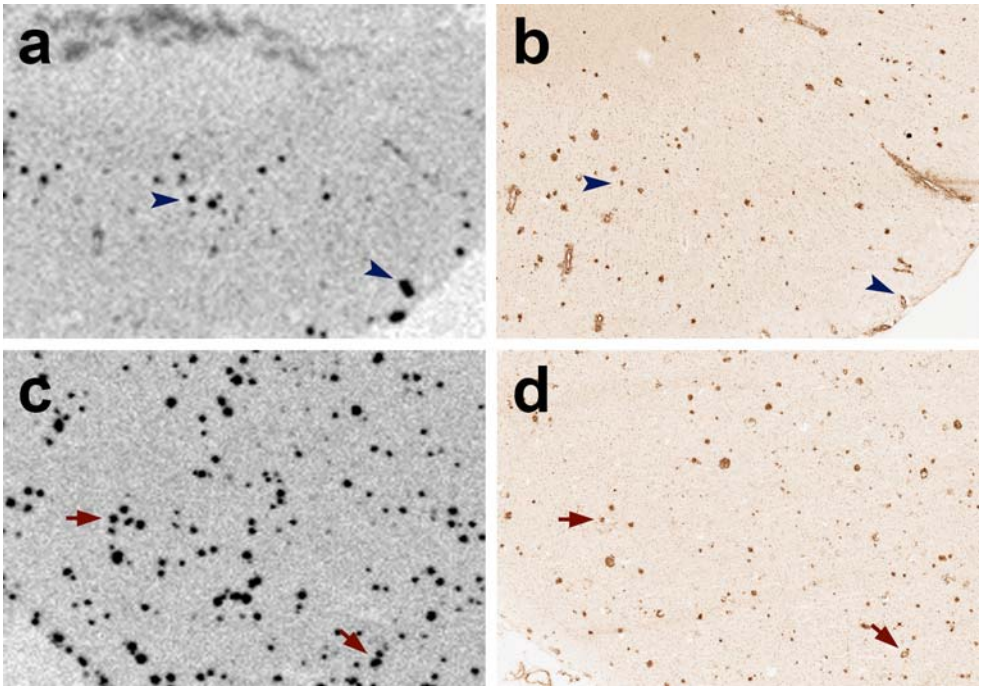

Figure 5.7. ^{3}H-PIB autoradiography in temporal cortical sections from case AD1 and a PIB-sensitive AD case (AD5). (A) At a 1.0nM concentration, ^{3}H-PIB binds to few cortical plaques and lightly to some blood vessels in the superior temporal cortex of AD1. (B) In an adjacent cryosection, immunohistochemistry with the 6E10 antibody to Aβ reveals abundant senile plaques as well as CAA in this cortical region. The blue arrowheads denote PIB-positive Aβ plaques and CAA, although the greater part of the Aβ-immunoreactive plaques and vessels did not bind to PIB by autoradiography. (C) In case AD5, ^{3}H-PIB autoradiography and (D) 6E10 immunohistochemistry on adjacent cryosections demonstrate heavy, PIB-positive senile plaque deposition in the superior temporal cortex. Red arrows indicate PIB-positive Aβ lesions identified in adjacent cryosections.

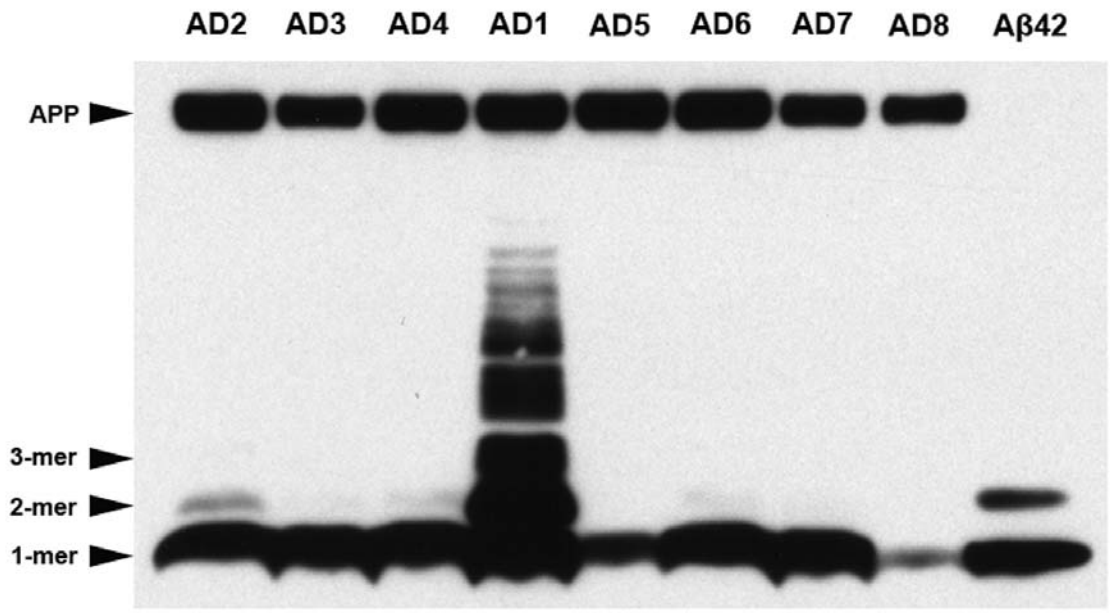

Figure 5.8. Western blot analysis of multimeric Aβ and APP in AD temporal cortex**.** Temporal cortical homogenates containing 60μg of total protein from case AD1 and seven other AD cases were separated by SDS-PAGE and immunoblotted with antibody 6E10 to the N-terminal region of Aβ. A preparation of synthetic Aβ42 (10 ng) is in the far right lane, as a positive control. Strong bands of monomeric Aβ were detected in all AD cases examined. Light bands corresponding to Aβ dimers were detected only in some of the AD lanes under these conditions. In AD1, 6E10 immunoblotting revealed high levels of dimeric and trimeric Aβ, as well as several higher molecular weight, Aβ-immunoreactive bands between 17 KDa and 44KDa. Note that 6E10 also recognizes the Aβ epitope in APP (top band), which was not increased in AD1. When the total protein content in AD1 temporal cortex was diluted to 6.78μg to normalize total Aβ levels to those seen in the comparison AD cases, the higher molecular weight bands, though lighter, were still detected by 6E10 immunoblot analysis, indicating that the presence of

these bands cannot be accounted for simply by the overall quantity of Aβ in AD1 temporal cortex (data not shown).

		AD1	AD12
TBS	a-42	(1-42)	1-42 4-42 (19-42)
	4G8/6E10	1-40 1-34; 1-38; 1-37; 1-36; 2-40; 1-33 1-29; 1-28; 2-28; 1-19; 1-18. 1-16	1-40; 1-40ox 1-34; 4-40 (4-34; 1-42; 1-42ox)
SDS	a-42	1-42 3-42 (7-42)	1-42 (1-42ox; 4-42; 3-42; 5-42)
	4G8/6E10	1-40 1-38; 2-40; 1-39; 1-37; 1-36; 1-28 1-22; 1-18 (2-28; 1-24)	1-40 1-40ox; 1-42 (1-42ox; 1-35; 1-34; 1-24; 1-16)
FA 70%	a-42	1-42; 3-42 1-42ox; 4-42ox; 5-42ox; 6-42; 7-42 8-42ox; 9-42ox; 11-42 (17-42ox)	-------
	4G8/6E10	1-40; 1-40ox 1-39; 1-38; 1-28; 2-28; 1-36; 1-37 (1-22)	-------
FA 100%	a-42	3-42; 1-42ox; 1-42 4-42ox; 8-42ox; 9-42ox; 11-42	1-42 9-42; 8-42; 5-42; 2-42; 4-42; pE3-42 (3-42)
	4G8/6E10	1-40; 1-42 1-40ox; 1-42ox; 2-40; 1-38; 1-37 1-36 (1-28; 1-18)	9-40 1-40; 1-25; 1-23 (1-40ox; 1-42)

Figure 5.9. Immunoprecipitation/MALDI-TOF MS detection of Aβ peptides in the temporal cortex of case AD1 and a comparison PIB-sensitive AD case (AD12)**.** By mass spectrometry, we detected substantially more individual Aβ fragments in all cortical fractions of AD1 temporal cortex, as compared to three other AD cases (data from one comparison AD case shown). Numerous C-terminally truncated peptides (Aβ1-x) were

seen in the buffer (TBS)-soluble extract, yet Aβ42 was barely detectable. These same truncated peptides also were detected in SDS-soluble extract, along with Aβ40 and Aβ42. N-terminally truncated peptides (Aβx-40 and Aβx-42) and full-length Aβ40 and Aβ42 predominated in formic acid-solubilized fractions (FA 70% and FA 100%) from AD1 cortex. This pattern of terminal-specific truncations in soluble and insoluble cortical fractions was not seen in the comparison AD cases or in a nondemented control case (not shown). The Aβ fragments written in red were particularly abundant, while those in parentheses were just barely detectable. a-42: Immunoprecipitation with monoclonal antibody 12F4, specific to Aβx-42; 4G8/6E10: Immunoprecipitation with two monoclonal antibodies, one to Aβ17-24 (4G8) and one to Aβ1-16 (6E10); TBS: Tris-buffered saline extract; SDS: sodium dodecyl sulfate-soluble extract; FA: formic acid-solubilized extract.

Results

APP, PSEN1, and PSEN2 gene sequencing

No mutations were detected in coding exons 3-18 and 50 bp of intronic junctions of the *APP* gene sequence in AD1 genomic DNA. Sequencing of all *PSEN1* and *PSEN2* coding exons and at least 25 base pairs of flanking sequence failed to identify any known AD-associated mutations or polymorphisms,that would result in amino acid sequence change to *PSEN1* or *PSEN2*. Conservative minor allele single nucleotide polymorphisms were identified in exons 3, 4, and 11 of *PSEN2* (listed in Table S5.4).

Histopathology

Immunohistochemically, subject AD1 had copious dense-cored and diffuse parenchymal senile plaques characteristic of advanced AD, as well as significant large vessel and capillary CAA and tau-positive neurofibrillary pathology (Figures 5.1, 5.2). Parenchymal and vascular Aβ lesions were detected throughout the temporal and occipital cortices of case AD1, with slightly more parenchymal deposits in the temporal cortex and a predilection for vascular amyloid deposition in occipital cortical regions (Figures 5.1a, 5.2). The presence of AD-typical lesions was confirmed by multiple antibodies to Aβ and tau, and by the Congo Red, Thioflavin-T and Campbell-Gallyas silver stains (not shown). Antibody R398 to Aβ42 disclosed a large variety of parenchymal and vascular lesions, similar to antibody 6E10, whereas antibody R361 to Aβ40 labeled primarily CAA and plaque cores (Figure 5.3). Antibody 8E1 to $A\beta_{pyr\text{-}glu}3\text{-}x$, like antibodies 6E10 and R398, stained a broad spectrum of vascular and parenchymal

Aβ deposits (not shown). Ultrastructurally, the senile plaques consisted of fibrillar material consistent with amyloid (Figure 5.1c), and the neurofibrillary pathology included filamentous ribbons typical of AD (Figure 5.1d). The antibody to α-synuclein did not show concomitant cortical Lewy bodies or Lewy neurites in this case (not shown).

^{3}H-PIB binding and Aβ analysis

PIB binding was markedly reduced in temporal and occipital cortical homogenates of case AD1 compared to 9 other clinically and pathologically confirmed AD subjects (Figure 5.4), and was in the range of the non-demented control cases (PIB also bound strongly to homogenates from the AD cases used as controls for the mass spectrometry analysis, below). Despite a paucity of high-affinity PIB binding sites, ELISAs disclosed levels of soluble and insoluble Aβ40 and Aβ42 that greatly exceeded those in both brain regions of all nine comparison AD cases in the core group (Tables 5.2, 5.3). The Aβ40:Aβ42 ratios for soluble and insoluble Aβ also were higher in AD1 than in the 9 other AD cases (Figure 5.4). A competition curve experiment with ^{3}H-PIB and unlabeled PIB in temporal cortical homogenates from AD1 and a comparison case (AD2) revealed a high-affinity PIB binding site in AD2 (Kd = 3.0nM and Bmax = 290 fmol), comparable to previously published reports [118, 141, 243], but not in AD1 (Figure 5.5). Similar results were seen in the occipital cortex (data not shown). Finally, mixing experiments with AD1 and AD2 temporal and occipital cortical homogenates revealed only an additive effect on PIB binding when equal parts of tissue from each case were simultaneously incubated with 1.0nM ^{3}H-PIB (Figure 5.6).

Autoradiography of 1nM ^{3}H-PIB binding in unfixed cryosections revealed some cortical plaques in the superior temporal cortex of case AD1. However, comparison with an adjacent cryosection that was immunostained with antibody 6E10 indicated that only a subset of potential plaques and CAA were labeled (Figure 5.7). In the temporal cortex of a comparison AD subject (AD5), ^{3}H-PIB autoradiography and 6E10 immunohistochemistry on adjacent cryosections showed substantial overlap of Aβ-immunoreactive and PIB-positive lesions (Figure 5.7).

Using antibody 6E10 for immunoblot analysis of temporal cortical extracts from AD1 and seven comparison AD cases, strong bands of 4KDa Aβ monomers were detected in all 8 cases. Light bands corresponding to Aβ dimers (~8KDa) were detectable in several of the AD cases. In the cortical extract from AD1, however, these Aβ dimer bands were of substantially greater intensity relative to the 7 comparison AD cases, and a strong immunoreactive band was detected at ~12 KDa, corresponding to trimeric Aβ. Additionally, numerous higher molecular weight bands migrating between 17 and 44 kDa were detected solely in AD1 temporal cortical tissue. APP levels (~100KDa) were similar in AD1 and the 7 comparison AD cases (Figure 5.8). Because our ELISA analyses indicate considerably higher total Aβ levels in AD1 tissue, an immunoblot was conducted with AD1 cortical extract that was diluted to reduce total protein, thereby yielding total Aβ levels that were comparable to the mean Aβ levels in the comparison AD cases. When Aβ levels are normalized as such, the higher molecular weight 6E10-immunoreactive bands, though weaker, are still visible (data not shown).

Aβ MALDI-TOF mass spectrometry

MALDI-TOF MS on immunoprecipitated buffer-soluble, SDS-soluble, and formic acid-soluble Aβ from AD1, three comparison (PIB-sensitive) AD cases and one nondemented control case revealed a pattern of N- and C-terminally truncated fragments unique to AD1 temporal cortex (Figure 5.9, data from 2 AD cases and the nondemented case not shown). Full-length Aβ40 and Aβ42 were detected in all fractions from all AD cases, although Aβ42 was barely detectable in AD1 buffer-soluble extract, suggesting that the peptide may be preferentially deposited in insoluble lesions and/or cleared from the brain (Figure 5.9). Numerous buffer-soluble, C-terminally truncated Aβ fragments were identified in AD1 tissue (Aβ1-38, Aβ1-37, Aβ1-36, Aβ1-34, Aβ1-33, Aβ1-29, Aβ1-28, Aβ1-19, Aβ1-18, Aβ1-16) but not in any of the 3 comparison AD cases. Insoluble Aβx-42 fragments with various N-terminal residues were identified in the AD1 insoluble extract, as were oxidized Aβ40, Aβ42, and Aβx-42 peptides, the majority of which were not seen in the comparison cases.

Discussion

Pittsburgh compound B has been shown to bind with high affinity to parenchymal senile plaques [140, 207, 244] and to cerebral β-amyloid angiopathy [13, 123] in Alzheimer's disease. Previous studies also have reported a significant positive correlation between PIB binding and Aβ levels [13, 118, 154, 264], further supporting the utility of this ligand in the antemortem diagnosis of AD and CAA. In assessing ^{3}H-PIB

binding to cortical tissue homogenates in a series of ten AD patients, however, we discovered a case of pathologically confirmed AD (case AD1) with particularly heavy cerebral Aβ deposition, yet negligible high-affinity binding of PIB.

To address potential reasons for the paucity of PIB binding in case AD1, we first considered the ways in which this patient differed from the other AD cases. Histopathologically, AD1 showed numerous diffuse parenchymal Aβ deposits, dense-cored Aβ plaques and neurofibrillary tangles typical of advanced AD, as well as substantial large vessel and capillary CAA (Figures 5.1, 5.2, 5.3 and 5.7). However, relative to PIB-sensitive AD cases, autoradiography with 1nM ^{3}H-PIB detected only a fraction of the senile plaques and CAA in AD1 (Figure 5.7). Comparison with the adjacent, Aβ-immunostained sections did not indicate preferential binding of PIB to a particular type of Aβ lesion. Although AD1 had substantial CAA, some degree of CAA is usual in AD [11], and vascular amyloid was present (albeit to a lesser degree) in most of the other cases that we examined. Furthermore, PIB has been shown to be a sensitive marker for CAA *in vivo* [13, 123] and *in vitro* [165]. Finally, in addition to CAA, abundant dense and diffuse Aβ plaques were present in the cortical samples from AD1 (Figure 5.1), yet, despite a heavy burden of Aβ lesions of multiple types, high-affinity PIB binding was unexpectedly meager.

Next, we used ELISA to measure the overall quantity of Aβ and found that the levels of both soluble and insoluble Aβ40 and Aβ42 in AD1 greatly *exceeded* those in the comparison group of nine AD patients. We then asked whether the relative amounts of Aβ40 and Aβ42 might influence PIB binding. As is usual for AD patients with prominent CAA [146, 235], the Aβ40:Aβ42 ratio was particularly high in AD1 (temporal

cortex: Aβ40:Aβ42 = 1.42, vs. 0.22 in the comparison AD group; occipital cortex: Aβ40:Aβ42 = 2.94, vs. 0.04 in the comparison group). However, PIB binding has been shown to correlate strongly with levels of both Aβ40 and Aβ42 in brain tissue [264], and PIB also binds with low stoichiometry but equal affinity to synthetic, aggregated Aβ40 and Aβ42 *in vitro* [141]. Hence, neither a paucity of Aβ nor the absolute amounts of the two major isoforms of Aβ is a likely explanation for the deficiency of high-affinity PIB binding in this case. However, the influence of the ratio of Aβ isoforms on PIB binding to Aβ generated *in vivo* deserves further study.

To rule out the presence of a diffusible cortical element in case AD1 that specifically inhibits the high-affinity binding of PIB to Aβ, we then incubated ^{3}H-PIB with mixtures of cortical homogenates from AD1 and a typical PIB-sensitive AD case (AD2). Both in temporal and occipital cortices, PIB binding to AD2 cortical homogenate was neither enhanced nor decreased in the presence of AD1 cortical homogenate, indicating an absence of diffusible factors in the AD1 cortex that inhibit high-affinity PIB binding to Aβ. These data also argue against a diffusible substance in typical AD tissue that stimulates PIB binding to Aβ, as the mixture of AD2 and AD1 cortical homogenates failed to increase PIB binding beyond the sum of the values achieved in the individual homogenates, despite very high amounts of Aβ in the AD1 cortical homogenate.

There is evidence to suggest that PIB binds with high affinity to parenchymal lesions containing N-terminally-truncated and modified $A\beta_{pyr\text{-}glu}3\text{-}x$ peptide isoforms, and that the low stoichiometry of PIB binding to Aβ in the transgenic mouse brain may be attributable to a dearth of such modified Aβ isoforms [113, 167]. In case AD1, however, an N-terminal-specific antibody to $A\beta_{pyr\text{-}glu}3\text{-}x$ labeled a substantial majority of

parenchymal and vascular Aβ deposits in the temporal and occipital cortices. By mass spectrometry of temporal cortical samples, we did identify a pattern of N- and C-terminally truncated Aβ peptides unique to AD1: Aβ1-x fragments predominated in the soluble extract, and Aβx-42 peptides were detected mainly in the insoluble extract (Figure 5.9). The heterogeneity of C-terminal Aβ fragments in the PIB refractory case may represent the atypical action of carboxyl peptidase(s) in AD1 brain. The possibility of anomalous peptidase activity and/or Aβ clearance mechanisms in this subject, as well as the effect of modified Aβ isoforms on PIB binding affinity, remain to be established. Importantly, these data indicate that deficient high-affinity PIB binding to cortical homogenate from this case is not attributable to an absence of modified or truncated Aβ isoforms that are generally found in mature plaques of the AD brain. Furthermore, in conjunction with the extract-mixing experiments (above), the findings suggest that the presence of abundant Aβ1-x fragments in the soluble extract does not inhibit PIB binding when introduced into cortical extracts from other AD cases.

We then analyzed the distribution of multimeric Aβ by SDS-PAGE/Western blot, and detected Aβ monomers and dimers in both AD1 and most of the comparison AD cases. However, Aβ immunoblots also yielded a dense series of low and higher molecular weight Aβ-immunoreactive bands in AD1 that were not identified, under identical conditions, in any of the comparison AD cases (Figure 5.8). Normalization of total Aβ levels indicated that these bands could not be attributed solely to the heavy Aβ load in AD1. Whether these oligomers are indicative of an alternative Aβ folding/aggregation pathway unique to this case, and whether the presence of these oligomers somehow inhibits PIB biding, warrants further investigation. Again, however,

the absence of an inhibitory effect of AD1 extract on PIB binding in other AD cases (above) argues against the presence of such an inhibitory factor, at least in a readily diffusible form.

The E4 subtype of apolipoprotein E has been linked to an increased likelihood of developing both AD [47, 223] and CAA [98, 229], and to the overall severity of cerebral β-amyloidosis [117, 292, 296]. However, like AD1, seven of the nine AD cases in the comparison group also were hemizygous for *ApoE4*, and one was homozygous, yet all of these individuals displayed strong *in vitro* binding of ^{3}H-PIB, as did the case that was *ApoE3/3*. Consequently, apolipoprotein E genotype *per se* does not account for the anomalous PIB binding in AD1. Genetic analysis of the common AD-associated loci in the genes for APP, presenilin1 and presenilin 2 revealed no obvious mutations or functional polymorphisms that might explain the paucity of high-affinity PIB binding in AD1.

Although the PIB-refractory AD case was not imaged with ^{11}C-PIB prior to death, our *in vitro* findings, using a concentration of free ^{3}H-PIB similar to that achieved in the brain parenchyma of ^{11}C-PIB-scanned patients [244], suggest the possibility that the PET signal would have been diminished or absent in this patient, despite the presence of copious cerebral Aβ. Currently, few cases of suspected AD have been imaged with PIB and then characterized pathologically and biochemically post-mortem; consequently, the frequency of PIB-refractory cases in the AD population is unknown. Although there is compelling evidence that PIB binds only weakly to Aβ deposits in nonhuman species [141, 243, 264], our present results, in conjunction with other findings [62, 140, 162,

197], suggest that PIB imaging may not detect all Aβ lesions in some humans as well [62, 140, 162, 197].

In summary, we describe a case of pathologically confirmed AD with heavy cerebral β-amyloidosis yet negligible high-affinity PIB binding in cortical homogenates. On a mechanistic level, the presence of PIB-refractory Aβ in a confirmed case of Alzheimer's disease implies the existence of molecular strains of Aβ that could be functionally dissimilar with regard to the pathogenesis of AD [160], similar to the heterogeneity of prion strains [45, 77]. In this light, PIB and other binding agents could serve as specific, early diagnostic tools that distinguish polymorphic AD phenotypes, as well as selective *in vitro* molecular probes for strain-like structural variants of multimeric Aβ [160]. Until the prevalence of PIB-refractory Aβ in senescent humans can be established, our findings indicate that limited ^{11}C-PIB retention in PET images of suspected AD cases should be interpreted with caution.

Supplementary Tables

Table S5.1. Primers used to sequence coding exons of *APP*

Exon	Primer	Sequence
Exon 3	APP Exon 3 Forward Primer	cggaaaaagtcagagaccttg
	APP Exon 3 Reverse Primer	ttcattctgaggcagggaac
Exon 4	APP Exon 4 Forward Primer	aaaggtagtagggtcttgattgg
	APP Exon 4 Reverse Primer	tgggttacggatagtagcactg
Exon 5	APP Exon 5 Forward Primer	ccaaagtgtaacccatgctaaa
	APP Exon 5 Reverse Primer	aactctgtgatgggtgactga
Exon 6	APP Exon 6 Forward Primer	gcatccccttttagcaactg
	APP Exon 6 Reverse Primer	gttgggcggagtcttgtaga
Exon 7	APP Exon 7 Forward Primer	tctagtcctggtggccagtt
	APP Exon 7 Reverse Primer	ctgcggagactctgagcaat
Exon 8	APP Exon 8 Forward Primer	ggttttgttggagggacca
	APP Exon 8 Reverse Primer	caagctgtctggcaaaatca
Exon 9	APP Exon 9 Forward Primer	gctgcacagtgtctcatggt
	APP Exon 9 Reverse Primer	ccttcctaggcagcatgttc
Exon 10	APP Exon 10 Forward Primer	tgggaggtcaaatattcttcag
	APP Exon 10 Reverse Primer	tgggactatgaacaatcacacg
Exon 11	APP Exon 11 Forward Primer	agggttggagagtgcaagaa
	APP Exon 11 Reverse Primer	atggaatggacaggggttg
Exon 12	APP Exon 12 Forward Primer	ttagaaggcagacctgcaaaa
	APP Exon 12 Reverse Primer	tcagaaaatgccaaaccaca
Exon 13	APP Exon 13 Forward Primer	tgtatctacctgcagtgcttgg
	APP Exon 13 Reverse Primer	ctagttccagcctgacagtttc
Exon 14	APP Exon 14 Forward Primer	tcttgtgagctgcgactttg
	APP Exon 14 Reverse Primer	tggcagtttacatgctttgc
Exon 15	APP Exon 15 Forward Primer	tggttcttttctggctgctc
	APP Exon 15 Reverse Primer	tcggaacttgggaaatgaag
Exon 16	APP Exon 16 Forward Primer	caggtttcccttacccttca
	APP Exon 16 Reverse Primer	gcgctcagcctagcctattt
Exon 17	APP Exon 17 Forward Primer	caaccagttgggcagagaat
	APP Exon 17 Reverse Primer	cacggtaagttgcaatgaatg
Exon 18	APP Exon 18a Forward Primer	cgttctgctccaagatgtca
	APP Exon 18a Reverse Primer	ctggctaaggggctatgtga
	APP Exon 18b Forward Primer	cattatcgccttttgacagc
	APP Exon 18b Reverse Primer	tgcttacaatgaacagggattc
	APP Exon 18c Forward Primer	gtgggagttcagctgcttct
	APP Exon 18c Reverse Primer	gttggccccaacttcctact

Table S5.2. Primers used to sequence coding exons of *PSEN1*

	Forward	**Reverse**
Exon 3	ttgcggtccttagacagctt	ttctcagaggtgaggggaga
Exon 4	tcatagtgacgggtctgttgtt	tcgctctctcaactgctcct
Exon 5	ggtgagttggggaaaagtga	ttacacatgcacctggcttc
Exon 6	gttgtggtgagctgagatcg	gcaaggagcaacagaagaatg
Exon 7	tgtttgggagccatcacat	ggcattcctgtgacaaacaa
Exon 8	acccccaccagttcacct	ctgcaggagttccaggaatg
Exon 9	ggcagcattaggaagactgg	tgggcattatcatagttctcaag
Exon 10	agcccatgctttgtggttta	gctacctaaaggaatccatgact
Exon 11	cacagctgaagcctaattttg	aatgtgtggccagggtagag
Exon 12	aaccccaaaaggaaaatattcag	Ccgggcctatcatatctcct

Table S5.3. Primers used to sequence coding exons of *PSEN2*

	Forward	**Reverse**
Exon 3	ttgtgtccaagtctccaggtc	catcagggaatgaatgtctgg
Exon 4	ccaaaaatccgtgcattaca	gctgcaggtacagtgaccaa
Exon 5	ccctagcaggtccagaatca	tctaaaggcggctgtttcac
Exon 6	agagcattcaggcttgggta	catgcccatgtccacttgt
Exon 7	ccaggttgggactgaatgg	agcacctgccctccttgt
Exon 8	cggggatagtttgacaagga	gcccagtcaactctgaaagc
Exon 9	ggtcctgtgcaggctttct	actcatgcctctcagggaag
Exon 10	acccctttcttggagctttgt	cctcatgccctcctccac
Exon 11	tgggccagagtttctcttct	tggtctcaagctgacccttc
Exon 12	actggtcctcgaacaagctc	cctcctcaccaagtaaacacg

Table S5.4. Individual minor allele single nucleotide polymorphisms identified in *APP*, *PSEN1* and *PSEN2* from genomic DNA sequencing of Case AD1

Location	**SNP ID**	**Allele**	**Allele Type**
PSEN2, Exon 3	rs6759	T	Minor
PSEN2, Exon 3	rs11405	C	Minor
PSEN2, Exon 4	rs1042740	T	Minor
PSEN2, Exon 11	rs2855562	G	Minor

Chapter 6

In vivo Characterization of Naturally Occurring, Pathogenic and Benign Aβ Multimers

Introduction

AD is a cerebral proteopathy, a brain disease caused by aberrant protein folding and aggregation. The cerebral proteopathies comprise a subset of over 40 disorders of various systems in which a functional, endogenous protein misfolds into a toxic species, either spontaneously or through the exogenous introduction of a similarly misfolded protein that serves as a folding template for disease transmission [289]. Other cerebral proteopathies include Huntington's disease, frontotemporal dementia, Parkinson's

disease, and the prion diseases, each of which can be attributed to the toxic gain of function of a single, distinct protein. Intriguingly, the toxic protein multimers in many of these phenotypically diverse disorders share a common higher order structural motif and, very likely, a common mechanism of toxicity [85]. From extensive studies of the initiation, transmission, and progression of the prion diseases, we know that a protein alone can be an infective disease agent that propagates in a new host via a mechanism of protein folding, or templating [101, 232]. The heritable information appears to lie in the structure of the folded proteins, and it is the structure itself that dictates the cellular characteristics of the infectious protein, such as disease incubation time, virulence, and toxicity [42]. Proteins with an identical amino acid sequence can fold into distinct molecular "strains", which in turn underlie unique disease phenotypes, and these strains generally are faithfully propagated between organisms of the same species [78].

Several molecular polymorphisms have been detected within β-sheet structures of Aβ fibrils from AD brains and synthetic peptide preparations, supporting the concept of Aβ strains [214, 277]. Recently developed amyloid-binding ligands exhibit striking conformational specificity, and may be able to differentiate structurally polymorphic Aβ fibrils at both *in vivo* and *ex vivo* levels of analyses [203, 207]. Pittsburgh Compound B (PIB) is a radiolabeled positron emission tomography (PET) ligand that binds specifically and with high affinity to naturally occurring Aβ deposits in the brains of AD subjects [118, 141, 244]. PIB binds with substantially diminished stoichiometry to aggregated Aβ in nonhuman primate and transgenic mouse brain, as well as to synthetic Aβ fibrils [141, 243], indicating that high-affinity PIB binding may be specific for a toxic form, or strain, of multimeric Aβ.

We have previously shown that cerebral Aβ peptide populations in aged chimpanzees, rhesus macaques, and squirrel monkeys are strikingly similar to the full-length, truncated, and modified Aβ isoforms that accumulate in the AD brain, but that the higher-order structure of nonhuman primate Aβ can be distinguished from that of AD by a paucity of high-affinity PIB binding sites [242, 243]. Therefore, multimeric Aβ in cognitively normal humans and in aged nonhuman primates may represent relatively benign strains of the folded peptide, as compared to the toxic Aβ aggregates found in AD.

In this study, we used the *in vivo* seeding model of Aβ-amyloidosis to characterize multimeric Aβ from AD and aged squirrel monkey brains, which are hypothesized to accumulate toxic and benign strains, respectively. Cortical extracts from both AD subjects and aged APP transgenic mice contain soluble Aβ "seeds" which induce the early misfolding and deposition of Aβ peptides when injected directly into the brains of young APP transgenic mice [129]. However, the morphology of seeded Aβ is determined by the nature of the Aβ "seeds" *and* the cortical environment of the host transgenic mouse [181, 286]. Cortical homogenates from different AD cases and Aβ-depositing transgenic mice induce morphologically distinct patterns of Aβ deposition. Furthermore, mice carrying various combinations of AD-like transgenes, under the control of diverse promoters, exhibit predilections for particular morphologies of seeded Aβ [181]. As such, seeding studies allow for the *in vivo* characterization of naturally occurring Aβ strains.

For the first time, we show that Aβ-rich cortical extracts from AD and aged nonhuman primates are similarly capable of seeding the early deposition of extracellular

Aβ in the PSAPP transgenic mouse brain. We also show that Aβ multimers from AD and aged squirrel monkeys are able to induce the formation of Aβ deposits with high-affinity PIB binding sites, which are not normally produced in the PSAPP mouse brain. Further characterization of naturally occurring, toxic and benign Aβ multimers in this seeding model may help to clarify the crucial events involved in the initiation and propagation of toxic misfolded proteins in Alzheimer's disease.

Materials and Methods

Subjects

Postmortem cortical tissue from five pathologically confirmed, end-stage AD cases (3 females, 2 males, ages 61-91) and two female nondemented human control cases (ages 57 and 75) were used in this study. All human postmortem material was obtained from the Emory University Alzheimer's Disease Research Center Brain Bank in accordance with federal and institutional guidelines, and the samples were coded to ensure the anonymity of the subjects. Nonhuman primate tissue was collected from five aged squirrel monkeys (one 23-year-old female and 4 males, ages 17-21) and 2 younger male squirrel monkeys, ages 10 and 14. Cortical tissue from squirrel monkey 06-5Ss was a generous gift from Dr. David Lyons (Stanford University, Palo Alto, CA), and cortical tissue from all other animals was collected at the Yerkes National Primate Research Center from aged animals that had died of causes unrelated to brain disease. All PSAPP mice used in this study carried co-segregating transgenes for APPSwe and PSEN1dE9, under the PrP promoter, and had been backcrossed for at least 8 generations [28]. PSAPP

mice were generously provided by Dr. James Lah of the Center for Neurodegenerative Disease at Emory University.

Tissue preparation

Bilateral tissue blocks from the superior temporal gyrus were dissected from all cases used in this study. Blocks from one hemisphere were snap-frozen and stored at -80°C. For preparation of tissue homogenates for Aβ ELISA and PIB-binding assays, blocks were weighed and then Dounce-homogenized in 5 volumes of Tris-buffered saline homogenization buffer (50mM Tris-HCL and 150mM NaCl containing complete protease inhibitor cocktail [Santa Cruz Biochemicals, Santa Cruz, CA]). Aliquots were stored at -80°C until use.

For the preparation of seeding injectates, tissue blocks were weighed, Dounce-homogenized in 4 volumes of 0.1M phosphate-buffered saline (1x PBS), vortexed, and then sonicated 3 times for 5 seconds. The samples were centrifuged at 3,000 x g for 5 minutes at 4°C, and aliquots of the supernatant ("injectate") were stored at -80°C until just before use [286].

Contralateral tissue blocks and mouse brains from the first experiment were immersion-fixed in PBS-buffered, 4% paraformaldehyde, cryoprotected in 30% sucrose, and then sectioned on a cryostat at 50μm and 40μm, respectively. Sections were stored at -20°C in antifreeze containing 30% ethylene glycol and 30% sucrose.

Unfixed mouse brains collected from the second and third seeding experiments (see below) were processed for autoradiography, immunohistochemistry, and radioligand binding experiments, all on ice. The right hemisphere was nicked along the ventral

cortex for identification purposes and the brains were coronally bisected in a brain matrix at the rostrocaudal level of the injection site. The rostral-most block was snap-frozen, sectioned on a cryostat at 12μm, and affixed to silanized slides. Block B2, caudal to the injection site, was slabbed caudally at the level of the rostral cerebellum, and the right and left hippocampi then were dissected from block B2 with a sterile #11 scalpel blade. The hippocampi were weighed, homogenized in 9 volumes of TBS homogenization buffer, and the aliquots were stored at -80°C. The remainder of block B2 was immersion-fixed in PBS-buffered 4% paraformaldehyde for 24 hours, embedded in paraffin wax, and processed for histochemical examination.

Stereotaxic mouse surgeries

In the first series of seeding experiments, eight 4-month old, female PSAPP mice were anesthetized with isoflurane gas. 2.5μl of 10% AD or squirrel monkey injectate (AD: OS02-159, E04-172; SM: 83GO, 84L, *n*=2 for all cases) were stereotaxically injected into the hilus of the dentate gyrus at a rate of 0.5μl/min, using the following coordinates: -2.2 A/P; +/-1.8 ML; -1.9 DV [75]. Sham injections of sterile PBS were administered in the contralateral hippocampus. Post-operatively, mice received an injection of 0.05 mg/kg buprenorphine to minimize discomfort. In the second series of experiments, 27 two-month old PSAPP mice received unilateral intrahippocampal injections of AD or squirrel monkey cortical extract, using the same coordinates described above. The injectates were individually diluted in order to standardize the total levels of Aβ peptide in all injectates (Table 6.2). In the contralateral hippocampus, the mice received a control injection of cortical extract that was essentially devoid of fibrillar

Aβ, i.e. from nondemented humans or younger squirrel monkeys, at the same dilution as the Aβ-rich injectates (Table 6.2).

For the final, third seeding experiment, all five AD or squirrel monkey injectates (10% w/v) were mixed together at 1:1 ratios and vortexed for one minute to create "mixed injectates". Eight 11.5 week-old mice were injected unilaterally with 2.5μl of the mixed injectate (AD *n*=5, squirrel monkey *n*=3) at the coordinates noted above, and with 2.5μl of 1x PBS into the contralateral hemisphere as a control. All 43 animals were incubated for 4 months after surgery, after which the 8 animals from Series 1 were euthanized by overdose of isoflurane and transcardially perfused with ice-cold phosphate-buffered 4% paraformaldehyde. The 27 animals from Series 2 and the 8 animals from Series 3 were euthanized by overdose of isoflurane, and the unfixed brains were collected by dissection on an ice-cooled plate.

Antibodies

Antibodies used for histochemical processing were: monoclonal anti-Aβ antibody 6E10, raised against Aβ1-16 (1:25,000, Covance, Princeton, NJ), polyclonal antibodies R361 and R398, to Aβ32-40 and Aβ33-42, respectively (both at 1:15,000, generously provided by Dr. Pankaj Mehta, Institute for Basic Research of Developmental Disabilities, Staten Island, NY), monoclonal antibody to NeuN (1:5000, Chemicon, Temecula, CA), polyclonal antibody to glial fibrillary acidic protein (α-GFAP, 1:5,000, Dako, Carpinteria, CA), and the monoclonal Iba1 antibody as a marker for microglia (1:10,000, Osaka, Japan) [241].

Immunohistochemistry

For immunohistochemical labeling of Aβ deposits in cortical tissue sections, endogenous peroxidase was blocked with 3% H_2O_2 in methanol and then Aβ epitopes were revealed by incubation with 100% formic acid for 10 minutes. Nonspecific binding was blocked by a one hour incubation in 2% normal serum (horse serum for mouse monoclonal and goat serum for rabbit polyclonal antibodies) and 0.2% Tween-20 (Sigma-Aldrich, St. Louis, MO) in 1xPBS ("blocking solution"). Without rinsing, sections were then incubated in primary antibody diluted in blocking solution, shaking overnight at 4°C. After rinsing in 1xPBS on the second day, sections were incubated in biotinylated secondary antibody (1:200 in blocking solution) for one hour, rinsed, then incubated for 30 minutes in avidin-biotin enzyme complex from the Vectastain Elite kit (Vector Laboratories, Burlingame, CA), all at room temperature. Antigen-antibody-horseradish peroxidase complexes were revealed with diaminobenzidine as the chromogen (Vector Labs). As a negative control, non-immune mouse IgG or rabbit serum was used in place of monoclonal and polyclonal antibodies, respectively. AD tissue was used as a positive control in all experiments.

For cellular localization of Aβ-immunoreactive deposits by double immunofluorescence labeling, after overnight incubation with monoclonal antibody 6E10 as described above, sections were rinsed and incubated in biotinylated anti-mouse antibody (1:200 in blocking solution, Jackson ImmunoResearch Laboratories, West Grove, PA) for one hour, rinsed, and then incubated for one hour with fluorescein-conjugated streptavidin (1:500 in blocking solution, Jackson), all at room temperature. Sections were extensively rinsed in 1xPBS and then incubated for one hour in blocking

solution at room temperature, followed by overnight incubation with primary antibody (GFAP, Iba1 or NeuN), diluted in blocking solution, at 4°C. On day 3, the sections were rinsed in 1xPBS and incubated for one hour in Rhodamine Red-X-conjugated anti-mouse or anti-rabbit secondary antibody (Jackson). Slide-mounted sections were coverslipped with Dakocytomation fluorescence mounting medium (Dako).

Light microscopic images were captured with a Leica DMLB microscope (Leica, Wetzlar, Germany) and Spot XPlorer and Flex digital cameras (Diagnostic Instruments, Sterling Heights, MI). Confocal images were taken with a Zeiss LSM 510 laser scanning confocal microscope (Carl Zeiss, Oberkochen, Germany). Besides cropping, images were not further manipulated prior to publication.

Aβ ELISA

Cortical homogenates were spun at 100,000g for 60 minutes at 4°C in a TLA 100.4 rotor (Beckman Coulter, Fullerton, CA) and the supernatant was removed as the "soluble fraction." Pellets were probe-sonicated for 30 seconds in 70% formic acid, centrifuged at 14,000g for 30 minutes at 4°C, and the clear supernatant, or the "insoluble fraction," was removed. Both fractions were aliquoted and stored at -80°C. To measure total Aβx-40 and Aβx-42 in cortical extracts, formic acid-solubilized protein extracts were neutralized with Tris base, pH 11.0. Soluble and neutralized insoluble cortical extracts were diluted in sample buffer (1:2 to 1:5,000) and peptides were measured by enzyme-linked immunosorbance assays, according to manufacturer's instructions (The Genetics Company, Schlieren, Switzerland). Samples were read at 450nm on a Biotek Synergy multidetection plate reader (Biotek, Winooski, VT).

Autoradiography

Slide-mounted frozen cryosections were brought up to room temperature in air-tight containers and then immersion-fixed in 10% ethanol/PBS for 20 minutes. Sections were incubated in 1.0nM ^{3}H-PIB (SA=82Ci/mmol, custom synthesis, GE Healthcare, UK) in 5% ethanol/PBS for one hour at room temperature, rinsed 2 times with 10% ethanol/PBS and 2 times with ddH_2O, both on ice, and then air-dried before exposing directly to ^{3}H-Hyperfilm (GE Amersham, UK). After 4 weeks exposure, the film was developed with D19 developer solution (Kodak, New Haven, CT) and images were captured with a QICAM digital camera (QImaging, Surrey, BC, Canada). Adjacent cryosections were immunostained with Aβ antibody 6E10, as described above.

For "radiodotblot" analysis of high-affinity PIB binding sites, 2μl of clarified temporal cortical homogenates (20% w/v) or 3μl hippocampal homogenates (10% w/v), were pipetted in duplicate onto silanized "Superfrost Plus" microscope slides (Fisher Thermo Scientific, Waltham, MA), dried on a slide warmer at 37°C overnight, and stored in an airtight container at -80°C until use. "Dot blot" slides were processed in the same manner as slide-mounted cryosections, described above. Intensity in a prescribed region of interest for each sample was quantified using Photoshop. Group means were compared using an unpaired t-test with a 95% CI.

Table 6.1. Case List

Case	Group	Age	Sex	PMI	Braak	ApoE
OS02-159 (AD1)	AD	61	m	5.5	V/VI	3/4
OS01-128 (AD2)	AD	91	f	2.5	V/VI	3/4
E05-04 (AD3)	AD	64	f	4.5	VI	3/4
E05-87 (AD4)	AD	61	m	4	V/VI	3/4
E04-172 (AD5)	AD	87	f	6	V/VI	3/4
E04-34	ND	57	f	17	0	3/3
OS02-35	ND	75	f	6	0	3/3
06-5Ss (SM1)	SM	23	f	<3		
83GO (SM2)	SM	20	m	1		
90T (SM3)	SM	18	m	1		
84L (SM4)	SM	21	m	1		
86J (SM5)	SM	17	m	1		
92AC	SM	14	m	1		
06-2Ss	SM	10	m	1		

AD: Alzheimer's disease; ND: Non-demented human; SM: Squirrel monkey; m: male; f: female

Table 6.2. Seeding Experiment 2: Aβ-normalized injectates, contralateral control cases, and quantitative soluble and insoluble Aβ ELISA data

				Soluble Fraction			Insoluble Fraction		
Case	**Inject. (%)**	**Ctl**	**N**	**Aβ40**	**Aβ42**	**Total Aβ**	**Aβ40**	**Aβ42**	**Total Aβ**
AD1	10	E04-34	2	0.50	0.05	0.55	39.84	174.88	214.72
AD2	10	OS02-35	3	0.08	0.07	0.15	17.75	196.38	214.13
AD3	5	E04-34	3	0.07	0.12	0.12	3.88	444.72	448.59
AD4	4	E04-34	1	1.59	0.09	1.68	275.37	352.57	627.94
AD5	10	OS02-35	2	0.01	0.03	0.04	7.65	217.09	224.74
SM1	6.67	92AC	3	0.02	0.07	0.09	18.63	317.88	336.52
SM2	3.33	92AC	3	7.11	1.41	8.52	497.06	252.49	749.55
SM3	6	06-2Ss	3	0.03	0.10	0.13	2.71	356.88	359.59
SM4	4	06-2Ss	3	8.12	2.07	10.19	366.78	229.97	596.75
SM5	20	92AC	3	0.31	0.32	0.63	8.32	90.96	99.28

Figures

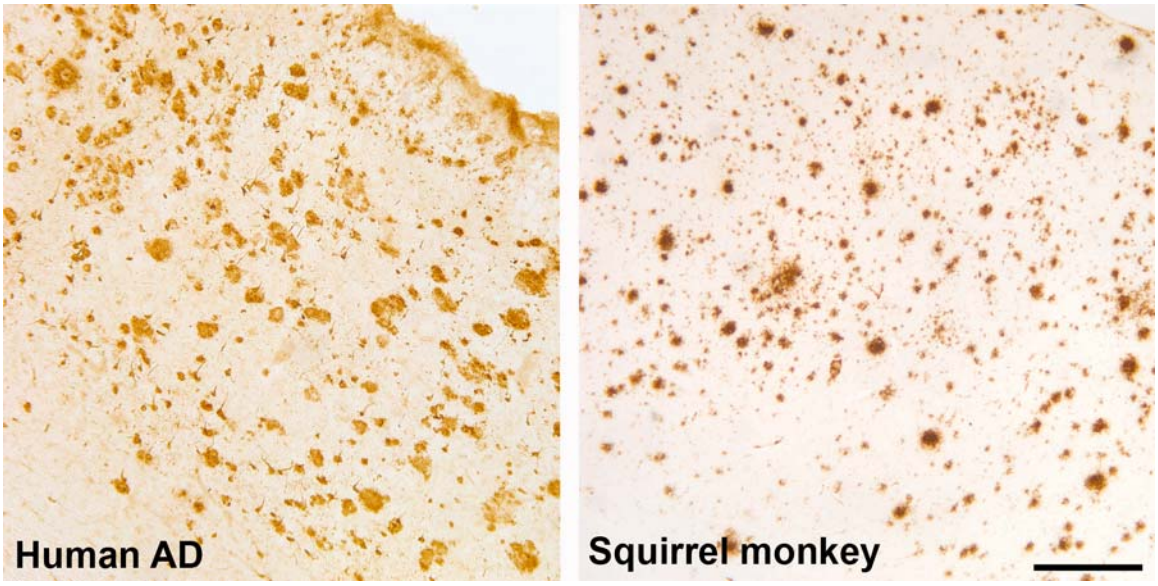

Figure 6.1. **Profound cerebral β-amyloid deposition in Alzheimer's disease and in an aged squirrel monkey**. Temporal cortical sections from AD (E04-172) and squirrel monkey (06-5Ss) cases immunostained with an antibody to Aβx-40 (R361). Both cases exhibit numerous diffuse and cored Aβ deposits (golden brown) throughout all cortical layers. Bar = 200μm.

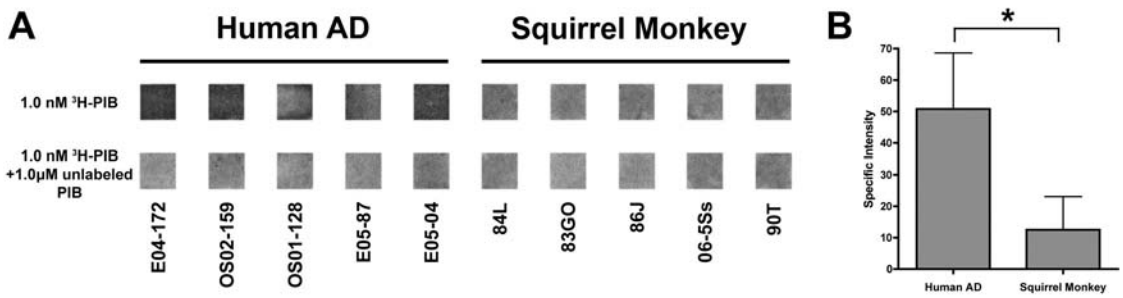

Figure 6.2. Radiodotblot detection of substantial high-affinity ^{3}H-PIB binding in AD compared to aged squirrel monkey cortical homogenates. (**A**) Aβ-rich temporal cortical homogenates (300μg wet tissue) from AD cases and squirrel monkeys (*n*=5 each) were analyzed by ^{3}H-PIB radiodotblot. In the top row, dried homogenates were incubated with 1.0nM ^{3}H-PIB. Samples in the bottom row were co-incubated with 1.0 nM ^{3}H-PIB and 1.0μM unlabeled PIB to determine the levels of nonspecific ligand binding. Shown here are identical regions of interest from a single film exposure. Darker signal indicates the presence of specifically bound radioligand. (**B**) Densitometric quantification of signal from the radiodotblot experiment, in which nonspecific signal (+ unlabeled PIB) was subtracted from positive signal detected after incubation with 1.0nM ^{3}H-PIB. PIB binding was significantly higher in AD human cortical homogenates compared to squirrel monkey cortical homogenates. Means (in Specific Intensity) - AD Human: 50.78, SD=17.85; Squirrel monkey: 12.50, SD=10.56, p = 0.0033. Bars = standard deviation.

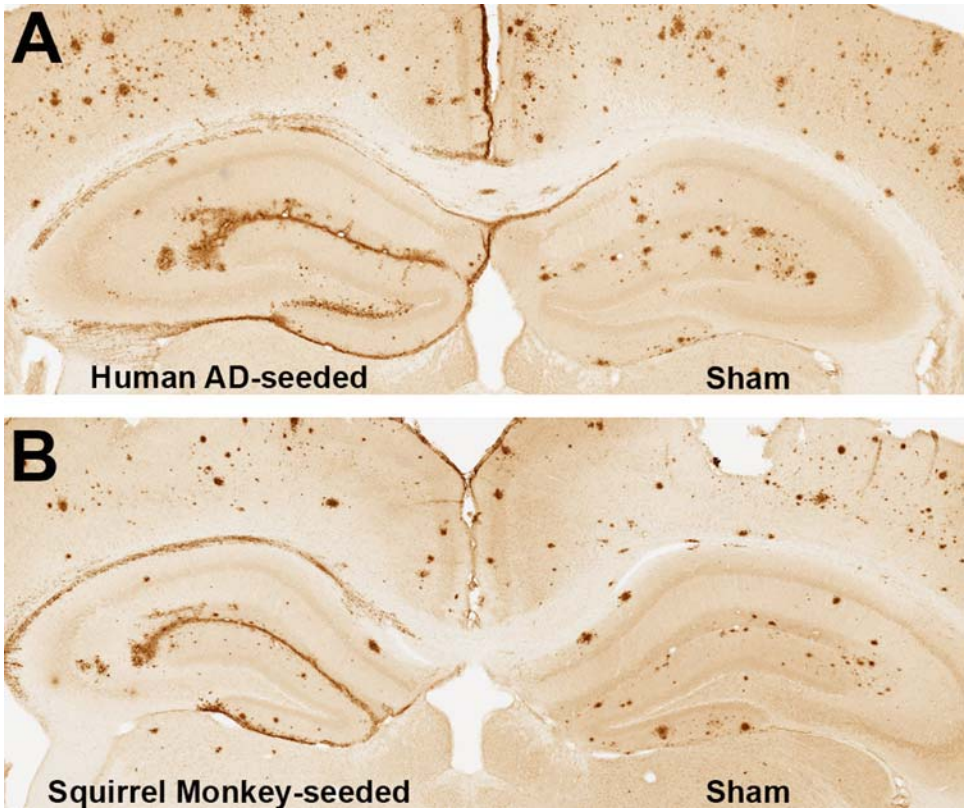

Figure 6.3. Aβ-rich cortical homogenates from both AD cases and squirrel monkeys seed the deposition of Aβ in PSAPP mouse hippocampus. (**A**) 10% AD extract (OS02-159) injected into the dentate gyrus of a 4-month old PSAPP mouse induced heavy Aβ deposition in the dentate granule cell layer, the hippocampal fissure and along the pial surface. Seeded Aβ deposition also is apparent along the corpus callosum dorsal to the hippocampus, exhibiting substantial lateral spread in both directions. Note the apparent decrease in independent hippocampal plaques in the seeded hemisphere compared to the contralateral hippocampus, which was injected with 1xPBS. (**B**) Injection of aged squirrel monkey cortical extract (84L) induced a strikingly similar pattern of seeded Aβ deposition in the hippocampus and white matter of this PSAPP

mouse. 40μm-thick fixed-frozen sections were immunostained with an antibody to Aβ42 (R398). Objective: 5x.

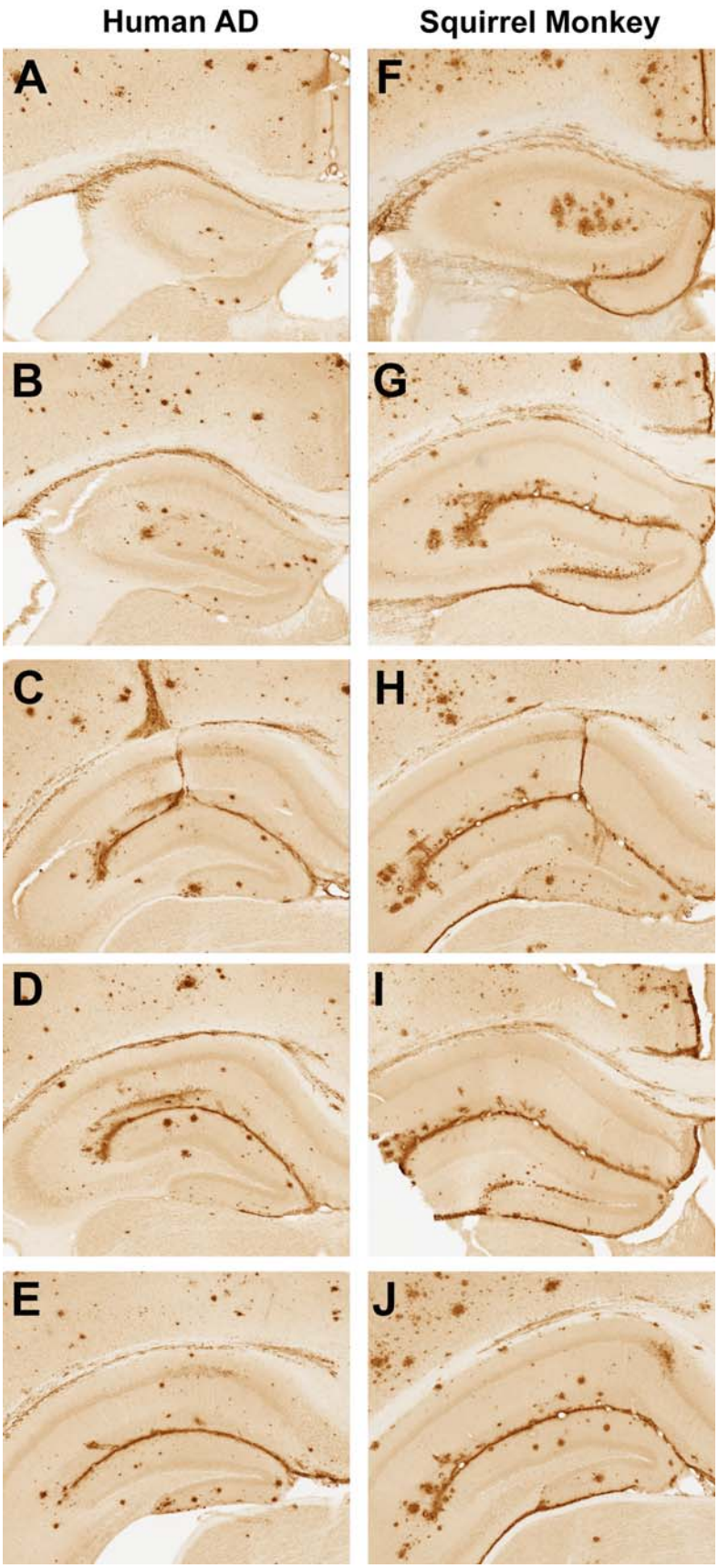
Human AD
Squirrel Monkey
A
F
B
G
C
H
D
I
E
J

Figure 6.4. AD and monkey-seeded Aβ deposition spreads throughout most of the rostro-caudal extent of the PSAPP mouse hippocampus. (**A-E**) AD cortical extract induced Aβ deposition throughout all hippocampal cell layers, the hippocampal fissure and the corpus callosum near the injection site. (**F-J**) Squirrel monkey cortical extract (84L) induced induced a similar pattern of Aβ deposition. Both AD and squirrel monkey-seeded Aβ exhibits substantial spread both rostrally and caudally, often reaching the limits of the hippocampal formation in the injected hemisphere. 40μm-thick fixed-frozen sections were immunostained with an antibody to Aβ42 (R398). Objective: 5x.

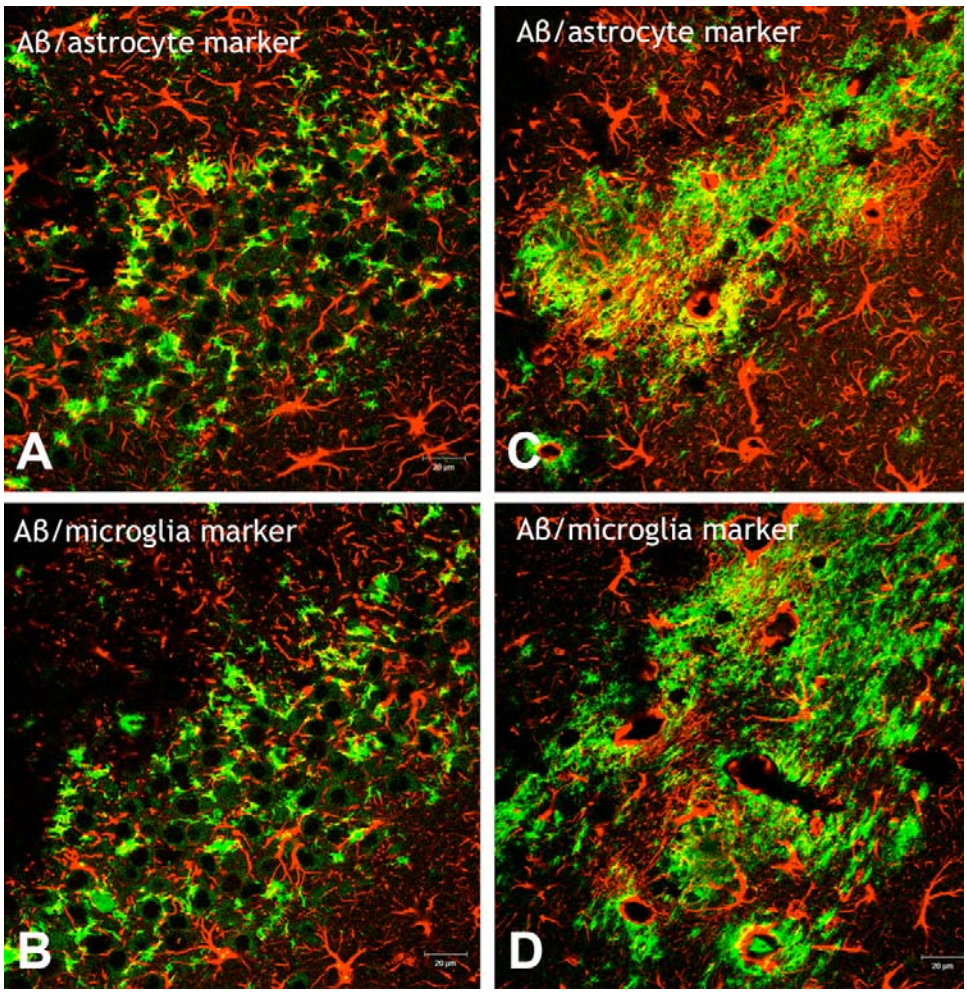

Figure 6.5. **Both AD and monkey-seeded Aβ is predominantly extracellular.** (**A, B**) Double immunofluorescence and confocal microscopy with antibodies to Aβ and glial cells (GFAP for astrocytes and Iba1 for microglia) in the CA3 region of an AD extract-injected mouse reveal little colocalization of Aβ and either glial marker. (**C, D**) In the corpus callosum above the hippocampus of monkey-injected PSAPP mouse brain, there is some colocalization of Aβ in GFAP-positive astrocytes, but no aggregated Aβ was detected in Iba1-labeled microglial cells. Aggregated Aβ also was detected in white

matter astrocytes in AD extract-injected animals. Aβ/NeuN double immunofluorescence did not reveal any intraneuronal Aβ aggregates (data not shown). Bars = 20μm.

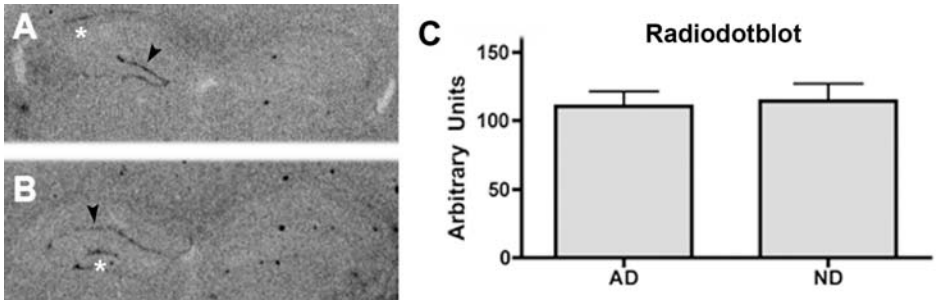

Figure 6.6. **Injectates containing mixed AD extracts and mixed squirrel monkey extracts both seed high-affinity PIB binding sites in PSAPP mouse brain (Experiment #3). (A**) 1.0 nM ^{3}H-PIB autoradiography on a 12μm cryosection from a "mixed AD extract"-injected animal reveals high-affinity PIB binding along the dentate gyrus (black arrowhead) and in the corpus callosum (above white asterisk), presumably within seeded Aβ deposits, as there is no PIB-positive material detected in the sham-injected hippocampus in this 6-month old mouse. (**B**) PIB-positive Aβ deposits are detected along the hippocampal fissure (black arrowhead) as well as in the dentate gyrus (above white asterisk) in the squirrel monkey extract-injected hemisphere of a PSAPP mouse. (**C**). 1.0 nM ^{3}H-PIB radiodotblot analysis of hippocampal homogenates from AD extract-injected and nondemented human cortical extract-injected hemispheres reveal no difference in PIB binding between the two hippocampi, despite the presence of a small amount of seeded Aβ in the AD extract-injected hippocampus by autoradiography, possibly reflecting the differential sensitivity of the two assays.

Results

Aβ deposition in AD and aged nonhuman primate brain

We previously showed that cerebral Aβ40 and Aβ42 peptides accumulate at comparable levels in end-stage AD and very old squirrel monkeys. Here we confirm by immunohistochemistry with Aβ-specific antibodies that the broad morphological spectrum of Aβ plaques in the AD brain is recapitulated to a certain extent in aged squirrel monkeys, although there is considerable inter-animal variability, and the plaques overall tend to be smaller in squirrel monkeys (Figure 6.1). In the 5 aged squirrel monkeys examined in this study, we identified diffuse, compact, and neuritic parenchymal plaques containing Aβ1-x, Aβx-40 and Aβx-42 peptides. Aβ-immunoreactive material also was detected in capillaries and large vessels of all 5 squirrel monkeys, whereas cerebral β-amyloid angiopathy was much less frequent in the 5 AD subjects examined (not shown). In some instances, parenchymal Aβ plaque density appeared substantially greater in AD cortex compared to squirrel monkey cortex, and plaques in AD temporal cortex were distributed throughout cortical layers 2 to 6 while squirrel monkey plaque deposition was more focal in nature, and not seen in all cortical layers.

In an earlier study, we used autoradiography and microplate radioligand binding assays to demonstrate that ^{3}H-PIB binds to high affinity sites with high stoichiometry in Aβ-rich AD cortex, whereas ^{3}H-PIB binds with much lower stoichiometry to Aβ-rich squirrel monkey cortex. Here we employed a new technique, the “radiodotblot”, in which cortical homogenates are dried onto slides and then ^{3}H-PIB binding is analyzed by

standard autoradiographic techniques. We have shown that this simple quantitative technique is reliable for the detection of radioligand binding sites. By radiodotblot analysis, we confirm that homogenates from AD cortex contain abundant high-affinity PIB binding sites, while squirrel monkey cortical homogenates exhibit little to no high-affinity PIB binding (Figure 6.2).

In vivo seeding with AD and aged squirrel monkey cortical extract

Aβ immunohistochemistry on fixed-floating PSAPP mouse brain sections from the first series of seeding experiments revealed that cortical homogenates from all 4 subjects (2 AD and 2 squirrel monkey cases) induced the anomalous deposition, or seeding, of hippocampal Aβ in the injected hemisphere. AD and squirrel monkey extracts both induced similar patterns of extracellular β-amyloid deposition when injected into the hilus of the dentate gyrus in murine hippocampus (Figure 6.3). Seeded β-amyloid accumulated along the hippocampal fissure and exhibited extensive spread into the rostral and caudal boundaries of the hippocampal formation (Figure 6.4). Aβ deposition also was induced along the CA1 and CA3 cellular layers and around the dentate gyrus granule cells, and variability was likely due to slight differences in injection sites. Seeding along the cellular layers also exhibited substantial rostrocaudal spread. In the sham-injected hippocampi of the transgenic mice, there was substantial parenchymal plaque deposition, which is typical for this transgenic strain at 8 months of age (Figure 6.3). Fewer such plaques were seen in the seeded hemisphere, suggesting that the exogenously introduced Aβ seeds had somehow shifted the endogenous Aβ aggregation pathway. Seeded Aβ was also detected in the corpus callosal white matter pathway

above the hippocampus, possibly as a result of extract leakage along the needle track. Aβ deposits in the white matter tracts exhibited spread across the corpus callosum into the contralateral hemisphere in some of the animals (Figure 6.3). Aβ seeding has been described previously in the entorhinal cortex of the injected hemisphere, but we did not see entorhinal seeding in any of these animals, possibly due the heavy amount of endogenous plaque deposition in the 8-month old mice.

To determine if seeded Aβ aggregates were intraneuronal, intraglial, or extracellular, we used confocal microscopy and double immunofluorescence with the 6E10 antibody raised to Aβ1-16 and a microglial, astrocytic, or neuronal marker. In both AD and monkey-seeded mice, we did not detect any colocalization of Aβ and NeuN, indicating that Aβ was not aggregating within hippocampal neurons (data not shown). There was also very little colocalization of 6E10-immunoreactive Aβ deposits and either of the glial markers, although some Aβ was detected within astrocytes in white matter tracts of all seeded animals (Figure 6.5).

Seeding of high-affinity PIB binding sites in transgenic mouse brain

Aβ plaques in the brains of transgenic mice contain a very low stoichiometry of high-affinity PIB binding sites per molecule of Aβ [141]. To determine if Aβ seeded by PIB-positive Aβ multimers from the AD brain contains high-affinity PIB binding sites, slide-mounted, rostral hippocampal cryosections and dot blots of caudal hippocampal homogenates were incubated with 1.0nm ^{3}H-PIB for autoradiographic analysis. Quantitative radiodotblots did not reveal detectable high-affinity PIB binding in any hippocampal homogenates (Figure 6.6C). However, autoradiography on intact

cryosections did reveal high-affinity PIB binding sites in the hippocampus of PSAPP mice that were injected with mixed extracts containing Aβ multimers from all 5 AD subjects in this study (Figure 6.6A). Surprisingly, a similar pattern of PIB-positive β-amyloid was also detected in mice that had been injected with mixed cortical extracts from squirrel monkeys (Figure 6.6B).

Discussion

In this study, we used an *in vivo* transgenic mouse model of cerebral β-amyloidosis to characterize naturally occurring Aβ multimers from the brains of AD and aged squirrel monkey subjects. According to the β-amyloid cascade hypothesis of AD pathogenesis, the aggregation of Aβ peptides into toxic Aβ multimers initiates the neurodegenerative cascade in the AD brain. However, Aβ with the same amino acid sequence as in humans also aggregates in the brains of aged nonhuman primates, in the absence of severe neurodegeneration or dementia. Aβ peptides can fold into structurally and functionally polymorphic strains [85, 181, 215], and we hypothesized that Aβ in the aged nonhuman primate brain represents a benign strain of the peptide, which is highly fibrillogenic but does not fold into toxic multimers.

We have assessed the ability of cerebral Aβ from aged monkeys to seed β-amyloidosis in the PSAPP transgenic mouse brain in order to validate this paradigm for the *in vivo* study of permissive templating (i.e., the propagation of protein strain polymorphisms). Aβ-rich cortical extracts from both AD and APP transgenic mouse brain have been shown to seed β-amyloid deposition in several different mouse models of

cerebral β-amyloidosis. However, this seeding effect cannot be replicated with synthetic Aβ peptides, suggesting that only certain strains of Aβ can template protein folding *in vivo* [129, 181]. For the first time, we showed that Aβ-rich cortical extract from a nonhuman primate, the squirrel monkey, can seed Aβ deposition *in vivo*, and that monkey-seeded β-amyloid accumulates and spreads at levels comparable to those seen in AD cortical extract-seeded β-amyloidosis. When injected into the hilus of the dentate gyrus, clarified homogenates from both monkey and AD temporal cortex produced pronounced deposition of Aβ, particularly along the hippocampal fissure and just beneath the superficial pia mater. After only one injection of cortical extract, seeded Aβ is seen throughout most of the rostrocaudal extent of the hippocampal fissure, similar to what has been shown in previous studies. Both monkey and AD cortical extracts also induce Aβ deposition around the dentate gyrus granule cells, along the CA1 and CA3 cellular layers, and among the white matter tracts of the corpus callosum. Seeded Aβ along the hippocampal cellular layers and within white matter tracts also exhibits extensive spread in both the rostral and caudal directions. Using double immunofluorescence and confocal microscopy, we demonstrated that the majority of seeded Aβ deposits are extracellular, despite a sometimes stellate appearance along the pyramidal cell layers. Further study is warranted to determine if the spread of seeded β-amyloid in this model is a result of physical diffusion, cell-to-cell trafficking/axonal transport, or both mechanisms in concert.

We have previously shown that Aβ from the brains of Alzheimer patients and nonhuman primates differs in the high-affinity binding to Pittsburgh Compound B, a PET radioligand that binds with high specificity to Aβ deposits in the living AD brain. In this

study, we replicated these findings using a novel "radiodotblot" technique with cortical homogenates from a cohort of 5 aged squirrel monkeys and 5 comparison AD cases. The radiodotblot technique allows for the quantification of PIB binding in cortical homogenates without a liquid scintillation counter, while maintaining a satisfactory signal-to-noise ratio. Additionally, the homogenate is dried onto a glass side before incubation with ^{3}H-PIB, so there is no need for membrane filtration, and no chance that any smaller, more soluble Aβ oligomers are washed away. The differential binding of PIB in our radiodotblot experiment adds to the evidence that Aβ folds into structurally distinct strains in AD and aged squirrel monkey brain.

Previous seeding studies with APP transgenic mouse cortical extracts injected into single and double transgenic Aβ-producing mice have shown that the morphology of seeded β-amyloid is determined by the strain of the exogenously introduced Aβ "seeds" and also by the transgenic makeup of the injected mouse. We therefore hypothesized that Aβ seeds from AD and aged squirrel monkey brain would induce donor-specific patterns of molecular folding in seeded amyloid in PSAPP mice. Specifically, we hypothesized that AD cortical extracts would seed plaques that bind PIB with high affinity in the transgenic mice, whereas squirrel monkey cortical extracts would not. To test this hypothesis, we quantified high-affinity PIB binding in seeded hippocampal homogenates using radioligand binding microplate assays. PIB binding in homogenized hippocampi was also measured with radiodotblot experiments. Finally, we simultaneously assayed PIB binding by autoradiography on intact cryosections from the same animals.

Using both radiodotblot analysis *and* liquid scintillation-based binding assays of hippocampal homogenates, we were unable to detect high-affinity ^{3}H-PIB binding in

either AD-seeded or monkey-seeded amyloid. Autoradiography is an integrating method of radioligand binding detection while liquid scintillation-based techniques rely on a count rate method of radioligand quantification. Our radiodotblot experiments settle any ambiguity between microplate binding assays (count rate) and film autoradiography, by utilizing integrating autoradiography on the same tissue homogenate samples as the binding assays to show that high-affinity PIB binding cannot be detected in any of these homogenized tissue samples.

However, autoradiography on cryosections from the same seeded mice did reveal the presence of PIB-positive seeded amyloid. We clearly detected high-affinity PIB binding within seeded Aβ deposits in the hippocampus, whereas no PIB binding could be detected in the contralateral, age matched control extract-injected hemisphere. The contradictory results we obtained using ^{3}H-PIB radiodotblot and autoradiography analyses highlight the different sensitivities of the two assays, although both use integrating methods of specifically-bound radioligand detection. PIB binding is likely concentrated within single plaque deposits in seeded hippocampi, and the signal:noise ratio is too low within homogenized tissue. Tissue homogenization may also alter ligand binding sites within protein aggregates.

Our cryosection autoradiography data suggest that *in vivo* seeding consists of high fidelity protein templating, and supports the use of this model to study the misfolding and bioactivity of other proteins that form toxic multimers in the human brain. With longer incubation periods, the model may also be used to study the cellular effects of Aβ and other toxic protein aggregates. The induction of PIB-positive amyloid by *both* AD and squirrel monkey extract further suggests that seeded Aβ in the transgenic mouse brain

may very well fold into novel Aβ strains that maintain structural characteristics of endogenous Aβ from both the agent (AD or squirrel monkey) and the host (transgenic mouse).

This is this first demonstration that Aβ-rich cortical extracts from aged nonhuman primates are able to induce the deposition of Aβ *in vivo*. Based on the general similarities in cerebral β-amyloidosis between aged nonhuman primates and humans with AD [242, 243], it is perhaps not surprising that cortical extracts from both groups induce profuse β-amyloidosis that spreads throughout the physical boundaries of the mouse hippocampus. More unexpected is the finding that Aβ-rich extracts from AD *and* squirrel monkey brains can induce the formation of high-affinity PIB binding sites in seeded Aβ deposits. Additional studies to fully characterize and quantify PIB binding components in seeded PSAPP mouse brains are currently underway. The creation of a mouse model of Aβ deposition with AD-like, high-affinity PIB binding sites could be a valuable tool for the identification of early events in the Aβ misfolding pathway that initiates the pathogenesis of Alzheimer's disease.

Chapter 7.

Discussion

I present in this dissertation a comprehensive analysis of cerebral Aβ peptide populations in aged nonhuman primates and in humans who had died in the final stages of Alzheimer's disease. The multimerization and accumulation of Aβ initiates the neurodegenerative cascade in the AD brain, but Aβ with the human-type amino acid sequence also aggregates profusely in nonhuman primates without gross neuronal loss or dementia. As a potential explanation for the existence of toxic and benign forms of a single peptide, I hypothesized that cerebral Aβ aggregates are structurally polymorphic between humans and nonhuman primates. Specifically, I hypothesized that, even with the identical amino acid sequence, Aβ in different species can assume different 2-, 3- and/or 4-dimensional molecular configurations that may govern the pathogenicity of the

molecules. To test this hypothesis, I designed a comparative study of Aβ peptides in postmortem cortical tissue from nondemented humans, humans with AD, and three species of aged nonhuman primates: chimpanzees (our closest living relatives), rhesus macaques (an Old World monkey species), and squirrel monkeys (New World monkeys). In collaboration with laboratories at Emory University, the University of Kentucky, New York University, Mount Sinai School of Medicine, and the University of California at Los Angeles, I demonstrated that Aβ peptides are strikingly similar, both in terms of quantity and peptide fragment populations, in AD and aged nonhuman primate brain. However, I provide the first evidence that the higher-order structure of the peptide is distinct in the two groups. These results confirm and elaborate upon previous reports that cerebral APP processing and the age-related upregulation of the amyloidogenic processing pathway have been conserved throughout primate evolution. By including New World and Old World monkey species in this comparative study, the data further suggest that the cortical environment and/or the molecular chaperones that permit the toxic misfolding of Aβ peptides in the AD brain did not emerge until after the chimpanzee and human lineages diverged.

My experimental design was a phenotype-driven comparative study intended to bolster our understanding of what makes us human, as well as to shed light on the cellular and molecular mechanisms of a devastating, human-specific disease. The human and chimpanzee lineages diverged approximately 6 million years ago, and the two species share over 95% genome homology [1]. Despite these genetic similarities, the human neocortex is relatively larger, and we live substantially longer than chimpanzees or any other extant primate [114]. The benefits of increased brain size and extended lifespan are

considerable, and include higher level analytical thought and reasoning, complex social interactions and family networks, and intricate systems of written and spoken language that allow for long-lasting and near-universal forms of communication. However, the benefits of encephalization and longevity come at a cost for *Homo sapiens*, particularly in the form of age-related disease. Several evolutionary theories of aging provide potential explanations for these human-unique diseases of age, notably Williams' "antagonistic pleiotropy" theory and Medawar's theory of mutation accumulation [177, 303]. Both theories assert that a decreased selection for traits that are not expressed until after human reproductive cessation allows for the preservation of late-acting deleterious genes within the human genome [138]. For this dissertation project, the unique human susceptibility to Alzheimer's pathology is used as a paradigm to identify a detrimental molecular mechanism that may have evolved within the hominid lineage and contributes to the human senescent phenome. Further comparative study is necessary to determine if the mechanisms underlying the formation of human-specific multimeric Aβ exist as a result of antagonistic pleiotropy, and may therefore be involved in brain size or longevity, or if they might be the result of some deleterious, late-acting mutation that provides no reproductive benefit but escaped selection during hominid evolution.

Adventures in Tissue Collection

One of the more difficult obstacles to executing a comparative study of primate brain aging was the acquisition of a sufficient quantity and quality of tissue from each of the nonhuman primate species examined. There are limited numbers of nonhuman

primates in captivity, and few of them survive until the final quartile of the species lifespan, during which time cerebral Aβ is widely deposited. Cortical tissue from aged chimpanzees is particularly rare and valuable, as a moratorium on chimpanzee breeding in federally funded research facilities has been in effect since 1995, and tissues for postmortem analyses will no longer be available by the year 2037 [44]. Because most tissue samples are routinely fixed, an additional obstacle was the collection of unfixed cortical tissue, which was necessary for the biochemical analysis of Aβ proteins and my Aβ-seeding studies.

I obtained fixed and unfixed cortical specimens from AD and nondemented human subjects in collaboration with Dr. Marla Gearing of the Emory University Alzheimer's Disease Research Center. At the Yerkes National Primate Research Center, I collected fixed and unfixed tissue from a sizable cohort of aged nonhuman primates, including chimpanzees, rhesus macaques, and squirrel monkeys, thanks in large part to the support of Todd Preuss and his neuroanatomy laboratory. To enhance the number of monkeys, however, I then sent out tissue requests to nonhuman primate researchers around the country. After several fortuitous shipments and one North Carolina road trip, I finally acquired sufficient β-amyloid-laden tissue from the 3 nonhuman primate species to begin the proposed study.

Alzheimer's Pathology in a Chimpanzee?

Cerebral Aβ deposition in aged apes and monkeys has been reported by our group and several others in the United States and Asia [63, 81, 82, 137, 287]. Because of the

variability in age of onset for Aβ deposition, I screened fixed temporal cortical sections from all potential nonhuman primate subjects for β-amyloid load by Aβ immunohistochemistry. Fixed tissue from each case was processed with four antibodies to Aβ: monoclonal antibodies 4G8 and 6E10 to Aβ17-24 and Aβ1-16, respectively, and polyclonal antibodies R361 and R398, specific to the C-termini of Aβ40 and Aβ42, respectively, as well as AT8, a monoclonal antibody to hyperphosphorylated tau found within AD neurofibrillary tangles [241]. During one of these routine immunohistochemistry experiments, I was surprised to see intense AT8-immunoreactivity in a section of neocortex from an aged chimpanzee. The 41-year-old female had recently died from a massive hemorrhagic stroke, a pathological event that has only been reported in one other captive ape [72]. At the light microscopic level, I identified four distinct types of AT8-immunoreactive lesions: neuropil threads, "spaghetti-like" tau plaques, punctate tau plaques, and intraneuronal tau bundles with a fibrillar appearance. Immunostained tissue was further examined ultrastructurally, revealing intraneuronal paired helical filaments that were indistinguishable from those found in human neurofibrillary tangles. The discovery of AD-like neurofibrillary tangles in an aged chimpanzee was a direct challenge to one of the core assumptions underlying this comparative study, that nonhuman primates do not get Alzheimer's disease.

In Chapter 1, I presented the results of analyses of postmortem tissue from this chimpanzee, along with a cohort of comparison AD cases, in order to determine if this animal might be the first documented case of AD in a nonhuman species. I also did some detective work, talking to animal technicians who worked with the animal, and to behavioral laboratories that had evaluated her in studies of hand preference and

communication. I learned that she did not demonstrate any abnormal behaviors up until the day she suffered from the ischemic stroke. Although we did not include it in the report, she did display what Dr. William Hopkins described as "pathological left-handedness" on behavioral tasks in which normal chimpanzees did not favor a particular hand. He explained that, unlike humans, chimpanzees are normally not strongly left or right handed. The stroke occurred in the left hemisphere, which controls the right hand, but we can only speculate on any further relationship between the stroke (or susceptibility to stroke) and the hand preference. Fortuitously, she had been scanned by MRI 10 years prior to her death, as part of the handedness study in Dr. Hopkins's laboratory. No pre-existing cortical abnormalities were detected, although her fatal stroke was so large that it might have obscured evidence of an older, smaller stroke. Just before her death, she was quickly scanned at the Yerkes Imaging Center, which gave us dramatic, live images of the infarct.

Upon histological examination, the brain of this chimpanzee contained tau pathology throughout much of the neocortex, and also Aβ deposition in the form of moderate CAA and rare senile plaques. However, the Aβ and tau pathology did not satisfy diagnostic criteria for AD [271]. The Aβ plaques were generally sparse and focal in nature, and the tau plaques were not colocalized with Aβ deposits, as is usually the case in AD. Furthermore, the hippocampal formation, the region that is afflicted with tauopathy early and heavily in AD, was largely unaffected. The tau pathology in this case also did not fit the criteria for any other known human tauopathy, and tau gene sequencing did not reveal any mutations. We therefore concluded that, although this chimpanzee brain did exhibit the cellular mechanisms responsible for AD pathogenesis,

all current evidence of aging in nonhuman primate brain indicates that AD is a human-specific disease.

Aβ in Aged Nonhuman Primate Brain

Increasing evidence suggests that Aβ, like other disease-causing amyloidogenic proteins, folds into self-propagating structural polymorphs (strains) with distinct neurotoxic properties [85, 181, 215]. The existence of Aβ strains would reconcile the β-amyloid cascade hypothesis with the benign accumulation of Aβ plaques I have detected in the brains of aged nonhuman primates.

Exciting new work from Robert Tycko's lab at the National Institutes of Health has shown that structural polymorphisms in preparations of synthetic Aβ fibrils can be experimentally induced by altering the incubation conditions, a phenomenon also seen with synthetic tau and α-synuclein, the proteins that aggregate to cause frontotemporal dementia and Parkinson's disease, respectively [55, 76, 216]. Dr. Tycko and his collaborators have shown that, at the ultrastructural level, molecular polymorphisms exist in the amyloid structure of Aβ fibrils derived from the AD brain [214], and that mutant and full-length Aβ40 also aggregate into polymorphic amyloid fibrils [277]. More recently, they showed that intact Aβ fibrils isolated from the AD brain can efficiently template the folding of synthetic Aβ40 peptides, and have used this "seeding in a dish" model to produce substantial quantities of AD-like Aβ oligomers that promise to be valuable experimental tools in the search for AD therapeutics. The elegant work from

these labs indicates that both primary peptide sequence *and* environmental conditions can influence the molecular structure of fibrillar Aβ.

In addition to Aβ40 and Aβ42, APP proteolytic cleavage products include Aβ isoforms with various N- and C-terminal truncations, such as Aβ3-x, Aβx-38, and Aβx-43 [226, 239], and different Aβ isoforms have distinct cytotoxic effects [57]. Relative *quantities* of Aβ isoforms also influence the peptide's bioactivity; high levels of Aβ40 may actually be protective against Aβ42-induced toxicity [135, 176].

In the experiments outlined in Chapter 3, however, I found no striking qualitative differences between the Aβ peptide isoforms produced and/or deposited in the brains of AD patients compared to aged nonhuman primates, nor could I detect any quantitative differences in total cortical levels of Aβ40 or Aβ42. Only through Western blot analysis of whole cortical homogenates was I able to find a clue to possible structural differences between Aβ multimers in the two groups. SDS-stable Aβ dimers from AD and squirrel monkey subjects exhibited different patterns of immunoreactivity to antibodies 6E10 and 4G8, which were raised against non-overlapping regions of the Aβ sequence. In two AD cases with very high levels of 4G8-immunoreactive dimers, for example, 6E10 barely labeled the 8KDa dimer band. Slight alterations in quaternary structure of Aβ dimers and trimers could directly influence epitope availability, and thus antibody immunoreactivity in these experiments. It is important to note that all cortical homogenates were boiled in SDS detergent prior to gel electrophoresis, so my interpretation of these data is hypothetical and in need of further testing. I concluded Chapter 3 with the observation that there is not an AD-unique set of Aβ peptides that can be identified through quantitative and qualitative antibody-based techniques. However, the intriguing

immunoblot data provided a jumping off point for a new set of experiments in the search for defining characteristics of toxic and benign Aβ peptide strains: analysis of the higher-order structure of Aβ multimers.

Before I continue, there is a technical observation worth noting from the experiments and data analyses in Chapter 3. Numerous reports, all of which were based on immunohistochemical analysis, indicate that Aβ40 is the predominant isoform deposited in aged nonhuman primate brain [63, 81, 222]. However, my quantitative ELISA data revealed insoluble Aβ40:Aβ42 ratios below one for all nonhuman primate groups examined. This is the first biochemical analysis of the Aβ40 and Aβ42 isoforms in unfixed tissue from three nonhuman primate species, and it suggests that the immunohistochemical assessment of the relative contributions of Aβ40 and Aβ42 to total plaque deposition may overstate the contribution of Aβ40 to nonhuman primate plaques. One potential explanation for the overestimation of Aβ40:Aβ42 ratios by immunohistochemistry is that vascular β-amyloid, which is particularly prominent in nonhuman primates, is more densely packed than cortical plaques, and can only be reliably quantified through homogenization of unfixed cortical tissue, followed by denaturation with formic acid.

Aβ is Structurally Distinct in AD and Nonhuman Primate Brain

In 2003, William Klunk and Chester Mathis reported a new radiolabeled benzothiazole that bound specifically, and with high-affinity, to β-amyloid from AD cortical homogenates [143]. This agent, now known as Pittsburgh Compound B, bound

with substantially lower stoichiometry to synthetic Aβ40 and Aβ42, indicating that the ligand was specific for Aβ aggregates produced in the human brain. In addition to its utility in the early diagnosis of AD, radiolabeled PIB was an exciting new experimental tool that could be used to differentiate Aβ strains *in vitro*, and potentially to identify the structural attributes of toxic Aβ multimers. When I began my studies, Harry LeVine III had already been working with PIB in his laboratory at the University of Kentucky, and he agreed to screen some of my nonhuman primate cortical homogenates for high-affinity PIB binding components. The pilot study proved promising, and in Chapter 4, I presented a quantitative analysis of high-affinity ^{3}H-PIB binding in all of the Aβ-laden nonhuman primate tissue I could get my hands on.

Using microplate binding assays with 1.0nM ^{3}H-PIB (a concentration that is selective for the high-affinity binding sites that are the primary target in PET studies), I found that not a single nonhuman primate case, nor any of the nondemented human subjects, contained AD-like levels of high-affinity PIB binding sites. High-affinity PIB binding was a feature that reliably distinguished the human AD and nonhuman Aβ populations in this comparative study, and the finding was confirmed with autoradiography, competition binding assays, and cortical homogenate mixing experiments. For the first time, I had solid evidence that multimeric Aβ in nonhuman primate brain may comprise a structural variant of Aβ that is distinct from Aβ in the Alzheimer's brain.

Can PIB Distinguish Strains of Aβ in the AD Brain?

In the course of evaluating PIB-binding in a series of AD cases, I made the unexpected discovery that one of the pathologically-confirmed AD cases, like the aged nonhuman primates, was deficient in high-affinity PIB binding sites. In Chapter 5, I presented a thorough analysis of Aβ pathology in postmortem tissue from this PIB-refractory case, known as "AD1". Our laboratory embarked on a collaborative effort to determine why the Aβ in this particular human was different from the other AD cases in the cohort. With the help of colleagues in Emory's Department of Neurology, I found that there was nothing remarkable in her clinical history, no family history of neurodegenerative disease (except for one relative with Parkinson's disease), and no AD-associated mutations in the APP or presenilin genes. Intriguingly, AD1 cortex contained more total Aβ40 *and* Aβ42, a greater variety of truncated Aβ isoforms, and more low-molecular weight SDS-soluble Aβ oligomers than any of the other 9 AD cases in the comparison cohort. Despite this abundance of Aβ peptide, the stoichiometry of high affinity PIB binding sites to Aβ molecules in case AD1 was as low as in each of the nonhuman primate cases I examined in the earlier study. This is the first pathologically and biochemically substantiated report of deficient PIB binding to Aβ-laden AD cortex, and adds to growing evidences that a lack of high-affinity PIB binding in PET scans does not rule out a diagnosis of AD [140, 263]. Furthermore, this finding supports our hypothesis that PIB is exquisitely sensitive to a particular (and as yet undefined) structural variation in multimeric Aβ, and that the characterization of these PIB-binding

aggregates may yield crucial insights into the mechanisms of Aβ multimer-induced neurotoxicity in the AD brain.

In vivo Seeding with Aβ Multimers from AD and Monkey Brain

After identifying probable structural polymorphisms in human and monkey β-amyloid, I looked for a valid model with which to study their distinct aggregation pathways. Inspired by the success of the *in vitro* Aβ seeding studies [215], I focused on an *in vivo* seeding model of β-amyloidosis. Clarified, Aβ-rich cortical homogenates from 5 aged squirrel monkeys were injected into the hippocampi of PSAPP transgenic mice, as were extracts from 5 AD cases, all of which were characterized in previous studies (Chapter 3). Despite structural differences between the two groups of Aβ seeds in these experiments, both Aβ strains were highly fibrillogenic. After 4 months of incubation, mice injected with both monkey extract and AD extract exhibited profuse extracellular, seeded β-amyloidosis throughout the hippocampus.

The next question was whether or not seeded Aβ deposits were actually produced by permissive templating, as seen with the experimental transmission of prion diseases. The presence or absence of high-affinity PIB binding sites in seeded Aβ might provide an answer, at least in the animals that were injected with AD cortical extracts. The answer I got, however, was far from simple. I analyzed PIB binding in seeded tissue in 3 different ways: homogenate radioligand binding assay, radiodotblot of hippocampal homogenates (a new technique I created in the course of these experiments), and film autoradiography on intact cryosections. The first technique relied on the counting of beta radiation by

liquid scintillation, while integrative autoradiography was used for ligand detection in the latter assays. I was unable to detect high-affinity ^{3}H-PIB binding in *any* seeded hippocampal homogenates, using both liquid scintillation and film autoradiography. However, since tissue homogenization increases the signal:noise ratio, I was concerned that increased background may have been obscuring any small PIB-binding signal in the mouse hippocampi. I overcame this technical issue by performing whole cryosection autoradiography on rostral coronal sections from the same seeded animals, and was indeed able to see concentrated ^{3}H-PIB binding along the hippocampal fissure and dentate gyrus in AD-injected mouse hippocampus, corresponding to the regions in which I originally detected seeded amyloid by Aβ immunohistochemistry.

AD cortical extract seeded the *in vivo* formation of AD-like β-amyloid with high-affinity PIB binding sites. However, PIB-positive seeded Aβ *also* was induced by *squirrel monkey* cortical extracts. Seeded PIB binding sites from both experimental groups were detected by ^{3}H-PIB autoradiography, but were very light and highly localized, even after 4 weeks of film exposure. It may be that the squirrel monkey extract does contain low levels of high-affinity PIB binding sites (as is the case for synthetic Aβ [143]), and that this conformation of Aβ, even at low levels, is a superior seed[6]. Alternatively, the murine (host) cortical environment may interact with the squirrel monkey (donor) Aβ to generate Aβ with high-affinity PIB-binding structural motifs in this model.

---

[6] By autoradiography, I *have* detected ^{3}H-PIB binding to vascular amyloid in squirrel monkey cryosections, but to a very small subset of total Aβ-immunoreactive amyloid, and at substantially lower levels than seen in AD tissue (unpublished data).

Significance and Future Directions

In the search for a cellular mechanism that underlies the human-specific vulnerability to Alzheimer's disease, I have provided evidence for structural polymorphisms in multimeric Aβ that distinguish nonhuman primates from humans with AD. The differential binding of PIB to Aβ aggregates in these two closely related groups is a particularly promising entrée into the use of new chemical probes for the identification of protein strains. To further characterize the structural basis of differences in high-affinity PIB binding sites, potential experimental directions include the determination of β-sheet content by Fourier-transform infrared spectroscopy (FTIR), identification of molecular fibril polymorphisms by NMR, or the assessment of amyloid packing by spectral shifts upon binding to luminescent conjugated polymers [35, 204, 214].

Further investigation is warranted to ascertain whether these structural polymorphisms underlie the benign or toxic nature of the naturally occurring peptide strains, as is seen in the prion diseases. Long-term *in vivo* seeding may be ideal for the determination of neurotoxicity or synaptotoxicity induced by structural variants of multimeric Aβ. Finally, the use of *in vivo* seeding to create a mouse model of Aβ amyloidosis with AD-like PIB binding components could lead to the development of new imaging agents and therapeutic interventions for Alzheimer's disease, particularly agents that prevent the formation and spread of toxic Aβ multimers.

References

1. (2005) Initial sequence of the chimpanzee genome and comparison with the human genome. Nature 437: 69-87.

2. Alzheimer's Disease: A Source Document (AsS Group, Ed. Washington, D.C., U.S. Government, 2008.

3. Agca C, Fritz JJ, Walker LC, Levey AI, Chan AW, Lah JJ, & Agca Y (2008) Development of transgenic rats producing human beta-amyloid precursor protein as a model for Alzheimer's disease: transgene and endogenous APP genes are regulated tissue-specifically. BMC Neurosci 9: 28.

4. Aguzzi A & Haass C (2003) Games played by rogue proteins in prion disorders and Alzheimer's disease. Science 302: 814-818.

5. Aisen PS, Gauthier S, Vellas B, Briand R, Saumier D, Laurin J, & Garceau D (2007) Alzhemed: a potential treatment for Alzheimer's disease. Curr Alzheimer Res 4: 473-478.

6. Aizenstein HJ, Nebes RD, Saxton JA, Price JC, Mathis CA, Tsopelas ND, Ziolko SK, James JA, Snitz BE, Houck PR, Bi W, Cohen AD, Lopresti BJ, DeKosky ST, Halligan EM, & Klunk WE (2008) Frequent amyloid deposition without significant cognitive impairment among the elderly. Arch Neurol 65: 1509-1517.

7. Allman J, McLaughlin T, & Hakeem A (1993) Brain weight and life-span in primate species. Proc Natl Acad Sci U S A 90: 118-122.

8. Alzheimer A (1907) Uber eine eigenartige Erkrankung der Hirnrinde. Allg Z Psychiat Psych-Gericht Med 64: 146-148.

9. Arriagada PV, Marzloff K, & Hyman BT (1992) Distribution of Alzheimer-type pathologic changes in nondemented elderly individuals matches the pattern in Alzheimer's disease. Neurology 42: 1681-1688.

10. Arslan MA, Csermely P, & Soti C (2006) Protein homeostasis and molecular chaperones in aging. Biogerontology 7: 383-389.

11. Attems J & Jellinger KA (2004) Only cerebral capillary amyloid angiopathy correlates with Alzheimer pathology--a pilot study. Acta Neuropathol 107: 83-90.

12. Austad SN & Fischer KE (1991) Mammalian aging, metabolism, and ecology: evidence from the bats and marsupials. J Gerontol 46: B47-53.

13. Bacskai BJ, Frosch MP, Freeman SH, Raymond SB, Augustinack JC, Johnson KA, Irizarry MC, Klunk WE, Mathis CA, Dekosky ST, Greenberg SM, Hyman BT, &

Growdon JH (2007) Molecular imaging with Pittsburgh Compound B confirmed at autopsy: a case report. Arch Neurol 64: 431-434.

14. Bai Y, Markham K, Chen F, Weerasekera R, Watts J, Horne P, Wakutani Y, Bagshaw R, Mathews PM, Fraser PE, Westaway D, St George-Hyslop P, & Schmitt-Ulms G (2008) The in vivo brain interactome of the amyloid precursor protein. Mol Cell Proteomics 7: 15-34.

15. Baily P, von Bonin G, & McCulloch W (1950) The Isocortex of the Chimpanzee. Univ. of Illionois Press, Urbana, Illinois.

16. Balch WE, Morimoto RI, Dillin A, & Kelly JW (2008) Adapting proteostasis for disease intervention. Science 319: 916-919.

17. Ballatore C, Lee VM, & Trojanowski JQ (2007) Tau-mediated neurodegeneration in Alzheimer's disease and related disorders. Nat Rev Neurosci 8: 663-672.

18. Bartus RT (2000) On neurodegenerative diseases, models, and treatment strategies: lessons learned and lessons forgotten a generation following the cholinergic hypothesis. Exp Neurol 163: 495-529.

19. Bennett DA, Schneider JA, Arvanitakis Z, Kelly JF, Aggarwal NT, Shah RC, & Wilson RS (2006) Neuropathology of older persons without cognitive impairment from two community-based studies. Neurology 66: 1837-1844.

20. Berchtold NC & Cotman CW (1998) Evolution in the conceptualization of dementia and Alzheimer's disease: Greco-Roman period to the 1960s. Neurobiol Aging 19: 173-189.

21. Bertram L & Tanzi RE (2008) Thirty years of Alzheimer's disease genetics: the implications of systematic meta-analyses. Nat Rev Neurosci 9: 768-778.

22. Bielschowsky M (1903) Die Ziele bei Impregnation der Neurofibrillen. Neurol Centralbl 22: 997-1006.

23. Bitan G, Fradinger EA, Spring SM, & Teplow DB (2005) Neurotoxic protein oligomers--what you see is not always what you get. Amyloid 12: 88-95.

24. Bitan G, Kirkitadze MD, Lomakin A, Vollers SS, Benedek GB, & Teplow DB (2003) Amyloid beta -protein (Abeta) assembly: Abeta 40 and Abeta 42 oligomerize through distinct pathways. Proc Natl Acad Sci U S A 100: 330-335.

25. Bitan G, Vollers SS, & Teplow DB (2003) Elucidation of primary structure elements controlling early amyloid beta-protein oligomerization. J Biol Chem 278: 34882-34889.

26. Bloom GS, Ren K, & Glabe CG (2005) Cultured cell and transgenic mouse models for tau pathology linked to beta-amyloid. Biochim Biophys Acta 1739: 116-124.

27. Bolmont T, Clavaguera F, Meyer-Luehmann M, Herzig MC, Radde R, Staufenbiel M, Lewis J, Hutton M, Tolnay M, & Jucker M (2007) Induction of tau pathology by intracerebral infusion of amyloid-beta -containing brain extract and by amyloid-beta deposition in APP x Tau transgenic mice. Am J Pathol 171: 2012-2020.

28. Borchelt DR, Ratovitski T, van Lare J, Lee MK, Gonzales V, Jenkins NA, Copeland NG, Price DL, & Sisodia SS (1997) Accelerated amyloid deposition in the brains of transgenic mice coexpressing mutant presenilin 1 and amyloid precursor proteins. Neuron 19: 939-945.

29. Borkowski R, Taylor TG, & Rush J (2000) Cerebral Infarction and Myocardial Fibrosis in a White-handed Gibbon (Hylobates lar). Journal of Zoo and Wildlife Medicine 65-70.

30. Braak H & Braak E (1991) Neuropathological stageing of Alzheimer-related changes. Acta Neuropathol 82: 239-259.

31. Braak H & Braak E (1994) Morphological criteria for the recognition of Alzheimer's disease and the distribution pattern of cortical changes related to this disorder. Neurobiol Aging 15: 355-356; discussion 379-380.

32. Braak H & Braak E (1996) Evolution of the neuropathology of Alzheimer's disease. Acta Neurol Scand Suppl 165: 3-12.

33. Brodmann K (1912) Anat. Anz. 41: 157-216.

34. Brody DL & Holtzman DM (2008) Active and passive immunotherapy for neurodegenerative disorders. Annu Rev Neurosci 31: 175-193.

35. Buchet R, Tavitian E, Ristig D, Swoboda R, Stauss U, Gremlich HU, de La Fourniere L, Staufenbiel M, Frey P, & Lowe DA (1996) Conformations of synthetic beta peptides in solid state and in aqueous solution: relation to toxicity in PC12 cells. Biochim Biophys Acta 1315: 40-46.

36. Bush AI & Tanzi RE (2008) Therapeutics for Alzheimer's disease based on the metal hypothesis. Neurotherapeutics 5: 421-432.

37. Caceres M, Lachuer J, Zapala MA, Redmond JC, Kudo L, Geschwind DH, Lockhart DJ, Preuss TM, & Barlow C (2003) Elevated gene expression levels distinguish human from non-human primate brains. Proc Natl Acad Sci U S A 100: 13030-13035.

38. Carey JR (2003) Longevity. The biology and demography of life span. Princeton University Press, Princeton, NJ.

39. Casas C, Sergeant N, Itier JM, Blanchard V, Wirths O, van der Kolk N, Vingtdeux V, van de Steeg E, Ret G, Canton T, Drobecq H, Clark A, Bonici B, Delacourte A, Benavides J, Schmitz C, Tremp G, Bayer TA, Benoit P, & Pradier L (2004) Massive CA1/2 neuronal loss with intraneuronal and N-terminal truncated

Abeta42 accumulation in a novel Alzheimer transgenic model. Am J Pathol 165: 1289-1300.

40. Catalano SM, Dodson EC, Henze DA, Joyce JG, Krafft GA, & Kinney GG (2006) The role of amyloid-beta derived diffusible ligands (ADDLs) in Alzheimer's disease. Curr Top Med Chem 6: 597-608.

41. Cervenakova L, Brown P, Goldfarb LG, Nagle J, Pettrone K, Rubenstein R, Dubnick M, Gibbs CJ, Jr., & Gajdusek DC (1994) Infectious amyloid precursor gene sequences in primates used for experimental transmission of human spongiform encephalopathy. Proc Natl Acad Sci U S A 91: 12159-12162.

42. Chien P, Weissman JS, & DePace AH (2004) Emerging principles of conformation-based prion inheritance. Annu Rev Biochem 73: 617-656.

43. Cleary JP, Walsh DM, Hofmeister JJ, Shankar GM, Kuskowski MA, Selkoe DJ, & Ashe KH (2005) Natural oligomers of the amyloid-beta protein specifically disrupt cognitive function. Nat Neurosci 8: 79-84.

44. Cohen J (2007) Animal studies. NIH to end chimp breeding for research. Science 316: 1265.

45. Collinge J & Clarke AR (2007) A general model of prion strains and their pathogenicity. Science 318: 930-936.

46. Conrad C, Vianna C, Schultz C, Thal DR, Ghebremedhin E, Lenz J, Braak H, & Davies P (2004) Molecular evolution and genetics of the Saitohin gene and tau haplotype in Alzheimer's disease and argyrophilic grain disease. Journal of Neurochemistry 89: 179-188.

47. Corder EH, Saunders AM, Strittmatter WJ, Schmechel DE, Gaskell PC, Small GW, Roses AD, Haines JL, & Pericak-Vance MA (1993) Gene dose of apolipoprotein E type 4 allele and the risk of Alzheimer's disease in late onset families. Science 261: 921-923.

48. Cork LC, Powers RE, Selkoe DJ, Davies P, Geyer JJ, & Price DL (1988) Neurofibrillary tangles and senile plaques in aged bears. J Neuropathol Exp Neurol 47: 629-641.

49. Cork LC & Walker LC (1993) Age-related lesions, nervous system. In: Monographs on Pathology of Laboratory Animals. Nonhuman Primates II. Springer-Verlag, Berlin, p^pp pp 173-183.

50. Cork LC WL (1993) Age-related lesions, nervous system. In: Monographs on Pathology of Laboratory Animals. Nonhuman Primates II. Springer-Verlag, Berlin, p^pp pp 173-183.

51. Cotman CW & Head E (2008) The canine (dog) model of human aging and disease: dietary, environmental and immunotherapy approaches. J Alzheimers Dis 15: 685-707.

52. Crowther RA (1991) Straight and paired helical filaments in Alzheimer disease have a common structural unit. Proc Natl Acad Sci U S A 88: 2288-2292.

53. Crystal H, Dickson D, Fuld P, Masur D, Scott R, Mehler M, Masdeu J, Kawas C, Aronson M, & Wolfson L (1988) Clinico-pathologic studies in dementia: nondemented subjects with pathologically confirmed Alzheimer's disease. Neurology 38: 1682-1687.

54. Cuello AC & Canneva F (2008) Impact of intracellular beta-amyloid in transgenic animals and cell models. Neurodegener Dis 5: 146-148.

55. Danzer KM, Haasen D, Karow AR, Moussaud S, Habeck M, Giese A, Kretzschmar H, Hengerer B, & Kostka M (2007) Different species of alpha-synuclein oligomers induce calcium influx and seeding. J Neurosci 27: 9220-9232.

56. de Magalhaes JP & Church GM (2007) Analyses of human-chimpanzee orthologous gene pairs to explore evolutionary hypotheses of aging. Mech Ageing Dev 128: 355-364.

57. Deshpande A, Mina E, Glabe C, & Busciglio J (2006) Different conformations of amyloid beta induce neurotoxicity by distinct mechanisms in human cortical neurons. J Neurosci 26: 6011-6018.

58. Dodart JC & May P (2005) Overview on rodent models of Alzheimer's disease. Curr Protoc Neurosci Chapter 9: Unit 9.22.

59. Dubois B, Feldman HH, Jacova C, DeKosky ST, Barberger-Gateau P, Cummings J, Delacourte A, Galasko D, Gauthier S, Jicha G, Meguro K, O'Brien J, Pasquier F, Robert P, Rossor M, Salloway S, Stern Y, Visser PJ, & Scheltens P (2007) Research criteria for the diagnosis of Alzheimer's disease: revising the NINCDS-ADRDA criteria. Lancet Neurol 6: 734-746.

60. Dulin F, Leveille F, Ortega JB, Mornon JP, Buisson A, Callebaut I, & Colloc'h N (2008) P3 peptide, a truncated form of A beta devoid of synaptotoxic effect, does not assemble into soluble oligomers. FEBS Lett 582: 1865-1870.

61. Duyckaerts C, Colle MA, Dessi F, Piette F, & Hauw JJ (1998) Progression of Alzheimer histopathological changes. Acta Neurol Belg 98: 180-185.

62. Edison P, Archer HA, Hinz R, Hammers A, Pavese N, Tai YF, Hotton G, Cutler D, Fox N, Kennedy A, Rossor M, & Brooks DJ (2007) Amyloid, hypometabolism, and cognition in Alzheimer disease: an [11C]PIB and [18F]FDG PET study. Neurology 68: 501-508.

63. Elfenbein HA, Rosen RF, Stephens SL, Switzer RC, Smith Y, Pare J, Mehta PD, Warzok R, & Walker LC (2007) Cerebral beta-amyloid angiopathy in aged squirrel monkeys. Histol Histopathol 22: 155-167.

64. Enard W, Khaitovich P, Klose J, Zollner S, Heissig F, Giavalisco P, Nieselt-Struwe K, Muchmore E, Varki A, Ravid R, Doxiadis GM, Bontrop RE, & Paabo S (2002) Intra- and interspecific variation in primate gene expression patterns. Science 296: 340-343.

65. Erwin JM, Nimchinsky EA, Gannon PJ, Perl DP, & Hof PR (2000) The Study of Brain Aging in Great Apes. In: Functional Neurobiology of Aging. Academic Press.

66. Ewing B & Green P (1998) Base-calling of automated sequencer traces using phred. II. Error probabilities. Genome Res 8: 186-194.

67. Ewing B, Hillier L, Wendl MC, & Green P (1998) Base-calling of automated sequencer traces using phred. I. Accuracy assessment. Genome Res 8: 175-185.

68. Fagan AM, Mintun MA, Mach RH, Lee SY, Dence CS, Shah AR, LaRossa GN, Spinner ML, Klunk WE, Mathis CA, DeKosky ST, Morris JC, & Holtzman DM (2006) Inverse relation between in vivo amyloid imaging load and cerebrospinal fluid Abeta42 in humans. Ann Neurol 59: 512-519.

69. Fillenbaum GG, van Belle G, Morris JC, Mohs RC, Mirra SS, Davis PC, Tariot PN, Silverman JM, Clark CM, Welsh-Bohmer KA, & Heyman A (2008) Consortium to Establish a Registry for Alzheimer's Disease (CERAD): the first twenty years. Alzheimers Dement 4: 96-109.

70. Finch CE & Sapolsky RM (1999) The evolution of Alzheimer disease, the reproductive schedule, and apoE isoforms. Neurobiol Aging 20: 407-428.

71. Fischer O (1907) Nekrosen mit drusigen Wucherungen der Neurofibrillen, eine egelmassige Veranderung der Hirnrinde bei seniler Demenz. Mschr. Psychiat. Neurol. 22: 361-372.

72. Fish PH, Carpenter JW, & Kraft S (2004) Diagnosis and treatment of a cerebral infarct in a chimpanzee (Pan troglodytes) Journal of Zoo and Wildlife Medicine 203-207.

73. Flood DG, Lin YG, Lang DM, Trusko SP, Hirsch JD, Savage MJ, Scott RW, & Howland DS (2007) A transgenic rat model of Alzheimer's disease with extracellular Abeta deposition. Neurobiol Aging

74. Fodero-Tavoletti MT, Smith DP, McLean CA, Adlard PA, Barnham KJ, Foster LE, Leone L, Perez K, Cortes M, Culvenor JG, Li Q-X, Laughton KM, Rowe CC, Masters CL, Cappai R, & Villemagne VL (2007) In vitro characterization of Pittsburgh Compound-B binding to Lewy bodies. J. Neurosci. 27: 10365-10371.

75. Franklin KBJ & Paxinos G (2007) The Mouse Brain in Stereotaxic Coordinates, 3rd Edition. Academic Press, San Diego.

76. Frost B, Ollesch J, Wille H, & Diamond MI (2009) Conformational diversity of wild-type Tau fibrils specified by templated conformation change. J Biol Chem 284: 3546-3551.

77. Gambetti P, Dong Z, Yuan J, Xiao X, Zheng M, Alshekhlee A, Castellani R, Cohen M, Barria MA, Gonzalez-Romero D, Belay ED, Schonberger LB, Marder K, Harris C, Burke JR, Montine T, Wisniewski T, Dickson DW, Soto C, Hulette CM, Mastrianni JA, Kong Q, & Zou WQ (2008) A novel human disease with abnormal prion protein sensitive to protease. Ann Neurol 63: 697-708.

78. Gambetti P, Parchi P, Capellari S, Russo C, Tabaton M, Teller JK, & Chen SG (2001) Mechanisms of phenotypic heterogeneity in prion, Alzheimer and other conformational diseases. J Alzheimers Dis 3: 87-95.

79. Games D, Adams D, Alessandrini R, Barbour R, Berthelette P, Blackwell C, Carr T, Clemens J, Donaldson T, Gillespie F, & et al. (1995) Alzheimer-type neuropathology in transgenic mice overexpressing V717F beta-amyloid precursor protein. Nature 373: 523-527.

80. Gearing M, Rebeck GW, Hyman BT, Tigges J, & Mirra SS (1994) Neuropathology and apolipoprotein E profile of aged chimpanzees: implications for Alzheimer disease. Proc Natl Acad Sci U S A 91: 9382-9386.

81. Gearing M, Tigges J, Mori H, & Mirra SS (1996) A beta40 is a major form of beta-amyloid in nonhuman primates. Neurobiol Aging 17: 903-908.

82. Gearing M, Tigges J, Mori H, & Mirra SS (1997) beta-Amyloid (A beta) deposition in the brains of aged orangutans. Neurobiol Aging 18: 139-146.

83. Geula C, Nagykery N, & Wu CK (2002) Amyloid-beta deposits in the cerebral cortex of the aged common marmoset (Callithrix jacchus): incidence and chemical composition. Acta Neuropathol (Berl) 103: 48-58.

84. Giannakopoulos P, Gold G, Kovari E, von Gunten A, Imhof A, Bouras C, & Hof PR (2007) Assessing the cognitive impact of Alzheimer disease pathology and vascular burden in the aging brain: the Geneva experience. Acta Neuropathol (Berl) 113: 1-12.

85. Glabe CG & Kayed R (2005) Common structure and toxic function of amyloid oligomers implies a common mechanism of pathogenesis. Neurology

86. Glenner GG & Wong CW (1984) Alzheimer's disease: initial report of the purification and characterization of a novel cerebrovascular amyloid protein. Biochem Biophys Res Commun 120: 885-890.

87. Goedert M (2004) Tau protein and neurodegeneration. Semin Cell Dev Biol 15: 45-49.

88. Goedert M (2009) Oskar Fischer and the study of dementia. Brain 132: 1102-1111.

89. Goedert M & Jakes R (2005) Mutations causing neurodegenerative tauopathies. Biochim Biophys Acta 1739: 240-250.

90. Goedert M, Jakes R, & Vanmechelen E (1995) Monoclonal antibody AT8 recognises tau protein phosphorylated at both serine 202 and threonine 205. Neurosci Lett 189: 167-169.

91. Goedert M, Klug A, & Crowther RA (2006) Tau protein, the paired helical filament and Alzheimer's disease. J Alzheimers Dis 9: 195-207.

92. Golde TE, Das P, & Levites Y (2009) Quantitative and mechanistic studies of abeta immunotherapy. CNS Neurol Disord Drug Targets 8: 31-49.

93. Gong Y, Chang L, Viola KL, Lacor PN, Lambert MP, Finch CE, Krafft GA, & Klein WL (2003) Alzheimer's disease-affected brain: presence of oligomeric A beta ligands (ADDLs) suggests a molecular basis for reversible memory loss. Proc Natl Acad Sci U S A 100: 10417-10422.

94. Gotz J, Chen F, van Dorpe J, & Nitsch RM (2001) Formation of neurofibrillary tangles in P301l tau transgenic mice induced by Abeta 42 fibrils. Science 293: 1491-1495.

95. Gotz J, Deters N, Doldissen A, Bokhari L, Ke Y, Wiesner A, Schonrock N, & Ittner LM (2007) A decade of tau transgenic animal models and beyond. Brain Pathol 17: 91-103.

96. Gotz J, Schild A, Hoerndli F, & Pennanen L (2004) Amyloid-induced neurofibrillary tangle formation in Alzheimer's disease: insight from transgenic mouse and tissue-culture models. Int J Dev Neurosci 22: 453-465.

97. Greenberg SG, Davies P, Schein JD, & Binder LI (1992) Hydrofluoric acid-treated tau PHF proteins display the same biochemical properties as normal tau. J Biol Chem 267: 564-569.

98. Greenberg SM, Rebeck GW, Vonsattel JP, Gomez-Isla T, & Hyman BT (1995) Apolipoprotein E epsilon 4 and cerebral hemorrhage associated with amyloid angiopathy. Ann Neurol 38: 254-259.

99. Grune T, Shringarpure R, Sitte N, & Davies K (2001) Age-related changes in protein oxidation and proteolysis in mammalian cells. J Gerontol A Biol Sci Med Sci 56: B459-467.

100. Haass C & Selkoe DJ (2007) Soluble protein oligomers in neurodegeneration: lessons from the Alzheimer's amyloid beta-peptide. Nat Rev Mol Cell Biol 8: 101-112.

101. Hardy J (2005) Expression of normal sequence pathogenic proteins for neurodegenerative disease contributes to disease risk: 'permissive templating' as a general mechanism underlying neurodegeneration. Biochem Soc Trans 33: 578-581.

102. Hardy J & Orr H (2006) The genetics of neurodegenerative diseases. J Neurochem 97: 1690-1699.

103. Hardy J, Pittman A, Myers A, Fung HC, de Silva R, & Duckworth J (2006) Tangle diseases and the tau haplotypes. Alzheimer Dis Assoc Disord 20: 60-62.

104. Hardy J & Selkoe DJ (2002) The amyloid hypothesis of Alzheimer's disease: progress and problems on the road to therapeutics. Science 297: 353-356.

105. Harper JD, Wong SS, Lieber CM, & Lansbury PT, Jr. (1999) Assembly of A beta amyloid protofibrils: an in vitro model for a possible early event in Alzheimer's disease. Biochemistry 38: 8972-8980.

106. Hartig W, Bruckner G, Schmidt C, Brauer K, Bodewitz G, Turner JD, & Bigl V (1997) Co-localization of beta-amyloid peptides, apolipoprotein E and glial markers in senile plaques in the prefrontal cortex of old rhesus monkeys. Brain Res 751: 315-322.

107. Hasegawa K, Yamaguchi I, Omata S, Gejyo F, & Naiki H (1999) Interaction between A beta(1-42) and A beta(1-40) in Alzheimer's beta-amyloid fibril formation in vitro. Biochemistry 38: 15514-15521.

108. Hashimoto M, Kazui H, Matsumoto K, Nakano Y, Yasuda M, & Mori E (2005) Does donepezil treatment slow the progression of hippocampal atrophy in patients with Alzheimer's disease? Am J Psychiatry 162: 676-682.

109. Hawkes K (2004) Human longevity: the grandmother effect. Nature 428: 128-129.

110. Hayflick L & Moorhead PS (1961) The serial cultivation of human diploid cell strains. Exp Cell Res 25: 585-621.

111. Herndon JG, Tigges J, Anderson DC, Klumpp SA, & McClure HM (1999) Brain weight throughout the life span of the chimpanzee. J Comp Neurol 409: 567-572.

112. Hesse C, Rosengren L, Andreasen N, Davidsson P, Vanderstichele H, Vanmechelen E, & Blennow K (2001) Transient increase in total tau but not phospho-tau in human cerebrospinal fluid after acute stroke. Neurosci Lett 297: 187-190.

113. Higuchi M (2009) Visualization of brain amyloid and microglial activation in mouse models of Alzheimer's disease. Curr Alzheimer Res 6: 137-143.

114. Hofman MA (1982) Encephalization in mammals in relation to the size of the cerebral cortex. Brain Behav Evol 20: 84-96.

115. Holzer M, Craxton M, Jakes R, Arendt T, & Goedert M (2004) Tau gene (MAPT) sequence variation among primates. Gene 341: 313-322.

116. Hsiao K, Chapman P, Nilsen S, Eckman C, Harigaya Y, Younkin S, Yang F, & Cole G (1996) Correlative memory deficits, Abeta elevation, and amyloid plaques in transgenic mice. Science 274: 99-102.

117. Hyman BT, West HL, Rebeck GW, Buldyrev SV, Mantegna RN, Ukleja M, Havlin S, & Stanley HE (1995) Quantitative analysis of senile plaques in Alzheimer disease: observation of log-normal size distribution and molecular epidemiology of differences associated with apolipoprotein E genotype and trisomy 21 (Down syndrome). Proc Natl Acad Sci U S A 92: 3586-3590.

118. Ikonomovic MD, Klunk WE, Abrahamson EE, Mathis CA, Price JC, Tsopelas ND, Lopresti BJ, Ziolko S, Bi W, Paljug WR, Debnath ML, Hope CE, Isanski BA, Hamilton RL, & DeKosky ST (2008) Post-mortem correlates of in vivo PIB-PET amyloid imaging in a typical case of Alzheimer's disease. Brain 131: 1630-1645.

119. Irizarry MC, McNamara M, Fedorchak K, Hsiao K, & Hyman BT (1997) APPSw transgenic mice develop age-related A beta deposits and neuropil abnormalities, but no neuronal loss in CA1. J Neuropathol Exp Neurol 56: 965-973.

120. Jankowsky JL, Younkin LH, Gonzales V, Fadale DJ, Slunt HH, Lester HA, Younkin SG, & Borchelt DR (2007) Rodent A beta modulates the solubility and distribution of amyloid deposits in transgenic mice. J Biol Chem 282: 22707-22720.

121. Jerison HJ (1969) Brain Evolution and Dinosaur Brains. The American Naturalist 103: 575-588.

122. Jicha GA, Bowser R, Kazam IG, & Davies P (1997) Alz-50 and MC-1, a new monoclonal antibody raised to paired helical filaments, recognize conformational epitopes on recombinant tau. J Neurosci Res 48: 128-132.

123. Johnson KA, Gregas M, Becker JA, Kinnecom C, Salat DH, Moran EK, Smith EE, Rosand J, Rentz DM, Klunk WE, Mathis CA, Price JC, Dekosky ST, Fischman AJ, & Greenberg SM (2007) Imaging of amyloid burden and distribution in cerebral amyloid angiopathy. Ann Neurol 62: 229-234.

124. Jones KP, Walker LC, Anderson D, Lacreuse A, Robson SL, & Hawkes K (2007) Depletion of ovarian follicles with age in chimpanzees: similarities to humans. Biol Reprod 77: 247-251.

125. Jr. Otvos L, Szendrei GI, Lee VM-Y, & Mantsch HH (1993) Human and rodent Alzheimer beta-amyloid peptides acquire distinct conformations in membrane-mimicking solvents. European Journal of Biochemistry 211: 249-257.

126. Judge DS & Carey JR (2000) Postreproductive life predicted by primate patterns. J Gerontol A Biol Sci Med Sci 55: B201-209.

127. Kalaria RN (2000) The role of cerebral ischemia in Alzheimer's disease. Neurobiol Aging 21: 321-330.

128. Kalback W, Watson MD, Kokjohn TA, Kuo YM, Weiss N, Luehrs DC, Lopez J, Brune D, Sisodia SS, Staufenbiel M, Emmerling M, & Roher AE (2002) APP transgenic mice Tg2576 accumulate Abeta peptides that are distinct from the chemically modified and insoluble peptides deposited in Alzheimer's disease senile plaques. Biochemistry 41: 922-928.

129. Kane MD, Lipinski WJ, Callahan MJ, Bian F, Durham RA, Schwarz RD, Roher AE, & Walker LC (2000) Evidence for seeding of beta -amyloid by intracerebral infusion of Alzheimer brain extracts in beta -amyloid precursor protein-transgenic mice. J Neurosci 20: 3606-3611.

130. Kanemaru K, Iwatsubo T, & Ihara Y (1996) Comparable amyloid beta-protein (A beta) 42(43) and A beta 40 deposition in the aged monkey brain. Neurosci Lett 214: 196-198.

131. Karaman MW, Houck ML, Chemnick LG, Nagpal S, Chawannakul D, Sudano D, Pike BL, Ho VV, Ryder OA, & Hacia JG (2003) Comparative analysis of gene-expression patterns in human and African great ape cultured fibroblasts. Genome Res 13: 1619-1630.

132. Katzman R & Kawas C (1999) The epidemiology of dementia and Alzheimer disease. In: Alzheimer's Disease. Raven, New York, p^pp 105-122.

133. Kayed R, Sokolov Y, Edmonds B, McIntire TM, Milton SC, Hall JE, & Glabe CG (2004) Permeabilization of lipid bilayers is a common conformation-dependent activity of soluble amyloid oligomers in protein misfolding diseases. J Biol Chem 279: 46363-46366.

134. Kiatipattanasakul W, Nakayama H, Yongsiri S, Chotiapisitkul S, Nakamura S, Kojima H, & Doi K (2000) Abnormal neuronal and glial argyrophilic fibrillary structures in the brain of an aged albino cynomolgus monkey (Macaca fascicularis). Acta Neuropathol (Berl) 100: 580-586.

135. Kim J, Onstead L, Randle S, Price R, Smithson L, Zwizinski C, Dickson DW, Golde T, & McGowan E (2007) Abeta40 inhibits amyloid deposition in vivo. J Neurosci 27: 627-633.

136. Kim KS, Miller, D.L., Sapienza, V.J., Chen, C.M.J., Bai, C., Grundke-Iqbal, I., Currie, J.R., and Wisniewski, H.M. (1988) Production and characterization of monoclonal antibodies reactive to synthetic cerebrovascular amyloid peptide. Neurosci Res Commun 121-130.

137. Kimura N, Tanemura K, Nakamura S, Takashima A, Ono F, Sakakibara I, Ishii Y, Kyuwa S, & Yoshikawa Y (2003) Age-related changes of Alzheimer's disease-associated proteins in cynomolgus monkey brains. Biochem Biophys Res Commun 310: 303-311.

138. Kirkwood TB & Austad SN (2000) Why do we age? Nature 408: 233-238.

139. Klunk WE, Engler H, Nordberg A, Bacskai BJ, Wang Y, Price JC, Bergstrom M, Hyman BT, Langstrom B, & Mathis CA (2003) Imaging the pathology of Alzheimer's disease: amyloid-imaging with positron emission tomography. Neuroimaging Clin N Am 13: 781-789, ix.

140. Klunk WE, Engler H, Nordberg A, Wang Y, Blomqvist G, Holt DP, Bergstrom M, Savitcheva I, Huang GF, Estrada S, Ausen B, Debnath ML, Barletta J, Price JC, Sandell J, Lopresti BJ, Wall A, Koivisto P, Antoni G, Mathis CA, & Langstrom B (2004) Imaging brain amyloid in Alzheimer's disease with Pittsburgh Compound-B. Ann Neurol 55: 306-319.

141. Klunk WE, Lopresti BJ, Ikonomovic MD, Lefterov IM, Koldamova RP, Abrahamson EE, Debnath ML, Holt DP, Huang GF, Shao L, DeKosky ST, Price JC, & Mathis CA (2005) Binding of the positron emission tomography tracer Pittsburgh compound-B reflects the amount of amyloid-beta in Alzheimer's disease brain but not in transgenic mouse brain. J Neurosci 25: 10598-10606.

142. Klunk WE, Wang Y, Huang GF, Debnath ML, Holt DP, & Mathis CA (2001) Uncharged thioflavin-T derivatives bind to amyloid-beta protein with high affinity and readily enter the brain. Life Sci 69: 1471-1484.

143. Klunk WE, Wang Y, Huang GF, Debnath ML, Holt DP, Shao L, Hamilton RL, Ikonomovic MD, DeKosky ST, & Mathis CA (2003) The binding of 2-(4'-methylaminophenyl)benzothiazole to postmortem brain homogenates is dominated by the amyloid component. J Neurosci 23: 2086-2092.

144. Koch HJ, Uyanik G, & Fischer-Barnicol D (2005) Memantine: a therapeutic approach in treating Alzheimer's and vascular dementia. Curr Drug Targets CNS Neurol Disord 4: 499-506.

145. Komori T, Arai N, Oda M, Nakayama H, Mori H, Yagishita S, Takahashi T, Amano N, Murayama S, Murakami S, Shibata N, Kobayashi M, Sasaki S, & Iwata M (1998) Astrocytic plaques and tufts of abnormal fibers do not coexist in corticobasal degeneration and progressive supranuclear palsy. Acta Neuropathol (Berl) 96: 401-408.

146. Kumar-Singh S (2008) Cerebral amyloid angiopathy: pathogenetic mechanisms and link to dense amyloid plaques. Genes Brain Behav 7 Suppl 1: 67-82.

147. Kuo Y-M, Kokjohn TA, Beach TG, Sue LI, Brune D, Lopez JC, Kalback WM, Abramowski D, Sturchler-Pierrat C, Staufenbiel M, & Roher AE (2001) Comparative analysis of amyloid-beta chemical structure and amyloid plaque morphology of transgenic mouse and Alzheimer's disease brains. J. Biol. Chem. 276: 12991-12998.

148. Kuo YM, Emmerling MR, Vigo-Pelfrey C, Kasunic TC, Kirkpatrick JB, Murdoch GH, Ball MJ, & Roher AE (1996) Water-soluble Abeta (N-40, N-42) oligomers in normal and Alzheimer disease brains. J Biol Chem 271: 4077-4081.

149. Kuo YM, Emmerling MR, Woods AS, Cotter RJ, & Roher AE (1997) Isolation, chemical characterization, and quantitation of A beta 3-pyroglutamyl peptide from neuritic plaques and vascular amyloid deposits. Biochem Biophys Res Commun 237: 188-191.

150. Kuo YM, Kokjohn TA, Beach TG, Sue LI, Brune D, Lopez JC, Kalback WM, Abramowski D, Sturchler-Pierrat C, Staufenbiel M, & Roher AE (2001) Comparative analysis of amyloid-beta chemical structure and amyloid plaque morphology of transgenic mouse and Alzheimer's disease brains. J Biol Chem 276: 12991-12998.

151. Lambert MP, Barlow AK, Chromy BA, Edwards C, Freed R, Liosatos M, Morgan TE, Rozovsky I, Trommer B, Viola KL, Wals P, Zhang C, Finch CE, Krafft GA, & Klein WL (1998) Diffusible, nonfibrillar ligands derived from Abeta1-42 are potent central nervous system neurotoxins. Proc Natl Acad Sci U S A 95: 6448-6453.

152. Lashuel HA, Hartley D, Petre BM, Walz T, & Lansbury PT, Jr. (2002) Neurodegenerative disease: amyloid pores from pathogenic mutations. Nature 418: 291.

153. Lee VM-Y, Goedert M, & Trojanowski JQ (2001) Neurodegenerative Tauopathies. Annual Review of Neuroscience 24: 1121-1159.

154. Leinonen V, Alafuzoff I, Aalto S, Suotunen T, Savolainen S, Nagren K, Tapiola T, Pirttila T, Rinne J, Jaaskelainen JE, Soininen H, & Rinne JO (2008) Assessment of {beta}-Amyloid in a Frontal Cortical Brain Biopsy Specimen and by Positron Emission Tomography With Carbon 11-Labeled Pittsburgh Compound B. Arch Neurol

155. Leissring MA, Farris W, Chang AY, Walsh DM, Wu X, Sun X, Frosch MP, & Selkoe DJ (2003) Enhanced proteolysis of beta-amyloid in APP transgenic mice prevents plaque formation, secondary pathology, and premature death. Neuron 40: 1087-1093.

156. Lemere CA, Blusztajn JK, Yamaguchi H, Wisniewski T, Saido TC, & Selkoe DJ (1996) Sequence of deposition of heterogeneous amyloid beta-peptides and APO E in Down syndrome: implications for initial events in amyloid plaque formation. Neurobiol Dis 3: 16-32.

157. Lesne S, Koh MT, Kotilinek L, Kayed R, Glabe CG, Yang A, Gallagher M, & Ashe KH (2006) A specific amyloid-beta protein assembly in the brain impairs memory. Nature 440: 352-357.

158. LeVine H, 3rd (2004) Alzheimer's beta-peptide oligomer formation at physiologic concentrations. Anal Biochem 335: 81-90.

159. LeVine III H & Walker LC (2006) Models of Alzheimer's disease. In: Handbook of Models for Human Aging. Academic Press, Burlington, p^pp 121-134.

160. LeVine III H & Walker LC (2008) Molecular polymorphism of Abeta in Alzheimer's disease. Neurobiol Aging

161. Lewis J, Dickson DW, Lin WL, Chisholm L, Corral A, Jones G, Yen SH, Sahara N, Skipper L, Yager D, Eckman C, Hardy J, Hutton M, & McGowan E (2001) Enhanced neurofibrillary degeneration in transgenic mice expressing mutant tau and APP. Science 293: 1487-1491.

162. Li Y, Rinne JO, Mosconi L, Pirraglia E, Rusinek H, Desanti S, Kemppainen N, Nagren K, Kim BC, Tsui W, & de Leon MJ (2008) Regional analysis of FDG and PIB-PET images in normal aging, mild cognitive impairment, and Alzheimer's disease. Eur J Nucl Med Mol Imaging 35: 2169-2181.

163. Lin H, Zhu YJ, & Lal R (1999) Amyloid beta protein (1-40) forms calcium-permeable, Zn2+-sensitive channel in reconstituted lipid vesicles. Biochemistry 38: 11189-11196.

164. Liu L, Orozco IJ, Planel E, Wen Y, Bretteville A, Krishnamurthy P, Wang L, Herman M, Figueroa H, Yu WH, Arancio O, & Duff K (2008) A transgenic rat that develops Alzheimer's disease-like amyloid pathology, deficits in synaptic plasticity and cognitive impairment. Neurobiol Dis 31: 46-57.

165. Lockhart A, Lamb JR, Osredkar T, Sue LI, Joyce JN, Ye L, Libri V, Leppert D, & Beach TG (2007) PIB is a non-specific imaging marker of amyloid-beta (Abeta) peptide-related cerebral amyloidosis. Brain 130: 2607-2615.

166. Lockhart A, Ye L, Judd DB, Merritt AT, Lowe PN, Morgenstern JL, Hong G, Gee AD, & Brown J (2005) Evidence for the presence of three distinct binding sites for the thioflavin T class of Alzheimer's disease PET imaging agents on beta-amyloid peptide fibrils. J Biol Chem 280: 7677-7684.

167. Maeda J, Ji B, Irie T, Tomiyama T, Maruyama M, Okauchi T, Staufenbiel M, Iwata N, Ono M, Saido TC, Suzuki K, Mori H, Higuchi M, & Suhara T (2007) Longitudinal, quantitative assessment of amyloid, neuroinflammation, and anti-amyloid treatment in a living mouse model of Alzheimer's disease enabled by positron emission tomography. J Neurosci 27: 10957-10968.

168. Mahley RW, Huang Y, & Weisgraber KH (2007) Detrimental effects of apolipoprotein E4: potential therapeutic targets in Alzheimer's disease. Curr Alzheimer Res 4: 537-540.

169. Mahley RW & Rall SC, Jr. (1999) Is epsilon4 the ancestral human apoE allele? Neurobiol Aging 20: 429-430.

170. Makarava N & Baskakov IV (2008) The same primary structure of the prion protein yields two distinct self-propagating states. J Biol Chem 283: 15988-15996.

171. Mandelkow E, von Bergen M, Biernat J, & Mandelkow EM (2007) Structural principles of tau and the paired helical filaments of Alzheimer's disease. Brain Pathol 17: 83-90.

172. Mann DM, Yates PO, Marcyniuk B, & Ravindra CR (1986) The topography of plaques and tangles in Down's syndrome patients of different ages. Neuropathol Appl Neurobiol 12: 447-457.

173. Masoro EJ & Austad SN (2006) Handbook of the biology of aging. Sixth ed. Academic Press,

174. Masters CL, Simms G, Weinman NA, Multhaup G, McDonald BL, & Beyreuther K (1985) Amyloid plaque core protein in Alzheimer disease and Down syndrome. Proc Natl Acad Sci U S A 82: 4245-4249.

175. Mathis CA, Wang Y, & Klunk WE (2004) Imaging beta-amyloid plaques and neurofibrillary tangles in the aging human brain. Curr Pharm Des 10: 1469-1492.

176. McGowan E, Pickford F, Kim J, Onstead L, Eriksen J, Yu C, Skipper L, Murphy MP, Beard J, Das P, Jansen K, Delucia M, Lin WL, Dolios G, Wang R, Eckman CB, Dickson DW, Hutton M, Hardy J, & Golde T (2005) Abeta42 is essential for parenchymal and vascular amyloid deposition in mice. Neuron 47: 191-199.

177. Medawar PB (1952) An Unsolved Problem of Biology. H. K. Lewis, London.

178. Mestre-Frances N, Keller E, Calenda A, Barelli H, Checler F, & Bons N (2000) Immunohistochemical analysis of cerebral cortical and vascular lesions in the primate Microcebus murinus reveal distinct amyloid beta1-42 and beta1-40 immunoreactivity profiles. Neurobiol Dis 7: 1-8.

179. Metuzals J, Robitaille Y, Houghton S, Gauthier S, Kang CY, & Leblanc R (1988) Neuronal transformations in Alzheimer's disease. Cell Tissue Res 252: 239-248.

180. Meyer-Luehmann M, Coomaraswamy J, Bolmont T, Kaeser S, Schaefer C, Kilger E, Neuenschwander A, Abramowski D, Frey P, Jaton AL, Vigouret J-M, Paganetti P, Walsh DM, Mathews PM, Ghiso J, Staufenbiel M, Walker LC, & Jucker M (2006) Exogenous induction of cerebral beta-amyloidogenesis is governed by agent and host. Science 313: 1781-1784.

181. Meyer-Luehmann M, Coomaraswamy J, Bolmont T, Kaeser S, Schaefer C, Kilger E, Neuenschwander A, Abramowski D, Frey P, Jaton AL, Vigouret JM, Paganetti P, Walsh DM, Mathews PM, Ghiso J, Staufenbiel M, Walker LC, & Jucker M (2006) Exogenous induction of cerebral beta-amyloidogenesis is governed by agent and host. Science 313: 1781-1784.

182. Meyer-Luehmann M, Spires-Jones TL, Prada C, Garcia-Alloza M, de Calignon A, Rozkalne A, Koenigsknecht-Talboo J, Holtzman DM, Bacskai BJ, & Hyman BT (2008)

Rapid appearance and local toxicity of amyloid-beta plaques in a mouse model of Alzheimer's disease. Nature 451: 720-724.

183. Miller JA, Oldham MC, & Geschwind DH (2008) A systems level analysis of transcriptional changes in Alzheimer's disease and normal aging. J Neurosci 28: 1410-1420.

184. Mintun MA, Larossa GN, Sheline YI, Dence CS, Lee SY, Mach RH, Klunk WE, Mathis CA, DeKosky ST, & Morris JC (2006) [11C]PIB in a nondemented population: potential antecedent marker of Alzheimer disease. Neurology 67: 446-452.

185. Miravalle L, Calero M, Takao M, Roher AE, Ghetti B, & Vidal R (2005) Amino-terminally truncated Abeta peptide species are the main component of cotton wool plaques. Biochemistry 44: 10810-10821.

186. Morimoto RI & Cuervo AM (2009) Protein homeostasis and aging: taking care of proteins from the cradle to the grave. J Gerontol A Biol Sci Med Sci 64: 167-170.

187. Morrissette DA, Parachikova A, Green KN, & LaFerla FM (2009) Relevance of transgenic mouse models to human Alzheimer disease. J Biol Chem 284: 6033-6037.

188. Mosconi L, Mistur R, Switalski R, Tsui WH, Glodzik L, Li Y, Pirraglia E, De Santi S, Reisberg B, Wisniewski T, & de Leon MJ (2009) FDG-PET changes in brain glucose metabolism from normal cognition to pathologically verified Alzheimer's disease. Eur J Nucl Med Mol Imaging

189. Mucke L, Masliah E, Yu GQ, Mallory M, Rockenstein EM, Tatsuno G, Hu K, Kholodenko D, Johnson-Wood K, & McConlogue L (2000) High-level neuronal expression of abeta 1-42 in wild-type human amyloid protein precursor transgenic mice: synaptotoxicity without plaque formation. J Neurosci 20: 4050-4058.

190. Muller T, Meyer HE, Egensperger R, & Marcus K (2008) The amyloid precursor protein intracellular domain (AICD) as modulator of gene expression, apoptosis, and cytoskeletal dynamics-relevance for Alzheimer's disease. Prog Neurobiol 85: 393-406.

191. Murphy MP, Beckett TL, Ding Q, Patel E, Markesbery WR, St Clair DK, LeVine H, 3rd, & Keller JN (2007) Abeta solubility and deposition during AD progression and in APPxPS-1 knock-in mice. Neurobiol Dis 27: 301-311.

192. Nakamura S, Kiatipattanasakul W, Nakayama H, Ono F, Sakakibara I, Yoshikawa Y, Goto N, & Doi K (1996) Immunohistochemical characteristics of the constituents of senile plaques and amyloid angiopathy in aged cynomolgus monkeys. J Med Primatol 25: 294-300.

193. Nakamura S, Okabayashi S, Ageyama N, Koie H, Sankai T, Ono F, Fujimoto K, & Terao K (2008) Transthyretin Amyloidosis and Two Other Aging-Related Amyloidoses in an Aged Vervet Monkey. Vet Pathol 45: 67-72.

194. Nakamura S, Tamaoka A, Sawamura N, Kiatipattanasakul W, Nakayama H, Shoji S, Yoshikawa Y, & Doi K (1997) Deposition of amyloid beta protein (A beta) subtypes [A beta 40 and A beta 42(43)] in canine senile plaques and cerebral amyloid angiopathy. Acta Neuropathol (Berl) 94: 323-328.

195. Nalivaeva NN, Fisk LR, Belyaev ND, & Turner AJ (2008) Amyloid-degrading enzymes as therapeutic targets in Alzheimer's disease. Curr Alzheimer Res 5: 212-224.

196. Necula M, Kayed R, Milton S, & Glabe CG (2007) Small molecule inhibitors of aggregation indicate that amyloid beta oligomerization and fibrillization pathways are independent and distinct. J Biol Chem 282: 10311-10324.

197. Nelissen N, Vandenbulcke M, Fannes K, Verbruggen A, Peeters R, Dupont P, Van Laere K, Bormans G, & Vandenberghe R (2007) Abeta amyloid deposition in the language system and how the brain responds. Brain 130: 2055-2069.

198. Nelson PT, Greenberg SG, & Saper CB (1994) Neurofibrillary tangles in the cerebral cortex of sheep. Neurosci Lett 170: 187-190.

199. Nelson PT, Marton L, & Saper CB (1993) Alz-50 immunohistochemistry in the normal sheep striatum: a light and electron microscope study. Brain Res 600: 285-297.

200. Nelson PT & Saper CB (1995) Ultrastructure of neurofibrillary tangles in the cerebral cortex of sheep. Neurobiol Aging 16: 315-323.

201. Nelson PT, Stefansson K, Gulcher J, & Saper CB (1996) Molecular evolution of tau protein: implications for Alzheimer's disease. J Neurochem 67: 1622-1632.

202. Nieuwenhuis-Mark RE (2009) Diagnosing Alzheimer's dementia in Down syndrome: Problems and possible solutions. Res Dev Disabil

203. Nilsson KP (2009) Small organic probes as amyloid specific ligands - Past and recent molecular scaffolds. FEBS Lett

204. Nilsson KP, Aslund A, Berg I, Nystrom S, Konradsson P, Herland A, Inganas O, Stabo-Eeg F, Lindgren M, Westermark GT, Lannfelt L, Nilsson LN, & Hammarstrom P (2007) Imaging distinct conformational states of amyloid-beta fibrils in Alzheimer's disease using novel luminescent probes. ACS Chem Biol 2: 553-560.

205. Nitsch RM & Hock C (2008) Targeting beta-amyloid pathology in Alzheimer's disease with Abeta immunotherapy. Neurotherapeutics 5: 415-420.

206. Noda A, Murakami Y, Nishiyama S, Fukumoto D, Miyoshi S, Tsukada H, & Nishimura S (2008) Amyloid imaging in aged and young macaques with [11C]PIB and [18F]FDDNP. Synapse 62: 472-475.

207. Nordberg A (2008) Amyloid plaque imaging in vivo: current achievement and future prospects. Eur J Nucl Med Mol Imaging 35 Suppl 1: S46-50.

208. Oddo S, Caccamo A, Shepherd JD, Murphy MP, Golde TE, Kayed R, Metherate R, Mattson MP, Akbari Y, & LaFerla FM (2003) Triple-transgenic model of Alzheimer's disease with plaques and tangles: intracellular Abeta and synaptic dysfunction. Neuron 39: 409-421.

209. Oddo S, Caccamo A, Tran L, Lambert MP, Glabe CG, Klein WL, & Laferla FM (2005) Temporal profile of Abeta oligomerization in an in vivo model of Alzheimer's disease: A link between Abeta and tau pathology. J Biol Chem

210. Ohm TG & Meske V (2006) Cholesterol, statins and tau. Acta Neurol Scand Suppl 185: 93-101.

211. Orgogozo JM, Gilman S, Dartigues JF, Laurent B, Puel M, Kirby LC, Jouanny P, Dubois B, Eisner L, Flitman S, Michel BF, Boada M, Frank A, & Hock C (2003) Subacute meningoencephalitis in a subset of patients with AD after Abeta42 immunization. Neurology 61: 46-54.

212. Osborne R (2008) Myriad stumbles, Wyeth closes on Alzheimer's. Nat Biotechnol 26: 841-843.

213. Otvos L, Jr., Feiner L, Lang E, Szendrei GI, Goedert M, & Lee VM (1994) Monoclonal antibody PHF-1 recognizes tau protein phosphorylated at serine residues 396 and 404. J Neurosci Res 39: 669-673.

214. Paravastu AK, Leapman RD, Yau WM, & Tycko R (2008) Molecular structural basis for polymorphism in Alzheimer's beta-amyloid fibrils. Proc Natl Acad Sci U S A 105: 18349-18354.

215. Paravastu AK, Qahwash I, Leapman RD, Meredith SC, & Tycko R (2009) Seeded growth of beta-amyloid fibrils from Alzheimer's brain-derived fibrils produces a distinct fibril structure. Proc Natl Acad Sci U S A 106: 7443-7448.

216. Petkova AT, Leapman RD, Guo Z, Yau WM, Mattson MP, & Tycko R (2005) Self-propagating, molecular-level polymorphism in Alzheimer's beta-amyloid fibrils. Science 307: 262-265.

217. Petkova AT, Yau WM, & Tycko R (2006) Experimental constraints on quaternary structure in Alzheimer's beta-amyloid fibrils. Biochemistry 45: 498-512.

218. Piccini A, Russo C, Gliozzi A, Relini A, Vitali A, Borghi R, Giliberto L, Armirotti A, D'Arrigo C, Bachi A, Cattaneo A, Canale C, Torrassa S, Saido TC, Markesbery W, Gambetti P, & Tabaton M (2005) beta-amyloid is different in normal aging and in Alzheimer disease. J Biol Chem 280: 34186-34192.

219. Pike KE, Savage G, Villemagne VL, Ng S, Moss SA, Maruff P, Mathis CA, Klunk WE, Masters CL, & Rowe CC (2007) Beta-amyloid imaging and memory in non-demented individuals: evidence for preclinical Alzheimer's disease. Brain 130: 2837-2844.

220. Pittman AM, Myers AJ, Abou-Sleiman P, Fung HC, Kaleem M, Marlowe L, Duckworth J, Leung D, Williams D, Kilford L, Thomas N, Morris CM, Dickson D, Wood NW, Hardy J, Lees AJ, & de Silva R (2005) Linkage disequilibrium fine mapping and haplotype association analysis of the tau gene in progressive supranuclear palsy and corticobasal degeneration. J Med Genet 42: 837-846.

221. Podlisny MB, Tolan DR, & Selkoe DJ (1991) Homology of the amyloid beta protein precursor in monkey and human supports a primate model for beta amyloidosis in Alzheimer's disease. Am J Pathol 138: 1423-1435.

222. Poduri A, Gearing M, Rebeck GW, Mirra SS, Tigges J, & Hyman BT (1994) Apolipoprotein E4 and beta amyloid in senile plaques and cerebral blood vessels of aged rhesus monkeys. Am J Pathol 144: 1183-1187.

223. Poirier J, Davignon J, Bouthillier D, Kogan S, Bertrand P, & Gauthier S (1993) Apolipoprotein E polymorphism and Alzheimer's disease. Lancet 342: 697-699.

224. Popa-Wagner A, Schroder E, Walker LC, & Kessler C (1998) beta-Amyloid precursor protein and beta-amyloid peptide immunoreactivity in the rat brain after middle cerebral artery occlusion: effect of age. Stroke 29: 2196-2202.

225. Portelius E, Zetterberg H, Andreasson U, Brinkmalm G, Andreasen N, Wallin A, Westman-Brinkmalm A, & Blennow K (2006) An Alzheimer's disease-specific beta-amyloid fragment signature in cerebrospinal fluid. Neurosci Lett 409: 215-219.

226. Portelius E, Zetterberg H, Gobom J, Andreasson U, & Blennow K (2008) Targeted proteomics in Alzheimer's disease: focus on amyloid-beta. Expert Rev Proteomics 5: 225-237.

227. Potempska A, Mack K, Mehta P, Kim KS, & Miller DL (1999) Quantification of sub-femtomole amounts of Alzheimer amyloid beta peptides. Amyloid 6: 14-21.

228. Povinelli DJ & Preuss TM (1995) Theory of mind: evolutionary history of a cognitive specialization. Trends Neurosci 18: 418-424.

229. Premkumar DR, Cohen DL, Hedera P, Friedland RP, & Kalaria RN (1996) Apolipoprotein E-epsilon4 alleles in cerebral amyloid angiopathy and cerebrovascular pathology associated with Alzheimer's disease. Am J Pathol 148: 2083-2095.

230. Preuss TM, Caceres M, Oldham MC, & Geschwind DH (2004) Human brain evolution: insights from microarrays. Nat Rev Genet 5: 850-860.

231. Price DL, Martin LJ, Sisodia SS, Wagster MV, Koo EH, Walker LC, Koliatsos VE, & Cork LC (1991) Aged non-human primates: an animal model of age-associated neurodegenerative disease. Brain Pathol 1: 287-296.

232. Prusiner SB (1986) Prions are novel infectious pathogens causing scrapie and Creutzfeldt-Jakob disease. Bioessays 5: 281-286.

233. Quist A, Doudevski I, Lin H, Azimova R, Ng D, Frangione B, Kagan B, Ghiso J, & Lal R (2005) Amyloid ion channels: a common structural link for protein-misfolding disease. Proc Natl Acad Sci U S A 102: 10427-10432.

234. Raby CA, Morganti-Kossmann MC, Kossmann T, Stahel PF, Watson MD, Evans LM, Mehta PD, Spiegel K, Kuo YM, Roher AE, & Emmerling MR (1998) Traumatic brain injury increases beta-amyloid peptide 1-42 in cerebrospinal fluid. J Neurochem 71: 2505-2509.

235. Revesz T, Holton JL, Lashley T, Plant G, Frangione B, Rostagno A, & Ghiso J (2009) Genetics and molecular pathogenesis of sporadic and hereditary cerebral amyloid angiopathies. Acta Neuropathol

236. Roberson ED, Scearce-Levie K, Palop JJ, Yan F, Cheng IH, Wu T, Gerstein H, Yu GQ, & Mucke L (2007) Reducing endogenous tau ameliorates amyloid beta-induced deficits in an Alzheimer's disease mouse model. Science 316: 750-754.

237. Roertgen KE, Parisi JE, Clark HB, Barnes DL, O'Brien TD, & Johnson KH (1996) A beta-associated cerebral angiopathy and senile plaques with neurofibrillary tangles and cerebral hemorrhage in an aged wolverine (Gulo gulo). Neurobiol Aging 17: 243-247.

238. Roher AE, Lowenson JD, Clarke S, Wolkow C, Wang R, Cotter RJ, Reardon IM, Zurcher-Neely HA, Heinrikson RL, Ball MJ, & et al. (1993) Structural alterations in the peptide backbone of beta-amyloid core protein may account for its deposition and stability in Alzheimer's disease. J Biol Chem 268: 3072-3083.

239. Roher AE, Palmer KC, Yurewicz EC, Ball MJ, & Greenberg BD (1993) Morphological and biochemical analyses of amyloid plaque core proteins purified from Alzheimer disease brain tissue. J Neurochem 61: 1916-1926.

240. Rohme D (1981) Evidence for a relationship between longevity of mammalian species and life spans of normal fibroblasts in vitro and erythrocytes in vivo. Proc Natl Acad Sci U S A 78: 5009-5013.

241. Rosen RF, Farberg AS, Gearing M, Dooyema J, Long PM, Anderson DC, Davis-Turak J, Coppola G, Geschwind DH, Pare JF, Duong TQ, Hopkins WD, Preuss TM, & Walker LC (2008) Tauopathy with paired helical filaments in an aged chimpanzee. J Comp Neurol 509: 259-270.

242. Rosen RF, III LeVine H, Pohl J, Preuss TM, Reed M, Tomidokoro Y, Farberg A, Rosene DL, Voytko ML, Lah JJ, Murphy MP, Gearing M, Ghiso JA, & Walker LC. Mass spectrometric detection of modified cerebral Abeta peptides in Alzheimer’s disease, aged humans, and aged nonhuman primates. Program # 170.22. In: 2006 Abstract Viewer/Itinerary Planner. Program No. 170.22 Washington, DC, Society for Neuroscience, 2006.

243. Rosen RF, Walker LC, & Levine H, 3rd (2009) PIB binding in aged primate brain: Enrichment of high-affinity sites in humans with Alzheimer's disease. Neurobiol Aging

244. Rowe CC, Ng S, Ackermann U, Gong SJ, Pike K, Savage G, Cowie TF, Dickinson KL, Maruff P, Darby D, Smith C, Woodward M, Merory J, Tochon-Danguy H, O'Keefe G, Klunk WE, Mathis CA, Price JC, Masters CL, & Villemagne VL (2007) Imaging beta-amyloid burden in aging and dementia. Neurology 68: 1718-1725.

245. Rowe JW & Kahn RL (2000) Successful aging and disease prevention. Adv Ren Replace Ther 7: 70-77.

246. Roychaudhuri R, Yang M, Hoshi MM, & Teplow DB (2009) Amyloid beta-protein assembly and Alzheimer disease. J Biol Chem 284: 4749-4753.

247. Sadowski MJ, Pankiewicz J, Scholtzova H, Mehta PD, Prelli F, Quartermain D, & Wisniewski T (2006) Blocking the apolipoprotein E/amyloid-beta interaction as a potential therapeutic approach for Alzheimer's disease. Proc Natl Acad Sci U S A 103: 18787-18792.

248. Saido TC, Yamao-Harigaya W, Iwatsubo T, & Kawashima S (1996) Amino- and carboxyl-terminal heterogeneity of beta-amyloid peptides deposited in human brain. Neurosci Lett 215: 173-176.

249. Saumier D, Aisen PS, Gauthier S, Vellas B, Ferris SH, Duong A, Suhy J, Oh J, Lau W, Garceau D, Haine D, & Sampalis J (2009) Lessons Learned in the Use of Volumetric MRI in Therapeutic Trials in Alzheimer's Disease: The ALZHEMEDTM (Tramiprosate) Experience. J Nutr Health Aging 13: 370-372.

250. Scarpini E, Scheltens P, & Feldman H (2003) Treatment of Alzheimer's disease: current status and new perspectives. Lancet Neurol 2: 539-547.

251. Schultz C, Dehghani F, Hubbard GB, Thal DR, Struckhoff G, Braak E, & Braak H (2000) Filamentous tau pathology in nerve cells, astrocytes, and oligodendrocytes of aged baboons. J Neuropathol Exp Neurol 59: 39-52.

252. Schultz C, Hubbard GB, Tredici KD, Braak E, & Braak H (2001) Tau pathology in neurons and glial cells of aged baboons. Adv Exp Med Biol 487: 59-69.

253. Selkoe DJ (1999) Biology of Beta-amyloid Precursor Protein and the Mechanism of Alzheimer Disease. In: Alzheimer Disease, Second ed. Lippincott Williams & Wilkins, Philadelphia, p^pp.

254. Selkoe DJ (2003) Aging, amyloid, and Alzheimer's disease: a perspective in honor of Carl Cotman. Neurochem Res 28: 1705-1713.

255. Selkoe DJ, Bell DS, Podlisny MB, Price DL, & Cork LC (1987) Conservation of brain amyloid proteins in aged mammals and humans with Alzheimer's disease. Science 235: 873-877.

256. Seneca N, Cai L, Liow JS, Zoghbi SS, Gladding RL, Hong J, Pike VW, & Innis RB (2007) Brain and whole-body imaging in nonhuman primates with [11C]MeS-IMPY, a candidate radioligand for beta-amyloid plaques. Nucl Med Biol 34: 681-689.

257. Serdons K, Verduyckt T, Vanderghinste D, Cleynhens J, Borghgraef P, Vermaelen P, Terwinghe C, Leuven FV, Laere KV, Kung H, Bormans G, & Verbruggen A (2009) Synthesis of 18F-labelled 2-(4'-fluorophenyl)-1,3-benzothiazole and evaluation as amyloid imaging agent in comparison with [11C]PIB. Bioorganic & Medicinal Chemistry Letters 19: 602-605.

258. Shankar GM, Li S, Mehta TH, Garcia-Munoz A, Shepardson NE, Smith I, Brett FM, Farrell MA, Rowan MJ, Lemere CA, Regan CM, Walsh DM, Sabatini BL, & Selkoe DJ (2008) Amyloid-beta protein dimers isolated directly from Alzheimer's brains impair synaptic plasticity and memory. Nat Med 14: 837-842.

259. Shughrue PJ, Acton PJ, Breese RS, Zhao WQ, Chen-Dodson E, Hepler RW, Wolfe AL, Matthews M, Heidecker GJ, Joyce JG, Villarreal SA, & Kinney GG (2008) Anti-ADDL antibodies differentially block oligomer binding to hippocampal neurons. Neurobiol Aging

260. Simons EL (1972) Primate evolution: an introduction to man's place in nature. Macmillan, New York.

261. Spence KW & Yerkes RM (1937) Weight, growth and age in chimpanzee. Am J Phys Anthrop 22: 229-246.

262. Striedter GF (2005) Principles of brain evolution. Sinauer Associates, Inc., Sunderland, MA.

263. Svedberg MM, Hall H, Hellstrom-Lindahl E, Estrada S, Guan Z, Nordberg A, & Langstrom B (2008) [(11)C]PIB-amyloid binding and levels of Abeta40 and Abeta42 in postmortem brain tissue from Alzheimer patients. Neurochem Int

264. Svedberg MM, Hall H, Hellstrom-Lindahl E, Estrada S, Guan Z, Nordberg A, & Langstrom B (2009) [(11)C]PIB-amyloid binding and levels of Abeta40 and Abeta42 in postmortem brain tissue from Alzheimer patients. Neurochem Int 54: 347-357.

265. Takahashi RH, Almeida CG, Kearney PF, Yu F, Lin MT, Milner TA, & Gouras GK (2004) Oligomerization of Alzheimer's beta-amyloid within processes and synapses of cultured neurons and brain. J Neurosci 24: 3592-3599.

266. Tanaka M, Chien P, Naber N, Cooke R, & Weissman JS (2004) Conformational variations in an infectious protein determine prion strain differences. Nature 428: 323-328.

267. Tanaka M, Chien P, Yonekura K, & Weissman JS (2005) Mechanism of cross-species prion transmission: an infectious conformation compatible with two highly divergent yeast prion proteins. Cell 121: 49-62.

268. Tanaka M, Collins SR, Toyama BH, & Weissman JS (2006) The physical basis of how prion conformations determine strain phenotypes. Nature

269. Tekirian TL, Saido TC, Markesbery WR, Russell MJ, Wekstein DR, Patel E, & Geddes JW (1998) N-terminal heterogeneity of parenchymal and cerebrovascular Abeta deposits. J Neuropathol Exp Neurol 57: 76-94.

270. Thal DR, Capetillo-Zarate E, Del Tredici K, & Braak H (2006) The development of amyloid beta protein deposits in the aged brain. Sci Aging Knowledge Environ 2006: re1.

271. Thal DR, Rub U, Schultz C, Sassin I, Ghebremedhin E, Del Tredici K, Braak E, & Braak H (2000) Sequence of Abeta-protein deposition in the human medial temporal lobe. J Neuropathol Exp Neurol 59: 733-748.

272. Thinakaran G & Koo EH (2008) Amyloid precursor protein trafficking, processing, and function. J Biol Chem 283: 29615-29619.

273. Todar K. Todar's Online Textbook of Bacteriology, 2008.

274. Tomidokoro Y, Lashley T, Rostagno A, Neubert TA, Bojsen-Moller M, Braendgaard H, Plant G, Holton J, Frangione B, Revesz T, & Ghiso J (2005) Familial Danish dementia: co-existence of Danish and Alzheimer amyloid subunits (ADan AND A{beta}) in the absence of compact plaques. J Biol Chem 280: 36883-36894.

275. Toyama H, Ye D, Ichise M, Liow JS, Cai L, Jacobowitz D, Musachio JL, Hong J, Crescenzo M, Tipre D, Lu JQ, Zoghbi S, Vines DC, Seidel J, Katada K, Green MV, Pike VW, Cohen RM, & Innis RB (2005) PET imaging of brain with the beta-amyloid probe, [11C]6-OH-BTA-1, in a transgenic mouse model of Alzheimer's disease. Eur J Nucl Med Mol Imaging 32: 593-600.

276. Tyas SL, Snowdon DA, Desrosiers MF, Riley KP, & Markesbery WR (2007) Healthy ageing in the Nun Study: definition and neuropathologic correlates. Age Ageing 36: 650-655.

277. Tycko R, Sciarretta KL, Orgel JP, & Meredith SC (2009) Evidence for Novel -Sheet Structures in Iowa-mutant -Amyloid Fibrils. Biochemistry

278. Uddin M, Wildman DE, Liu G, Xu W, Johnson RM, Hof PR, Kapatos G, Grossman LI, & Goodman M (2004) Sister grouping of chimpanzees and humans as revealed by genome-wide phylogenetic analysis of brain gene expression profiles. Proc Natl Acad Sci U S A 101: 2957-2962.

279. Vamathevan JJ, Hasan S, Emes RD, Amrine-Madsen H, Rajagopalan D, Topp SD, Kumar V, Word M, Simmons MD, Foord SM, Sanseau P, Yang Z, & Holbrook JD (2008) The role of positive selection in determining the molecular cause of species differences in disease. BMC Evol Biol 8: 273.

280. van Groen T, Kiliaan AJ, & Kadish I (2006) Deposition of mouse amyloid beta in human APP/PS1 double and single AD model transgenic mice. Neurobiol Dis 23: 653-662.

281. Varki A & Altheide TK (2005) Comparing the human and chimpanzee genomes: searching for needles in a haystack. Genome Res 15: 1746-1758.

282. Vassar R (2001) The beta-secretase, BACE: a prime drug target for Alzheimer's disease. J Mol Neurosci 17: 157-170.

283. Vinters HV, Wang ZZ, & Secor DL (1996) Brain Parenchymal and Microvascular Amyloid in Alzheimer's Disease. Brain Pathology 6: 179-195.

284. Walker L & Cork L (1999) The Neurobiology of Aging in Nonhuman Primates. In: Alzheimer Disease, 2nd edition ed. Lippincott Williams & Wilkins, Philadelphia, p^pp.

285. Walker L, Levine H, & Jucker M (2006) Koch's postulates and infectious proteins. Acta Neuropathol (Berl) 112: 1-4.

286. Walker LC, Callahan MJ, Bian F, Durham RA, Roher AE, & Lipinski WJ (2002) Exogenous induction of cerebral beta-amyloidosis in betaAPP-transgenic mice. Peptides 23: 1241-1247.

287. Walker LC & Cork LC (1999) The Neurobiology of Aging in Nonhuman Primates. In: Alzheimer Disease, 2nd edition ed. Lippincott Williams & Wilkins, Philadelphia, p^pp.

288. Walker LC & LeVine H, 3rd (2000) The cerebral proteopathies. Neurobiol Aging 21: 559-561.

289. Walker LC & LeVine H, 3rd (2002) Proteopathy: the next therapeutic frontier? Curr Opin Investig Drugs 3: 782-787.

290. Walker LC, Levine H, 3rd, Mattson MP, & Jucker M (2006) Inducible proteopathies. Trends Neurosci 29: 438-443.

291. Walker LC, Masters C, Beyreuther K, & Price DL (1990) Amyloid in the brains of aged squirrel monkeys. Acta Neuropathol (Berl) 80: 381-387.

292. Walker LC, Pahnke J, Madauss M, Vogelgesang S, Pahnke A, Herbst EW, Stausske D, Walther R, Kessler C, & Warzok RW (2000) Apolipoprotein E4 promotes

the early deposition of Abeta42 and then Abeta40 in the elderly. Acta Neuropathol 100: 36-42.

293. Walker LC, Rosen RF, & Levine H, 3rd (2008) Diversity of Abeta deposits in the aged brain: a window on molecular heterogeneity? Rom J Morphol Embryol 49: 5-11.

294. Walsh DM & Selkoe DJ (2007) A beta oligomers - a decade of discovery. J Neurochem 101: 1172-1184.

295. Wang Y, Klunk WE, Huang GF, Debnath ML, Holt DP, & Mathis CA (2002) Synthesis and evaluation of 2-(3'-iodo-4'-aminophenyl)-6-hydroxybenzothiazole for in vivo quantitation of amyloid deposits in Alzheimer's disease. J Mol Neurosci 19: 11-16.

296. Warzok RW, Kessler C, Apel G, Schwarz A, Egensperger R, Schreiber D, Herbst EW, Wolf E, Walther R, & Walker LC (1998) Apolipoprotein E4 promotes incipient Alzheimer pathology in the elderly. Alzheimer Dis Assoc Disord 12: 33-39.

297. Watson D, Castano E, Kokjohn TA, Kuo YM, Lyubchenko Y, Pinsky D, Connolly ES, Jr., Esh C, Luehrs DC, Stine WB, Rowse LM, Emmerling MR, & Roher AE (2005) Physicochemical characteristics of soluble oligomeric Abeta and their pathologic role in Alzheimer's disease. Neurol Res 27: 869-881.

298. Wen Y, Yang SH, Liu R, Perez EJ, Brun-Zinkernagel AM, Koulen P, & Simpkins JW (2007) Cdk5 is involved in NFT-like tauopathy induced by transient cerebral ischemia in female rats. Biochim Biophys Acta 1772: 473-483.

299. Whitwell JL, Shiung MM, Przybelski SA, Weigand SD, Knopman DS, Boeve BF, Petersen RC, & Jack CR, Jr. (2008) MRI patterns of atrophy associated with progression to AD in amnestic mild cognitive impairment. Neurology 70: 512-520.

300. Wilcock GK, Black SE, Hendrix SB, Zavitz KH, Swabb EA, & Laughlin MA (2008) Efficacy and safety of tarenflurbil in mild to moderate Alzheimer's disease: a randomised phase II trial. Lancet Neurol 7: 483-493.

301. Wilcock GK & Esiri MM (1982) Plaques, tangles and dementia. A quantitative study. J Neurol Sci 56: 343-356.

302. Williams DR (2006) Tauopathies: classification and clinical update on neurodegenerative diseases associated with microtubule-associated protein tau. Intern Med J 36: 652-660.

303. Williams GC (1957) Pleiotropy, natural selection, and the evolution of senescence. Evolution 11: 398-411.

304. Ye L, Morgenstern JL, Gee AD, Hong G, Brown J, & Lockhart A (2005) Delineation of positron emission tomography imaging agent binding sites on beta-amyloid peptide fibrils. J Biol Chem 280: 23599-23604.

305. Ye L, Morgenstern JL, Lamb JR, & Lockhart A (2006) Characterisation of the binding of amyloid imaging tracers to rodent Abeta fibrils and rodent-human Abeta co-polymers. Biochem Biophys Res Commun 347: 669-677.

306. Ye L, Velasco A, Fraser G, Beach TG, Sue L, Osredkar T, Libri V, Spillantini MG, Goedert M, & Lockhart A (2008) In vitro high affinity alpha-synuclein binding sites for the amyloid imaging agent PIB are not matched by binding to Lewy bodies in postmortem human brain. J Neurochem 105: 1428-1437.

307. Young RD, Epstein L, & Coles LS (2009) Validated worldwide supercentenarians, living and recently deceased. Rejuvenation Res 12: 65-68.